

Sheffield Hallam University

The prediction of applied force and torque during flat hot rolling.

GONZALEZ, Jose Antonio.

Available from the Sheffield Hallam University Research Archive (SHURA) at:

<http://shura.shu.ac.uk/19698/>

A Sheffield Hallam University thesis

This thesis is protected by copyright which belongs to the author.

The content must not be changed in any way or sold commercially in any format or medium without the formal permission of the author.

When referring to this work, full bibliographic details including the author, title, awarding institution and date of the thesis must be given.

Please visit <http://shura.shu.ac.uk/19698/> and <http://shura.shu.ac.uk/information.html> for further details about copyright and re-use permissions.

POLYTECHNIC LIBRARY
POND STREET
SHEFFIELD S1 1WB

6802

7924517014



**Sheffield City Polytechnic
Eric Mensforth Library**

REFERENCE ONLY

This book must not be taken from the Library

PL/26

R5193

ProQuest Number: 10696998

All rights reserved

INFORMATION TO ALL USERS

The quality of this reproduction is dependent upon the quality of the copy submitted.

In the unlikely event that the author did not send a complete manuscript and there are missing pages, these will be noted. Also, if material had to be removed, a note will indicate the deletion.



ProQuest 10696998

Published by ProQuest LLC (2017). Copyright of the Dissertation is held by the Author.

All rights reserved.

This work is protected against unauthorized copying under Title 17, United States Code
Microform Edition © ProQuest LLC.

ProQuest LLC.
789 East Eisenhower Parkway
P.O. Box 1346
Ann Arbor, MI 48106 – 1346

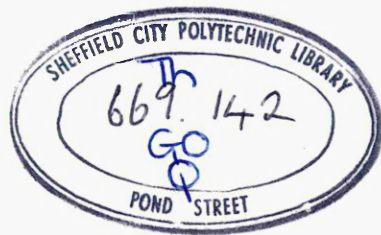
THE PREDICTION OF APPLIED FORCE AND TORQUE
DURING FLAT HOT ROLLING.

by

JOSE ANTONIO GONZALEZ BSc. MIMechE.

This thesis is submitted in part fulfilment of the requirements for the degree of Doctor of Philosophy in Industrial Metallurgy of the Council of National Academic Awards. The work was carried out at Sheffield City Polytechnic, Department of Metallurgy, in collaboration with Swinden Laboratories, British Steel Corporation.

January, 1981.



7924517-01

ABSTRACT

THE PREDICTION OF APPLIED FORCE AND TORQUE DURING FLAT HOT ROLLING.

by

JOSE ANTONIO GONZALEZ.

A mathematical model has been used to calculate the roll force and torque produced under a wide range of flat hot rolling conditions. The technique used is based on the numerical solution to the Von Karman equation developed by Alexander and applied to cold rolling conditions. In the present work, extensions have been made that allow the use of a yield stress which is dependent upon temperature, rate of deformation and extent of inhomogeneity of the deformation process. Like Alexander, the present model considers also the effect of both: the elastic zone at each end of the deformation region and of roll flattening on force and torque. A prerequisite for these calculations has been the experimental determination of the temperature gradients in the plate during rolling, the coefficient of friction between plate and rolls and the flow stress of the material at relevant temperatures and strain rates; the last named data being supplemented by published data on similar material. The results have been compared with experimentally determined force and torque required to roll mild steel plates at temperatures between 900°C and 1200°C, under unlubricated conditions.

The coefficients of friction associated with percentage reductions of between 30% and 45% were within the range 0.2 - 0.45. The thickness of the scale, the rolling velocity and the temperatures at the plate surface appeared to control the magnitude of the coefficient of friction. The peripheral layers of the plates underwent a severe quench, caused by rapid heat transfer to the rolls: the associated temperature reduction increased with increasing roll pressures and contact time. The resulting temperature gradient was included in the calculation using a geometric mean of the individual temperature measurements. At rolling temperatures between 900°C and 1000°C and reductions up to 35%, the degree of agreement between the experimental and calculated roll forces and torques were $\pm 13\%$ and $\pm 15\%$ respectively, although the use of Suzuki's flow stress data reduced these discrepancies to about $\pm 6\%$ and $\pm 11\%$ respectively in most cases. However the use of higher reductions or higher temperatures led to poorer agreement between calculation and experiment ($\pm 25\%$ and $\pm 35\%$ in the case of roll force and torque respectively).

The research described was carried out during the period of March 1977 to April 1980 in the Department of Metallurgy at Sheffield City Polytechnic and financed by La fundacion Gran Mariscal de Ayacucho (Venezuela). No part of this thesis has been submitted for a degree at any other University or College.

During the period of this work the author attended the following lectures, which constituted part of the M.Sc. in Metallurgical Process Management at Sheffield City Polytechnic:

- Module I: Process Metallurgy
 Mechanical Metallurgy
 Advanced Thermodynamics
- Module II: Numerical Methods and Programming
 Economic Analysis and Financial Control
- Module III: High Strength Alloys
 Heat Treatment and Transformations
 Automatic and Computer Aided Control of Metallurgical -
 Processes.
 Oxygen Steelmaking
 Quality Control
 Continuous Casting
- Module IV: Case studies in the subject areas of:-
 High Strength Alloys
 Oxygen Steelmaking
 Hot Rolling Schedule (Appendix I of this thesis).

Acknowledgements.

The author would like to thank his supervisor Dr. A.J.Fletcher for his guidance at all stages of the writing of this thesis, and Messrs. V.G.Gibson and M.Gleave for their contribution to this research.

He would also like to thank the technical staff of both the Metallurgy Department and the Department of Mechanical and Production Engineering at Sheffield Polytechnic for their help and cooperation; also the staff of computer services. Particular thanks to Messrs. R.Day and D.Wilkinson for their assistance during the experimental stage of this work.

Finally, I am heavily indebted to my wife, Jane, for her untiring effort throughout the typing and revision of this thesis, and for her continuous moral support.

. . . por la continua búsqueda . . .

CONTENTS

Abstract		i
Preface		ii
Figures and Tables		vii
Notation		xiii
CHAPTER 1	Introduction.	1
CHAPTER 2	The Theory of Rolling.	2
	2.1 Introduction.	2
	2.2 The differential equation governing variation in roll pressure during a pass.	3
	2.3 Early Theories of Rolling.	5
	2.4 Orowan's Theory of Rolling.	15
	2.5 Approximate Theories.	21
	2.6 Alternative Theories.	26
	2.7 Alexander's solution to the Von Karman equation.	30
	2.8 Roll flattening.	31
	2.9 The yield stress applicable in hot rolling.	34
	2.10 Coefficient of friction between slab and rolls during hot rolling.	39
	2.11 Roll force and torque.	46
	2.12 Validity of the theories of hot rolling.	49
CHAPTER 3	Numerical Solution to the Basic Von Karman Equation.	
	3.1 Introduction.	53
	3.2 Basic differential equation under homogeneous deformation	53
	3.3 Basic differential equation under inhomogeneous deformation.	56
	3.4 Yield stress variation during hot rolling.	57
	3.5 Roll force per unit width.	58
	3.6 Roll torque per unit width.	59
	3.7 Elastic arcs of contact.	60
	3.8 Roll flattening.	62
	3.9 Calculation technique.	63
	3.10 Data used in roll pressure calculations.	65
	3.11 Computer Programmes.	66

CHAPTER 4	Experimental Procedure.	
4.1	The Rolling Mill.	69
4.1.1	Mill power supply.	69
4.2	Mill instrumentation.	70
4.2.1	Tachogenerator.	70
4.2.2	Light-activated switch.	71
4.2.3	Temperature measurements.	72
4.2.4	Load cells.	73
4.3	Determination of the rolling power and roll torque.	74
4.3.1	Frictional power.	75
4.3.2	Idling power.	76
4.3.3	Dynamic power.	77
4.3.4	Rolling power and roll torque.	77
4.3.5	Experimental determination of the frictional power under load.	78
4.4	Recording Instruments.	79
4.5	Reheating furnaces.	82
4.6	Cam plastometer.	83
4.6.1	Cam design.	84
4.6.2	Instrumentation of the cam plastometer.	85
4.7	Rolling Programme.	87
4.7.1	The condition, composition and dimension of the plates.	89
4.7.2	Reheating and rolling.	90
4.8	Determination of the coefficient of friction.	91
4.9	Hot compression tests.	92
CHAPTER 5	Experimental Results.	
5.1	Introduction.	94
5.2	Roll force measurements.	94
5.3	Roll torque measurements.	96
5.4	Determination of the coefficient of friction during rolling.	97
5.5	Temperature measurements during rolling.	98
5.6	Yield stress data of the material undergoing rolling.	101

CHAPTER 6	Calculated Results.	
6.1	The magnitude of the mechanical properties and rolling conditions used in the calculation of roll force and torque.	103
6.2	Effect of the coefficient of friction on roll force.	104
6.3	Effect of the mean temperature of rolling on roll force.	108
6.4	Effect of the coefficient of friction on roll torque.	109
6.5	Effect of the mean temperature of rolling on roll torque.	117
6.6	Effect on roll force and torque of the transversal distribution of roll pressure.	119
CHAPTER 7	Discussion.	
7.1	Distribution of temperatures in the deforming material.	121
7.2	The effect of the coefficient of friction on the calculated roll force and torque.	126
7.3	Values of the coefficient of friction obtained by experiment.	129
7.4	Inhomogeneity of the deformation process.	131
7.5	Comparison between calculated and measured values of roll force.	135
7.6	Comparison between calculated and measured values of roll torque.	137
7.7	Limitations in the accuracy of the measured and calculated forces and torques.	139
7.8	Conclusions.	143
Bibliography.		145
Appendix I	Case Study	152
Appendix II	Computer Print-out	159
Appendix III	Temperature Calculations	165

2.2.1	Roll gap geometry.	167
2.3.1	Comparison of Siebel's and Von Karman's roll stress distributions.	168
2.3.2	Variation of the radial pressure and shear stresses along the arc of contact - after Tselikov ⁽⁵⁾ .	168
2.3.3.	Distribution of normal and tangential pressures along the arc of contact according to the theories shown - after El Wasiri ⁽⁹⁾ .	169
2.4.1	Compression between two rough inclined platens.	170
2.4.2	Illustrating the calculation of horizontal force in the strip between the rolls (Orowan).	170
2.4.3	Variation of w with a for various values of μ - after Orowan ⁽⁴⁾ .	170
2.4.4	Comparison of measured and calculated roll pressure distribution for smooth ($\mu=0.14$) and rough ($\mu=0.4$) rolls.	171
2.5.1	Exit side of a typical friction hill, showing the difference between the Denton and Crane method and that of El Kalay and Sparling - after Denton et al. ⁽¹⁷⁾	172
2.6.1	Geometrical construction of the slip line field solution - after Alexander ⁽²¹⁾ .	173
2.9.1	True stress/true strain curves in the hot working temperature range: (a) 3% silicon steel, (b) mild steel - after Sellars et al. ^(41a) .	174
2.10.1	Variation of the coefficient of friction in unlubricated hot rolling conditions - after Roberts ⁽⁵⁰⁾ .	175
2.10.2	Distribution of shear stresses and coefficients of friction along the arc of contact - after Matsuura et al. ⁽⁵¹⁾ .	175
3.2.1	Longitudinal section of a strip between two rolls.	176
3.4.1	Variation of the mean strain rate of a section along the arc of contact for a typical rolling pass.	177
3.10.1	Variation of Young's modulus with temperature for two steel compositions - after BISRA Research Report ⁽⁶⁷⁾ .	178
Table A	Flow stress constants of 0.17% C steel at different temperatures.	178a
3.11.1	Flow chart for the numerical solution to the Von Karman equation to predict roll force and torque per unit width.	179

4.1.1 (Plate)	The rolling mill and ancillary instruments	180
4.2.2	Light-activated switch and its location on the exit table of the rolling mill.	181
4.2.3	Location of thermocouples inside a plate, (a) two thermocouples, (b) four thermocouples.	182
4.2.4	Calibration curves of the load cells.	183
4.3.5	Experimental values of the roll neck friction coefficient/drive efficiency ratio at various loads.	184
4.6	Cam plastometer and enlarged section of the die assembly.	185
4.6.1	Cam profiles.	186
4.6.2	Calibration curves of the instrumentation of the cam plastometer.	187
4.8.1	Relation between the coefficient of friction and the forward slip at various reductions and entry thicknesses, (a) $h = 9.5$ mm (b) $h = 12.7$ mm. (c) $h = 16$ mm (d) $h = 19$ mm.	188 189
5.2	Typical recording of the load cells.	190
5.2.1	Relation between mean roll force and reduction measured at 900°C .	191
5.2.2	" " 1000°C .	192
5.2.3	" " 1100°C .	193
5.2.4	" " 1200°C .	194
5.3.1	Simultaneous recordings of voltage, current and angular velocity of the rolls during a test at 900°C and 40% reduction, (a) associated roll power consumption.	195
5.3.2	Relation between mean roll torque and reduction measured at 900°C .	196
5.3.3	" " 1000°C .	197
5.3.4	" " 1100°C .	198
5.3.5	" " 1200°C .	199
Table 1	Rolling parameters determined in experimental work.	200
5.4.1	Forward slip variation with the percentage reduction measured at 900°C .	201
5.4.2	" " 1000°C .	202
5.4.3	" " 1100°C .	203
5.4.4	" " 1200°C .	204

5.4.5	Forward slip variation with percentage reduction under lubricated conditions at 960°C.	205
5.4.6	" dry " "	206
5.5.1	Temperature variations at the centre and sub-surface of a plate before and during rolling for various reductions, 18%-45%, and mean entry temperatures, 900-1100°C.	207
5.5.2	" 34% " " " 800-950°C.	208
5.5.3	" 34% " " " 850°C.	209
5.5.4	Typical recording from an insulated thermocouple inserted in a plate being deformed.	210
5.5.5	Correction to allow voltage interference in a re-welded thermocouple.	210
5.5.6	Temperature variation at several depths of a plate during contact time using insulated thermocouples, (a) at mean entry temperature 870°C and 30% reduction, (b) " " " " 820-900°C and 10-40% red.	211
5.5.7	Temperature variation at several depths of a plate during contact time using rewelded thermocouples, (a) mean entry temperature 900-1050°C and 15% reduction. (b) " " " 1000°C and 30% reduction. (c) " " " 1050°C and 30% reduction. (d) " " " 1050°C and 40% reduction.	212 213 213 214
5.6.1	Typical traces of the load/time and displacement/time recorded in a cam plastometer.	215
5.6.2	Uniaxial yield stress/strain curves of 0.17% C steel at 900°C.	216
5.6.3	" 1000°C.	217
5.6.4	" 950 - 970°C.	218
5.6.5	" 980 - 1050°C.	219
6.2.1	Relation between calculated roll force and reduction under homogeneous deformation and using published flow stress data ($\mu=0.2 - 0.6$) at 900°C.	220
6.2.2	" " " " " " 1000°C.	221
6.2.3	" " " " " " 1100°C.	222
6.2.4	" " " " " " 1200°C.	223

6.2.5	Relation between calculated roll force and reduction under homogeneous deformation and using flow stress data determined in the present work ($\mu=0.2-0.6$) at 900°C.	224
6.2.6	" " " " " " " " 1000°C.	225
6.2.7	Relation between calculated roll force and reduction under inhomogeneous deformation and using published flow stress data ($\mu=0.2 - 0.6$) at 900°C.	226
6.2.8	" " " " " " 1000°C.	227
6.2.9	" " " " " " 1100°C.	228
6.2.10	" " " " " " 1200°C.	229
6.2.11	Relation between calculated roll force and reduction under inhomogeneous deformation and using flow stress data determined in the present work ($\mu=0.2-0.6$) at 900°C	230
6.2.12	" " " " " " " " 1000°C	231
6.3.1	Relation between calculated roll force and reduction showing the effect of a $\pm 5\%$ variation in the nominal temperature of rolling and using published flow stress data ($\mu=0.4$) - nominal temperature 900°C.	232
6.3.2	" " " " " 1000°C.	233
6.3.3	" " " " " 1100°C.	234
6.3.4	" " " " " 1200°C.	235
6.4.1	Relation between calculated roll torque and reduction under homogeneous deformation using published flow stress data ($\mu=0.2-0.6$) at 900°C.	236
6.4.2	" " " " " 1000°C.	237
6.4.3	" " " " " 1100°C.	238
6.4.4	" " " " " 1200°C.	239
6.4.5	Variation of the relative position of the neutral angle with the percentage reduction ($\mu=0.2-0.6$) at 900°C.	240
6.4.6	" " " " " " " " 1000°C.	241
6.4.7	Variation of the lever arm with percentage reduction at 900°C.	242
6.4.8	" 1000°C.	243
6.4.9	Variation of the relative position of the neutral angle with the percentage reduction ($\mu=0.2-0.6$) at 1100°C.	244
6.4.10	Roll pressure and yield stress distributions along the arc of contact under homogeneous deformation and using published yield stress data at 1100°C and 1200°C ($\mu=0.4$ reduction 30%)	245

6.4.11	Variation of the lever arm with percentage reduction at 1100°C.	246
6.4.12	" 1200°C.	247
6.4.13	Relation between calculated roll torque and reduction under homogeneous deformation using flow stress data determined in the present work ($\mu=0.2-0.6$) at 900°C.	248
6.4.14	" " " " " " " " 1000°C.	249
6.4.15	Calculated roll pressure distributions under homogeneous deformation using both published flow stress data and that determined in the present work, (900°C, $\mu=0.2$, $r=33\%$).	250
6.4.16	Relation between roll torque and reduction under inhomogeneous deformation using published flow stress data ($\mu=0.2-0.6$) at 900°C.	251
6.4.17	" " " " 1000°C.	252
6.4.18	" " " " 1100°C.	253
6.4.19	" " " " 1200°C.	254
6.4.20	Roll pressure distribution assuming both homogeneous and inhomogeneous deformation and using published flow stress data (900°C, $\mu=0.6$, $r=18\%$).	255
6.4.21	Relation between roll torque and reduction under inhomogeneous deformation using flow stress data determined in the present work ($\mu=0.2-0.6$) at 900°C.	256
6.4.22	" " " " " " " " 1000°C.	257
6.5.1	Relation between calculated roll torque and reduction showing the effect of a $\pm 5\%$ variation in the nominal temperature of rolling and using published flow stress data ($\mu=0.4$) - nominal temperature 900°C.	258
6.5.2	" " " " 1000°C.	259
6.5.3	" " " " 1100°C.	260
6.5.4	" " " " 1200°C.	261
6.6.1	Distribution of stresses across roll gap mid-way between exit and entry planes - after Sansome ⁽⁶⁶⁾ .	262
6.6.2	Transversal distribution of peak roll pressures for various cross sectional shapes of the material between the rolls - after Polukhine ⁽⁶³⁾ .	262
6.6.3	Roll force distribution across strip width - after Matsuura et al. ⁽⁵¹⁾ .	262

Table 2	Correcting factors to allow for transversal drop of roll pressure distribution.	265
7.1	Measured and calculated temperature profiles at several instants during the time of contact.	266
Table 3	Values of coefficient of friction determined from several empirical relationships.	267
7.4.1	Reconstructed disposition of the hot junction of thermocouples in rolled plates.	268
7.4.2	Relation between theoretical and experimental values of the neutral angle and percentage reduction (Series A)	269
7.5.1	Comparison between calculated and measured values of roll force for the rolling conditions in Series A at 880 - 940°C.	270
7.5.2	Comparison between calculated and measured values of roll force for the rolling conditions in Series A at 950°C.	271
7.5.3	Comparison between calculated and measured values of roll force for the rolling conditions in Series A at 1080°C.	272
7.5.4	Comparison between calculated and measured values of roll force for the rolling conditions in Series A at 1150°C.	273
7.5.5	Comparison between measured and calculated roll forces in Series A using published flow stress data.	274
7.5.6	Comparison between measured and calculated roll forces in Series A using flow stress data determined in the present work.	275
7.6.1	Comparison between calculated and measured values of roll torque for the rolling conditions in Series A at (a) 880 - 940°C.	276
7.6.2	(b) 950°C.	277
7.6.3	(c) 1080°C.	278
7.6.4	(d) 1150°C.	279
7.6.5	Comparison between measured and calculated roll torque in Series A using published flow stress data.	280
7.6.6	Comparison between measured and calculated roll torque in Series A using flow stress data determined in the present work.	280
7.7	Distribution of roll pressure and shear stress/roll pressure ratio along the arc of contact(1100°C,r=40%).	281

1. Introduction.

The rolling mill section of a plant represents, normally, the largest single item of investment, which demands that a mill should be operated as efficiently as possible. The objective of rolling theories, then, is to enable the roll separating force and the torque to be predicted so that optimum scheduling, operation and control of a mill can be attained in order to produce the maximum tonnage at the lowest cost.

A large number of rolling theories have been proposed to estimate roll force and torque for a wide variety of rolling conditions, and simplified methods, representing a compromise between accuracy and speed of calculation, have been adopted in the rolling industry. Predictions in cold rolling theory have reached acceptable levels of accuracy, whereas hot rolling theories often produce discrepancies, owing to crude assumptions made in their derivation.

The lack of understanding of many aspects of the hot rolling process arises from the difficulties associated with the experimental work. As a result, fundamental research, concerned with the mechanics of deformation of the metal at high temperatures in the roll gap, becomes essential so as to achieve accurate estimates of roll force and torque for rolling mill design and scheduling purposes. This has become feasible with the widespread availability of digital computers and the amount of data accumulated over recent years on the resistance to deformation of metals at high temperatures.

In the present work, a mathematical model, translated into computer programmes, has been constructed, which provides quick and satisfactory predictions of experimentally determined roll force and torque, and enables factors affecting rolling loads in flat hot rolling to be studied.

2. The Theory of Rolling.

2.1 Introduction.

The theory of rolling is concerned with the relationships between the external forces applied and the mechanical properties of the material undergoing deformation. Such relationships are established through an analysis of the distribution of stresses inside the material between the rolls. Since considerable difficulties are encountered in the direct determination of the frictional forces between the material and roll surfaces and of the changes of the material properties during deformation, simplified assumptions are introduced into any theory of rolling.

Rolling theories were initiated with the work of Von Karman⁽¹⁾ and Siebel⁽²⁾ who, in order to simplify the actual problem, analysed only the case of flat rolling without spread, rather than that of the more complicated section rolling where there is considerable spread. They considered the forces acting on a vertical slice of the material being rolled in order to derive a differential equation from which the variation of roll pressures applied to the deforming material could be determined. Integration of this pressure distribution over the contact length between the material and the rolls allowed the roll force and torque to be determined.

In order to obtain satisfactory solutions to the determination of the roll pressures, roll force and torque under a wide range of rolling conditions, a number of theories, which basically follow the assumptions introduced by Von Karman, have been proposed.

2.2 The differential equation governing the variation in the roll pressure during the rolling pass.

Most of the early theories of rolling⁽¹⁻⁴⁾ relied on assumptions that were basically the same as those introduced by Von Karman⁽¹⁾ viz:

- (i) Plane sections in the material perpendicular to the direction of rolling remain plane during rolling. i.e. homogeneous deformation is present.
- (ii) There is no lateral spread of the material if the thickness of the sheet is small compared with its width.
- (iii) The Von Misses criterion of yielding in plane strain applies. When the principal stresses in the plane sections are q and p , this condition reduces to: $q-p=1.15Y$
- (iv) The plane strain yield stress $2K=1.15Y$ is constant throughout the contact length.
- (v) The coefficient of friction, μ , between the material and the roll, is constant over the arc of contact.
- (vi) There is no elastic deformation of the rolls in the arc of contact.
- (vii) The elastic deformations of the material are negligible in comparison with the plastic deformations.
- (viii) The peripheral velocity of the rolls is uniform.

Fig.221 represents a longitudinal section of a strip in transit through the roll gap. Von Karman considered a slice of the material bounded by two parallel planes, AA and BB, which were assumed to remain plane as the material passed through the roll gap.

During rolling the strip is reduced in thickness from h_1 to h_2

and since it does not spread laterally, this vertical compression produces elongation in the rolling direction. Thus, the following relationship applies,

$$h_1 v_1 = h v = h_2 v_2$$

where v_1 and v_2 are the mean velocities of the strip entering and leaving the roll gap and v is the velocity at any intermediate thickness h .

The roll surface velocity v_R must have some value between v_1 and v_2 . The point where the roll and strip move at the same velocity is defined as the neutral point. On the entry side the roll moves more rapidly than the strip, while the reverse is the case on the exit side. Thus the frictional forces at the surfaces always act toward the neutral point. This condition produces a roll pressure distribution which includes a maximum pressure at the neutral point. This characteristic shape of the roll pressure distribution is referred to as the friction hill (see Fig. 2.3.1).

If the equilibrium of the horizontal forces in the absence of acceleration, i.e. at a constant roll velocity, is considered, we arrive at,

$$\frac{d(ph)}{d\theta} = \pm R \tau \sin \theta + T \cos \theta \quad (2.2.1)$$

where the upper sign refers to the exit side of the neutral point and the lower sign to the entry side.

The roll pressure S is related to the vertical stress q by a balance between the vertical forces,

$$q = S(1 \mp \tau \theta)$$

with the application of Von Mises' yield criterion,

$$q - p = 2K$$

thus,

$$p = s(1 \mp \mu \tan \theta) - 2k \quad (2.2.2)$$

substituting in Eq. 2.2.1 we get

$$d/d\theta [h(s \mp \mu \tan \theta - 2k)] = 2R(s \sin \theta \pm \mu \cos \theta) \quad (2.2.1a)$$

where the thickness h is given by the geometry of the circular arc of contact as:

$$h = h_2 + 2R(1 - \cos \theta)$$

2.3 Early theories of rolling.

In practice the yield stress of the material in hot rolling is a function of temperature, rate and amount of plastic strain and degree of homogeneity of the deformation, which greatly increases the difficulties associated with the solution of Von Karman's equation. In addition, the actual arc of contact is elliptical rather than circular⁽⁴⁾ and the plane sections (AA and BB in Fig. 2.2.1) are subject to a change in shape as they move towards the exit plane XX. Many workers have attempted to overcome these difficulties by the use of approximate solutions to the Von Karman equation (Eq. 2.2.1a).

Von Karman himself⁽¹⁾ replaced the radial pressure S acting on the section by the vertical pressure Q . Furthermore, he assumed that X was small compared with R so that $Rd\theta = dx$. In addition $\sin \theta = x/R$ was considered with $\cos \theta = 1$, and $h_x = h_2/2 + x^2/2R$

and
$$\frac{dh_x}{dx} = \frac{x}{R}$$

Hence Eq. (2.2.1) was replaced by:

$$h_x dp/dx + p x/R = s(x/R \pm \mu) \quad (2.3.2)$$

which, together with the application of the Von Mises yield criterion gave,

$$h_x dp/dx = 2k(x/R \pm \mu) \pm \mu p \quad (2.3.2a)$$

Eq. 2.3.2a can be written in terms of the radial pressure in the form

$$ds/dx = A(x)s + B(x) \quad (2.3.2b)$$

where $A(x) = \pm \mu/h_x$

and $B(x) = \frac{2K(x)}{h_x(R)}$

The formal solution of the linear Eq. 2.3.2b is given by,

$$s = \exp\left[-\int A(x)dx\right] \left[\int \exp\left(\int A(x)dx\right) B(x)dx + C \right] \quad (2.3.3)$$

where the sign of the function $A(x)$ is taken as positive on the exit and negative on the entry side, and the constant C is determined by the boundary conditions of the exit and entry sides respectively.

Eq. 2.3.3 can be solved only by expanding the integrand inside the brackets in a series. Thus, the final result obtained is cumbersome and not completely accurate.

Siebel⁽²⁾ assumed that the radial pressure was equal to the yield stress $2K$ and that the thickness of the material remained constant on the entry and exit sides of the arc of contact. This implied that $\frac{dh}{dx} = 0$ except at the neutral point. Further approximations were $\sin\theta = A = x/R$ so $d\theta = x/R$ and $\cos\theta = 1$ which resulted in a simplified expression:

$$h dp/dx = 2K(x/R \pm \mu) \quad (2.3.2a)$$

which gave the following solutions:

$$p^+ = \frac{2K}{h} \left[\frac{x^2}{R} + \mu x \right] + C_1$$

$$p^- = \frac{2K}{h} \left[\frac{x^2}{R} - \mu x \right] + C_2$$

C_1, C_2 are constants

Although Siebel's theory served to explain many of the phenomena observed in rolling, it is not sufficiently accurate for quantitative

calculations, as it neglects the cumulative effect of the horizontal pressure on the friction hill equation and hence the maximum pressure obtained is too low. (8)

T.L. Smith achieved a simplification of the basic Von Karman equation^(8b) assuming that the arc of contact was parabolic. Thus,

$$h = [h_2 + \Delta h (x/L)^2] \quad \text{so } dh/dx = 2\Delta h x/L^2$$

and an expression for the roll pressure distribution was obtained,

$$\left(\frac{h_2}{2} + \frac{\Delta h x^2}{2L^2}\right) \frac{ds}{dx} = 2K \frac{\Delta h x}{L^2} \pm \mu s \quad (2.3.4)$$

which, after rearrangement, gave:

$$\frac{d(s/2K)}{d(x/L)} = \frac{2\Delta h \left(\frac{x}{L} \mp \frac{s}{2K} \frac{L}{\Delta h} \mu\right)}{1 + \Delta h x^2/h_2 L^2}$$

Thus, from the above equation a distribution of $s/2K$ against the relative position x/L could be obtained by selecting values of $L\mu/\Delta h$ and h_1 .

The solutions of Siebel and Von Karman were compared by Trinks^(8a), assuming the same rolling conditions, and presented on a graph, shown in Fig. 2.3.1; where it can be noted that Von Karman's solution produces a much higher maximum pressure, whose position coincides with the neutral point given by the corresponding equation, i.e. when either $p^+ = p^-$ or $s^+ = s^-$.

Tselikov⁽⁵⁾ introduced $a = \Delta h/L^2$ and $b = h_2/2$ to write Eq. 2.3.4.

as:

$$ds = (2Kax \pm \mu s) \frac{2dx}{ax^2 + b} \quad (2.3.4a)$$

and introduced a new variable u :

$$x = \sqrt{\frac{b}{a}} \tan u$$

then

$$u = \frac{1}{2} x \sqrt{\frac{a}{b}}, \quad du = \sqrt{\frac{a}{b}} \frac{dx}{1 + ax^2/b}$$

The value of U was substituted into Eq. 2.3.4a to arrive at a solution of the form;

$$S = \exp -mu \left[4K \int \exp mu \frac{1}{2} x \sqrt{\frac{a}{b}} dx + C \right] \quad (2.3.3a)$$

where

$$m = \frac{2\mu}{\sqrt{ab}}$$

Thus the solution given by Eq. (2.3.3a) was similar to the general solution to the approximate Von Karman's equation, given by Eq. (2.3.5).

It was then considered that when $\Delta h < h_2$ and $U < 1$ the integrand could be expanded in a series, so that Eq. 2.3.3a assumed the form,

$$S^- = C_0 \exp -mu - \frac{4K}{m^2} (1 - mu)$$

for the entry zone

and

$$S^+ = C_1 \exp mu - \frac{4K}{m^2} (1 + mu)$$

for the exit zone.

The constants C_0 and C_1 were determined from the boundary conditions at the entry plane EE , where $X=L$, $S=2K-\delta_A$ and $U=U_0 = \frac{1}{2} \sqrt{\frac{\Delta h}{h_2}}$; and at the exit plane XX , where $X=0$, $S=2K-\delta_B$ and $U=0$.

Thus the final solution of Eq. 2.3.4a was expressed for the entry and exit zone respectively as:

$$S^- = 2K \left\{ \left[\xi + \frac{2}{m^2} (1 - mu_0) \right] \exp m(u_0 - u) - \frac{2}{m^2} (1 - mu) \right\}$$

and

$$S^+ = 2K \left\{ \left[\xi + \frac{2}{m^2} \right] \exp mu - \frac{2}{m^2} (1 + mu) \right\}$$

where $\xi_0 = 1 - \delta_0/2k$

and $\xi_1 = 1 - \delta_0/2k$

Subsequently Tselikov suggested an alternative method to calculate the rolling pressure assuming small angles of contact. He used a similar approach to that of Von Karman to obtain an equation of the form,

$$2s(t_2\theta \pm \mu)dx = d(hp) \quad (2.3.4b)$$

Eq. 2.2.2. was also included, i.e.

$$p = s(1 \mp \mu t_2\theta) - 2k$$

so

$$dp = (1 \mp \mu t_2\theta) ds$$

These values for p and dp with $dh/2t_2\theta = dx$ were substituted in Eq. 2.3.4b which divided through by $1 \mp \mu t_2\theta$ resulted in,

$$\left[\left(1 + \frac{t_2\theta \pm \mu}{(1 \mp \mu t_2\theta)t_2\theta} \right) \left(s - \frac{2k}{1 \mp \mu t_2\theta} \right) \right] dh + hds = 0 \quad (2.3.4c)$$

It was assumed that for small angles of contact, θ may be considered constant and equal to half the contact angle. Then Eq. 2.3.4c was written as

$$\frac{ds}{(1+\xi) - S_0} = -\frac{dh}{h} \quad (2.3.4d)$$

where

$$\xi = \frac{t_2\theta \pm \mu}{(1 \mp \mu t_2\theta)t_2\theta}$$

and

$$S_0 = \frac{2k}{1 \mp \mu t_2\theta}$$

were constant.

After integration Eq. 2.3.4d became,

$$\frac{1}{1+\xi} \ln \left\{ (1+\xi) s - S_0 \right\} = \ln \frac{1}{h} + C_0 \quad (2.3.5)$$

The constant C_0 is found from the boundary conditions. Thus, when $h=h_1$ and $S=S_1$ Eq.(2.3.5) becomes

$$S^- = \frac{S_0}{1+\xi} \left[\left\{ \frac{S_1}{S_0} (1+\xi) - 1 \right\} \left(\frac{h_1}{h} \right)^{1+\xi} + 1 \right] \quad (2.3.5a)$$

for the entry side, with

$$\xi = \frac{\mu \theta - \mu}{(1 + \mu \mu \theta) \mu \theta}$$

and

$$S_0 = 2K / (1 + \mu \mu \theta)$$

While for the exit side, when $h=h_2$ and $S=S_2$ Eq.(2.3.5) becomes

$$S^+ = \frac{S_0}{1+\xi} \left[\left\{ \frac{S_2}{S_0} (1+\xi) - 1 \right\} \left(\frac{h_2}{h} \right)^{1+\xi} + 1 \right] \quad (2.3.5b)$$

with

$$\xi = \frac{\mu \theta + \mu}{(1 - \mu \mu \theta) \mu \theta}$$

and

$$S_0 = 2K / (1 - \mu \mu \theta)$$

Later Tselikov, ⁽⁵⁾ in contrast with previous solutions, recognized the fact that the material did not necessarily slip at all points of the arc of contact and postulated that a zone occurred in the vicinity of the neutral point where there was zero relative motion between roll and strip. This zone, where sticking friction conditions occurred, separated zones at each end of the arc of contact, where relative motion between roll and slab was possible (Fig.2.3.2). Tselikov obtained an expression for the pressure distribution in the latter zones using the method already outlined; in the case of the sticking zone, a solution was reached by first determining the magnitude of the frictional forces, which appear on the contact surfaces. This was done assuming

that the frictional forces varied according to a law which is approximately linear, then

$$\tau = \frac{K(h-h_n)}{l_s \tan \theta} \quad (2.3.6)$$

An approximate expression was then proposed to calculate the length of the sticking zone l_s , which in hot rolling was $l_s \approx (0.5-2.0) h_m$, thus denoting $\tan \theta = \frac{d(h/2)}{dx} = \alpha$ and $\mu S = \tau$. Eq. 2.3.4a was rewritten as,

$$ds = K \left[2 - \frac{h-h_0}{l_s \tan \theta} \right] \frac{dh}{h} \quad (2.3.4c)$$

The plus sign in front of the second term inside the brackets vanished, since Eq. 2.3.6 gave the friction stress for the whole sticking zone.

The integrated expression of Eq. 2.3.4c was given by:

$$S = S_c + K \left[A(h_c - h) - (2 + Ah_0) \ln h_c/h \right] \quad (2.3.7)$$

where

$$A = 1/l_s \tan^2 \theta$$

and S_c was the radial pressure at the point C determined from Eq. 2.3.5a and h_c is the associated thickness of the cross section.

It was proposed that h_0 in Eq. 2.3.7. could be found by equating the values of the radial pressure given by Eq. 2.3.5b and Eq. 2.3.7 at the point D, so:

$$h_0 = \frac{S_c - S_D + A(h_c - h_D)}{A \ln h_c/h_D} - \frac{2}{A}$$

Nadai (3) obtained a differential equation of the form,

$$\frac{d}{dx} (hp) \pm 2\tau + 2Sx/R = 0 \quad (2.3.8)$$

which again described the stress distribution within the arc of contact.

Here the case of applied tension was considered and the yield criterion

became $S + p = 2K$. In addition, dimensionless groups were introduced:

$\eta = 9/2K$, $\beta^2 = h^2/R$, $Z = x/R$; and for small angles of contact the thickness

of the material within the roll gap was given by:

$$h = h_2 + x^2/R = h_2(1 + Z^2)$$

Eq. 2.3.8 was rewritten as:

$$(1+z^2)dy/dz \mp 2\tau/\beta 2K = 2Z \quad (2.3.8a)$$

Nadai also investigated the effect of three conditions of friction on the distribution of pressure along the arc of contact. These were:-

(i) A constant coefficient of friction.

In this case the frictional stress was given by $\tau = \pm \mu S$ and for a constant coefficient of friction

$$2\tau/\beta 2K = 2\mu y/\beta = K_1 y$$

So Eq. 2.3.8a can be written as

$$(1+z^2)(dy/dz) \mp K_1 y = 2Z \quad (2.3.8b)$$

Eq. 2.3.8b was integrated by introducing the variable θ such that

$z = \tan \theta$, whence $d\theta = dz/(1+z^2)$ and,

$$dy/d\theta - K_1 y = 2 \tan \theta$$

from which

$$y = S/2K = \exp \mp K_1 \theta (C + 2 \int \exp \pm K_1 \theta \tan \theta d\theta) \quad (2.3.9)$$

It was considered that in most cases the integral in Eq. 2.3.9 could be computed by replacing $\tan \theta$ by a series, thus,

$$y = S/2K = C \exp K_1 \theta - 2(1 \pm K_1 \theta)/K_1^2 \quad (2.3.9a)$$

using Eq. 2.3.9a Nadai calculated the pressure distribution for a number of cases of rolling. These showed that the application of front or back tension only, or of both together, reduces the roll pressure and shifts the position of the neutral plane.

(ii) A constant shear stress at the surface.

In this case the shear stress was assumed constant, and after introducing the dimensionless number $K_2 = 2\tau/\beta 2K$ Eq. 2.3.8a became:

$$dy/dz = \pm \frac{K_2}{1+z^2} + \frac{2Z}{1+z^2}$$

which upon integration gave:

$$y = S/2K = \pm K_2 \tan^{-1} Z + \ln(1+Z^2) + C \quad (2.3.9b)$$

(iii) A variable shear stress at the surface.

In this case the surface friction was assumed to be proportional to the relative velocity of slip. Nadai pointed out that the above assumption was rather doubtful due to the fact that little was known about the conditions of friction when lubricated strips were rolled.

The suggested relationship between the frictional shear stress (τ) and the relative velocity between rolls and strip ($v - v_R$) was,

$$\tau = \frac{\eta}{\delta} (v - v_R)$$

where η = mean value of the lubricant viscosity at the rolling pressure.

δ = mean thickness of the oil layer.

Considering that the thickness of the strip was given by, $h = h_2(1 + Z^2)$

then $v = \sqrt{2}h_2/h = \sqrt{2}/(1 + Z^2)$

and $v_R = \sqrt{2}/(1 + Z_0^2)$

so

$$\tau = \frac{\eta\sqrt{2}}{\delta} \left(\frac{1}{1 + Z^2} - \frac{1}{1 + Z_0^2} \right)$$

where Z_0 was the value of Z corresponding to the neutral point.

After introducing $\tau_0 = \frac{\eta\sqrt{2}}{\delta}$ and $K_3 = \frac{2\tau_0}{\beta 2K}$, Eq. 2.3.8a took the form,

$$(1 + Z^2) \frac{dy}{dZ} = K_3 \left(\frac{1}{1 + Z^2} - \frac{1}{1 + Z_0^2} \right) + 2Z$$

Hence after integration,

$$y = \frac{3}{2} \frac{1}{2K} = 1 + \ln(1 + Z^2) + \frac{K_3}{2} \left[\frac{Z}{1 + Z^2} - \left(\frac{1 - Z_0^2}{1 + Z_0^2} \right) \frac{1}{Z} \right] \quad (2.3.9c)$$

Fig. 2.3.3 shows the distribution of roll pressure and shear stress along the arc of contact calculated using the theories of Tselikov, Von Karman, Siebel and Nadai, as presented by El Waziri⁽⁹⁾. These curves were applicable to the rolling of wide strip without applied tensions, with a 50% reduction and a coefficient of friction $\mu = 0.2$.

It should be noted that in the solutions of Nadai and Tselikov the sharp maximum pressure has been replaced by rounded peaks as these curves were obtained from Eqs. 2.3.9c and 2.3.7 respectively, which do not involve the intersection of two separate relationships between roll pressure and position along the arc of contact. Additionally, in both cases the neutral point does not coincide with the position of the maximum pressure.

Ekelund⁽⁶⁾ assumed that slipping conditions occurred at the entry side of the arc of contact, while shearing or sticking conditions were present from the neutral point to the exit plane. A balance of horizontal forces was used to obtain an expression of the form:

$$\frac{1}{2}(h_1+h_2)dp = 2qRd\theta(\mu\cos^2\theta - \cos\theta\sin\theta) \quad (2.3.10)$$

The yield criteria was expressed as $p = q - \bar{K} = \bar{K}[f(x) - 1]$, where \bar{K} represented the mean strength of the material. Introducing $K_1x + K_2 = \mu\cos^2\theta - \cos\theta\sin\theta$, $2K_3 = \frac{1}{2}(h_1+h_2)$ and $x = R(\sin\theta_1 - \sin\theta)$, Eq. 2.3.10 was integrated to give,

$$p = \bar{K}[f(x) - 1]K_3 = \int_0^x \bar{K}f(x) \cdot (K_1x + K_2)dx$$

from which

$$p = \frac{4}{3} \bar{K} \exp(C_1x^2 + C_2x) - 1$$

which was approximated to,

$$p = \frac{4}{3} \bar{K} (C_1x^2 + C_2x)$$

where

$$C_1 = 2(\mu\sin\theta_1 + \cos\theta_1) / R(h_1+h_2)$$

and

$$C_2 = \mu\cos^2\theta_1 - \sin\theta_1\cos\theta_1 / (h_1+h_2)$$

The Ekelund method was semi-empirical because it contained a large number of approximations, often very arbitrary, which were selected to obtain agreement with the results of certain experiments on the hot rolling of steel.⁽⁹⁾

Most of the theories reviewed above aimed at methods of calculation that were simple enough to be of practical use in rolling mill practice. To achieve this, drastic simplifications were necessary, which led in some cases, to serious disagreement with experimental results. Usually it was not clear which of the several assumptions and approximations was responsible. On the other hand agreement between theoretical and experimental results may be attributed to the fortuitous cancellation of several errors. ⁽⁴⁾

2.4. Orowan's Theory of Rolling.

Orowan aimed to discard as many simplifications as possible, and derived a more accurate solution from which simplified theories, valid for restricted rolling conditions, could be evolved. The Orowan solution was also suitable as a standard against which existing theories could be assessed. ⁽⁴⁾

The first part of Orowan's work was concerned with developing a method to calculate the roll pressure using the assumptions of homogeneous deformation and slipping conditions. Eq. 2.2.1 was rewritten as:

$$df/d\theta = 2Rs \cos \theta (\tan \theta \pm \mu) \quad (2.4.1)$$

With $S = \eta$ and $p = f/h$, the yield criteria became $S = f/h + 2K$

and the final expression of 2.4.1 was:

$$-df/d\theta + A(\theta)f(\theta) + B(\theta) = 0 \quad (2.4.1a)$$

where

$$A(\theta) = 2R/h \cos \theta (\tan \theta \pm \mu)$$

and

$$B(\theta) = 2R(2K) \cos \theta (\tan \theta \pm \mu)$$

The general solution of Eq. 2.4.1a was given by:

$$f(\theta) = \exp \int_{\theta_1}^{\theta} A(\theta) d\theta \left[\int_{\theta_1}^{\theta} \frac{B(\theta)}{\exp \int_{\theta_1}^{\theta} A(\theta) d\theta} d\theta + f_1 \right] \quad (2.4.2)$$

where f_1 was the initial value of $f(\theta)$ at either the entry or exit plane where f_1 was the initial value of $f(\theta)$ at either the entry or exit plane.

Orowan considered that the integral $\int A(\theta)$ could be solved if the roll flattening was ignored, but the formulae were too complicated for practical use. The second integral contained $2k(\theta)$ which was given by experimentally determined curves. Thus, it was proposed to obtain a graphical solution.

Orowan compared two of the measurements of roll pressure by Siebel and Lueg⁽⁷⁾ with the results given by the homogeneous graphical method. The measured roll pressures taken at or extrapolated to the centre of the strip where plane strain was assumed, were obtained using both smooth and rough rolls. In the first case Orowan considered a low value of $\mu = 0.14$ and calculated an approximate yield stress distribution along the roll gap using the yield stress data published by Siebel and Pomp^(7a). It was found that at a low value of μ such a graphical method gave results which were comparable with those obtained by early theories^(1,2,3). However when a high value of μ was considered in the case of rough rolls, the graphical method produced roll pressures that were too high. Orowan suggested that here the frictional stress exceeded the shear yield stress of the material and therefore theories that assumed slipping friction - $\tau = \mu S$ - were unsuitable in such cases. He concluded that if the frictional stress rises to the magnitude of the shear yield stress, plastic shear will occur in the interior of the deforming material, while the surface will stick to the rolls. In addition Orowan suggested that sticking conditions would appear first at the neutral point and that the zone of sticking friction would be extended towards both entry and exit planes as the coefficient of friction increased.

In order to study the effect of inhomogeneous deformation on roll pressures, Orowan followed Prandtl's analysis⁽¹⁰⁾ of the compression of a slab between two rough parallel flat platens; which showed that the stress distribution was defined by,

$$q = C + \frac{2K}{h}x$$

$$t = C + \frac{2K}{h}x - 2K\sqrt{1 - \frac{4y^2}{h^2}}$$

$$\tau = -\frac{2Ky}{h}$$

where C is a constant, h is the distance between the platens, X and Y are the coordinates with origin at the centre of the slab.

Since the roll surfaces are neither parallel nor plane, Orowan used the analysis due to Nadai⁽¹¹⁾, in which the material is compressed between plane rough platens inclined at a small angle 2θ . In Fig. 2.4.1 an element of the deforming material subtends an angle θ with the centre line of the material and the stresses on this element are also indicated. Nadai proved that in such a case Prandtl's solutions become,

$$t = S - 2K\sqrt{1 - \theta^2/\rho^2} \quad (2.4.3) \quad \tau = -\frac{K}{\rho}\theta \quad (2.4.4)$$

These equations are valid only in the case where the flow of the material is towards the thinnest edge of the wedge shaped slab. Although Nadai's solution applies specifically to this case, Orowan assumed that this solutions also held for material flowing in the opposite direction. Underwood⁽⁸⁾ pointed out that Nadai's solution applies only to small angles of inclination of the platens, limiting the application of the resulting theory of rolling to small angles of contact.

Eq. 2.4.3. and Eq. 2.4.4. refer specifically to the case in which the material sticks to the platens. Orowan considered that the stress distributions given by these equations could be applied in the case in

which the surfaces of the material slip on the platens if a semi-angle θ^* of a hypothetical wedge shaped slab sticking to the platens was calculated, so that the shear stress at the surface of a wedge of semi-angle $\theta < \theta^*$ should be equal to $\mu S < K$. Thus, the value of θ^* was related to θ by

$$\theta^* = \frac{K}{\mu S} \theta$$

Substituting θ^* for θ in Eq. 2.4.3 and Eq. 2.4.4 gives

$$f = S - 2K \sqrt{1 - \left(\frac{2\mu S}{2K}\right)^2 \left(\frac{\theta}{\theta}\right)^2} \quad (2.4.3b)$$

$$\tau = -\frac{\mu S \theta}{\theta} \quad (2.4.4b)$$

Orowan assumed that the stress distribution along the surface AB in Fig. 2.4.2. could be approximately the same as if the strip was compressed between two inclined platens tangential to the rolls at A and B; so that Eq. 2.4.4.b and Eq. 2.4.3.b describe the stress distribution along section AB.

The element df in the basic Eq. 2.4.1 acting across the surface element $rd\theta = hds/2\sin\theta$ consisted of the horizontal components of both the radial and the shear stresses.

Upon integration across the surface AB, the contribution of the radial stress component $f \cos\theta r d\theta$ to $f(\theta)$ gave

$$f_f(\theta) = hs - \frac{hK}{\sin\theta} \int_0^\theta \left[\sqrt{1 - \left(\frac{\mu S}{K}\right)^2 \left(\frac{\theta}{\theta}\right)^2} \right] \cos\theta d\theta \quad (2.4.5)$$

The integrand in Eq. 2.4.5, known as Orowan's inhomogeneity factor - w(a) -, is essentially a function of the parameter $a = \mu S/k$ as shown in Fig. 2.4.3 .

Thus Eq. 2.4.5 was abbreviated to:

$$f_f(\theta) = hs - hKw(a) \quad (2.4.5a)$$

The contribution of the shear stress τ to the total horizontal force $f(\theta)$

was obtained by integration of its horizontal component $\tau \sin \theta ds$.

along the surface AB. Hence,

$$\int \tau(\theta) = \pm h \mu s \left(\frac{1}{\theta} - \frac{1}{\frac{1}{2}\theta} \right)$$

Therefore the total horizontal force was given by,

$$f(\theta) = \int_1(\theta) + \int_2(\theta) = h \left[s \left\{ 1 \pm \mu \left(\frac{1}{\theta} - \frac{1}{\frac{1}{2}\theta} \right) \right\} - 2Kw(a) \right] \quad (2.4.6)$$

Orowan proposed that under slipping conditions the shear stress contribution $\int_2(\theta)$ could be neglected while sticking conditions were associated with $a=1$ and $w(a) = \pi/4$. Hence, in the former case,

$$f(\theta) = hs - 2Kh w(a) \quad (2.4.6a)$$

and for the latter case,

$$f(\theta) = h \left[s - 2K \left\{ \frac{\pi}{4} \mp \frac{1}{2} \left(\frac{1}{\theta} - \frac{1}{\frac{1}{2}\theta} \right) \right\} \right] \quad (2.4.6b)$$

The values of s obtained from Eqs. 2.4.6a and 2.4.6b were substituted into the basic differential Eq. 2.4.1. Thus, Orowan obtained expressions in which a non-uniform pressure distribution across the thickness of the material undergoing deformation was included, viz.

$$df/d\theta = f(\theta) \frac{2R}{h} (\sin \theta \pm \mu \cos \theta) + 2R 2Kw(a) (\sin \theta \pm \mu \cos \theta) \quad (2.4.7)$$

$$df/d\theta = f(\theta) \frac{2R}{h} \sin \theta + 2R 2K \left[\frac{\pi}{4} \mp \frac{1}{2} \left(\frac{1}{\theta} - \frac{1}{\frac{1}{2}\theta} \right) \right] (\sin \theta \pm \frac{1}{2} \cos \theta) \quad (2.4.7a)$$

Since Eq. 2.4.7a is of the same form as Eq. 2.4.1a the general solution given by Eq. 2.4.2 was used. So that,

$$f(\theta) = Z(\theta) \left[\int_{\theta_1}^{\theta} \frac{B(\theta)}{Z(\theta)} d\theta + f_0 \right] \quad (\text{c.f. } 2.4.2)$$

with $Z(\theta) = \exp \left[\int_{\theta_1}^{\theta} \frac{2R}{h} \sin \theta d\theta \right]$

$$B(\theta) = 2R 2K \left[\frac{\pi}{4} \mp \frac{1}{2} \left(\frac{1}{\theta} - \frac{1}{\frac{1}{2}\theta} \right) \right] (\sin \theta \pm \frac{1}{2} \cos \theta)$$

The analytical solution of $Z(\theta)$ and the graphical integration of $B(\theta)/Z(\theta)$ enabled Orowan to obtain a solution in the case of sticking friction. With slipping friction the integration of the first term of

the right hand side of Eq.2.4.7 can be done in finite terms, but there is an additional complication, because $w(a)$ in the second term of the right hand side depends on $s(\theta)$ and thus implicitly on $\int(\theta)$. However, as $w(a)$ varies little with $\int(\theta)$, Orowan proposed an approximate technique by which the variable inhomogeneity factor could be included. Thus, an initial value of $w(a)$ calculated from the known radial pressure at entry, was used to determine $\int(\theta)$ in the next interval in the arc of contact. This implied that $w(a)$ was considered constant over such an interval. The function $w(a)$ was then recalculated with the associated value of $s(\theta)$ and used to determine the next value of $\int(\theta)$, as in general no second approximation of $w(a)$ in each interval was necessary. An analogous procedure was followed in the exit side.

Orowan compared the measurements of roll pressure made by Siebel and Lueg⁽⁷⁾ at both high and low values of the coefficient of friction, with the results calculated with the inhomogeneous graphical method. Only a slight discrepancy was obtained between the two sets of values, which occurred close to the point of maximum pressure. Here the results of the graphical method showed a sharp peak, while the experimental results indicated a gradual change in pressure at this point(Fig.2.4.4.). Orowan attributed this change of the roll pressure distribution around the neutral point, to zones of zero plastic deformation whose presence was thought to have little effect upon the calculated values of roll loads.

The complexity of Orowan's method undoubtedly caused some workers to develop alternative solutions applicable only to particular rolling conditions. A characteristic of such solutions was the use of simplifying assumptions. Typical examples were the solution of Bland and Ford⁽¹²⁾ for cold rolling and Sims⁽¹⁴⁾ for hot rolling. These are referred to below as approximate theories.

2.5 Approximate Theories.

Bland and Ford⁽¹²⁾ considered a flattened roll radius and small angles of contact. This enabled the following approximations to be introduced $\sin\theta \approx \theta$, $\cos\theta \approx 1$ and $h = h_2 + R'\theta^2$; therefore Eq. 2.4.1 was reduced to

$$\frac{df}{d\theta} = 2sR'(\theta \pm \mu) \quad (2.5.1)$$

and with the condition of plasticity approximated to $s - 2k = p$

$$\text{so } \frac{d}{d\theta} [h(s - 2k)] = 2sR'(\theta \pm \mu)$$

which, after rearranging, became,

$$2kh \frac{d}{d\theta} \left(\frac{s}{2k} \right) + \left(\frac{s}{2k} - 1 \right) \frac{d}{d\theta} (2kh) = 2sR'(\theta \pm \mu) \quad (2.5.1a)$$

It was then assumed that

$$\left(\frac{s}{2k} - 1 \right) \frac{d}{d\theta} (2kh) \ll 2kh \frac{d}{d\theta} \left(\frac{s}{2k} \right)$$

This arises because the material work-hardens as rolling proceeds and the thickness of the plate is reduced: thus $2k$ increases as h decreases. Furthermore, the coefficient $\left(\frac{s}{2k} - 1 \right)$ is small when low coefficients of friction are used. Hence, Eq. 2.5.1a was reduced to

$$\frac{d}{d\theta} \left(\frac{s}{2k} \right) / \left(\frac{s}{2k} \right) = \frac{2R'}{h} (\theta \pm \mu)$$

which, after integration gave,

$$\frac{s}{2k} = C \left[\frac{h}{R'} \exp \pm \mu H \right]$$

and

$$H = 2 \sqrt{\frac{R'}{h_2}} \tan^{-1} \left(\sqrt{\frac{R'}{h_2}} \theta \right)$$

In order to integrate readily the resulting pressure distribution a mean value of the yield stress was introduced, viz.,

$$\bar{k} = \frac{1}{\theta_1} \int_0^{\theta_1} k d\theta$$

This method was shown to give close agreement with Orowan's homogeneous graphical solution, except for the cases of high back tension with rapid work-hardening. Under these conditions the term $\left(\frac{s}{2k} - 1 \right) \frac{d}{d\theta} (2kh)$ may not be negligible.

Under these circumstances, the solution of Bland and Sims⁽¹³⁾ allows a determination of roll pressure to be made by including the effect of front and back tension to arrive at,

$$s^+ = \left(\frac{2Kh}{h_2} - t_2 \right) \exp \mu H$$

$$s^- = \left(\frac{2Kh}{h_1} - t_1 \right) \exp \mu (H_1 - H) \quad t_1, t_2 \text{ applied tensions}$$

Later Sims⁽¹⁴⁾ assumed that sticking friction would occur over the whole arc of contact and that the shear yield stress would remain constant during the rolling pass. The compression process was approximated to the deformation of a strip between two rough inclined platens, following Orowan, to obtain,

$$s/h = \left(s - \frac{\pi}{4} 2K \right)$$

This relationship was substituted in the equilibrium Eq. 2.4.1, together with the approximations $\sin \theta \approx \theta$ and $\cos \theta = 1$ and $1 - \cos \theta = \theta^2/2$. Thus Eq. 2.4.1 became,

$$\frac{d}{d\theta} h \left(\frac{s}{2K} - \frac{\pi}{4} \right) = 2R' \theta \frac{s}{2K} \pm R' \quad (2.5.1b)$$

Integration of Eq. 2.5.1b gave

$$\left(\frac{s}{2K} \right)^+ = \frac{\pi}{4} \ln \left(\frac{h}{h_2} \right) + \frac{\pi}{4} + M(\theta) \quad (2.5.2)$$

$$\left(\frac{s}{2K} \right)^- = \frac{\pi}{4} \ln \left(\frac{h}{h_1} \right) + \frac{\pi}{4} + M(\theta_1) - M(\theta) \quad (2.5.2a)$$

where

$$M(\theta) = \sqrt{\frac{R'}{h_2}} \frac{1}{2} \sqrt{\frac{R'}{h_2}} \theta$$

Sims proposed that mean values of the yield stress could be obtained by the use of an equation of the form $\bar{\sigma} = A(r) + B(r) \ln \bar{\lambda}$ where $A(r)$ and $B(r)$ are constants that could be determined from experimental yield stress data obtained at strain rates equal to the mean rolling strain rates and various reductions. It was also shown that the geometry of the roll gap led to an expression of the mean strain

rate given by

$$\bar{\lambda} = \frac{2\pi N}{60\sqrt{r}} \sqrt{\frac{R'}{h}} \ln \frac{1}{1-r}$$

Cook and McCrum⁽³⁴⁾ obtained a graphical method based on Sims' solution by which roll force and torque could be determined. This method was limited to the case of the hot rolling of flat sections.

Orowan and Pascoe⁽¹⁵⁾ made a further approximation to Orowan's exact solution, which was applicable only in the case when the length of the arc of contact was much greater than the thickness of the strip. It was then assumed that because the planes tangential to the roll surfaces are parallel at the exit plane, the slope of the pressure distribution at this point must be the same as that produced by the compression of the material between horizontal platens set h_0 apart. Thus, the condition of equilibrium for a vertical segment of the compressed material was

$$-h_0 dp + 2\tau dx = 0$$

and from the condition of plasticity under plane strain $q - p = 2k$
so $dp = dq$, and $h_0 dq = 2\tau dx$ (2.5.3)

Thus, assuming sticking conditions, under hot rolling Eq. 2.5.3 was integrated to

$$q = q_0 + \frac{k}{2h_0} x$$

where q_0 is the vertical pressure at entry, which under inhomogeneous deformation and vanishing horizontal pressure becomes $q_0 = 2k\psi(\alpha)$

The slope of the pressure distribution at the exit side was given by

$$\tan \alpha = \frac{dq}{dx} = \frac{k}{2h_0}$$

Recently El Kalay and Sparling⁽¹⁶⁾ proposed an approximate method to use in flat hot rolling including the Orowan inhomogeneity factor $w(\alpha)$. The method was a combination of both: Bland and Ford's solution⁽¹²⁾ to calculate roll pressures in the zones immediately adjacent to the

entry and exit planes where slipping was assumed and Sims' solution in the middle portion of the roll gap where sticking occurred. Thus, it was shown that $w(a)$ could be expressed as

$$w(a) = \sqrt{1 - 1.5326(\mu s/2k)^2} \quad (2.5.4)$$

and at entry and exit, $(s/2k) = \frac{1}{\sqrt{1 + 1.5326\mu^2}}$

so that the pressure distribution under slipping conditions was given

by (c.f. Eq. 2.5.2),

$$(s/2k)^+ = \frac{1}{\sqrt{1 + 1.5326\mu^2}} \frac{h}{h_2} \exp \mu H$$

$$(s/2k)^- = \frac{1}{\sqrt{1 + 1.5326\mu^2}} \frac{h}{h_1} \exp \mu (H_1 - H)$$

At those positions where $s/2k = 1/2\mu$ sticking conditions were assumed, and the $s/2k$ ratio increased from these positions towards the neutral point according to Sims' expressions (c.f. Eq. 2.5.2 and 2.5.2a)

$$(s/2k)^+ = \frac{1}{2\mu} + \frac{\mu}{4} \ln \frac{h}{h_f} + \frac{R}{h_2} \left(\frac{1}{2} \sqrt{\frac{R}{h_2}} \theta - \frac{1}{2} \sqrt{\frac{R}{h_2}} \theta_f \right) \quad (2.5.5)$$

$$(s/2k)^- = \frac{1}{2\mu} + \frac{\mu}{4} \ln \frac{h}{h_b} + \frac{R}{h_2} \left(\frac{1}{2} \sqrt{\frac{R}{h_2}} \theta_b - \frac{1}{2} \sqrt{\frac{R}{h_2}} \theta \right) \quad (2.5.5a)$$

where f, b refer to conditions on the boundaries of the sticking region on exit and entry sides respectively.

Denton and Crane⁽¹⁷⁾ observed that the above method assumed the inhomogeneity factor to be constant throughout the slipping zones and considered that since $w(a)$ is a function of $\mu s/k$ it must therefore decrease steadily from both entry and exit planes towards the neutral point, until the value of μ/k is attained which then remained constant throughout the sticking zone. Hence, a modification to El Kalay's solution was developed which included a variable inhomogeneity factor in the zones where slipping friction occurred. The simplified equilibrium equation of Bland and Ford (Eq. 2.5.1a) together with the

condition of plasticity given by Orowan i.e. $\frac{1}{h} = S - 2kw(a)$ enabled

Denton and Crane to obtain,

$$\left(\frac{S}{2k} + w(a)\right) \frac{d}{d\theta} (hk) + hk \frac{d}{d\theta} \left(\frac{S}{2k} - w(a)\right) = 2R's(\theta \pm \mu) \quad (2.5.1c)$$

It was also assumed, after Bland and Ford⁽¹²⁾ that

$$\left(\frac{S}{k} - w(a)\right) \frac{d}{d\theta} (hk) \ll hk \frac{d}{d\theta} \left(\frac{S}{k} - w(a)\right)$$

and considering $\frac{d}{d\theta} \left(\frac{S}{k} - w(a)\right) = \frac{d(S/k)}{d\theta} \left(1 - \frac{dw(a)}{d(S/k)}\right)$

Eq.2.5 was rewritten as,

$$\frac{d(S/k)}{d\theta} \left(1 - \frac{dw(a)}{d(S/k)}\right) = 2R's(\theta \pm \mu)$$

Next it was shown, using the expression of $w(a)$ obtained by El Kalay⁽¹⁶⁾

that,

$$\frac{dw(a)}{d(S/k)} = - \frac{1.5326\mu^2(S/k)}{w(a)}$$

Thus Eq.2.5.1c was finally expressed as,

$$\frac{d(S/k)}{d\theta} \left[\frac{1}{(S/k)} + \frac{0.7663\mu^2}{\{1 - 0.38315\mu^2(S/k)\}^{1/2}} \right] = \frac{2R's(\theta \pm \mu)}{h}$$

which, after integration, and assuming $h = h_2 + R'\theta^2$ gave,

$$\ln(S/k) + 1.236\mu \sin^{-1}(0.69\mu S/k) = \ln\left(\frac{h}{R'}\right) \pm 2\mu \sqrt{\frac{R'}{h_2}} \tan^{-1} \sqrt{\frac{R'}{h_2}} \theta + C$$

In the sticking zone the modified Sims solution, as given by El Kalay, (Eq. 2.5.5 and 2.5.5a) was adopted.

Denton and Crane also made a comparison between the solutions on the exit side given by their method and that used by El Kalay et al.⁽¹⁶⁾

(Fig. 2.5.1.). This showed that with the former method slipping friction

occurred over a larger fraction of the arc of contact with a

corresponding reduction of the roll load. It should be noted that the

function $w(a)$ included in Fig. 2.5.1. was defined as ,

$$w(a) = 2\sqrt{1 - 0.38315(\mu S/k)^2} \quad \text{c.f. Eq.2.5.4.}$$

2.6 Alternative Theories.

Alternative theories of rolling which do not incorporate the basic Von Karman equation, have been developed using either slip-line fields or approximations to this method i.e. upper bounds. In addition shear plane and hydrodynamic theories have also been put forward.

(i) Slip-line field theory.

Slip-line fields consist of two orthogonal families of curves, showing the direction of maximum shear at every point in the deformation zone. These lines are designated the α and β lines (Fig.2.6.1A). Slip-line fields always refer to plane strain and the material is assumed to be incompressible and ideally plastic.

The stresses at any point can be determined by the shear stress and a hydrostatic pressure $p = (\delta_1 + \delta_2 + \delta_3)/3$. The Hencky⁽¹⁸⁾ equations enable the variation of the hydrostatic pressure along slip-lines to be determined, viz.,

$$p + 2k\phi = C_1 \text{ along an } \alpha \text{ line}$$

$$p - 2k\phi = C_2 \text{ along a } \beta \text{ line}$$

where ϕ is the angle of rotation of the tangent to an α line with respect to an axis of reference; and C_1 and C_2 are constant.

There are two types of slip-line field; those in which the system is in static equilibrium, and those where the metal flow attains a steady-state condition. The rolling process is an example of the latter. In such a case it is essential to verify that the chosen slip-line field conforms to the requirements of steady velocity, compatible with that of the rigid parts of the material undergoing deformation.

Deformation along slip-lines is due to pure shear. Since direct strain does not occur along these lines, they are not associated with

any changes in velocity. Hence, each line may be considered to be a rigid link. This condition was expressed by Geiringer^(18a) in the form

$$du - v d\phi = 0 \quad \text{along an } \alpha \text{ line}$$

$$dv - u d\phi = 0 \quad \text{along a } \beta \text{ line}$$

where u and v are the velocities along α and β lines respectively.

Hill⁽¹⁹⁾ described a method for the numerical calculation of slip-line fields. However, in the case of the statically undetermined rolling process i.e. the steady-state case, the use of Hill's method to obtain an acceptable slip-line field which satisfies the velocity boundary conditions would prove very laborious.

Prager⁽²⁰⁾ suggested a geometrical construction to solve the slip-line field equations. The geometrical representation takes the form of three diagrams; the physical plane, showing the slip-line field, the stress plane, representing the stress variation along the slip-lines, and the hodograph. representing the velocity of any point in the physical plane.

According to Prager's method the state of stress of any point along a slip-line could be represented by a cycloid traced by a mohr circle rolling along either the top or bottom tangent parallel to the σ_y/k axis of the stress plane (Fig. 2.6.1 B). Alexander⁽²¹⁾ extended this method to solve the compression between rough inclined platens, assuming that such a solution gave a possible slip-line field for the hot rolling process. The original slip-line field was modified to allow for the effect of rotation of the roll surface. The final solution was obtained after a few trials for a single geometry of rolling ($R/h_f=58$ and $r=33\%$). Thus, Alexander demonstrated that with the geometrical method of Prager, adjustments of an assumed slip-line field to obtain an acceptable solution for hot rolling become possible by continual

inspection of the slip-line field and hodograph.

Later Ford and Alexander⁽²²⁾ proposed an approximate slip-line method to obtain solutions for various rolling geometries. Further simplifications were subsequently suggested by several workers^(24,25).

Denton and Crane⁽¹⁷⁾ summarised the results of the slip-line field solutions for the roll force and torque, and compared them with various other methods including those of Sims, Orowan and Pascoe and El Kalay et al. and with experimental results. The slip-line field results were comparable to those obtained by Sims⁽¹⁴⁾ and El Kalay et al.⁽¹⁶⁾, while the experimental results in general were smaller than the predictions of any of the theories considered. Comparisons of these slip-line solutions with a modified hot rolling theory derived by Denton and Crane (see Sect.2.5), established that any adequate method must include both a low coefficient of friction (0.2 - 0.4) and a variable inhomogeneity factor $w(a)$ throughout the arc of contact.

(ii) Shear plane theory.

Green and Wallace⁽²³⁾ have reached a simplified solution for hot rolling, where the material undergoing deformation was considered to be a rigid triangular area with its base representing the arc of contact. All deformations occurred along the sides of the triangle through pure shear. The forces created in the deformation zone were in equilibrium with the roll pressure and the frictional stresses at the arc of contact. The solution obtained was adequate for ingot rolling.

(iii) Hydrodynamic theory.

Kneschke^{26a} developed an alternative theory of rolling by interpreting the rolling process in terms of hydrodynamics in which the laws of mechanics of viscous media were applied. Thus, the differential equation,

$$\eta \frac{\partial^2 v}{\partial y^2} = \frac{ds}{dx}$$

described the flow of the material during the rolling process, where v represents the velocity component of the material in the rolling direction and η is the dynamic viscosity of the material undergoing deformation.

The application of the formulae of the hydrodynamic theory to predict roll force and torque requires a knowledge of the dynamic viscosity of the material (η) which is not yet available⁽²⁶⁾. Thus, a quantitative solution is not possible. However, Kneschke, using the assumption that the outermost layer of the deforming material sticks to the roll surface, arrived at solutions which were, to a large extent, qualitatively in agreement with the present understanding of the rolling process and with experimental results.

Alternatively, Ichinoi and Tonizawa⁽²⁷⁾ assumed that a fluid film exists between the strip and the roll surface, in which case a theory of hydrodynamic lubrication could be applied, while Von Karman's equation was employed to describe the plastic deformation of the material.

The rolling pressure curve obtained was similar to that derived by Nadai⁽³⁾ for the case when the shearing stress was assumed proportional to the relative velocity between the material and the rolls (see Sect.2.3).

Although these alternative theories seem to represent the rolling process adequately, the use of such methods has been very limited in practice.

2.7 Alexander's solution to the Von Karman equation.

With the widespread availability of digital computers, the approximate methods that have been previously used to achieve analytical solutions to the differential equation describing the roll pressure distribution lose much of their value, since it is now possible to use numerical techniques that do not require many of the simplifications introduced in early methods.

Alexander⁽²⁸⁾ presented a comprehensive solution to the basic Von Karman equation where the mixed frictional conditions $\tau \leq K$ introduced by Orowan⁽⁴⁾ and the variation of the yield stress through the arc of contact was incorporated together with the contribution of the elastic zones of the material to the roll force and torque according to the expressions due to Bland and Ford⁽³³⁾.

In order to solve the linear first order differential equation a numerical technique, which incorporated the fourth order Runge Kutta method of integration, was developed. First an approximated value of the roll force was calculated, to give a realistic value to the deformed roll radius and hence the angle of contact. A yield stress distribution along the contact arc was then determined. Next, a solution to the differential equation was obtained by means of the Runge Kutta method at each interval along the arc of contact. The resulting roll pressure distribution, given by the overlapping of the entry and exit side solutions, was integrated by trapezoidal rule to determine the specific roll force, the latter being then corrected to include the contributions of the elastic zones of the material at both ends of the arc of contact. The whole procedure was repeated until consistent values of both the roll force and the deformed roll radius were reached. Finally, values of specific roll torque were calculated according to

early approximate formulae and an accurated expression which included the roll flattening effect.

Alexander showed in this work, mainly concerned with cold rolling, the large errors involved in using some approximate solutions, such as those due to Bland and Ford⁽¹²⁾, Sims⁽³⁴⁾ and Hill⁽³⁵⁾ in the prediction of roll torque; and concluded that future studies of the hot rolling problem could be directed towards refinements of the computer programme so as to include the effects of both temperature and strain rate variation on the yield stress, and of the actual frictional conditions between the material and the roll surfaces.

2.8 Roll flattening.

Although the surface of the roll in contact with the material being rolled is deformed, the arc of contact was assumed to remain circular. The general nature of this deformation is indicated in Fig. 3.2.1 where the shape of the rigid roll is compared with that of the deformed roll. Here it can be seen that the roll flattening increases the contact length and shifts the exit plane from the line joining the centre of the rolls.

Prescott⁽³⁰⁾ assumed that an elliptical distribution of pressure was applied over the roll surface, and determined the radial deformation of the roll caused by the stress distribution over that part of the surface where it is applied, which could be expressed as:

$$\frac{1}{R'} = \frac{1}{R} - \frac{4(1-\nu^2)P}{\eta E d^2} \quad (\text{Eq.2.8.1})$$

where P is the total force per unit width and d is one half of the length of the arc of contact.

Hitchcock⁽³¹⁾ presented an approximate analysis which enabled the length of the flattened arc of contact to be determined. Thus,

$$2d = \sqrt{\left(\frac{8R(1-\nu^2)P_s}{\eta E}\right)^2 + \Delta h R} + \frac{8R(1-\nu^2)P_s}{\eta E}$$

where $P_s = P/2d$

Later Underwood⁽⁸⁾ showed that Hitchcock's formula, which can only be solved by iteration, could be modified so as to obtain an expression for the deformed roll radius, viz.

$$R' = R \left(1 + \frac{16(1-\nu^2)P}{\eta E \Delta h}\right)$$

According to Bland and Ford⁽³³⁾ the total length of the arc of contact, including those points where the strip is elastically deformed, was given by,

$$2d = \sqrt{R'} \sqrt{\delta + \delta_2 + \delta_t} + \sqrt{\delta_2} t$$

where $\delta = h_1 - h_2$
 $\delta_2 = h_2(1-\nu^2)(2K - t_2)/E$
 $\delta_t = \nu(1+\nu)(h_2 t_2 - h_1 t_1)/E$

Therefore Eq. 2.8.1. was rewritten as,

$$\frac{R'}{R} = 1 + \frac{2cP}{(\sqrt{\delta + \delta_2 + \delta_t} + \sqrt{\delta_2})^2}$$

where

$$c = 16(1-\nu^2)/\eta E$$

0.0223 mm²/kN for cast iron rolls

0.0108 mm²/kN for steel rolls

0.0022 mm²/kN for chill cast iron rolls.

Orowan⁽⁴⁾ 0.0123 mm²/kN for

presented experimental evidence which indicated that the shape of the arc of contact left impressed into the strip after the upper roll was lifted, was not even approximately circular, since the roll surface appeared to be concave around the zone of the maximum pressure, unless the flattening was very slight.

Bland⁽³²⁾ developed a method by which the elastic distortion of the roll surface might be determined when it was subjected to a non-uniform pressure distribution. Thus, an initial radial pressure distribution was found using an estimated value of a deformed roll radius; thence the roll profile associated to such a radial pressure

was determined by means of equations describing the elastic distortion of the rolled material. The resulting roll profile enabled a new roll pressure distribution to be obtained and the whole process was repeated until compatible values of radial pressure and roll profile were attained.

Bland established that the main feature of the deformed arc of contact was the depression in the region of the maximum pressure. However, he found that the difference between the forces obtained using both Hitchcock's formula and the successive approximations method, was within the limits of error introduced in the calculation of the elastic distortion of the rolls by the latter method. Therefore, Bland concluded that Hitchcock's formula was the most suitable technique by which roll flattening could be taken into account.

2.9. The yield stress applicable in hot rolling.

In order to apply the theories of rolling, a knowledge of the values of yield stress, relevant to the material undergoing deformation, is required. In hot rolling the chief factors influencing the yield stress are; the type of material, the amount and rate of deformation and the temperature.

The main difficulties involved in the determination of the appropriate yield stress characteristics were to reproduce experimentally the temperatures and rates of compression encountered in the hot rolling process and until quite recently such yield stress data was available in very limited quantities.

The relationship between yield stress and strain at high temperatures and strain rates has been the subject of several investigations. Nadai and Manjoine ^{36a} determined such relationships in the case of a series of different steels and examined the effect of temperature and strain rate on tensile strength. Inohue ^{36b} measured the yield stress obtained with a wide range of steels and established a general relationship between a yield stress, strain rate and temperature. Fink et al. ^(36b) determined the yield stress of various steels during high speed compression tests by means of a drop hammer. In all tests of this kind the strain rate varied during the deformation process and at different temperatures different mean strain rates were employed ^(37b).

Some work has been done on the effect of variations in strain rate during deformation by the use of the cam plastometer, which can carry out a compression test at a constant strain rate within the range 0.2 - 100 per sec (s^{-1}). Alder and Phillips ⁽³⁸⁾ used such an instrument to measure the flow stress of: aluminium, copper and 0.17 C steel in the strain rate range 1 - 40 s^{-1} and up to a strain of 50%, while Cook ⁽³⁷⁾

obtained data on twelve steels in the strain rate range $1.5 - 100 \text{ s}^{-1}$ and between the temperatures of 900°C to 1200°C . Likewise Arnold and Parker⁽³⁹⁾ determined the yield stress of aluminium and some non-ferrous alloys, while Bailey and Singer⁽⁴⁰⁾ carried out plane strain compression tests on various non-ferrous metals and alloys. It appears to be that the most comprehensive series of results on yield stress, using both cam plastometer and a drop hammer, was carried out by Suzuki et al.⁽³⁶⁾, whose work on a wide range of materials has been presented in the form of data sheets.

Theoretical predictions of roll force and torque developed during rolling, assumed that under hot working conditions the metal behaves as an ideal plastic-solid; therefore in the calculation of rolling loads it is usual to establish first a mean strain rate representative of a specific rolling operation. Available yield stress curves obtained at a constant strain rate equivalent to the mean strain rate during rolling and at the relevant temperature, enables a mean yield stress to be determined by integration over the strain of interest. Sims⁽¹⁴⁾ suggested the following expressions:

$$K_p = \frac{1}{\theta_1} \int_0^{\theta_1} K d\theta \quad \text{for roll force calculations}$$

$$K_a = \frac{1}{r} \int_0^r K de \quad \text{for roll torque calculations}$$

Cook and McCrum⁽³⁴⁾ used this procedure to develop graphical methods by which roll force and torque in flat hot rolling could be calculated, Unfortunately the above equations neglected any effect that the variation of the strain rate during deformation may have on the yield stress.

During hot deformation ferritic and austenitic steels undergo work-hardening until a critical strain is attained beyond which a recovery process and a dynamic recrystallization is initiated in each

case^(41a), resulting in a drop in yield stress as deformation proceeds (Fig.2.9.1). In general the yield stress at a given strain increases with increasing strain rate and decreases with increasing temperature. Thus, the interaction of these parameters during deformation determines the shape of the yield stress curve.

Many workers have proposed various equations to describe the effects of temperature, strain and strain rate on the yield stress, either separately or conjointly. The most common relationships used to represent data obtained at constant temperatures are the power law, viz.,

$$\delta = \delta_0 \dot{\epsilon}^n \quad (2.9.1.)$$

and the semi-logarithmic formula of Ludwick⁽⁴¹⁾,

$$\delta = B \ln \dot{\epsilon} + \delta_0 \quad (2.9.2.)$$

where δ_0, n, B are constants.

It was noted that Eq. 2.9.1 fitted results below a certain stress level, while Eq.2.9.2. only fitted data obtained at high stresses⁽³⁸⁾. Hence an empirical relationship was proposed⁽⁴¹⁾;

$$\dot{\epsilon} = A (\sinh \alpha \delta)^{n'} \quad (2.9.3)$$

which after rearrangement reduces to Eq.2.9.1 at low stresses ($\alpha \delta < 0.8$) and to Eq.2.9.2 at high stresses ($\alpha \delta > 1.2$). This gave a good correlation between predicted and experimental data obtained over a wide range of strain rates, for various non-ferrous metals and several ferritic and austenitic alloys⁽⁴¹⁾.

The activation energy, which could be associated with the dynamic recrystallization process during hot deformation and which in low C steels remains constant over a wide range of strain rates, enabled a temperature compensated strain rate parameter to be obtained⁽⁴²⁾

$$Z = \dot{\epsilon} \exp(Q/RT) = A (\sinh \alpha \delta)^{n'} \quad (2.9.4.)$$

where T is absolute temperature, R is the gas constant and Q is

the activation energy, which values have been obtained experimentally for various metals⁽⁴³⁾.

Sellars and Tegart⁽⁴¹⁾ showed that the empirical relationship given by Eq. 2.9.4 applied over a wide range of strain rates at high temperature.

McGregor and Fisher⁽⁴¹⁾ introduced an alternative concept of a velocity-modified temperature (T_v) where the effects of strain rate and temperature were combined, thus

$$T_v = T(1 - k \ln \dot{\epsilon} / \dot{\epsilon}_0)$$

$$\delta = f(T_v)$$

where k and $\dot{\epsilon}_0$ are constant.

Simple empirical formulae have also been proposed to fit yield stress strain data obtained at constant temperatures and strain rates,⁽⁴¹⁾

$$\delta = K \dot{\epsilon}^m \quad (2.9.5)$$

$$\delta = \delta_0 + B \ln \dot{\epsilon} \quad (2.9.6)$$

$$\delta = \delta_0 + B [1 - \exp(-C \dot{\epsilon})]^m \quad (2.9.6a)$$

$$\delta = A [1 - \exp(-C \dot{\epsilon}^{mn})]^{-1/n} \quad (2.9.5c)$$

where $A, B, C, K, \delta_0, m, n$, are constants of the material dependent on strain rate and temperature. Eq. 2.9.5 and Eq. 2.9.6 apply adequately to low strain levels corresponding to that portion of the stress strain curve that showed substantial work-hardening, while at higher strains Eq. 2.9.5a and Eq. 2.9.6a were more appropriate. Furthermore, at small strains, Eq. 2.9.5a and Eq. 2.9.6a reduced to Eq. 2.9.5 and Eq. 2.9.6 respectively.

In order to calculate the yield stress appropriate to any combination of strain, strain rate and temperature, it has been suggested that the equations relating stress and strain can be combined with the relationships between stress and temperature, and stress and strain rate. Thus, Sellars and Tegart⁽⁴¹⁾ proposed

empirical equations of the form,

$$\Delta = (BZ)^{1/n} \epsilon^m \quad (2.9.7)$$

$$\Delta = \epsilon^m / \beta \ln BZ \quad (2.9.7a)$$

$$\Delta = \epsilon^m / \alpha \sinh^{-1}(BZ)^{1/n} \quad (2.9.7b)$$

where B, α, β, m, n are constants.

Similarly Lubahn et al. (42) arrived at,

$$\Delta = CG^T \left(\frac{\dot{\epsilon}}{\dot{\epsilon}_0} \right)^D \epsilon^{(E-F) \ln(\dot{\epsilon}/\dot{\epsilon}_0)} \quad (2.9.8)$$

where $C, G, \dot{\epsilon}_0, D, E, F$ are constants of the material.

The use of such equations is of considerable value in the calculation of working forces in hot rolling, since the experimental data applicable to particular deformation conditions is not usually available.

2.10 Coefficient of friction between slab and rolls during hot rolling.

Most of the existing methods used to determine the external friction are indirect and dependent for their validity upon the assumptions made. It was generally assumed that only sliding friction occurred on the contact surfaces between the tool and the metal; and therefore, the external friction was subject to Coulomb's law. Even more often it was considered that the coefficient of friction was constant along the surfaces in contact.

Trinks⁽⁴⁴⁾ used a crude method to determine coefficients of friction by placing hot steel specimens on variously inclined smooth steel plates and it was observed whether the specimens lay still or slid down. These simple tests gave an average coefficient of friction of 0.4.

Male and Cockroft⁽⁴⁵⁾ developed a technique, which involved the compression of flat-ring shaped specimens at elevated temperatures, between plane parallel platens. It was found that under frictionless conditions, both internal and external diameter increased, whereas at a high coefficient of friction the internal diameter decreased. Hence, the coefficient of friction was related^{to} the change of the internal diameter by a given amount of reduction of the ring thickness. Thus it was established that under dry conditions and over the temperature range 700 - 1000 °C the coefficient of friction between mild steel samples and the platens, decreased from 0.57 to 0.38 as the temperature was increased. These results were, in general, in fair agreement with the limited data available from industrial processes. However the major disadvantage of the method was that no mathematical expression could be used to convert the results of the tests into values of coefficients of friction.

Later Gleave et al.⁽⁴⁶⁾ used the ring compression technique, under

both dry and lubricated conditions, in low C and stainless steel specimens. It was found that over the temperature range 1000 - 1300°C and dry conditions, the coefficient of friction using low C steel was lower than that obtained with stainless steel, possibly due to the partial lubricating action of the scale formed in the C steel. Additionally it was established that under lubricated conditions, the use of glass and graphite caused a decrease in the coefficient of friction as the temperature was increased.

Alternative compression tests have also been conducted to determine coefficients of friction at high temperatures⁽⁴⁷⁾, but, however valid the assumptions made to obtain values of μ , such indirect methods cannot be fully recommended to establish actual frictional conditions during hot rolling.

In order to determine experimentally the average coefficient of friction during hot rolling, techniques based on either the maximum angle of bite or the amount of forward slip are currently used. In addition coefficients of friction expressed as a function of roll force and torque by means of approximate rolling theories, enabled values of μ to be established from the measurements of rolling loads.

El Kalay et al.⁽¹⁶⁾ published data concerning the rolling of low C steel bars over the temperature range 1000 - 1200°C, under conditions of light, medium and heavy scaling and using both smooth and rough rolls. This enabled Roberts⁽⁵⁰⁾ to compute the coefficient of friction for each set of rolling conditions, based on a simplified mathematical model, where both the roll force and torque were related to the coefficient of friction. These results were then plotted against the logarithm of the roll roughness/scale index ratio as shown in Fig. 2.10.1. Thus, the following relationship was proposed, suitable in the cases of

unlubricated hot rolling of low C steels,

$$\mu = 3.6 \exp \left[-4.910 / (459 + T) \right] + 0.063 \ln (\rho / \delta)$$

where T is the steel temperature ($^{\circ}\text{C}$), ρ is the roughness (μ in.) and δ is the 'scale index' of the material ($\text{lb} \times 10^3 / \text{ft}^2$).

In the case of well de-scaled work pieces, rolled under conditions of good lubrication, the following expression was given,

$$\mu = 2.77 \times 10^{-4} \exp(-2.61 \times 10^{-4} / (459 + T)) + 0.21$$

which was considered only approximate since the coefficient of friction would be expected to be dependent upon such factors as roll velocity, the geometry of the rolling pass and the properties of the lubricant.

i. Technique utilising the maximum possible entry angle.

Ekelund⁽⁶⁾ derived a coefficient of friction from the maximum possible entry angle produced when a rectangular bar was brought into contact with the rolls and showed that at the onset of rolling . The entry angle was measured between the tangent to the roll at the entry plane and the central line of the bar. From these results Ekelund deduced the following expressions:-

$$\mu = 1.05 - 0.0005 T \quad \text{for cast iron and rough rolls}$$

$$\mu = 0.8(1.05 - 0.0005 T) \quad \text{for chilled and smooth steel rolls.}$$

Later Batchinov^{48a} proposed a modification to Ekelund's formulae to include the effect of the velocity of rolling. Thus,

$$\mu = a k_1 (1.05 - 0.0005 T) \quad (2.10.3.)$$

where k_1 depends on the rolling velocity and $a=1$ or 0.8 when rough or smooth rolls are used.

Tafel^(49a) presented a graphical relationship between the maximum entry angle and the peripheral velocity of the rolls, which applied to the rolling of mild steels at 1200°C with either rough or smooth rolls. Wusatowski et al.⁽⁴⁸⁾ carried out similar rolling tests

on mild steel bars at 1100 °C over a wide range of rolling velocities. The results obtained suggested that the coefficient of friction in hot rolling varied between 0.25 - 0.7.

Wusatowski pointed out that the value of the coefficient of friction obtained with this technique, related only to the point of entry where a specific velocity exists between the slab and rolls; and since the slip velocity varied along the arc of contact, such a value of μ could not represent the mean coefficient of friction.

In the case when a steady state rolling is established the rolls will start to slip on the slab surfaces if the average horizontal component of the roll force equals that of the surface friction. Such condition, considering a small angle of contact, can be approximately expressed as:-

$$P \sin \alpha/2 = \mu P \cos \alpha/2$$

$$\tan \alpha/2 = \mu$$

Thus, this angle of contact is twice the maximum entry angle at the start of a rolling pass, which indicates that during steady state rolling the coefficient of friction could be lower than that at the initial moment of entry.

ii. Technique involving measurement of the relative velocity between rolls and slab (Forward slip).

The amount of forward slip is defined by the difference between the exit velocity of the rolled material and the peripheral velocity of the rolls, expressed as a percentage of the latter.

Ekelund⁽⁶⁾ assumed homogeneous deformation and slipping conditions along the arc of contact, to show that the forward slip was related to the neutral angle by the expression,

$$\Phi = (1 - \cos \theta_n) \left(2R / h_2 \cos \theta_n - 1 \right) \quad (2.10.4)$$

From the equilibrium of horizontal forces within the arc of contact, the neutral angle was approximately expressed as,

$$\theta_n = \theta/2 - \frac{1}{\mu}(\theta/2)^2 \quad (2.10.5)$$

This equation required that the radial pressure remains uniform within the arc of contact.

The coefficient of friction could then be determined from the measured forward slip and by combining the above equations (2.10.4-5). However, the values of the coefficient of friction obtained by this method were limited by the validity of the assumptions made to obtain these equations.

Siebel⁽⁴⁹⁾ determined the coefficient of friction by measuring the value of the forward slip using various entry thicknesses for a given value of $h_2/2R$ until a maximum value of the forward slip was reached, ($\frac{d\Phi}{d\theta} = 0$). It can then be shown that a maximum forward slip would occur when $\mu = \theta$. Siebel also investigated the conditions governing the forward slip and showed that for any given ratio $h_2/2R$ the maximum forward slip increased as the coefficient of friction increased. Furthermore, the effect of an increase in the temperature of the material was a reduction in the amount of forward slip. Values of the coefficient of friction using ground steel rolls, were thus given by the expression,

$$\mu = 0.55(1.05 - 0.0005T) \quad (2.10.6)$$

Values of forward slip were usually determined by measuring the distance, l , between marks left on the rolled material by two fine holes drilled into the surface and along the circumference of the top roll, a distance, d , apart; thus the ratio $(t-d)/d$ defined the forward slip. Wusatowski⁽⁴⁸⁾ claimed that measurements of the forward slip made on the surface of the material did not represent the true situation, since the metal flow near the surface was entirely different from that in the

interior of the slab.

Pavlov^{49b} designed a device to determine the coefficient of friction at the moment when skidding began between the surfaces of the material and the rolls by applying a braking force on the strip. With this system the roll force and the braking force were measured and the coefficient of friction was calculated from the equation,

$$\mu = \frac{Q}{2P} + \frac{1}{2} \alpha \quad (2.10.7)$$

where Q is the braking force applied in the rolling direction, P is the vertical roll force, α is the angle of contact.

In Eq. 2.10.7 it is assumed that slipping conditions occur at all points along the arc of contact. Wusatowski⁽⁴⁸⁾ claimed that these conditions were unrepresentative of those normally found during rolling.

2.10.1 Variation of the coefficient of friction along the arc of contact.

All the work reviewed so far involved the assumption that μ is constant throughout the arc of contact. Presumably because of the extreme difficulty of measuring μ at various points along the contact length, there is little data which can be used to postulate a probable variation of μ with position inside the arc of contact. In the absence of more positive information several workers have proposed expressions for the variation of μ . Hitchcock^{31a} stated that, from experimental evidence, μ between sliding bodies was greatest at low velocities, and suggested the following relationship between μ and position within the arc of contact,

$$\mu = \mu_n - \frac{R^2}{2} (\sin\theta - \sin\theta_n)^2$$

where μ_n is the coefficient of friction at the neutral point. According to this expression μ is a maximum at the neutral point and decreases towards the entry and exit planes.

Nadai⁽³⁾ investigated the influence of a variable coefficient of

friction on the roll pressure distribution. The frictional shear was assumed to be proportional to the relative velocity of slip between the rolls and the material, i.e. $\tau = \eta \frac{v - v_r}{\delta}$ (see Sect. 2.3). According to this equation the frictional shear and hence μ is zero at the neutral point.

Khayyat and Lancaster⁽⁵²⁾ used a photo-elastic technique to investigate the distribution of contact stresses during rolling of pure lead with rolls made from a hard, transparent resin. It was shown that a significant variation of the shear stress/normal pressure ratio occurred along the arc of contact, which indicated that the coefficient of friction, as given by the above ratio, was variable.

(51, 51a)

Recently experimental measurements of both the radial pressure and shear stress along the arc of contact have been made by means of two pressure-transmitting pins inserted, one normal and the other oblique to the roll surface.

Matsuura et al.⁽⁵¹⁾ applied the above technique to measure the roll pressures and shear stresses along the length and width of the arc of contact using ^{low} low C steel strips. It was found that the coefficient of friction increased towards the entry and exit planes and became zero at the neutral point during cold rolling. A distribution of shear stress and μ along the arc of contact is shown in Fig. 2.10.2.

Zengler^(51a) also carried experiments on lead at 90°C, aluminium and low C steel at 440 and 1110°C respectively, showing that the distribution of shear stresses along the arc of contact decreased towards the neutral point. This might suggest that a similar variation of the coefficient of friction could be expected during hot rolling.

2.11 Roll force and torque.

Considering a surface element of the roll $R'd\theta$. The normal force acting upon the surface element is $S R'd\theta$ and the tangential force $T R'd\theta$. The vertical component of the normal force is $S R'd\theta \cos\theta$ and that of the tangential force is $T R'd\theta \sin\theta$. Hence, the total vertical force acting upon either roll per unit width of the rolled material is,

$$P = R' \left[\int_0^{\theta_1} S \cos\theta d\theta - \int_0^{\theta_n} T \sin\theta d\theta + \int_{\theta_n}^{\theta_1} T \sin\theta d\theta \right] \quad (2.11.1)$$

Orowan⁽⁴⁾ considered that for small angles of contact the contribution of the tangential force could be neglected and $\cos\theta \approx 1$. Thus, Eq.2.11.1 was simplified to,

$$P = R' \int_0^{\theta_1} S d\theta \quad (2.11.1a)$$

Sims⁽³⁴⁾ also assumed that the vertical pressure equalled the normal roll pressure for small angles of contact. Hence, substituting Sims' expression (Eqs. 2.5.2 and 2.5.2a) into Eq.2.11.1a,

$$P = R' 2K_p \left[\int_{\theta_n}^{\theta_1} \left\{ \frac{\bar{n}}{4} \ln \frac{h}{h_1} + \frac{\bar{n}}{4} + M(\theta) - N(\theta) \right\} d\theta + \int_0^{\theta_n} \left\{ \frac{\bar{n}}{4} \ln \frac{h}{h_2} + \frac{\bar{n}}{4} + M(\theta) \right\} d\theta \right] \quad (2.11.2)$$

which after integration becomes,

$$P = R' 2K_p \left[\frac{\bar{n}}{2} \sqrt{\frac{h_2}{R'}} \frac{1}{2} \sqrt{\frac{r}{1-r}} - \frac{\bar{n}\theta_1}{4} - \ln \frac{h_0}{h_2} + \frac{1}{2} \ln \frac{h_1}{h_2} \right] \quad (2.11.2c)$$

where $h_0 = h_2 \sqrt{\frac{R'}{r}}$

and the neutral angle can be found by equating Eqs.2.5.2 and 2.5.2a.

Thus,

$$\frac{\bar{n}}{4} \ln(1-r) = 2 \sqrt{\frac{R'}{h_2}} \frac{1}{2} \sqrt{\frac{r}{1-r}} \theta_n - \sqrt{\frac{R'}{h_2}} \frac{1}{2} \sqrt{\frac{r}{1-r}}$$

Orowan and Pascoe⁽¹⁵⁾ derived expressions for the total roll force for both wide and narrow plates by assuming that the drop of the roll pressure towards the edges of the material could be calculated approximately in the same manner as the slope at the exit side of the friction hill (see Sect.2.5). They showed that when the initial ratio width/

thickness was 6, the roll force was given by,

$$P = 2KW \sqrt{RAh} \left(\frac{\pi}{4} + \frac{\sqrt{RAh}}{4h_1} \right)$$

In cases where the width/thickness ratio was within 2 - 6 then,

$$P = 2K\bar{W} \left[0.8 + 0.25 \frac{\sqrt{RAh}}{h} - \frac{2h_m h_1}{3W \sqrt{RAh}} \left(\frac{\sqrt{RAh}}{2h_1} - 0.2 \right)^3 \right]$$

where $h_m = (2h_1 + h_2)/3$

$$\bar{W} = (2w_2 + w_1)/3$$

Finally, for narrow stock, $w_1/h_1 < 1.5$

$$P = 2K\bar{W} \sqrt{RAh}$$

i. Roll torque.

The tangential force per unit width acting upon a surface element of the roll is $T'R'd\theta$, and the torque exerted by this force about the roll centre is $R'T'R'd\theta$. The total torque per unit width acting upon one roll and ignoring the contribution of the radial forces, is then given by,

$$G = R'R \int_{\theta_n}^{\theta_1} T'd\theta - \int_0^{\theta_n} T'd\theta \quad (2.11.3)$$

or

$$G = \mu R'R \int_{\theta_n}^{\theta_1} \sin\theta d\theta - \int_0^{\theta_n} \sin\theta d\theta \quad \text{if } T = \mu S$$

The determination of the torque by the use of the above equation involves the calculation of the difference between two quantities of the same order of magnitude which may lead to substantial errors if the position of the neutral angle is not most accurately determined. Therefore Bland and Ford⁽¹²⁾ developed an alternative expression by considering the moment of the vertical pressure with respect to the roll axis $S \cos R'd\theta \times R \sin\theta$. Thus, the total roll torque, considering small angles of contact, so $\cos\theta \approx 1$, $\sin\theta \approx \theta$ and including the contribution of both front and back tensions, was given by,

$$G = RR' \left[\int_0^{\theta_1} \theta d\theta + \frac{h_1 - h_2}{2R'} \right] \quad (2.11.4)$$

Alternatively, Sims⁽¹⁴⁾ derived an expression for hot rolling considering the moment due to vertical forces only, so,

$$G = RR' \int_0^{\theta_1} s \theta d\theta \quad (2.11.4a)$$

and using Eqs. 2.5.2 and 2.5.2a, given by Sims' method, then,

$$G = R'RK_G \left[\int_{\theta_n}^{\theta_1} \left\{ \frac{\mu}{4} \ln \frac{h}{h_1} + \frac{\mu}{4} + M(\theta_1) - M(\theta) \right\} \theta d\theta + \int_0^{\theta_n} \left\{ \frac{\mu}{4} \ln \frac{h}{h_2} + \frac{\mu}{4} + M(\theta) \right\} \theta d\theta \right] \quad (2.11.5)$$

and after integration this equation reduces to:

$$G = RR' 2K_G (\theta_{1/2} - \theta_n)$$

Hill⁽³⁵⁾ considered the effect of roll flattening on the torque, in which the centre of the arc of contact is not on the line joining the roll centres. Since the roll pressure distribution in Hitchcock's method is symmetrical about the mid-point of the arc of contact, Hill assumed that the centre of the latter lay on the line joining the mid-point, C, to the roll centre at a distance $(R' - R)$ beyond the roll centre (Fig. 3.2.1).

The lever arm of the radial force $sR'd\theta$ about the spindle axis was approximated to $\pm (R' - R) (\theta_{1/2} - \theta)$ the sign being dependent on the side of C on which the surface element lay. Thus, the total torque including the contribution of the tangential forces ($\mu sR'd\theta \cdot R$) was expressed as,

$$G = R'R\mu \left[\int_{\theta_n}^{\theta_1} s d\theta - \int_0^{\theta_n} s d\theta \right] + \left(\frac{R'}{R} - 1 \right) \int_0^{\theta_1} s (\theta - \theta_{1/2}) d\theta \quad (2.11.6)$$

Next, by considering the equilibrium of the horizontal forces acting on the strip and assuming $\cos\theta \approx 1$, $\sin\theta \approx \theta$ the following expression was obtained;

$$h_2 t_2 - h_1 t_1 = 2R' \int_0^{\theta_1} s \theta d\theta - \mu \left[\int_{\theta_n}^{\theta_1} s d\theta - \int_0^{\theta_n} s d\theta \right] \quad (2.11.7)$$

Hence, by combining Eq.2.11.6 and Eq.2.11.7 an expression was derived where the coefficient of friction is eliminated; thus,

$$G = RR' \int_0^{\theta_1} s \theta d\theta + \frac{(h_1 t_1 - h_2 t_2)}{2R'} + \left(\frac{R'}{R} - 1\right) \int_0^{\theta_1} s(\theta - \theta/2) d\theta \quad (2.11.8)$$

Finally, by introducing the approximate expression of roll force given by Eq.2.11.1a, Eq.2.11.8 was reduced to,

$$G = R'^2 \int_0^{\theta_1} s \theta d\theta + \frac{R'}{2} (h_1 t_1 - h_2 t_2) - \frac{1}{2} (R' - R) \theta_1 P \quad (2.11.8a)$$

2.12 Validity of the theories of hot rolling.

It can be concluded that in general the route followed in establishing the rolling loads is to consider, first, the equilibrium of vertical and horizontal forces on a vertical slice of the material between the rolls, and to use a yield criterion to relate the horizontal stresses to the vertical stresses and thereby obtain a differential equation relating the vertical pressure to the position along the deformation zone. Integration of the equation results in a vertical pressure distribution throughout the deformation zone and hence roll force and torque can be determined.

Various workers compared theoretical values of roll force and torque against measurements in both experimental and production mills in order to establish the validity of several methods commonly used in hot rolling practice.

Sims presented measured roll forces obtained by S.K.F. Co. (35) using mild steel strips rolled at temperatures between 1000 -1200 °C. These results were then compared with calculated values given by Eq. 2.11.2a and using mean yield stress values from experimental data obtained at high temperatures on 0.17% C steel by means of a cam plastometer. Sims also compared roll force and torque measurements made on lead strips rolled at room temperature and under dry conditions, with calculated values based on yield stress data from uniaxial compression

tests on lead and published in the same work⁽³⁵⁾. A satisfactory agreement between theoretical and measured results was obtained in both cases over a wide range of reductions.

Stewartson⁽⁵³⁾ reported a large number of roll force measurements on mild steel rolled in a 42 - in. plate mill. The results showed considerable scatter attributed to difficulties involved in temperature and thickness measurements. These results were compared with calculated values obtained with the formulae of Ekelund, Crowan & Pascoe, and Sims. It was shown that using Ekelund's formula the mean of the calculated forces was about 33% lower than the measured values and the scatter about this mean exceeded $\pm 25\%$; the Crowan and Pascoe formula showed no better agreement than in the previous case at lower reductions. Since predictions with the Crowan and Pascoe formula should improve when the plate thickness/length of contact ratio is less than unity⁽¹⁵⁾, which represented reductions of over 10% in Stewartson's results, the majority of the calculated loads above 10% reductions were within a range of +50 to -10% above the measured values. One source of error admitted by Stewartson may be in the values of yield stress which were calculated back and extrapolated from a small number of experimental roll load measurements. Values of force calculated with Sims' formula based on yield stress data obtained by BISRA and later published by Cook and McCrum⁽³⁴⁾ showed the closest agreement with measured loads at reductions over 10%. However, at lower reductions all three formulae gave results which were some 50% lower than those measured.

Sims and Wright^(53a) carried out extensive checks of the accuracy of the Cook and McCrum method, referred to as the BISRA method, against measurements of roll force and torque obtained on six types of production mill: a blooming mill, a slabbing mill, a 2-high strip mill, a 2-high

roughing mill, a 4-high strip mill and a plate finishing mill. The calculated results were found to diverge significantly from the measured ones for values of R/h_2 up to about 20 - 25. This was attributed mainly to errors in the method of measuring the thickness of the rolled material as determined from the roll gap settings and the mill modulus. There was, in addition, a considerable discrepancy between the measured and calculated torques in the 4-high strip mill owing to the effect of interstand tension. Sims and Wright concluded that, in general, rolling theory will predict reliable values of rolling loads when R/h_2 is greater than about 25, the roll torque being underestimated by theory in this range of R/h_2 . The limitations of the rolling theory over this range of values of R/h_2 was attributed to both the change in the mode of deformation between the rolls when the thickness/length of contact ratio is equal to or greater than 2, and the inaccuracies involved when the angle of contact becomes so large that approximations of its trigonometrical functions are no longer acceptable.

Most of the early methods to predict rolling loads relied upon the assumption of homogeneous deformation; the achievement of which (i.e. initial plane sections remaining plane during rolling), is in principle impossible, since friction between the material and roll surfaces restricts the flow of the peripheral layers. Furthermore, experimental evidence of the deflection of cross sections of the deforming material had been obtained, the most satisfactory of which appears to be that produced by Jones et al.⁽⁶¹⁾, using steel plates with MnS inclusions initially oriented perpendicular to the rolling direction. The deformation pattern of these inclusions after hot rolling established that initial vertical sections did not remain plane during deformation. Hence, Crowan's method by which the effect of inhomogeneous deformation can be

included, remains the most accurate treatment of the rolling process. A recent work by Alexander⁽²⁸⁾ showed how the basic approach by Orowan can be incorporated into computer programmes providing thus a quick and accurate way to solve any rolling problem.

Nevertheless, the validity of more accurate methods depends on the availability of relevant flow stress data at high temperatures and various strain rates. Reliable data has been obtained from experiments with cam plastometers, but the increase in hot rolling speeds demands data at even higher strain rates. In addition, experimental evidence indicated that the coefficient of friction between the material and the rolls varies along the arc of contact so that it becomes extremely difficult to establish the actual frictional conditions of a specific rolling operation.

3 A Numerical Solution to the basic Von Karman Equation.

3.1 Introduction.

A mathematical model has been produced by which predictions of both roll force and torque, developed over a wide range of flat hot rolling conditions, can be made. The basic Von Karman equation, describing the distribution of roll pressure along the arc of contact, takes into account the effect of a variable flow stress of the material undergoing deformation and of both homogeneous and inhomogeneous deformation, together with a mixed frictional condition $\mu \leq k$ and a deformed roll radius. Since the resulting differential equation possesses no analytical solution, the numerical technique involving the fourth-order Runge Kutta method and originally developed by Alexander⁽²⁸⁾ for the cold rolling process, was extended to the hot rolling case. The following sections will therefore describe the mathematical basis of the model by considering the analysis relevant to the plastic and elastic deformations of flat sections at high temperatures and varying strain rates.

3.2 Basic differential equation under homogeneous deformation.

The analysis presented in this section relies upon the following assumptions:-

- (i) Vertical sections of the material in the direction of rolling remain plane during deformation.
- (ii) There is no lateral spread of the material if the thickness of the strip is small compared with its width.
- (iii) Plastic deformation occurs throughout the material between the rolls, though in the vicinity of both the entry and exit planes elastic deformation and elastic recovery take place respectively.
- (iv) The yield stress of the material varies throughout the zone of deformation under isothermal conditions.

- (v) The frictional stresses, between the material and roll surfaces, are proportional to the radial pressure but cannot exceed the shear yield stress of the material.
- (vi) The deforming arc of contact between the strip and the rolls remains circular.
- (vii) The peripheral velocity of the rolls is uniform.

Fig.3.2.1 represents a longitudinal section of a strip in transit through the roll gap. The state of stress of the material between the rolls is triaxial: a vertical stress, q , a horizontal stress acting in the direction of rolling, p , and a stress parallel to the roll axis preventing free lateral spread Δ_2 . Since the assumption of homogeneous deformation implies that no shear stresses arise between the surfaces of vertical sections, the horizontal stress, p , together with the transversal stress Δ_2 and the vertical stress, q , are considered principal stresses. Then if plastic strain in the transverse direction is ignored,

$$\epsilon_2 = \frac{1}{E_p} [\Delta_2 - 0.5(q+p)] = 0$$

so

$$\Delta_2 = (q+p)/2$$

The Von Misses maximum shear strain energy criterion states that plastic yielding occurs, when

$$(\Delta_1 - \Delta_2)^2 + (\Delta_2 - \Delta_3)^2 + (\Delta_1 - \Delta_3)^2 = 6GA = \text{constant}$$

The critical value of the shear strain energy can be determined considering the case of yielding in a pure torsion test when $\Delta_1 = K$, $\Delta_2 = 0$, $\Delta_3 = -K$ thus, $GA = K^2$.

Hence the use of the Von Misses criterion in a triaxial stress system and under plane strain conditions leads to,

$$q - p = 2K$$

The vertical stress, q , is constant within a vertical section

due to the absence of shear stresses along its surfaces and assuming that the yield stress through a section is uniform, the horizontal stress, p , must be therefore a constant. Hence the equilibrium of horizontal forces per unit width acting on the vertical slice AA of the strip leads to ,

$$df/d\theta = d(ph) = 2R's \sin\theta \pm \tau \cos\theta \quad (3.2.1)$$

where the upper sign refers to the exit side and the lower to the entry side of the arc of contact.

A balance of vertical forces within the slice AA and the use of the yield criterion permits the above equation to be expressed in terms of the radial pressure,

$$d[h(s - 2K \mp \tau \frac{1}{2}\theta)]/d\theta = 2R'(s \sin\theta \pm \tau \cos\theta) \quad (3.2.1a)$$

Two frictional conditions were assumed between the rolls and the material surfaces:

1. A dry frictional stress proportional to the radial pressure

$\tau = \mu s$, in which case Eq. 3.2.1a applicable to slipping conditions was written as,

$$ds/d\theta = \rho_1(\theta)s + \rho_2(\theta) \quad (3.2.2)$$

where

$$\rho_1(\theta) = \pm \mu \sec\theta \left(\frac{2R'}{h} + \sec\theta \right) / (1 \mp \mu \frac{1}{2}\theta)$$

and

$$\rho_2(\theta) = \left(\frac{2R'}{h} 2K \sin\theta + \frac{d(2K)}{d\theta} \right) / (1 \mp \mu \frac{1}{2}\theta)$$

A limiting frictional stress $\tau = K$ which produced sticking

- ii. A limiting frictional stress $\tau = K$ which produced sticking conditions, so Eq. 3.2.1a was expressed as,

$$ds/d\theta = \rho_3(\theta) \quad (3.2.3)$$

where

$$\rho_3(\theta) = 2K \left\{ \frac{2R'}{h} \sin\theta (1 \pm \frac{1}{2}\theta) \pm \left(\frac{R'}{h} \cos\theta - \frac{1}{2} \sec^2\theta \right) \right\} / (1 \pm \frac{1}{2}\theta) + \frac{d(2K)}{d\theta}$$

The values of the radial pressure at both the entry and exit

planes can be found by combining the equilibrium equation of vertical forces and the yield criterion; thus at the entry plane, where $K=K_1$ and $p=t_{e1}$ (the effective back tension, see Sect.3.7), the radial pressure becomes,

$$S_1 = 2K_1 - t_{e1} - \tau \frac{1}{\sin \theta} \quad (3.2.4)$$

and at the exit plane, where $\theta=0$, $K=K_2$ and $p=t_{e2}$ (the effective front tension, see Sect.3.7),

$$S_2 = 2K_2 - t_{e2} \quad (3.2.4a)$$

3.3 Basic differential equation under inhomogeneous deformation.

A radial pressure distribution during inhomogeneous deformation was obtained following Orowan's analysis⁽⁴⁾, in which it was assumed that the stress distribution inside the deforming material could be approximated to that produced by the compression of the slab between two inclined platens, so that the horizontal compressive stress acting across the strip thickness was given by the following equation (see Sect.2.4),

$$f_h = s \left(1 \pm \mu \left(\frac{1}{\theta} - \frac{1}{\sin \theta} \right) \right) - 2Kw(a) \quad (3.3.1)$$

It was assumed after Orowan that under slipping friction and small contact angles the coefficient $\mu \left(\frac{1}{\theta} - \frac{1}{\sin \theta} \right)$ could be eliminated. Thus, the variation of the horizontal stress along the deformation zone could be expressed as, (replacing the value of s in terms of from Eq.3.3.1 into 3.2.1a),

$$\frac{d(f/h)}{d\theta} = g_1(\theta) f/h + g_2(\theta)$$

where $g_1(\theta) = 2R'(\pm \mu \cos \theta)/h$

and $g_2(\theta) = 2R' 2Kw(a) (\sin \theta \pm \mu \cos \theta)/h$

Under sticking conditions the frictional stress contribution to the horizontal stress becomes $\tau=K$ so $a = \mu S/K = 1$ and the inhomogeneity factor⁽⁴⁾ reaches a constant value $w(a) = \sqrt{1/4}$ (see Fig.2.4.3) and Eq.3.3.1

reduces to,

$$\left\{ \frac{1}{h} = S - 2K \left\{ \frac{R}{4} + \frac{1}{2} \left(\frac{1}{\theta} - \frac{1}{2\theta} \right) \right\} \right.$$

and Eq.3.2.1a can be rewritten as,

$$\frac{d(1/h)}{d\theta} = \rho_3(\theta) \quad (3.3.3)$$

where $\rho_3(\theta) = 2K \left\{ 2K \left\{ \frac{R}{4} + \frac{1}{2} \left(\frac{1}{\theta} - \frac{1}{2\theta} \right) \right\} \right\} \sin\theta \pm \frac{1}{2} \cos\theta$

Finally, the associated radial pressure can be found by means of the yield criterion expressed by Orowan as,

$$\frac{1}{h} = S - 2K \omega(\alpha) \quad (3.3.6)$$

3.4 Yield stress variation during hot rolling.

During hot deformation the chief factors influencing the yield stress of the material are, the amount of strain, strain rate and temperature. Since isothermal conditions were assumed throughout the deformation zone an empirical relationship proposed by Lubhan et al. (42) which fitted adequately the yield stress data used in this work, enabled the effect of strain and strain rate at a constant temperature to be included, viz.

$$\sigma_T = C \dot{\epsilon}^G \epsilon^{D+H \ln \dot{\epsilon}} \quad (3.4.1)$$

where ϵ and $\dot{\epsilon}$ are the uniaxial strain and strain rate respectively and C, D, G, H are constants.

Since in flat rolling the effective strain is given by, $\bar{\epsilon} = \frac{2}{\sqrt{3}} \ln(h_0/h)$ and the effective strain rate by $\dot{\bar{\epsilon}} = \frac{2}{\sqrt{3}} \dot{\epsilon}$, the effective yield stress under plane strain becomes,

$$2K \left|_T = \frac{2}{\sqrt{3}} C \left(\frac{2}{\sqrt{3}} \dot{\epsilon} \right)^G \frac{2}{\sqrt{3}} \ln \left(\frac{h_0}{h} \right)^{D+H \ln \left(\frac{2}{\sqrt{3}} \dot{\epsilon} \right)}$$

The variation of the strain rate during rolling can be derived by considering first the mean strain rate within a vertical section to be given by,

$$\dot{\epsilon} = \frac{1}{h} \frac{dh}{dt} = \frac{1}{h} \frac{dh}{dx} \frac{dx}{dt}$$

under slipping conditions, $\frac{dx}{dt} = v = v_0 \frac{h_0}{h}$

From the geometry of the pass $h=h_2+2R'(1-\cos\theta)$, $x=R'\sin\theta$ and $V_n=V_r \cos\theta$, thus, $dh/dx=2tg\theta$, and the strain rate can be expressed as,

$$\dot{\epsilon}_s = 2V_r h_0 \cos\theta_0 \tan\theta/h_2 \quad (3.4.2)$$

It can be shown similarly that under sticking conditions the strain rate becomes,

$$\dot{\epsilon}_k = 2V_r \sin\theta/h \quad (3.4.2a)$$

The variation of the mean strain rate of section along the arc of contact, assuming both complete sticking or slipping conditions, is shown in Fig.3.4.1 for a typical rolling pass.

The values of $\dot{\epsilon}_s$ and $\dot{\epsilon}_k$ given by Eqs.3.4.2 and 3.4.2a can be then replaced in Eq.3.4.1 and the rate of change of the yield stress along the arc of contact will be then given by,

$$\frac{d(\sigma_k)}{d\theta} = \frac{\sigma_k}{h} \left[(h-4R'\theta^2)G + H \ln \left(\frac{2}{3} \frac{h_0}{h} \right) \right] - \frac{(H \ln \dot{\epsilon}_s) 2R' \sin\theta}{\ln v/h} \quad \text{under slipping conditions,}$$

and

$$\frac{d(\sigma_k)}{d\theta} = \frac{\sigma_k}{h} \left[(h-2R'\theta^2)G + H \ln \left(\frac{2}{3} \frac{h_0}{h} \right) \right] - \frac{(H \ln \dot{\epsilon}_k) 2R' \sin\theta}{\ln h/h} \quad \text{under sticking conditions.}$$

3.5 Roll force per unit width.

On the assumption that the deformed arc of contact remains circular, the radial pressure distribution must be considered symmetrical about the mid-point of the contact length and the resulting roll force must be then applied mid-way along the arc of contact (Fig. 3.2.1). Since the radial force acting upon a surface element is $sR'd\theta$ and the frictional force is $\pm \tau R'd\theta$ the component in the direction of the resultant roll force of both the radial force and the tangential force will be $s \cos(\theta-\theta/2)R'd\theta$ and $\pm \tau \sin(\theta-\theta/2)R'd\theta$ respectively. The resultant roll force excluding the contribution of the elastic zones of the material at both ends of the contact arc, will be given by,

$$P = R' \int_{\theta_0}^{\theta_1} s \cos(\theta-\theta/2) d\theta + R' \left[\int_{\theta_0}^{\theta_1} \tau \sin(\theta-\theta/2) d\theta - \int_{\theta_0}^{\theta_1} \tau \sin(\theta-\theta/2) d\theta \right] \quad (3.5.1)$$

3.6 Roll torque per unit width.

In order to determine the moments produced by both the radial and tangential forces about the roll axis, the position of the centre of the deforming arc of contact must be established. Since the radial pressure distribution was considered symmetrical about the mid-point C, the centre of the deformed arc of contact must lie along the line joining the roll centre and the mid-point C (Fig.3.2.1). The position of the centre of the deforming arc of contact should then be given by the intersection of the line through OC and a vertical line traced at the point where the tangent to the roll surface is horizontal. Therefore, taking into account the vertical and horizontal distances between the centres of the roll and of the deforming arc of contact, and excluding the contribution of the elastic zones of the material, the resultant torque per roll will be given by⁽³⁵⁾,

$$G = R' \int_{\theta_n}^{\theta_1} [(s \cos \theta + (r \sin \theta)) \{ R' \sin \theta - (R' - R) \sin \frac{1}{2} \theta \}] - (s \sin \theta - r \cos \theta) \\ \times \{ R' \cos \theta - (R' - R) \cos \frac{1}{2} \theta \}] d\theta + R' \int_{\theta_2}^{\theta_n} [(s \cos \theta - (r \sin \theta)) \{ R' \sin \theta - (R' - R) \\ \times \sin \frac{1}{2} \theta \}] - (s \sin \theta + r \cos \theta) \{ R' \cos \theta - (R' - R) \cos \frac{1}{2} \theta \}] d\theta$$

or

$$G = R'(R-R) \int_0^{\theta_1} s \sin(\theta - \frac{1}{2} \theta) d\theta + R' \int_{\theta_n}^{\theta_1} [R' - (R' - R) \cos(\theta - \frac{1}{2} \theta)] d\theta - R' \int_0^{\theta_n} [R' - (R' - R) \cos(\theta - \frac{1}{2} \theta)] d\theta \quad (3.6.1)$$

Approximate expressions of the roll torque originally developed for cold rolling, as proposed by various workers^(12, 14, 35) will also be included in this model, viz.,

$$G = R'R \left(\int_0^{\theta_1} s \theta d\theta + \frac{h_1 - h_2}{2R'} \right) \quad (2.11.4)$$

$$G = R'R 2K_0 (\frac{1}{2} \theta_1 - \theta_n) \quad (2.11.5a)$$

$$G = R'^2 \int_0^{\theta_1} s \theta d\theta + \frac{R}{2} (h_1 t_1 - h_2 t_2) - \frac{1}{2} (R' - R) \theta_1 P \quad (2.11.8a)$$

3.7 Elastic arcs of contact.

At both ends of the deformation zone there must be an area of contact between the strip and the rolls where the material is only elastically deformed. The effect of this is to increase the length of the arc of contact beyond the points where the strip undergoes plastic deformation and hence to augment the total roll force by the contribution of the elastic zones. Bland and Ford⁽³³⁾ developed expressions by which the total normal force in the elastic zones can be obtained. First it was considered that, since the strip is in contact with the rolls, the normal displacement along the elastic recovery zone of length a , was given as,

$$v = \frac{\nu(1+\nu)h^2}{E} \frac{1}{2} + \frac{1}{2R'}(a^2 - x^2) \quad (3.7.1)$$

After applying the generalised Hooke's law in plane strain and assuming no shear stresses across vertical sections it was shown that,

$$\int_0^a \delta_y dx = \frac{1-\nu^2}{E} \frac{h}{2} \int_0^a \delta_y dx - \frac{\nu(1+\nu)h}{E} \frac{a}{2} \quad (3.7.2)$$

where $\int_0^a \delta_y dx$ represents the contribution to the roll force from the elastic recovery zone. Thus, solving the integral of the left hand side of Eq.3.7.2, the roll force contribution was,

$$P_{E2} = \int_0^a \delta_y dx = \frac{2Ea^2}{3(1-\nu^2)R'h_2}$$

In order to determine the length of the elastic recovery zone, it was postulated that the mean vertical stress $\bar{\delta}_y$ on the elastic side, taken with the horizontal stress $\frac{1}{2}$, satisfies the yield criterion.

Hence, defining $\bar{\delta}_y$ as,

$$\bar{\delta}_y = \left\{ \frac{1}{h_2/2} \int_0^{h_2/2} \delta_y dx \right\}_{x=0} = \frac{1}{h_2/2} \int_0^{h_2/2} \left(\frac{E}{1-\nu^2} \epsilon_{yy} + \frac{\nu}{1-\nu} \frac{1}{2} \right) dy \Big|_{x=0}$$

which was then expressed in terms of the normal displacement at $x=0$ to arrive at,

$$\bar{\delta}_y = \frac{E}{(1-\nu^2)} v_{x=0} + \frac{\nu}{1-\nu} \frac{1}{2} = \frac{a^2 E}{h_2(1-\nu^2)R'}$$

so that the yield criterion was expressed as,

$$\bar{\sigma}_y = 2K - \frac{1}{2} = \frac{\sigma^2 E}{h_2(1-\nu^2)R'} \quad (3.7.3)$$

Hence, after substituting the value of σ obtained from Eq.3.7.3 into Eq.3.7.2 the contribution from the elastic recovery zone is given by,

$$P_{E2} = \frac{2}{3} (2K - \frac{1}{2}) \sqrt{\frac{h_2 R' (1-\nu^2) (2K - \frac{1}{2})}{E}} \quad (3.7.4)$$

Next, Bland and Ford considered that at the end of the plastic zone the horizontal force applied to both roll surfaces was $2\mu P_{E2}$, thus the effective front tension over a section of thickness h_2 was therefore,

$$\frac{1}{2} t_2 = \frac{1}{2} - \frac{2\mu P_{E2}}{h_2}$$

By a similar analysis Bland and Ford showed that the contribution to the total roll force from the elastic compression zone at entry was given by,

$$P_{E1} = \frac{(1-\nu^2) \sqrt{R'}}{4 \sqrt{h_1 - h_2}} \frac{(2K - \frac{1}{2})^2}{E} \quad (3.7.5)$$

and the effective back tension was,

$$\frac{1}{2} t_1 = \frac{1}{2} - \frac{2\mu P_{E1}}{h_1}$$

It can be seen that the effective tensions $\frac{1}{2} t_1$ and $\frac{1}{2} t_2$ depend on P_{E1} and P_{E2} respectively, so that Eqs.3.7.4 and 3.7.5 must be solved by iteration.

Finally, the total value of the roll force per unit width, ignoring the inclination of P_{E1} and P_{E2} to the line of action of P and the shear stresses along the elastic arc, is given by,

$$P_T = P + P_{E1} + P_{E2}$$

while the total value of the roll torque per unit width per roll could be expressed by,

$$G_T = G + G_{E1} + G_{E2}$$

where
and

$$G_{E1} = \mu R P_{E1}$$

$$G_{E2} = -\mu R P_{E2}$$

$$(3.7.6)$$

$$(3.7.6a)$$

3.8 Roll flattening.

The radius of the flattened arc of contact was determined following Prescott's analysis⁽³⁰⁾ by which the radial deformation, caused by an elliptical stress distribution over the length of the roll surface (2d), can be given in terms of the elastic properties of the roll as (see Sect.2,8),

$$\frac{1}{R'} = \frac{1}{R} - \frac{4(1-\nu^2)P}{\pi E d^2} \quad (3.8.1)$$

According to Bland and Ford⁽³³⁾ the total length of the arc of contact must include those portions immediately adjacent to the plastic deformation zone, where elastic deformation at entry and elastic recovery at exit take place. Thus, the total length was approximated to,

$$2d = \sqrt{R'(h_i - h_m)} + \sqrt{R'(h_2 - h_m)} \quad (3.8.2)$$

where h_i , h_m and h_2 are the thicknesses at entry, minimum and exit respectively (Fig.3.2.1).

The analysis outlined in the previous section(3.7) enabled Bland and Ford to find expressions for the strip thicknesses along the elastic zones and Eq.3.8.2 was rewritten as,

$$2d = \sqrt{R(\delta + \delta_{e2} + \delta_f)} + \sqrt{R\delta}$$

where

$$\begin{aligned} \delta &= h_i - h_2 \\ \delta_{e2} &= h_2 - h_m = \frac{h_2(1-\nu^2)}{E} (2K_2 - \frac{1}{K_2}) \\ \delta_f &= \frac{\nu(1+\nu)}{E} (h_2 \frac{1}{K_2} - h_i \frac{1}{K_1}) \end{aligned}$$

Therefore the final expression to determine the deformed roll radius, after re-arrangement of Eq.3.8.1 is,

$$\frac{R'}{R} = 1 + \frac{cP}{(\delta + \delta_{e2} + \delta_f + \sqrt{\delta})^2}$$

where $c = 16(1-\nu^2)/\pi E$ is constant for the material of the rolls.

3.9 Calculation technique.

The technique used to solve the basic differential equations which assume homogeneous deformation, was based on the work presented by Alexander⁽²⁸⁾. Thus, an initial value of the deformed radius was obtained by estimating a roll force for a given mean strength of the material and percentage reduction. Hence, a realistic value of the angle of contact could be determined.

In order to reach consistent values of the total roll force and the associated deformed roll radius the following procedure was adopted:

1. The angle of contact was split into $2n$ divisions.
2. Values of the radial pressure both at entry and exit planes were calculated using Eq.3.2.4 and Eq.3.2.4a.
3. The yield stress at each angular position was calculated for the associated values of strain and strain rate as given by Eq.3.4.1a.
4. The radial pressure at each angular position from the exit plane towards the entry plane was determined by means of the fourth-order Runge Kutta method to integrate Eq.3.2.2 or Eq.3.2.3 depending on the frictional state defined by the shear stress at the previous angular position $\mu S_i - \tau_{ik}$.
5. The radial pressure at each angular position from the entry plane towards the exit plane was determined in the same manner as described in stage 4.
6. The intersection of both the radial pressure distribution determined from the exit and entry sides enabled a feasible radial pressure distribution along the arc of contact to be determined.
7. The resulting roll pressure distribution was then integrated over the arc of contact by trapezoidal rule to determine the roll force per unit width, P .
8. The contribution of the entry and exit elastic zones of the material to the roll force was then determined by means of Eq.3.7.5 and Eq.3.7.4

9. A new value of the roll radius for the total roll force $P_t = P_1 + P_2$, was calculated and a corrected value of the angle of contact was determined.

Stages 1-9 were then repeated until compatibility was reached between the most recent value of the total roll force and the associated value of the deformed roll radius.

Following the above calculations the moments about the roll axis of both the shear stresses and the radial stresses were integrated by trapezoidal rule over the arc of contact, to obtain approximate values of the roll torque according to Eq.3.6.1, Eq.2.11.4 and Eq.2.11.80.

Finally, an accurate estimation of the roll torque was made using Eq.3.6.1 and including the contributions of the elastic zone of the strip at the entry and exit planes, as given by Eq.3.7.6 and Eq.3.7.60 respectively.

In the case of inhomogeneous deformation, in order to include the effect of a variable inhomogeneity factor, $w(a)$, on the radial pressure distribution, Stages 4 and 5 of the calculation procedure were modified. Since $w(a)$ was a function of the radial pressure, the latter could only be found at each angular position by iteration until consistent values of both the radial pressure and the inhomogeneity factor were reached.

Thus, initial values of $w(a)$ and the horizontal pressure were calculated at the exit plane using Eq.2.5.4, viz., $w(a) = \sqrt{1 - 1.5326(4S/2R)^2}$ and Eq.3.3.4 respectively. The horizontal pressure at the first angular division was then found by means of the Runge Kutta method, which integrated Eq.3.3.2 or Eq.3.3.3, depending on the frictional state defined by the radial pressure at the exit plane. An associated value of the radial pressure at the first angular division was then determined and the inhomogeneous factor re-calculated. A corrected value of the horizontal pressure was then obtained at that division and the process was repeated until an inhomogeneous factor consistent with the radial pressure was reached.

3.10 Data used in roll pressure calculations.

A requisite in the calculation of roll pressures needed to accomplish a given reduction at specific rolling conditions, is the determination of the strength of the material undergoing deformation at the relevant temperatures and rates of strain.

The data defining the rolling conditions comprised: the coefficient of friction, determined from forward slip measurements (see Sect.5.4), the entry and exit thickness, the roll radius, the peripheral velocity of the rolls and the external tensions.

The flow stress data was obtained by means of hot compression tests on specimens from the rolling material and supplemented by published data on similar material. The experimental data obtained at 900, 950, 1000 and 1050 °C and strain rates over the range $5 - 10 \text{ s}^{-1}$ is presented in Sect.5.6. A reasonable fit of the experimental data over the strain of interest ($\epsilon = 0.5$) was obtained using an empirical equation of the form $\sigma = K\dot{\epsilon}^m$; the constants of which were determined by a least-square method. The stress-strain expressions enabled the constants in Eq.3.4.1 to be found; thus the effects of strain and strain rate on the flow stress at the above temperatures were included. At intermediate temperatures the constants were determined by linear interpolation. Following the above procedure, the associated constants to fit the data published by Suzuki⁽³⁶⁾ were also found. Table A lists such constants at various temperatures for both sets of flow stress data.

Additional information to define the material elastic properties was comprised of Young's modulus and Poisson's ratio. The former varies linearly within the range of hot rolling temperatures according to published data⁽⁶⁷⁾ plotted in Fig.3.10.1 and a mean value of the latter ($\nu = 0.336$) was used in all calculations.

3.11 Computer Programmes.

The calculation technique outlined in Section 3.9 was translated into computer programmes following Alexander's work. The flow chart of the programmes is shown in Fig.3.11.1 and the various features of the latter, presented in Appendix II for the case of inhomogeneous deformation, will now be described.

The central problem is to determine the distribution of roll pressures, and S(I) is the computer notation of the M ordinates of pressure distributed over the arc of contact, where M is an odd number of ordinates, so that the arc of contact will have an even number of divisions.

The Common and External statements are required by the particular functions and sub-routines used in a programme, while the Dimension statement defines the functions in arrays. The mechanical properties of the material and the conditions and geometry of rolling are then read and written out. Tests are then made to increase the exit thickness if the reduction cannot be accomplished using the selected value of the coefficient of friction at entry, and to decrease the values of front and back tensions if they exceed the exit and entry yield stress in plane strain respectively, since it would imply that the strip is being deformed by tension exclusively, which is not the case considered here. The permissible values of front and back tension and exit thickness are then written out.

An approximate value of roll force is then calculated, to give initial realistic values to the deformed radius and hence the total angle of contact, denoted as RD and PHI1 respectively. Plastic deformation, assuming that yielding is initiated at 0.2% nominal strain, will then occur over an angle of contact given by,

$$PHI2 = \text{ARCOS}(\text{COS}(PHI1) + 0.002 * H1 / (2 * RD))$$

The values $S(1)$ and $S(M)$ at the boundaries of the plastic arc of contact and the values of K , denoted as $XK(I)$, over the arc of contact are then determined. The fourth-order Runge Kutta method, defined by the sub-routine RK, then solves the differential equation, and $SEN(I)$ denotes the solution at each division from $S(1)$ up to $S(M)$, using the entry boundary conditions, while $SEX(L)$ denotes the solution from $S(M)$ down to $S(1)$ associated with the exit boundary conditions. The actual value of $S(I)$ at each division must then be the lesser of both: the entry and exit solutions. The frictional conditions μS or K , whichever is the smaller, is ensured by the IF statements:

```
IF (XMU*SEX(L).LT.XK(I)) CALL RK (PHI,SEX(L),DPHI,DS,G1,G2),
or IF (XMU*SEX(L).GE.XK(I)) CALL RK (PHI,SEX(L),SPHI,DS,G4,G3).
```

In the case of inhomogeneous deformation the horizontal pressure of each division $PEX(L)$ is found first and then related to the associated radial pressure $SEX(L)$, as described in the calculation technique.

The ordinates between which $SEN(I)$ and $SEX(L)$ intersect, which represent the neutral point, can be determined by the IF statement;

```
IF (SEX(I).GE.SEN(I). AND.SEN(I+1):GE.SEX(I+1) GO TO 61.
```

Statement 61 then calculates the fraction of the interval in which θ_n PHIN. occurs. If that statement is not satisfied. the programme is arranged to declare that no solution is possible and write out the distribution of $SEN(I)$ and $SEX(I)$.

Since an initial value of the neutral angle (PHN) must be assumed in order to calculate the strain rate distribution over the arc of contact (Eq.3.4.2), the calculated value of θ_n replaces the initial one to determine a new strain rate distribution and the whole process is repeated until the absolute value $(PHN-PHIN)/PHN \leq 0.001$, where $PHIN$ is the most recent value of θ_n calculated.

The radial pressure at the neutral point (SN) is then determined and the pressure distribution integrated over the arc of contact by trapezoidal rule, in order to determine the roll force per unit width P , due to plastic deformation. The contributions to the roll force of the elastic zones at both ends of the deformation zone ($PE1$ and $PE2$) are then determined. Then the total roll force $P_1 = P + PE1 + PE2$, is used to obtain a new value of the roll radius and the process is iterated J times until the absolute value $(P_1 - P)/P_1$ is less than 0.00001 , where P_1 is the most recent value of P calculated. $GE1$ and $GE2$, the contributions of the elastic zones to the roll torque are then calculated and finally the various estimates of torque are made according to the various formulae discussed. The most accurate estimate is $GAC12$, as given by Eq.3.6.1, with $GE1$ and $GE2$ added. Finally, the programmes are arranged to write out the relevant parameters.

4. Experimental Procedure.

A description is given below of the rolling mill and ancillary equipment used in the experimental work.

4.1 The Rolling Mill.

The mill is a 2-high, single stand, reversing type, supplied with rolls for both hot and cold rolling. The rolls are 257 mm (10") in diameter by 380 mm (15") in barrel length, with necks mounted in bronze bearings supported by steel chocks. The roll neck bearings are lubricated by a fluid film, and each bearing is designed for nominal roll forces up to 650 kN (65 tons) to provide a 3000 hour service life at 45 rev/min. The upper chocks are positioned by a screw-down gear driven by a 0.74 kW (1 hp) electric motor. The maximum lift of the top roll is 70 mm. The roll gap setting is indicated by a pointer on a disc with graduated markings, which is attached to each screw-down pin. This arrangement allows the roll gap to be set within to 0.25 mm. The rolls consist of Nichillite alloy (Ni bearing chilled rolls) with a shore scleroscope hardness of 40 and with a cylindrically smooth finish of C.L.A. $\sim 0.8 \mu\text{m}$ (32 μin), as measured on a grinding scale for surface finishing. The mean roll diameter, measured along the roll axis is 257.155 ± 0.025 mm.

4.1.1. Mill power supply.

The mill is driven by a 0/60 kW/60 kW (0/80 hp/80 hp), D.C. separately excited motor, coupled through a double reduction gearbox to a pair of helical pinions. Each pinion is connected to a roll by a spindle fitted with flexible couplings. The motor-generator set, which runs at a constant speed of 1440 rev/min, comprises: an 82.0 kW (110 hp) induction motor to drive the set, a 7.5 kW, 230 V (10 hp) constant voltage exciter for field excitation and supply to the control circuits, and

67 kW (90 hp) generator to feed the mill motor. The output voltage of the generator can be adjusted from 0 to 230 V by the variation of its field excitation. Thus, the mill motor speed can be brought up to 500 rev/min by increasing the input voltage, but a further increase up to 1500 rev/min can be obtained by the weakening of the motor field. In order to transfer power to the mill the voltage of the exciter is brought through a rheostat to a maximum of 230 V. Further operations are carried out using push-button controls installed in the mill console. The mill, together with its ancillary instruments, is shown in Fig.4.1.1.

4.2. Mill Instrumentation.

In the present investigation, the main characteristics to be studied during the rolling operation were:

- (i) peripheral velocity of the rolls
- (ii) exit velocity of the material
- (iii) rolling temperature
- (iv) roll force
- (v) rolling power
- (vi) roll torque

There follows a description of the various instruments and methods used to determine the above characteristics.

4.2.1. Tachogenerator.

To measure the peripheral velocity of the rolls initially, a friction tachometer was pressed against the surface of the top roll. Later it was found that the angular velocity of the rolls decreased at the onset of rolling, so the velocity of rolling could not be determined accurately by that method. Therefore it was necessary to select an instrument with an output signal proportional to the angular velocity of the rolls, which could be recorded continuously. For this purpose, the shaft of a

precision D.C. tachogenerator was attached to the centre point of the free end of the top roll. The tachogenerator (Servotek) gave an output of 7V per 1000 rev/min with a linearity better than 0.1 %.

4.2.2. Light-activated switch.

To measure the exit velocity of the material emerging from the rolls, a light activated switch, placed on the exit table, and a digital timer were used. The light switch consisted of a photodiode box, two thermal shields and two coated bundles of optic fibres. The arrangement was designed specifically for this work and is shown in Fig.4.2.2 . The thermal shields, made of aluminium, served to protect the photodiodes from high temperatures. The light beams, which passed through the windows of the shields were then transmitted to the photodiodes via optic fibres, these latter excluded any spurious effects due to reflected light from the surroundings. The photodiode box encased two photodiodes, each with an integrated circuit including a resistor and a capacitor, to set the light switching threshold. When the light beam reaching window A was interrupted, the device triggered the digital timer which was only stopped when the light beam reaching window B was interrupted. Since the two windows were 50mm apart the time lapse between the two actions, i.e. start and stop, determined the mean exit velocity of the front end of a slab emerging from the rolls. As the front end of a rolled slab was too thin to effectively interrupt the light beam reaching the photodiodes, a refractory block placed on the exit table, was pushed by the slab as it emerged from the rolls. The greater size of this block ensured an effective interruption of the incident light beam. Due to lack of space between the mill stands, the light source could not be placed directly opposite the light activated switch and it was difficult to get sufficient incident light to trigger

the light switch. Therefore the light from a tungsten lamp was reflected to the light switch using a mirror placed opposite to it. The whole arrangement is shown in Fig. 4.2.2.

4.2.3 Temperature measurements.

During rolling, temperature changes within the material often take place in a fraction of a second. Thus, a first requirement of the temperature measurement technique employed during rolling is that thermocouples inserted in the material should respond rapidly to the changes in temperature. Bradley et al.⁽⁵⁴⁾ examined the effect of the wire diameter on the thermocouple response and also investigated the ability of different thermocouple materials to withstand high pressures. As a result of their work 1.5mm Pyrotanax Chromel-Alumel thermocouples were selected for the present investigation. These possessed a hot junction insulated in a stainless steel sheath and a response time of 0.24 sec⁽⁵⁵⁾ with a standard accuracy of $\pm \frac{3}{4}\%$ ⁽⁵⁶⁾. This represented a suitable compromise between response speed and mechanical strength. To allow the re-use of the thermocouples, the hot junction had to be re-welded. Hence the sheath insulation was filed off to expose the thermocouple wires, which were welded together to produce an exposed hot junction. A response time of about 0.12 secs.⁽⁵⁵⁾, better than that quoted for a thermocouple with an insulated junction, was to be expected in this case.

Preliminary temperature measurements on slabs 12.5mm thick were carried out with a thermocouple inserted in a hole drilled in such a position that the hot junction lay on both the mid-width and mid-thickness planes, at a distance of 50mm from the back end of the slab. A second thermocouple was located on the mid-width plane near the top surface of the slab. This arrangement, shown in Fig. 4.2.3, was used to establish

the effect on the mean temperature of the material of both the heat generated inside the material by the deformation process and the quenching produced when the slab surface was in contact with the rolls. These temperature measurements allowed the mean temperature of rolling to be estimated.

A further investigation, which involved the ^{determination} ~~definition~~ of the temperature distribution across the thickness of the material as it passed through the deformation zone, was carried out using slabs 19mm thick (See Sect. 4.7). Thermocouples were inserted in four positions between the surface and the mid-thickness of the slab with one thermocouple on, and a second just below, the surface, and with two further thermocouples towards the centre. All the hot junctions were located as close as possible to the mid-width plane. The arrangement is shown in Fig. 4.2.3. Each thermocouple on the surface and at the sub-surface position (1 and 2 respectively in Fig. 4.2.3) was inserted in a hole drilled at an angle so that the former broke the slab surface, while the latter reached a point about 0.2mm below. This whole arrangement permitted the measurement of temperature changes, which were produced by the combination of the heat of deformation and the quenching effect of the rolls, in different layers of the material. Later these temperature measurements were used to establish temperature distributions within the deformation zone.

Attempts to hold the thermocouples in place either with high temperature cement or by welding were not successful. Therefore, lengths of mild steel wire were wedged into each hole to prevent movement of the hot junctions of the thermocouples.

4.2.4 Load cells.

The roll forces developed in a rolling operation were measured by

means of load-cells placed between the screw-down ends and the upper chocks. Each load-cell consisted of a columnar element integrated with its base and fabricated of a high strength steel. The load-cells were fitted with strain-gauge bridges cemented to their columns. The top of each column, the height/diameter ratio of which was about 1.2, was covered by a self aligning cap: thus the effect of any uneven loading was virtually eliminated. The strain-gauge bridges were supplied with 6V D.C. and their output was fed to an U.V. recorder via D.C. amplifiers.

The load-cells were already calibrated at the the start of this work but during the experimental period two recalibrations were carried out. This included the removal of the load-cells from the mill after which they were loaded into an Avery-Denison testing machine, which was itself regularly calibrated. Forces up to 500kN in 50kN steps were applied in both increasing and decreasing loading cycles. A check for additive measurements was also effected by testing both load-cells simultaneously. Fig. 4.2.4 shows the calibration curves obtained in each case.

4.3. Determination of the rolling power and roll torque.

The total power consumed by the mill motor was determined from the simultaneous measurements of the voltage, V , and armature current I_a , supplied, thus:

$$\sqrt{I_a} - I_a^2 R_a = E_b I_a \quad (4.3.1)$$

where $\sqrt{I_a}$ represents the total power supplied to the mill

$I_a^2 R_a$ is the armature copper losses, manifested by the heating of the armature windings.

and $E_b I_a$ is the power developed on the shaft of the motor.

In order to measure the armature resistance R_a , connected in series with a coil in the circuit of the D.C. compound motor, the mill was run for about 45 minutes without any load. This permitted a steady temperature to be obtained. The mill was then stopped and the series and armature resistance measured while the windings of the motor were still warm. The value of the total resistance was $R_0 = 0.14 \pm 1\%$. (Ohms)

The total driving power (P_m) developed on the motor shaft during a rolling pass, is divided into the following components:-
(48)

Rolling power - P_w - Power which is required to overcome the resistance to deformation of the rolled stock and the frictional forces between the rolls and the material surfaces.

Frictional power - P_f - Power necessary to overcome additional frictional losses during the pass, produced in the roll neck bearings, pinions and reduction gear.

Idling power - P_i - Power necessary to overcome frictional losses along the drive under no load.

Dynamic power - P_d - Power necessary to overcome inertia forces arising from variations in roll velocity.

Thus, the equation which expresses the driving power developed during a rolling pass is,

$$P_M = E_b I_a = P_w + P_f + P_i + P_d \quad (4.3.2)$$

The first three values represent a constant load on the drive, and their sum forms the static power. The procedure followed to determine the components of the driving power - P_m - is described below.

4.3.1 Frictional power.

The power to overcome the additional frictional losses consisted

of:-

(i) The frictional losses in the roll neck bearings (P_{f_1}). The force exerted on each roll neck, assuming the slab is central with the rolls, is $F/2$ and the frictional force at each roll neck is therefore $f_1 F/2$. Since this force acts at a distance $d/2$ (roll neck diameter = 184.2mm) from the roll centres, the frictional torque at each roll neck is $f_1 Fd/4$ and the total torque on the mill is then $f_1 Fd$. Values of the coefficient of friction f_1 in fluid-film bearings⁽⁵⁷⁾ are quoted within the range $f_1 \approx 0.001 - 0.005$.

(ii) The frictional losses along the driving gear, i.e. in the gearbox and pinions.

The sum of the rolling and additional friction power developed at the motor shaft is given by⁽⁴⁸⁾:

$$P_w + P_f = \frac{P_w + P_{f_1}}{\eta_1 \eta_2 \dots \eta_n} \quad (4.3.3)$$

$$\text{where } P_{f_1} = f_1 F d W r \quad (4.3.4)$$

and η_i is the efficiency of individual gears positioned between the motor and rolls. Values of efficiency for single reduction gear transmission are quoted within the range⁽⁴⁸⁾ $\eta = 0.95$ to 0.98 .

Here it can be noted that experimental values of both frictional losses (P_f) and rolling power (P_w) cannot be determined separately. An experimental technique, which is described in Section 4.3.5 was, adopted to obtain the additional frictional losses.

4.3.2 Idling power.

The idling power was determined by the measurement of the armature current and voltage supplied to the mill motor when no load was applied. Thus using Eq. 4.3.1 the idling power would be given by:

$$P_i = \sqrt{1 - I_a^2} R_a$$

However, these voltage and current measurements can only be made before or after rolling, when the velocity of the rolls is about 20% higher than when a slab is present in the roll gap. From several power measurements at zero load at various speeds, it was established that the idling power was approximately proportional to the angular velocity of the rolls. Therefore, it was assumed that the effective idling power at rolling velocity was given by,

$$P_i' = \frac{w_R}{w_i} P_i$$

4.3.3. Dynamic power.

The dynamic power is significant when the velocity of the rolls changes rapidly during the acceleration or deceleration of the mill. In the present work it was found that the angular velocity of the rolls was practically constant during the rolling pass, as can be seen from typical traces shown in Fig. 5.6.1 from the tachogenerator, so that the dynamic power could be ignored.

Thus, the driving power at a constant rolling velocity and for static power is given by:-

$$P_m = P_w + P_f + P_i' \quad (4.3.2a)$$

(c.f. Eq. 4.3.2.)

4.3.4 Rolling power and roll torque.

In order to obtain an expression for the rolling power, reference is made to Eq. 4.3.2a which, after the introduction of Eq. 4.3.3 becomes,

$$P_m = \frac{P_w + P_{f1}}{\eta_0} + P_i'$$

and the rolling power and total roll torque would be

given respectively by, $P_w = (P_m - P_i') \eta_0 - P_{f1} \quad (4.3.5)$

$$T_w = \frac{L}{w_R} [(P_m - P_i') \eta_0 - P_{f1} d w_R] \quad (4.3.6)$$

4.3.5 Experimental determination of the frictional power under load.

Determination of the power produced by the mill was carried out with the rolls pressed together and rotating at low speed. This enabled an experimental determination to be made of the additional frictional losses along the drive under load, as conditions of zero rolling power were present. To avoid over-loading the electric motor which drove the screw-down gear, the rolls were pressed together using a lever attached to the screw-down system, which was temporarily detached from the electric drive. Then, with the rolling power term eliminated in Eq. 4.3.20 and Eq. 4.3.3 the following expression gave the power generated; viz

$$P_f = P_1/\eta_0 = P_m - P_r'$$

Re-arranging and introducing Eq. 4.3.4, the ratio between the coefficient of friction f_1 and the overall efficiency of the drive, can be obtained viz,

$$\frac{f_1}{\eta_0} = \frac{P_m - P_r'}{F d \omega r}$$

Experimental values of the above ratio f_1/η_0 were obtained with several values of the roll force and plotted in Fig. 4.3.5. The results indicate that the ratio f_1/η_0 was practically independent of the roll force. In Fig. 4.3.5 the broken lines represent several constant ratios of f_1/η_0 . These in turn were determined assuming that the overall efficiency of the mill drive, which consisted of a double reduction gear box and pinions, was $\eta_0 = (0.95)^3$, while the coefficient of friction f_1 was varied between the range $f = 0.003 - 0.005$. Thus a combination of $f_1 = 0.0045$ and $\eta_0 = 0.857$ would approach the mean value, about 0.006, of the experimental results. These values of f_1 and η_0 were considered suitable for use in the estimation of the additional frictional losses during a rolling pass.

4.4. Recording Instruments.

Ultra-violet light recorder.

The roll force measurements were registered on an ultra-violet light recorder, in which a U.V. light beam was directed onto a mirror attached to a moving coil galvanometer and then reflected via a lens and mirror system onto a moving light-sensitive paper, where the light beam generated a trace. The deflection of the galvanometer and hence the movement of the light beam was a function of the magnitude of the input signal. Recording speeds of up to 1000mm/sec. could be obtained with this system. In order to give an adequate response, the frequency of the galvanometer needed to be at least 20 times higher than the frequency of the input signal⁽⁵⁸⁾. Since it was estimated that the signals from the load-cells increased within 0.1 - 0.2 seconds while the material filled the roll gap, a peak frequency of 10Hz for the input signals was assumed. Therefore a galvanometer of not less than 200Hz was required. In addition, since the sensitivity of the galvanometer was inversely proportional to its frequency response⁽⁵⁸⁾, it was difficult to obtain simultaneously both adequate sensitivity and response. This limitation could only be overcome by the inclusion of an amplifier between the signal source and the galvanometer. Therefore, a D.C. amplifier with stepped gain was installed in each measuring circuit.

To calibrate each circuit, the amplifier was supplied with a known voltage, whose magnitude was equal to the output voltage given by the load-cell under forces of 250kN and 500kN respectively. These in turn were determined from the calibration curves given in Fig.4.2.4. Various combinations of amplifier gains and galvanometers were tested

until a full scale displacement of the signal on the trace paper was accomplished. As a result, two galvanometers of 500Hz frequency each (SM500) were combined with one of two gains in the amplifiers (X100 and X200), and a recording speed of 12mm/sec was selected to cover the range of roll force measurements at each rolling temperature.

Potentiometric pen recorder.

A potentiometric pen recorder was used to record the armature current supplied to the motor mill, the output from the tachogenerator, and the e.m.f. from the thermocouples placed inside the slab. These signals were fed into a four-channel Rikadenki pen-recorder, which possessed a 250mm(10") full scale deflection per channel. An attenuator switch in each channel gave 11 levels of sensitivity - 10mV to 20V, which could be combined with recording speeds of up to 10mm/sec. on the trace paper. The voltage of the input signal was measured by comparison with a reference voltage from a resetting potentiometer in each channel. The difference between these two voltages caused the servo-operated pen-arm to move until the voltages were equal. The armature current supplied to the motor was determined indirectly by means of the measurement of the voltage drop across a current shunt installed in the switch gear panel of the mill. The current/voltage ratio was 4.66A/mV. It was considered that the maximum e.m.f. of the thermocouples was 50mV which corresponded to a temperature of about 1200°C. The output of the tachogenerator was estimated to reach a maximum of 70mV that, according to the specifications, represented 50 rev/min; this was equivalent to a rolling velocity of 350mm/sec. Finally, armature currents of up to 400 amps were expected, as established by a few rolling trails. Thus, each channel in the recorder was set to give a full scale displacement per 100mV input signal. The servo-mechanism, which drove

the pen arm in each channel, possessed a resolution of $\pm 0.07\%$ and a linearity of $\pm 0.15\%$ of the level of sensitivity, in addition to an intrinsic error of less than $\pm 0.25\%$ and a band width from D.C. to 6-8Hz quoted for these potentiometric instruments⁽⁵⁷⁾. The voltage applied to the mill motor and measured by a voltmeter installed in the switch-gear panel was recorded on an XY plotter which consisted of potentiometric systems to drive both axes. The X axis was fixed as a time base, while the Y axis recorded the voltage regulation produced during a rolling operation. A full scale displacement per 100V input signal was found suitable for recording most voltage variations.

Tape Recorder.

In the preliminary work on temperature measurements (Sect.4.2.3), the e.m.f. of the thermocouples was recorded on the potentiometric recorder already described. Later it was found that the response of this instrument did not permit an adequate record of the rapid temperature changes produced in the material inside the deformation zone. Therefore a device with fast response characteristics was required. Thus the temperature changes were recorded on a high speed tape recorder and then played back at low speed, which allowed the signals to be accurately traced on an XY plotter. The tape recorder (Racal thermionic) used a frequency modulation recording process, in which a carrier frequency was modulated by the input signal. On playback the resulting magnetic pattern stored on the tape was translated into the original input signal, via a filter which removed the carrier frequency. A four-track head installed in the instrument permitted simultaneous recordings of the e.m.f. of four thermocouples inserted in a slab. The band-width frequency response ranged between D.C. and 20kHz, with a signal to noise ratio of ± 48 dB at maximum tape speed. Seven tape

M

MECHANICAL & PRODUCTION ENGINEERING

USEFUL CLASS NUMBERS

Accountancy	657
Resistives	620.199
Automatic control engineering	629.8
/CAM	620.0042
Computer control	629.895
Sign	620.0042
Composites	620.104
Fluids	620.1064
Economics	330
Engineering	620-629
Factory operation	670.42
Queue	620.1123
Flexible manufacturing systems	670.427
Structure	620.1126
Thermodynamics	621.4
Pneumatic power	621.2
Thermodynamics	340
Machine theory	621.8

Management	658
Marketing	658.8
Materials	658.7
Production	658.5
Quality control	658.56
Manufacturing	670
Materials properties	620.112
Mathematics	510
Mechanics	620.1
Fluids	620.106
Metrology	
Engineering	620.004
General	389
Microprocessors	004.16
Noise	620.2
Nuclear engineering	621.48
Numerical control	621.902
Operational research	003
Physics	
General	530
Applied	621
Pneumatic engineering	621.5
Robotics	629.892
Steam engineering	621.1
Strain/stress	620.112
Elasticity	620.112
Plasticity	620.112
Structural theory	624.17
Technical drawing	604.2
Thermodynamics	621.402
Tools	621.9
Tribology	621.89
Vibration	620.3

speeds were available, from 2.38 cm/sec. up to 152.4 cm/sec. A twelve position attenuator knob in each channel was used to select the sensitivity in volts between 0.1 V. and 20 V. Thus a maximum recording speed of 152.4 cm/sec. and playback speeds of 20 cm/sec. and 2.38 cm/sec. were selected, together with a sensitivity up to 0.1 V, as the maximum e.m.f. expected from the thermocouples was 50 mV.

4.5. Reheating Furnaces.

Two types of electric furnaces were used to heat the plates prior to rolling: a muffle furnace with an embedded heating element, and two furnaces with silicon carbide elements. The first furnace, rated at 2.9 K.V.A., possessed a wire element wound along the length of the external surfaces of the chamber and embedded in a refractory cement to give rapid heating response. A Pt/Pt/13% Rh thermocouple was placed at the back of the chamber roof and together with an automatic controller with proportional action assured a temperature fluctuation of approximately 5°C. at 1000°C. The maximum working temperature was 1200°C. The chamber dimensions were 35.5 cm x 17.8 cm x 12.7 cm. The furnace with silicon carbide elements could be used at temperatures of up to 1400°C. with a power rating of 5.75 kW. The chamber was 45 cm x 18 cm x 17 cm and the heating elements were mounted transversely across the roof of the chamber. Again a Pt/Pt/13% Rh thermocouple and a proportional controller were used to control the furnace temperature. Later a second silicon carbide furnace with a power rating of 16.6 K.V.A. and chamber dimensions of 120 cm x 20 cm x 15 cm, was installed in the deformation laboratory. The heating chamber was divided into three zones. The power input of each zone was regulated by a thyristor capable of carrying a current of up to 40 amps. A controller with proportional action assured an homogeneous temperature along the chamber,

though manual control of the power drive in each thyristor could be used to minimize temperature gradients between zones. Thus, the furnace was capable of operating at temperatures of up to 1300°C with rapid response to temperature fluctuations along its chamber during charging and discharging operations.

4.6. Cam plastometer.

In order to obtain information about the relationship between temperature, strain rate and the flow stress of the material undergoing deformation, hot compression tests were carried out on cylindrical specimens 12.5 mm high x 7.5 mm in diameter, using a cam plastometer. The temperatures and strain rates used were close to those accomplished during the experimental rolling schedules (see Sect. 4.7). The data obtained was compared with published results that related to similar material and conditions^(36,37). This data allowed the mathematical model used in this work to calculate the yield stress of the deforming material. The cam plastometer, designed and built in the Department of Mechanical and Production Engineering at Sheffield Polytechnic, was essentially a cam-driven compression machine which operated at a constant strain rate. In Fig. 4.6. the cams (1)(2), which could impart two ranges of strain rate, were mounted on a cam shaft (6) which was supported by ball and roller bearings in a main frame (12). Power to rotate the cam shaft was derived from a heavy flywheel (4) which was belt driven by a 1.5 kW electric motor. An eccentric plate clutch mechanism transmitted the rotation of the flywheel to the cam shaft. The rotational motion of the cams was converted into the vertical movement of a piston by means of a cam follower which was mounted in a spring-loaded guide block (8). The downwards movement of the piston was transmitted to the cylindrical specimen through the upper moving

platen of a detachable die assembly.

The die assembly (9) was mounted on an adjustable spacer which rested on a load cell (13). The die assembly (Fig. 4.6.) consisted of a moving upper platen and a fixed lower platen, between which the specimen was axi-symmetrically compressed, and two cylindrical casings, separated by an air gap. These components were made of a Nimonic alloy. The complete die assembly was heated to the required temperature using a 2.9 kW muffle furnace. Thus, the arrangement minimised the heat losses of the specimen during its transfer from the furnace to the cam plastometer.

4.6.1 Cam design.

The surfaces of the cams originally installed in the plastometer were flattened, so that it was necessary to design a new set made from a high strength steel. First an estimation was made of the compression force required to accomplish a 50% deformation in 7.5 mm diameter x 12.5 mm high mild steel specimens at 900°C and 40 s⁻¹ strain rate under unlubricated conditions. Then a balance of forces acting between the cam and the follower was made to calculate the contact stresses developed between the surfaces of the cam and roller follower. This showed that the compressive stress applied on the surface of the cam would be of the order of 1365 N/mm² (90 ton/in²). Thus an EN 24 steel was selected, which had a quoted 0.2% proof yield stress of 1544 N/mm² (100 ton/in²) after heat treatment. This steel could be cut in the annealed condition as supplied, then hardened and tempered.

The profile of the cams was such that the specimen of an initial height h_0 , could be deformed at a constant true strain rate, i.e.

$$\ln h_0/h = \dot{\epsilon}t$$

If a cam has a basic circle of radius r_0 , and if the cam radius

changes to the value r_θ for a rotation θ , then it can be shown that the profile of the cam is defined by:

$$r_\theta = r_0 + h (1 - \exp(-\dot{\epsilon}\theta/w)) \quad (4.6.1)$$

where w was the angular velocity of the cam. If the cam was intended to impart a total strain rate $\dot{\epsilon}$ and the cam lift occurred over an arc θ_T , then $\dot{\epsilon} = \dot{\epsilon} w / \theta_T$

Therefore it was possible to vary the strain rate of the deforming specimens by variation of w and/or θ_T . Eq. 4.6.1 was used to determine the profiles of two cams with a different lift angle (θ_T) which would then impart two different strain rates during the rotation of the cams at a constant angular velocity. Thus, the set consisted of two cams with a maximum lift of 6.35 mm each produced by rotation of the cams through 48° and 25° respectively (Fig. 4.6.1).

The heat treatment of each cam involved heating to and holding at $830/850^\circ\text{C}$, followed by oil quenching and then tempering at 150°C . A hardness test on the surface gave the following values:-

		V.P.N.
Cam 1	$\theta_T = 49^\circ$	537 - 425
Cam 2	$\theta_T = 25^\circ$	570 - 505

A slight distortion was induced by this heat treatment. To partially correct this distortion the cams were ground only in the basic circle surfaces to a tolerance of ± 0.025 mm. However no grinding was attempted in the lobe of the cams. Later the actual strain rate characteristics of the cams when mounted in the shaft showed fluctuations during a hot compression test of $\pm 14\%$ of the nominal strain rate.

4.6.2 Instrumentation of the cam plastometer.

The stress load applied to a specimen during a hot compression

test was determined by means of a load cell placed under the die assembly. The load cell consisted of a steel column fitted with a network of strain gauges. These gauges were connected to a bridge, the output from which was fed into one channel of an ultraviolet recorder via a D.C. amplifier. The load cell was calibrated to a maximum of 50 kN and the load range of a recording could be conveniently changed by alteration of the amplifier gain. Compression strain was determined from the vertical displacement of a linear potentiometer attached to the piston of the cam follower. The output from the potentiometer was fed to a second channel in the ultraviolet recorder. To calibrate the linear potentiometer a dial indicator was placed under the piston of the cam follower, and the cam shaft was rotated manually. Thus, at each increment of 0.5 mm in the dial indicator, a recording of the output of the linear potentiometer was made. Calibration graphs of both the load cell and the linear potentiometer are shown in Fig 4.6.2. Elastic distortion of the cam plastometer must be considered in order to calculate the actual compressive strain. Such distortion was measured by compressing a specimen made of a high speed steel using a long lever attached to the flywheel. Since no plastic and negligible elastic deformation of the specimen was likely to occur, the output of the linear potentiometer was a measure of the elastic deformation of the frame of the cam plastometer under load. Fig. 4.6.2 shows the results obtained. The temperature of the specimen prior to compression was measured by means of a Chromel-Alumel thermocouple placed between the specimen and the lower platen of the die assembly. A clutch mechanism allowed the cam shaft to be engaged to the flywheel, when this was rotating at the test speed, so the compression of the specimen could be effected within a few seconds of withdrawal of the die assembly from the furnace.

4.7 Rolling Programme.

Initially, slabs 12.7 mm thick were rolled at nominal temperatures between 850°C and 950°C with percentage reductions in single passes of approximately 35% and mean strain rates of 2.5 per second. These tests enabled roll force and torque, amount of forward slip and temperatures inside the deforming material to be measured. Such preliminary results serve both: to provide experimental data relevant to the hot rolling conditions, and to correlate measured roll force and torque with the corresponding theoretical results given by the mathematical model developed in this work. In addition, a rolling test was carried out in quadruplicate at 1000°C and 40% reduction, in order to check the repeatability of the measurements of current and voltage supplied to the mill.

The preliminary work was conducted within a narrow range of temperatures, hence a rolling programme was subsequently prepared so that a wide range of temperatures, percentage reduction, and frictional conditions could be covered. The programme was divided into three series of experiments as described below.

Series A.

This series of experiments aimed to test the validity of the present mathematical model to predict values of roll force and torque measured over the range of temperatures covered by commercial hot rolling schedules. The experiments involved the rolling of mild steel plates under the following conditions:

Rolling temperatures (°C)	900, 1000, 1100 and 1200
Reduction during a single pass (%)	10, 20, 30, 40 and 45
Slab thickness at entry to the rolls (mm)	19.5 and 12.7
Average strain rates within the range 0.8 - 3.0 per second, were	

selected as a reasonable compromise between rolling velocities low enough for safe manual handling and rolling times short enough to avoid excessive cooling of the ingoing material. The experiments were carried out under unlubricated conditions and the plates were heated without any protective gas inside the furnace. This introduced variations in the quantity of surface scale formed on the plates. Since it had been concluded by El Kalay et al. (16) that changes in the quantity of scale were liable to cause variations in the frictional conditions, an experimental technique was developed to measure the amount of forward slip produced during every rolling operation in order to establish the associated coefficient of friction.

Series B.

Measurements of the amount of forward slip were carried out in this series in order to establish the validity of the forward slip method of determining the coefficient of friction under various percentage reductions and frictional conditions. The tests were carried out using rolling passes in triplicate and the plates were hot rolled using both: slightly lubricated and dry roll surfaces. To obtain lubricated conditions the surfaces of the rolls were oiled prior to rolling; while dry rolling conditions were produced by cleaning the roll surfaces thoroughly with carbon tetrachloride.

Series C.

The limited programme of temperature measurements carried out in series A was extended in this series, so that a more accurate estimation of the effective temperature of rolling could be made. Four thermocouples were inserted between the surface and centre of plates 19 mm thick which were hot rolled at temperatures between 800°C and 1100°C with percentage reductions within the range 10 - 40 %. Thus,

simultaneous temperature recordings could be made at several points inside the material while it lay within the rolls.

4.7.1 The condition, composition and dimension of the plates.

The plates used in the preliminary rolling tests and in experimental series A and C, were prepared from EN 2 bright drawn, mild steel plates with a dimensional tolerance, as supplied, of ± 0.125 mm. The mean composition of the steel, determined from a U.V.A.Q. analysis of three samples, was as follows:

C	Mn	Si	S	P	
0.17	0.79	0.21	0.036	0.010	(%mass)

A strip 12.7 mm thick and 100 mm wide was sawn into pieces 250 mm long to prepare the slabs used in experimental series A. The section of the plates was selected so that a width/thickness ratio of at least 8 was obtained. This ensured plane strain conditions during deformation across most of the width, and gave enough space to insert two thermocouples between the centre and the surface of the plate. A strip 19 mm thick and 200 mm wide was chosen for the experimental series C so that various thermocouples could be accommodated across the section of each plate. The width of the plates was limited to 150 mm in order to avoid overloading of the roll neck bearings during high percentage reductions and a length of 250 mm assured safe manual handling. The plates used in the experimental series B were prepared from slabs supplied in the as hot rolled condition, with a surface roughness of 5 - 20 μ m C.L.A. (190 - 790 μ in), which ensured high frictional conditions. The plates, available in two thicknesses, 16 mm and 9.5 mm, were cut into pieces 100 mm wide and 150 mm long.

4.7.2 Re-heating and rolling.

In the preliminary rolling tests, one or two plates were rolled in each operation, while in the subsequent series A and B four or five plates were prepared to be hot rolled in single passes at each temperature. These plates were re-heated in either a 2.9 kW muffle furnace or a 5.75 kW furnace with silicon carbide elements, and thermocouples inserted in two of these plates enabled a nominal rolling temperature throughout each operation to be established. In the experimental series C, two plates were deformed in single passes with reductions between 20 and 40% at each temperature and using a 16.6 kW furnace. Heating times of about 60 mins. were chosen to give a near uniform temperature distribution across the thickness of the plates, and to minimise the amount of surface scale formed. Temperature differences between the centre and surface of the plates were over a range of 30 - 40°C. During the re-heating period the roll surfaces were cleaned and the roll gap set to the required value. The mill was started 15 mins. before rolling commenced, which allowed the mill motor to warm up and the roll velocity to be set. At the end of the heating period the plates were transferred to the rolls in succession and alignment on the access table was completed within a few seconds of removal from the furnace. After which rolling was immediately carried out. The surface of the access table was insulated so as to prevent an excessive cooling of the plates before rolling. Throughout each rolling operation the angular velocity of the rolls was kept constant and the roll gap was re-set after each reduction.

The roll gap required to accomplish each nominal percentage reduction was calculated by,

$$h_0 = h_1(1 + \Delta l)(1 - r) - P/M$$

The total roll force, P, was estimated from preliminary results at various percentage reductions, while the mill spring - $M=1.15 \text{ MN/mm}$ was already determined at the start of this work. The correction for thermal expansion Δl is about 0.014 in low C steel⁽⁵⁹⁾ for the temperature range 900 - 1200 °C.

4.8. Determination of the coefficient of friction.

Values of the coefficient of friction during hot rolling were obtained through measurements of the amount of forward slip. These were calculated by simultaneous measurements of the exit velocity of the rolled material and the peripheral velocity of the rolls using the following expression,

$$\Phi = \frac{v_2 - v_r}{v_r} \quad (4.8.1)$$

A relationship between the amount of forward slip and the coefficient of friction could be derived. Thus, assuming constancy of volume, vertical cross sections during deformation and no lateral spread, then,

$$v_r = v_n = v_2 h_2 / h_n \cos \theta_n$$

and $h_n = h_2 + R \theta_n^2$ for small angles of contact.

Therefore, after rearrangement, Eq. 4.8.1 can be written as,

$$\Phi = \frac{h_n \cos \theta_n - h_2}{h_2} \approx \frac{R \theta_n^2}{h_2} \quad (4.8.1a)$$

Ekelund⁽⁶⁾ showed that the neutral angle could be approximated to,

$$\theta_n = \frac{\theta_1}{2} - \frac{1}{\mu} \left(\frac{\theta_1}{2} \right)^2 \quad (4.8.2)$$

This expression was obtained under the assumption that the roll pressure distribution was uniform along the arc of contact and that the coefficient of friction was constant. It can be shown, after combining Eqs. 4.8.1a and 4.8.2, that the amount of forward slip is given by,

$$\Phi = \frac{r}{4(1-r)} \left(1 - \frac{\theta}{2\mu} \right)^2 \quad (4.8.3)$$

Eq. 4.8.3 was used to calculate the relationship between the percentage forward slip and the coefficient of friction at specified

values of percentage reduction (r) and R/h_1 ratio, as shown in Figs.

4.8.1 a,b,c,d. Here the effect of roll flattening at each percentage reduction was estimated in order to obtain a realistic value of the angle of contact. It can be seen in the above Figs. that at any value of forward slip two values of μ are obtained. This is obviously impossible in physical terms, so it has been assumed that only the upper value of μ is significant in the case of hot rolling.

4.9. Hot compression tests.

In order to carry out hot compression tests in the cam plastometer, each mild steel specimen, placed inside the die assembly, was heated up to a temperature within the range 900 - 1100°C. It was estimated that a heating period of 15 - 20 mins. was sufficient time for the 12.5 mm x 7.5 mm cylindrical specimens to reach a homogeneous temperature. A thermocouple in contact with the specimen measured its surface temperature. During the heating period, the fly-wheel was set to a selected test speed. Since low angular velocities - < 30 rev/min. - introduced marked fluctuations in the fly-wheel velocity and on occasions it stalled during a compression, the tests were carried out at such velocities as to impart strain rates within a range of 3 - 10 per second. The transfer to and setting of the die assembly in the cam plastometer was followed immediately by the compression of the specimen; the total operation lasted a few seconds. The recorded values of the force and amount of deformation accomplished, were used to determine the variation of the yield stress of the material with strain at a constant strain rate and temperature. It was assumed that homogeneous deformation applied.

To achieve true homogeneous deformation it would be necessary to completely eliminate friction between the platens and the specimen

so preventing barrelling during compression. Cook⁽³⁷⁾ and Alder et al⁽³⁸⁾ tested different types of glass at high temperatures to determine the effectiveness of this as a lubricant in minimising barrelling during compression, and found that different compositions of glass were suitable within specific temperature ranges. Thus, in the present test an approach to homogeneous compression was made by the application of glass powder to both ends of the specimen prior to heating. Lubrication with a glass of composition 70% SiO₂, 13.5% Na₂O, 9.17% CaO produced only a very slight barrelling of the specimen so that it was assumed that the coefficient of friction between the platens and specimen surfaces was very low.

5. Experimental Results.

5.1 Introduction.

Experimentally determined values of roll force and roll torque were obtained using a wide range of hot rolling conditions. Simultaneously, measurements were made of the temperature distributions inside the material and of the amount of forward slip. The latter measurements were used to determine the mean coefficient of friction during rolling. Comparisons were then made with the corresponding values of roll force and roll torque calculated by the mathematical model described in Section 3. These comparisons served to establish the validity of the model in the hot rolling practice. In addition, a limited amount of yield stress data about the steel undergoing deformation was determined using a cam plastometer to conduct hot compression tests on cylindrical specimens.

5.2. Roll Force Measurements.

The total roll force developed during a rolling operation was obtained by the summation of the forces acting on the load cells placed between the screw-down ends and the upper chocks of the mill. Fig. 5.2 shows a typical recording of the output of the load cells, obtained in a rolling experiment at 900 °C that produced a 30% reduction. Strictly, the roll force measured by the load cells should be corrected by the addition of the weight of the top roll of about 2 kN.

Since the slabs had to be aligned off centre due to the position of the light-activated switch on the exit table, a difference between the forces acting on each load cell was produced, as can be seen in Fig. 5.2. Here it can also be noted that the roll force increased during the rolling operation, possibly due to the increase in work-hardening as the ingoing material cooled down. Mean values of roll force measured in the preliminary rolling experiments are presented

in Table 1 together with the relevant rolling parameters determined in each test. Figs. 5.2.1 - 5.2.4 show mean values of the roll force measurements obtained in each rolling test of the experimental Series A. These values were plotted against the percentage reductions for each of the nominal temperatures investigated. The percentage reduction in each pass was calculated from the mean initial and final thickness of the slab. These mean values were determined from measurements taken at various points along the width and length of each plate, using a micrometer with a tolerance of ± 0.005 mm. The slabs were measured at room temperature due to the difficulties of making such measurements at elevated temperatures. The measurements were then corrected to take the thermal expansion into account. This mean correcting factor is shown in Section 4.7.2 for temperatures between 900°C - 1200°C. The nominal temperature of each set of rolling tests was taken as the mean value of the measurements given by two thermocouples inserted near the surface and at the centre of the first plate in each set of tests (see Sect.4.2.3). The relevant rolling parameters for each nominal temperature are given in Table 1.

In Fig. 5.2.1 , where the results obtained at 900°C are shown, it is apparent that the roll force increased rapidly as the percentage reduction increased. In Figs. 5.2.2. - 5.2.4 , however, where the results at higher temperatures are plotted, it can be seen that the slope of the graph showing the relationship between roll force and percentage reduction became smaller as the nominal temperature was increased. Furthermore, it is evident that in general, an increase in the rolling temperature produced a decrease in the roll force at a given percentage reduction.

5.3 Roll Torque Measurements.

The total torque developed during a rolling operation was determined from simultaneous measurements of the angular velocity of the rolls and the current and voltage supplied to the mill. These measurements were used in the method described in Sect.4.3 to determine the rolling power and roll torque. Fig.5.3.1 shows instantaneous recordings of the voltage, current and angular velocity of the rolls during a test conducted at a nominal temperature of 900°C and 40% reduction; while in Fig.5.3.1a the corresponding values of the calculated input power are plotted. Here it can be seen that the input power increased during the rolling operation. This could be associated with the increase of work-hardening of the ingoing material as it cooled down. In Table 1 are the mean values of the roll torque obtained in the preliminary work. Figs.5.3.2 - 5.3.5 show mean values of the roll torque measured in the tests conducted in the experimental series A. These results were plotted against the percentage reduction at the corresponding nominal temperatures. It can be seen in Fig.5.3.2 that at 900°C the measured values of roll torque increased rapidly as the percentage reduction was increased, corresponding to the increase in pressure observed in the measurements of roll force (Fig. 5.2.1). The values of roll torque measured at 1000°C and 1100°C rose smoothly as the percentage reduction was increased; while at 1200°C (Fig.5.2.5) the rate of increase of the torque with the percentage reduction was significant, as opposed to the less rapid increase observed in the corresponding values of roll force (Fig.5.1.4). Although an increase in temperature produced a decrease in roll pressure, as indicated by the roll force measurements, the values of roll torque at 1000°C were very similar to those obtained at 900°C. This could be associated with the greater entry thickness used at the higher temperature.

5.4 Determination of the coefficient of friction during rolling.

Measurements of the forward slip were used to establish values of the coefficient of friction during rolling. The amount of forward slip was given by the difference between the exit velocity of the rolled material and the peripheral velocity of the rolls, expressed as a percentage of the latter. A tachogenerator coupled to the top roll permitted the velocity of the rolls to be determined. A typical trace is shown in Fig. 5.3.1. The velocity of the emerging plate was measured by means of a light activated switch placed on the exit table. The velocities of the rolls and the emerging plates measured in the experiments of series A, together with the associated values of forward slip, are presented in Table 1 for each of the rolling temperatures used. In Figs. 5.4.2 - 5.4.5 the values of forward slip are plotted against the amount of reduction. It can be seen that the general level of the forward slip decreased as the rolling temperature was increased from 1000°C to 1200°C (Figs. 5.4.3 - 5.4.5).

The measurements obtained in experimental series B using both lubricated and dry rolls are plotted in Figs. 5.4.6 and 5.4.7 respectively. These results indicated that, as the amount of deformation increased, the values of forward slip, using dry rolls, became higher than those produced with lubricated rolls. In addition, it can be seen that these tests, carried out in triplicate, gave scattered results at a given amount of deformation. This would suggest that the reproducibility of frictional conditions was difficult to attain. The values of the coefficient of friction for experimental series A, determined from the measurements of forward slip, and using the method described in Sect. 4.3, are presented in Table 1 .

5.5 Temperature measurements during rolling.

Temperature measurements allowed an estimate of the mean temperature of rolling to be made, so that the appropriate yield stress data could be used.

Preliminary measurements of temperature were obtained using thermocouples inserted at the centre and 2mm, initially, beneath the surface of plates 12.5mm thick. Figs. 5.5.1 - 5.5.3 show the temperature changes in the material during rolling processes at percentage reductions within the range of 18 - 45%. It can be seen that the centre of the slab underwent a temperature rise on entry to the rolls, due to the generation of heat that accompanied deformation. This temperature rise increased as the amount of deformation and strain rate were increased. At the same time, the material close to the surfaces underwent either a small rise or a significant drop in temperature. The quenching effect of the rolls could account for the drop in temperature. As a result, on exit from the rolls, there was a steep temperature gradient through the thickness of the slab. Subsequently, heat flowed from the centre to the surfaces of the material until an even temperature distribution was re-established. This is shown in Figs. 5.5.1 - 5.5.3 by a rapid decrease from the peak temperature at the centre and a corresponding increase at points close to the surface. Once the steep temperature gradient disappeared, it can be seen that thermal steady state conditions were attained.

The relatively slow response time of the potentiometric recorder, used in this preliminary work, meant that temperature changes in the material within the deformation zone could not be measured accurately. Furthermore, the thickness of the plates used did not allow several thermocouples to be accommodated for multiple measurements to be taken

simultaneously during the time of contact. Hence, this preliminary work led to the development of an improved experimental method, by which temperature variations inside the material could be more accurately determined.

The experiments included in series C involve the use of a fast response tape recorder, which recorded the temperature measurements at four points between the surface and the centre and in the mid-width plane of slabs 19mm thick (see Sect. 4.2.3). The strain rates and temperatures used were within the ranges covered by the experimental series A. Thus, the results obtained could be used both to explain the temperature changes observed previously in series A, and to attempt a more accurate estimation of the actual temperature of rolling.

Fig. 5.5.4 shows a typical recording from an insulated thermocouple inserted in the slab; the 'cycling' in the e.m.f. was attributed to the surrounding power supply, the effect of which could not be eliminated. Thus, the results presented were mean lines drawn through these ripples. Figs. 5.5.6a & 5.5.6b show the temperature changes inside the material, as measured by insulated thermocouples, using percentage reductions of between 10% and 40% and mean temperatures at entry within the range 320°C - 1900°C. The initial depth of the thermocouples beneath the surface of the plate is indicated in the above figures

A voltage interference in the e.m.f. of the re-welded thermocouples, indicated by an abrupt change in the voltage, occurred once the slab was in contact with the rolls. An electrostatic screening was attempted by earthing the stands of the mill, but without success. Hence, the recordings were corrected as indicated in Fig. 5.5.5. Figs. 5.5.7, a, b, c, d, show the temperature measured by re-welded thermocouples using percentages of reduction between 15% and 40%, and mean temperatures at

entry within the range of 900°C - 1050°C .

It can be seen from Figs. 5.5.7b and 5.5.7c that, at the same percentage reduction the temperature rise towards the centre of the slab was higher as the entry temperature was decreased. This would be associated with an increase in work-hardening, as the temperature fell, so that the energy of deformation increased. Alternatively, it can be seen in Figs. 5.5.7a and 5.5.7d that an increase in the amount of deformation produced only a small increase of the temperature rise. At positions closer to the surfaces, smaller temperature rises occurred, as the quenching effect of the rolls offset the heat due to deformation. On the contact surfaces a rapid quenching took place. The steep temperature gradient was eliminated within 1 - 2 seconds of the material emerging from the rolls.

5.6 Yield stress data of the material undergoing rolling.

A limited number of hot compression tests on cylindrical specimens of the rolling material was conducted using the cam plastometer. The experimental results enabled the yield stress of the material to be determined. The deforming load applied to the specimen throughout the compression was measured by means of a load cell placed under the bottom platen of the plastometer. The vertical displacement of the top platen was determined by means of a linear potentiometer. Typical traces of the load/time and displacement/time are shown in Fig. 5.6.1. The ripples seen in the load/time trace were associated with the combined effect of work-hardening and thermal softening,⁽³⁸⁾ whereas the unevenness in the displacement/time trace may suggest that vibrations occurred in the main frame during compression.

The method of obtaining yield stress and strain values from the experimental data was as follows. In each load/time trace ten equally spaced positions were marked. The deflection associated with each of these positions was then measured and converted into load values by means of the calibration curve of the load cell. By a similar procedure the corresponding deflections in the displacement/time trace were converted into vertical displacements of the top platen which, together with an allowance for elastic distortion of the machine, (dependent on the instantaneous value of the deforming load) enabled the specimen height to be calculated at each position. Following these calculations, the true strain and cross-sectional area of the specimen were determined together with the associated uniaxial stress applied. The instantaneous strain rate was computed by dividing the increment in strain between two consecutive moments by the associated time interval. While the nominal strain rate was given by the total strain

divided by the overall period of compression. The values of true stress strain established in this manner for the temperatures and strain rates investigated are drawn in Figs. 5.6.2 - 5.6.5.

A noticeable feature of the data was the drop of yield stress at high strains. It was attributed to the predominance of thermal softening over strain hardening as compression proceeded^(37,38). It was found that the experimental true stress strain data gave reasonable fit, over the strain of interest ($\epsilon=0.5$) with an empirical equation of the form: $\delta = K\epsilon^m$

The experimental data was fitted to the above equation using a least-squares method. The experimental points, the empirical curves, and the corresponding variances of fit of the equation are shown in Figs. 5.6.2 - 5.6.3.

Strictly, a constant rate of compression could not be attained. Fluctuations of about $\pm 14\%$ of the value of the nominal strain rate usually occurred during a compression and, on occasions the initial strain rate was 60 -70% higher than the nominal value. The instantaneous values of strain rate in each test are also included in Fig. 5.6.2 a-b. 6.9. It can be seen in Figs. 5.6.2 a-b 5.6.3 that the strain rate history during deformation in two tests conducted at a similar compression speed, had a significant effect on the yield stress characteristics of the material.

6. Calculated Results.

6.1. The magnitude of the mechanical properties and rolling conditions used in the calculation of roll force and torque.

The basic Von Karman equation⁽¹⁾ related the roll pressure within the arc of contact to the position at which this pressure is applied. This enabled the mathematical model proposed in this work to calculate the specific roll force and torque required to accomplish a rolling operation at given conditions. The roll pressure itself was determined by the yield stress of the material, the frictional shear between the roll and the material surfaces and the distribution of the stresses through the thickness of the material (degree of inhomogeneity of the deformation). In addition, the yield stress of the material was dependent on the strain, strain-rate and temperature. Thus, the ability of this mathematical model to predict the values of roll force and torque developed during the hot rolling process, relied upon the selection of the experimental data which could approach the actual conditions existing during deformation. Such data comprised: the entry and exit thickness of the material, velocity of rolling, temperature of rolling, coefficient of friction and distribution of yield stress within the deformation zone.

The above parameters were determined from measurements taken under actual rolling conditions, and published data on yield stress was verified by means of hot compression tests on specimens of the material undergoing deformation. However, considerable uncertainty existed as to:

the coefficient of friction, a most important factor in hot rolling, estimated using an approximate method (See Sect. 4.5)

the distribution of the yield stress due to a non-uniform temperature of the material within

the deformation zone.

the degree of the inhomogeneity of the deformation. Shearing through the material thickness was indicated by the barrelling of the rolled plates.

the distribution of the roll pressure across the width of the material, as plane strain conditions do not exist towards the edges of a plate.

The mathematical model developed in this work permitted the effect of the material properties and rolling conditions on the calculated values of roll force and torque to be studied.

6.2. Effect of the coefficient of friction on roll force.

In order to cover a wide range of rolling conditions, values of the specific roll force were calculated using the conditions under which the tests of series A were conducted. In the hot rolling of steel, the state of friction is considered to be a mixture of slipping and sticking conditions^(16,17), though some theories of hot rolling were based upon the assumption of sticking friction only. Sticking friction is produced at an interface when the shear stress reaches the shear yield stress of the material i.e $\tau = k$, and since the pressure of deformation cannot be less than the uniaxial yield stress of the material, sticking friction is said to occur when the coefficient of friction is $\mu = 0.567$. Thus, in order to cover most frictional conditions μ was selected within the range of 0.2 - 0.6. The study was conducted assuming both homogeneous and inhomogeneous deformation, and using both published flow stress data and the data from the material undergoing rolling, as follows:-

i. Homogeneous deformation and published flow stress data.

Figs. 6.2.1 - 6.2.4 show calculated values of a specific roll force assuming homogeneous deformation and using the flow stress data given by Suzuki et al. (36). The results are plotted against the percentage reductions accomplished at each of the rolling temperatures selected in series A. In Fig. 6.2.1 it can be seen that at a given value of the coefficient of friction and temperature, the specific roll force rose as the percentage reduction was increased. This was related to the lengthening of the arc of contact. Furthermore, at a given velocity of rolling, the mean strain rate increased with the amount of deformation causing an increase in the yield stress. In Fig. 6.2.1 it can also be seen that, up to an intermediate value of the coefficient of friction, a proportional increase in the roll force occurred as the coefficient of friction increased. However, higher values of the coefficient of friction produced only a further slight increase in the roll force.

In Fig. 6.2.2 the results obtained, using the rolling conditions at 1000°C, show a general increase of roll force with percentage reduction, though the magnitude of the results was lower than that obtained at 900°C. This was associated with the reduction of the yield stress as the temperature increased. It can also be observed that using values of friction higher than 0.2 the proportional increase of roll force to the amount of deformation was less steep than the corresponding increase at 900°C. At lower values of μ the rate of increase in both cases was similar.

In Figs. 6.2.1 - 6.2.2 the rolling process involved slipping friction only in any case below the line a - a. This line was found by establishing the values of μ , at a given amount of deformation, that initiated sticking conditions along the arc of contact. Between lines

a - a and b - b mixed frictional conditions were involved during rolling. Line b - b was found after determining those values of the coefficient of friction which produced total sticking conditions.

In Figs. 6.2.3 and 6.2.4 the results obtained at 1100°C and 1200°C showed that the values of roll force were proportional to the percentage reduction and that the magnitude of the effect decreased as the temperature was increased. It can also be seen, particularly in the results obtained at 1200°C, that an increase in the coefficient of friction produced only a slight increase in the values of the roll force. This indicated that as the temperature was increased the values of roll force were less affected by a change in the frictional conditions.

ii. Homogeneous deformation and flow stress data of the material undergoing rolling.

Figs. 6.2.5 and 6.2.6 show the re-calculated values of roll force using the flow stress data obtained from the hot compression tests on samples of the material used in the experiments. The results are plotted against the percentage reduction obtained at each of the rolling temperatures of series A. It can be seen that the roll force increased as the percentage reduction was increased, though at a given amount of deformation these results were slightly lower than those obtained using published flow stress data related to a similar steel composition (Figs. 6.2.1, 6.2.2).

iii. Inhomogeneous deformation and published yield stress data.

During inhomogeneous deformation the distribution of stresses through the thickness of the material causes initial vertical planes to warp as deformation proceeds. The effect of an internal distribution of stresses on the roll pressure was studied following Crowan's work⁽⁴⁾ (see Sect. 3.3). Figs. 6.2.7 - 6.2.10 show values of roll force that

were calculated using several coefficients of friction, published data on flow stress and assuming inhomogeneous deformation in each of the rolling experiments of series A. It can be noted that, for a given amount of deformation and temperature, both the values of roll force and their percentage increase, as the coefficient of friction was increased, were smaller than those obtained under homogeneous deformation.

iv. Inhomogeneous deformation and flow stress data of the material undergoing rolling.

A further approach to the actual conditions of deformation in hot rolling was made by assuming inhomogeneous deformation and including the flow stress data of the material used in the experiments. Thus, Figs. 6.2.11 and 6.2.12 show re-calculated values of roll force plotted against percentage reduction using several values of μ for the rolling conditions conducted at 900°C and 1000°C. It can be seen that the use of yield stress data obtained from the steel under consideration was associated with lower calculated values of roll force than those obtained with the use of the yield stress data published by Suzuki⁽³⁶⁾; these latter yield stress values were, of course, obtained from a steel of slightly different composition. This effect was similar to that observed in the cases where homogeneous deformation was assumed.

6.3. Effect of the mean temperature of rolling on roll force.

In order to estimate the variation of the results due to changes of the mean temperature of the material, values of roll force for the rolling conditions of series A were calculated using temperatures between $\pm 5\%$ of the nominal temperatures of rolling. The value of the coefficient of friction was kept constant and homogeneous deformation was assumed. Figs. 6.2.13 - 6.2.16 show the results at a coefficient of friction $\mu=0.4$, that placed the hot rolling in a mixed frictional

condition and at temperatures within the range $\pm 40^{\circ}\text{C}$ of the nominal rolling temperature. It can be noted that a change in temperature causes an opposite change in the magnitude of the results, as the yield stress is inversely proportional to the temperature.

6.4. Effect of the coefficient of friction on roll torque.

In order to study the effect of the frictional states over a wide range of rolling conditions on the values of the calculated roll torque, an accurate estimate of this parameter was selected, among the various expressions proposed (see Sect. 3.6.). Values of the specific roll torque were calculated using the rolling conditions covered in series A, and considering coefficients of friction between 0.2 and 0.6. A similar procedure was adopted in the calculation of roll torque to that described above (6.2 i - iv and 6.3) as applied to roll force.

1. Homogeneous deformation and published flow stress data.

Figs. 6.4.1 - 6.4.4 show calculated values of the specific roll torque assuming homogeneous deformation and using the flow stress data obtained by Suzuki et al.⁽³⁶⁾. The results are plotted against the percentage reduction at constant coefficients of friction and temperatures between the range 900 - 1200°C. It can be seen that the values increased as the deformation was increased. This effect is related to the increase in both the roll pressure and the length of the arc of contact, the latter causing a lengthening of the lever arm. It can be noted that the effect of the coefficient of friction was reduced as the state of friction approached complete sticking conditions. The lines a - a and b - b defined the limits of the state of friction in Figs. 6.4.1 and 6.4.2. It can also be seen that the rate of increase of the roll torque with an increase in deformation became exponential as

the coefficient of friction was raised, which contrasted with the linear rate of increase of the corresponding results of roll force. This effect is related to the increase of both the roll pressure and the value of the neutral angle, as the coefficient of friction was increased. In Fig. 6.4.5. are plotted the relative positions of the neutral angle to the total angle of contact, against the percentage reduction at various coefficients of friction. The marked influence of the coefficient of friction on the position of the neutral angle can be seen in this figure

In Fig. 6.4.2 the results obtained at 1000°C show an increase in the roll torque as the deformation increased at a given coefficient of friction. The relative positions of the neutral angle plotted against the amount of deformation at several values of μ are shown in Fig. 6.4.6. A comparison of these results with the values of roll torque calculated at 900°C shows that, at a given amount of deformation, the results are very similar, despite the difference in the magnitude of the corresponding values of roll force. This was associated to the longer lever arms produced in the rolling conditions at 1000°C as the entry thickness was increased. In Figs. 6.4.7 and 6.4.8 the lever arm is plotted against percentage reduction for the rolling conditions at 900°C and 1000°C. The effect of an increase in the entry thickness of the plate on the values of roll torque was more significant at a low coefficient of friction. This is indicated by the higher values of torque obtained at 1000°C in comparison to those calculated for the rolling conditions at 900°C.

In Fig. 6.4.3 the results obtained at 1100°C show an increase of roll torque proportional to the amount of deformation at a given coefficient of friction. The effect of the coefficient of friction was reduced as the magnitude of the roll torque increased. The values were substantially lower than those obtained at 900°C and 1000°C as could

be expected from a reduction in strength at higher temperatures. In Fig. 6.4.9 the relative position of the neutral angle to the angle of contact is plotted against the percentage deformation. Here it can be seen that at values of $\mu \geq 0.4$ the neutral point moved slightly towards the exit plane as the percentage reduction increased, whereas at a low coefficient of friction the situation was reversed.

In Fig. 6.4.4 the results calculated for the rolling conditions at 1200°C show a proportional increase in the values of roll torque with an increase in deformation. As the value of μ was increased, the increment of roll torque decreased, c.f. above results. The values of roll torque at 1200°C were similar to those obtained at 1100°C despite the reduction in the values of roll force as the temperature was increased. In Fig. 6.4.10 are plotted both the roll pressure distributions and the plane strain yield stress of the material, along the arc of contact under the rolling conditions used in the experiments at 1100°C and 1200°C. Here it can be noted that the stress strain characteristics at the higher temperature caused a shift of the position of the resultant roll force, producing a higher lever arm. The lever arm is plotted against the percentage reduction for the conditions at 1100°C and 1200°C in Figs. 6.4.11 and 6.4.12 respectively. Here it can be seen that the values of the lever arms were higher at 1200°C.

ii. Homogeneous deformation and flow stress data of the material undergoing rolling.

Figs. 6.4.13 and 6.4.14 show the re-calculated values of roll torque using the flow stress data from the steel undergoing deformation for the rolling conditions at 900°C and 1000°C. The results are plotted against the percentage reductions at each of the above temperatures and using several values of μ . It can be seen that the values were

proportional to the amount of deformation and increased as the coefficient of friction rose. However, the magnitude of the results was higher than that obtained when published flow stress data was used, c.f. Figs. 6.4.1 and 6.4.3. The difference between these results narrowed as the amount of deformation was increased. Although the values of roll force decreased when the flow stress data determined during the present work was taken into account, the stress strain characteristics produced, in this case, a neutral angle which was slightly smaller than that obtained with published flow stress data at a given amount of deformation (Fig. 6.4.15). Hence, in the former case, the net area under the frictional stress distribution, which is a measure of its contribution to the roll torque, was slightly higher, as shown in Fig. 6.4.15. The torques calculated at 1000°C also show a significant increment in relation to those based on published flow stress data, particularly at low amounts of reduction (Fig. 6.4.14).

iii. Inhomogeneous deformation and published flow stress data.

The effect of a non-uniform stress distribution inside the material due to inhomogeneous deformation was also considered. In Figs. 6.4.16 - 6.4.19 the re-calculated values of specific roll torque are plotted against percentage reductions for the rolling conditions at 900°C, 1000°C, 1100°C and 1200°C assuming several values of μ . Orowan's analysis was used to include the effect of inhomogeneous deformation⁽⁴⁾. In the results shown at 900°C (Fig. 6.4.16) it can be seen that the roll torque increased when either the amount of deformation or the value of μ was increased.

It can be noted from a correlation of these results with the corresponding ones which assume homogeneous deformation (Fig. 6.4.1) that at a low value of μ the effect of inhomogeneous deformation did

not introduce a substantial change in the results. However, at high values of the coefficient of friction the roll torque was higher than that calculated assuming homogeneous deformation at a given amount of reduction. Here, although the specific roll force decreased under inhomogeneous deformation, as established previously (Figs 6.2.1 and 6.2.7), the corresponding roll pressure distribution produced a neutral point slightly closer to the exit plane than in the results obtained assuming homogeneous deformation (Fig. 6.4.20). Consequently, the negative contribution from the exit side of the friction hill to the roll torque was smaller when inhomogeneous deformation was assumed.

In Fig. 6.4.17 the results obtained at 1000°C show a linear increase as the percentage reduction was increased. The coefficient of friction produced a proportional increase in the values of roll torque as opposed to the diminished effect observed at high values of friction, when homogeneous deformation was assumed (Fig. 6.4.2a). Sticking friction limits the effect of the coefficient of friction. Therefore, due to the decrease in roll pressure under inhomogeneous deformation (Fig. 6.4.20), higher values of the coefficient of friction were required to produce sticking friction than under homogeneous deformation.

In Fig. 6.4.18 the calculated values at 1100°C show a linear increase as the amount of reduction was increased. However, high values of the coefficient of friction had a reduced effect on the values of roll torque. Under mixed frictional conditions the values calculated were higher than those where homogeneous deformation was assumed (Fig. 6.4.3). At a low value of μ , where only slipping friction occurred, the results were similar in both cases.

Finally, in Fig. 6.4.19 the results obtained at 1200°C show that the rate of increase of the specific roll torque, as the percentage

reduction was increased, was less sensitive to changes in the values of μ . This is related to the decrease of the shear yield stress as temperature is increased, producing sticking conditions at relatively low values of μ . Instead of increasing the values of roll torque, as observed at lower temperatures, the effect of inhomogeneous deformation, for the conditions at 1200°C, was to decrease these values. (cf. 6.4.4.-19)

iv. Inhomogeneous deformation and flow stress data of the material undergoing rolling.

A further attempt was made to establish the effect of friction on the roll torque in a closer approach to the actual rolling conditions. Thus, inhomogeneous deformation was assumed using the flow stress data from the rolling material. Figs. 6.4.21 and 6.4.22 show re-calculated values of roll torque, plotted against percentage reductions at several values of μ for the rolling conditions of the experiments conducted at 900°C and 1000°C in series A.

In the results calculated at a rolling temperature of 900°C, shown in Fig. 6.4.21, it can be noted that the rate of increase of the roll torque was dependent on the state of friction, as previously observed in those results obtained under homogeneous deformation (Fig. 6.4.13). The effect of the inhomogeneity of the deformation was similar to that observed when published flow stress data was considered. Alternatively, the use of the flow stress data of the experimental steel introduced an increment in the magnitude of the roll torque at a given value of μ when compared with associated values based on published flow stress data (Fig. 6.4.16). This difference was practically constant under sticking friction, whereas, in a state of slipping friction, the difference narrowed as the amount of deformation was increased (cf. 6.4.16-21)

Fig. 6.4.22 shows that an almost linear increment in the results

obtained at 1000°C occurred as the percentage reduction was increased at a constant value of μ , and that the magnitude of the specific roll torque increased rapidly as the coefficient of friction was increased.

6.5 Effect of the mean temperature of rolling on roll torque.

Since it was established from experimental results that the distribution of temperature of the material within the deformation zone was not uniform (see Sect. 5.5), the effect of a variation of the nominal temperature of rolling on the magnitude of the results was also studied. Values of the specific roll torque for the rolling conditions covered in series A were calculated at temperatures between $\pm 40^\circ\text{C}$ of the nominal temperatures of rolling. Calculations were made assuming homogeneous deformation, a constant value of μ and considering the published flow stress data. Figs. 6.5.1 - 6.5.4 show the results plotted against the percentage reductions and within a narrow range of variation ($\pm 5\%$) of the nominal temperatures of rolling, i.e. 900°C, 1000°C 1100°C and 1200°C.

In Fig. 6.5.1 the results obtained at temperatures close to 900°C show that either an increase or a decrease of the mean temperature caused an opposite change in the torque, as the yield stress is inversely proportional to the temperature.

In Fig. 6.5.2 the results shown at temperatures in the vicinity of 1000°C indicated that a variation in the mean rolling temperature produced an effect on the values of roll torque which was greater as the temperature decreased. This effect became more apparent at low percentage reductions.

From the results obtained at temperatures close to 1100°C ^{Fig 6.5.3.} it can be noted that a change of the mean temperature caused only a small effect on the values of roll torque. Furthermore, at low deformations, if the

temperature was raised, the roll torque decreased until a minimum value was reached, after which, a further increase in temperature caused an increase in roll torque.

Finally, the results shown in Fig 6.5.4, obtained with temperatures at and below 1200°C, were almost unchanged by a reduction in temperature. Therefore, the values of roll torque were less sensitive to temperature fluctuations as the nominal temperature of rolling increased.

6.6 Effect on roll force and torque of the transversal distribution of roll pressures.

The state of stress along the centre of a plate undergoing deformation is triaxial with $\sigma_1 > \sigma_2 > \sigma_3$, while at the edges of the plate the lateral stress σ_2 vanishes. Therefore, applying the Von Misses criteria to this stress system, and introducing an index defined by the state of constraint⁽⁵⁾ as, $\xi = (\sigma_2 - \frac{\sigma_1 + \sigma_3}{2}) / \frac{\sigma_1 - \sigma_3}{2}$, the condition of plasticity reduces to,

$$\sigma_1 - \sigma_3 = \frac{2\sqrt{3}k}{\sqrt{3 + \xi^2}}$$

An approximate distribution of principal stresses in the transverse direction, mid-way between the entry and exit planes, may be represented by Fig.6.6.1⁽⁶⁶⁾. Tselikov⁽⁵⁾ presented a distribution of roll pressure, σ_1 , similar to that in the above Fig., in the case of contact areas with a width/length ratio between 1 - 4. In an analysis presented by Polukhine⁽⁶⁵⁾ a partial differential equation was derived to describe the variation of roll pressure across the contact area, viz.,

$$\left(\frac{\partial s}{\partial x}\right)^2 + \left(\frac{\partial s}{\partial y}\right)^2 = \left(\frac{1}{h/2} \frac{2\sqrt{3}Y_{0.02}}{\sqrt{3 + \xi^2}} \pm \tau\right)$$

x, y rolling and transverse direction respectively

The above equation needs an elaborate method for its solution and only the profiles of the peak pressures across the width, which depend upon the variation of the thickness of the material, in the transverse direction, are shown here (Fig.6.6.2).

Measurements of the roll pressure distribution at various distances from the centre of the slab carried out by Siebel and Lueg⁽⁷⁾, indicated that the roll surface conditions influenced the distribution of roll pressure towards the edges.

Matsuura et al.⁽⁵¹⁾ measured values of roll pressures across the width and determined the transverse variation of the specific roll

force using plates with several width/thickness ratios (Fig.6.6.3).

In order to include the effect of transverse roll pressure distribution, corrections to the specific roll force and torque, calculated under plane strain conditions, were carried out in the present work according to the expressions:

$$P = P' (P_m/P_c)$$

$$G = G' (P_m/P_c)$$

The effect of transverse pressure was, therefore, included using the mean value across the width, P_m , and the value at the centre of the plate, P_c , taken from published results (Figs.6.6.2 - 6.6.3) obtained from plates with width/thickness ratios comparable to those used in the present experiments (6 - 8). In Table 2 are presented the correcting factors (P_m/P_c) calculated from the experimental results given by various workers (7,51,65).

7. Discussion.

The objective of the present work has been the development of a mathematical model that will allow the accurate prediction of roll force and torque in hot rolling. The degree of success obtained must be tested by comparing the results of the calculations with those obtained experimentally over a wide range of rolling conditions. The validity of the calculated results relies on the use of both realistic data and assumptions within the mathematical model that do not seriously impair the accuracy of the calculations. Therefore this section discusses the selection of the data used in the mathematical model including consideration of the factors that influence deformation in the roll gap. The accuracy of the prediction made is then assessed by a comparison of the calculated and experimental values of roll force and torque and the factors which may be responsible for any discrepancies are analysed. Finally, the possibility of further improvements in the accuracy of the prediction is considered briefly.

7.1 Distribution of temperatures in the deforming material.

The selection of appropriate yield stress data relies upon the determination of temperature distribution in the deforming material. Temperature measurements were obtained using thermocouples inserted at various points between the surface and the centre of the plates used in the experiments. These measurements produced evidence of severe quenching taking place in the peripheral layers of the material undergoing deformation, causing, in some cases, temperature decreases in excess of 200°C between the entry and exit planes (Fig.5.5.7b). At the same time, the material towards the central layers underwent an increase of about $20 - 30^{\circ}\text{C}$ due to the generation of heat that accompanied deformation. Thus, a temperature gradient was created between the surface

and centre of the material as it moved towards the exit. The magnitude of this gradient was affected by various factors.

At a given roll velocity an increase in the amount of deformation produced an increase in the extent of cooling at the surface of the material being rolled, due to an increase in the contact time between the material and the rolls. Additionally, the associated increase in the roll pressure at high reductions improved the contact between the roll surfaces and the material, which thus produced a higher heat transfer coefficient at the surfaces. Some evidence of this latter effect appeared to be given by the difference in the reduction of temperature at the surfaces in two rolling passes conducted at entry temperatures of 1010 °C and 1050 °C (Figs. 5.5.7b and 5.5.7c). Here it can be seen that the reduction in surface temperature was higher at the lower entry temperature. This indicates that the values of the heat transfer coefficient might have been affected by the magnitude of the roll pressure, since both increase as the mean entry temperature of the material was decreased.

Pawelski et al. ⁽⁶⁴⁾ found that surface scale was a bad conductor of heat and even a very thin layer had a significant effect on the heat transfer in the hot rolling of steel. It is reasonable to assume that the thickening of the surface scale will increase its thermal resistance in accordance with $U = \Delta x / C$. Thus, the increase in scale thickness produced in series A experiments, as the rolling temperature was increased, should be associated with an increase in the thermal resistance at the surface. At the same time a reduction of frictional heat could also be expected, due to both: the lubricating effect of the scale as it thickened and the decrease in the frictional stresses as the roll pressures decreased at higher temperatures.

The peripheral layers of the plate 0.5 mm beneath the surface experienced either a small rise in temperature, near the entry plane only (Fig. 5.5.7a), or a reduction in temperature that was always less severe than that which occurred at the surface. The actual temperature change was due to the complex interaction between the quenching effect of the rolls, the frictional heat generation at the surface and the heat produced within the material by deformation.

The rising temperature towards the centre of the material appears to be controlled, at a given reduction, by the entry temperature. It can be seen in Fig. 5.5.2 (800-950°C) that a decrease in entry temperature produced a larger increase in the temperature at the centre. This could be related to the increase in the amount of work hardening associated with the decrease in rolling temperature. However, at a given entry temperature, an increase in the percentage reduction only produced a slightly larger temperature increase (Fig. 5.5.1 $r=18$ & 243%). In this case, the increase in the amount of work hardening and hence in the heat of deformation associated with the higher strains and strain rates, was offset by the increase in the surface area and time of contact, both of which increased the total amount of heat removed by the rolls.

The large temperature gradients which were generated towards the surfaces of the material, ensured that the average temperature of the deforming material at any instant was noticeably lower than the nominal temperature. This had the effect of raising the yield stress and hence the roll load, as shown in Sect. 6.2.5. Thus, the selection of the correct yield stress depended upon the accurate estimation of these temperature changes.

Several methods have been proposed to predict both temperature profiles and average temperature of rolling, as follows:

(i) Analytical solutions.

Bradley et al.⁽⁵⁴⁾ proposed an analytical solution to Fick's law of heat conduction, which was used to determine the slab temperature distribution. This solution assumed heat transfer in the radial direction only with no thermal resistance between the roll and plate surfaces. By this means, an average temperature drop for the total time of contact could be determined. Denton et al.⁽¹⁷⁾ considered that the rolls and the plate formed a continuous system and applied the solution of heat conduction related to an infinite body, in which the plate thickness was initially at a constant temperature and the regions on both sides of the plate were at zero temperature. In addition, a mean time of contact was used to determine an overall temperature drop. Unfortunately, such analytical solutions overestimated the actual temperature drop at any position along the deformation zone, when compared with experimentally determined results. This can be seen in Fig.7.1. where the calculated temperature profiles at several instants during the contact period were compared with temperature measurements made during one of the series C experiments. The effect of such overestimation in the temperature drop at a specific position and time would be an increase in the yield stress data to be used in the roll force and torque calculations, with a consequent distortion of the results obtained.

An alternative solution related to the cooling of a semi-infinite solid with thermal resistance at the surface could also be considered. This solution only applies for very short periods of time when the centre of the slab has not yet felt the effect of the changing temperatures close to the surface. For such a situation, providing the following initial and boundary conditions are satisfied,

$$T(x,0) = T_i$$
$$\lambda \frac{\partial T(0,t)}{\partial x} = h_0 [T(0,t) - T_f]$$

a solution is given as, ⁽⁶⁰⁾

$$\frac{T - \bar{T}_i}{T_f - \bar{T}_i} = \operatorname{erfc}\left(\frac{x}{2\sqrt{\alpha t}}\right) - \exp\left\{\operatorname{erf}\left[\frac{x}{2\sqrt{\alpha t}} + \frac{h_o}{\lambda}\sqrt{\alpha t}\right]\right\} \quad (7.1)$$

where

$$f = \frac{h_o}{\lambda}\sqrt{\alpha t}\left[\frac{x}{\sqrt{\alpha t}} + \frac{h_o}{\lambda}\sqrt{\alpha t}\right]$$

The order of magnitude of h_o could be established by considering the inverse of the thermal resistance of the surface scale ($1.0 \text{ W/m}^\circ\text{C}$); hence with a scale thickness of 0.5 mm h_o was approximately $2000 \text{ W/m}^2\text{C}$. Schneider ⁽⁶⁰⁾ presented a chart where the relationship between the dimensionless groups in Eq.7.1. was plotted, which enabled thermal profiles to be obtained at various stages in the rolling process. It was also found that such a solution overestimated temperature reductions when compared with measured results, as can be seen in Fig.7.1.

(ii) Finite differences.

Temperature distributions at various instants during the contact time were calculated in the present work by means of a finite difference solution to Fick's law, where several values of the surface heat transfer coefficient were assumed. It was established that a close agreement between theoretical and measured thermal profiles was obtained when values of h_o were within the range $12,000 - 50,000 \text{ W/m}^2\text{C}$ (See Appendix II). However, the mean temperature obtained from the selected profiles at various positions in the roll gap was not significantly different from the corresponding mean values obtained from the experimental measurements made at four different points across the plate thickness. Therefore the actual mean temperatures used in the present work were based on these experimental readings.

In the present model it was assumed that isothermal conditions existed inside the material undergoing deformation. Hence, it was decided that an effective rolling temperature could be given by the

average value of measured temperatures at a mid-way position between the entry and exit planes. In Fig.7.1. such average temperature was about 20°C below the mean entry temperature of 900°C. Hence, the effective temperature was considered to be 2% lower than the mean temperature of the ingoing material.

7.2 The effect of the coefficient of friction on the calculated roll force and torque.

Predictions of roll force and torque in flat hot rolling are commonly made, for practical purposes, by the use of methods which assume that the material sticks to the rolls at all points along the arc of contact. In such cases the coefficient of friction, apart from being high enough to produce sticking, has no further influence on the rolling load. However, in the experiments conducted in the present work, there was a difference between the velocity of the rolls and that of the emerging material, which indicated that slipping occurred between the rolls and the plate. In addition, lubricants are being introduced in hot rolling practice which reduce the coefficient of friction to the point where complete sticking conditions are improbable. Therefore, the calculation of rolling loads assuming sticking conditions exclusively is no longer acceptable. As a result the coefficient of friction becomes an adjustable parameter, whose value must be lower than that where sticking conditions exist.

An increase in the magnitude of the coefficient of friction produced an increase in the calculated roll force. The results plotted in Figs.6.2.1 - 6.2.12 showed that the magnitude of the contribution of the coefficient of friction to the roll force decreased as the state of friction approached complete sticking conditions, at which point the contribution of the frictional stresses to the roll pressures was

limited by the strength of the material, i.e. $\sigma = k$. It was also found that, as the rolling temperature was increased the threshold value of μ at which sticking conditions initiated was lowered. Thus, as the temperature was raised and the yield stress of the material decreased, the value of the coefficient of friction above which sticking conditions appeared was reduced. Hence, as the rolling temperature was increased from 900°C to 1200°C the upper value of μ which might significantly influence the roll force fell from 0.6 to 0.4 (Fig. 6.2.1 - 6.2.4).

The condition of plasticity under inhomogeneous deformation was expressed by Orowan⁽⁴⁾ as, $s-p=2kw(a)$ with the function $w(a)$ decreasing rapidly as sticking conditions were approached i.e. $a \approx 1$ (see Fig. 2.4.3). Thus, the slope of the friction hill - $ds/d\theta$ - at those segments of the contact arc where conditions close to sticking friction existed, was smaller than the corresponding slope under conditions of homogeneous deformation. Consequently the introduction of inhomogeneity of stress distribution into the calculation, by means of the inhomogeneity factor, $w(a)$, led to a reduction in the magnitude of the effect of μ on the roll force, particularly when the value of μ exceeded 0.4 (Fig. 6.2.7 - 6.2.10). It can also be seen that the level of roll pressure decreased when inhomogeneous deformation was considered. This was mainly associated with the reduction of the effective yield stress given by $kw(a)$.

The coefficient of friction has a more complex effect on the values of roll torque, being expressed as,

$$G = \mu R' R \int_{\theta_n}^{\theta_1} s d\theta - \int_0^{\theta_n} s d\theta \quad (7.2.1)$$

Thus, the roll torque depends upon both the roll pressure and the position of the neutral angle. It can be seen in Figs. 6.4.5 and 6.4.6 that the increase in the coefficient of friction caused an increase in

the neutral angle up to a maximum value, which remained constant at values of μ in excess of 0.4. Thus, as the coefficient of friction was increased the associated increase in both the roll pressure and the negative integrand in Eq.7.2.1 tended to counteract one another.

The majority of the calculated values of roll torque obtained under conditions of inhomogeneous deformation were smaller than the corresponding values obtained under homogeneous conditions. This arose because the effective yield stress was lower in the former case. Only when a high value of the coefficient of friction ($\mu=0.6$) was used did the introduction of inhomogeneity increase the roll torque. Since the values of μ most likely to occur in the experimental conditions were lower than 0.6, calculations under inhomogeneous deformation may be considered to reduce the values of roll torque.

The experimental values of roll force at 900°C and 1200°C (Figs. 5.1.1. and 5.1.4) showed a linear increase as the percentage reduction was increased. The corresponding calculated forces obtained at constant values of the coefficient of friction showed a similar relationship with the percentage reduction (Figs. 6.2.1. and 6.2.4). Likewise, the linear increase in the experimentally determined values of roll torque produced by the increase of the percentage reduction, compared well with the corresponding relationship between percentage reduction and the calculated roll torque, obtained with the use of a constant μ . These results seem to indicate that the value of the coefficient of friction was constant throughout the experiments conducted at 900°C and 1200°C. This was not the case with the experimental results of roll force and torque at 1000°C and 1100°C, which showed a reduction in the rate of increase of both parameters as the percentage reduction was increased. A similar rate of increase could be obtained in the corresponding

calculated results if the value of μ was assumed to be inversely proportional to the percentage reduction. This might indicate that the value of the coefficient of friction decreased as the percentage reduction was increased throughout the experiments conducted at 1000°C and 1100°C.

7.3 Values of the coefficient of friction obtained by experiment.

The forward slip results obtained in the present experimental programme give some indication of the factors affecting the frictional conditions in the rolling process. Thus, the results of the measurements made in the experiments of series B show that as the amount of reduction increased, the magnitude of the forward slip produced with dry rolls, became higher than that produced when lubrication was present (Figs. 5.4.6 and 5.4.8). In the preliminary rolling tests, the forward slip measurements at 900°C (Table 1) were much higher than the corresponding values in series A at a similar temperature (Fig. 5.4.2). Such high values of forward slip could be associated with the fact that the rolls might have become drier, as these preliminary tests were carried out after several plates had been rolled consecutively.

The values of the forward slip measurement obtained in the series B experiments were higher than those produced in each reduction in series A (Figs. 5.4.5 and 5.4.1 respectively). Those results may be explained by the bright drawn finish of the latter material, in contrast to that used in the former case, which possessed a surface finish of C.L.A. $\sim 3\mu\text{m}$ (120µin). Some evidence of the influence of surface finish on roll force has been obtained by El Kalay et al.⁽¹⁶⁾ who used low C steel bars with various amounts of scale. Furthermore, Roberts⁽⁵⁰⁾ used the above data to obtain an empirical relationship between coefficient of friction and a roll roughness/scale index ratio.

The general level of forward slip values decreased as the rolling temperature was increased from 1000°C to 1200°C (Figs. 5.4.2 - 5.4.6). The mean scale thickness of the rolled plates, measured when the material was cold, indicated that the amount of scale increased as the rolling temperature was increased. Thus, the increase in the thickness of the surface scale could have provided a more efficient lubricating layer between the rolls and the material, which was responsible for the reduction in the forward slip values and hence the coefficient of friction. This same effect could explain the results of El Kalay et al. who found that an increase in scale thickness reduced the rolling load by as much as 14%, using smooth rolls. However, the low values of the forward slip measured at 900°C during series A experiments do not seem to be directly related to the amount of scale produced, which was very small at this temperature - c.f. Table 1. It is tentatively suggested that a combination of high roll pressures and a thin layer of scale at such temperature could create a high surface heat transfer coefficient which would cause a pronounced reduction in temperature towards the surfaces of the material. This would lead to an increase in the shear yield stress and a consequent reduction in the shear strain at the peripheral layers. Thus, a reduction in the extent to which the central portion of the cross sections is deflected towards the entry plane could produce a reduction of the zone in which the material slips ahead of the rolls and could thus reduce the magnitude of forward slip (see Sect. 7.4). Furthermore, some of the observed differences in the amount of forward slip measured at 900°C and 1000°C could also have been associated with the increased entry thickness at the higher temperature, which would give rise to a higher contact angle and an increase in the value of the neutral angle. This effect would cause an increase

in the amount of forward slip, as given by Eq.4.8 viz., $\Phi = \frac{1}{2} \theta_n^2 (2R/h_2 - 1)$

According to the forward slip method, most values of the coefficient of friction associated with percentage reductions above 30% were within the range 0.2 - 0.45. These results were similar to published data on coefficient of friction in hot rolling of steel, based on amount of reduction between 30 - 50%. In Table 3 the values of μ obtained from several empirical relationships, compared well with the corresponding results of the present work at reductions over 30%, considering that such relationships were derived from values of μ determined by different experimental techniques at specific rolling conditions. At lower percentage reductions it was not possible to obtain meaningful values of the coefficient of friction. This arose because the theoretical relationship given in Fig.4.8.1.(a)(b)(c)(d) showed that the coefficient of friction became progressively less sensitive to variations in the amount of forward slip as the percentage reduction became smaller. However, in cases where a meaningful value of μ was not obtained, a significant lateral spread occurred, c.f. Table 1. This might suggest that the values of the coefficient of friction were relatively low ($\mu < 0.2$). The minimum value of μ at which it was possible to obtain a solution to the roll pressure distribution was ~ 0.16 . Hence, this value of the coefficient of friction has been used in the cases where the forward slip measurements could not determine values of μ .

The values of coefficient of friction given in Table 1 have been used in the calculations of roll force and torque.

7.4 Inhomogeneity of the deformation process.

Indirect experimental evidence of inhomogeneous deformation in the present work was obtained during the determination of temperature

measurements in series C, where simultaneous recordings were made from thermocouples which had originally been assembled in a vertical plane (see Sect.4.2.3). It was found, that, after rolled plates were cut, the thermocouple beads had been displaced from the original vertical plane, as indicated by the reconstructed shape of this plane after rolling, as shown in Fig.7.4.1. Experimental evidence of the deflection of cross sections in hot flat rolling has been provided in previous investigations, the most satisfactory of which is probably a recent work by Jones et al. (61), who used steel plates 12.5 mm thick with elongated MnS inclusions initially oriented perpendicular to the rolling direction. The deformation pattern of these inclusions after hot rolling established that initial vertical sections did not remain plane within the deformation zone and that the shearing of the peripheral layers of the material increased as the amount of deformation was increased.

In the present work, theoretical values of the neutral angle were obtained by the use of the mathematical model and assuming coefficients of friction within the range 0.2 - 0.6. The corresponding experimental values of the neutral angle at each reduction of series A, were determined by the use of forward slip measurements and Eq.4.8.1, viz. $\phi = R'\theta_n/h_2$. In Fig.7.4.2 the two sets of results are plotted against the percentage reduction. It can be seen that the experimental values in each reduction was higher than the corresponding theoretical results. This could be explained by following Potopkin's assumption (65) that instead of a neutral cross section with a uniform velocity, a neutral surface was present, the location of which could be defined as the geometric site of the points with a velocity equal to the horizontal component of the roll velocity at the neutral position along the arc of contact. This assumption was based on a theoretical investigation of

the metal flow kinematics by comparing calculated and experimental values of the neutral angle. Therefore, a deflection of the neutral position of the arc of contact, ahead of the central portion of the neutral surface, could explain the higher magnitude in the experimental values of the neutral angle.

The above results indicate that calculations of roll force and torque that are based on an assumption of homogeneous deformation do not represent the conditions in the deformation zone, and justify consideration of the stress distribution which originates from inhomogeneous deformation i.e. the Crowan analysis⁽⁴⁾.

7.5 Comparison between calculated and measured values of roll force.

Fig.7.5.1 compares the measured roll forces at effective temperatures of either 880°C or 940°C with those calculated at identical temperatures and under conditions as similar as possible to the experimental ones. The former included both the results obtained by the use of yield stress data determined in the present work, and also the corresponding forces calculated with the aid of Suzuki's yield stress data⁽³⁶⁾. Both the experimental and calculated forces increased as the percentage reductions increased, but at the highest reduction the calculated results were greater. This discrepancy was larger when Suzuki's data was employed. In the case of forces calculated with the aid of the yield stress values determined during the present work, the values differed from the experimental forces by between -13% and +17%.

In Fig.7.5.2 the calculated and measured forces are plotted against the percentage reduction used at an effective temperature of 950°C. Again both forces increased as the percentage reduction increased, with both calculated values usually higher than the corresponding experimentally determined value at percentage reductions above 30%. Furthermore, as in the previous case, the calculated values obtained by the use of the yield stress data determined during the present investigation gave the best agreement with the experimentally determined values. In this case, the magnitude of the discrepancies between calculated and experimental forces increased from 6% to 22% as the percentage reduction was increased from 12% to 42%.

At higher temperatures the most reliable yield stress data available was that due to Suzuki⁽³⁶⁾; though extrapolated data from

the yield stress values obtained at lower temperatures during the present work was also used. The calculated forces obtained by the use of Suzuki's data at an effective temperature of 1080°C (Fig.7.5.3) were either higher or lower than the corresponding experimental forces, depending on the percentage reduction used. Thus at reductions of less than 35% the calculated force was, on average 30% lower than the measured force, while at 45% reduction the reverse was the case with the former about 10% higher than the latter. In the case of the calculated forces based on the extrapolated yield stress data no significant improvement between the calculated and measured results was observed. Thus, the calculated results suggest a rather greater influence of percentage reduction on force than that suggested by the experimental measurements. The slope of the graph that represents the latter results is less steep than that obtained at lower temperatures.

Finally, at 1150°C , the calculated forces were, on average, lower than the measured values, as shown in Fig.7.5.4. There was, in this instance, no obvious relationship between the percentage reduction and the discrepancy between the two sets of values. As at 1080°C , the calculated relationship between force and percentage reduction showed a much steeper slope than was the case when the experimental forces were considered.

All the forces calculated with the aid of Suzuki's yield stress data have been plotted as abscissae in Fig.7.5.5 with the corresponding experimentally determined forces as ordinates; thus the solid line at 45° to the axis represents total agreement between the two sets of results. The data as a whole showed a scatter of $\pm 25\%$ about this line, with the low and high temperature results tending to lie below, and above this line respectively.

In Fig.7.5.6 the measured forces and the associated forces calculated with the use of the yield stress data determined during the present investigation are plotted as ordinates and abscissae respectively. Almost all the data showed a scatter of $\pm 25\%$ about the line representing total agreement between measured and calculated results, with nearly all data obtained at temperatures below 1000°C lying within $\pm 13\%$ of that line.

7.6 Comparison between calculated and measured values of roll torque.

Fig.7.6.1 compares the measured torques at effective rolling temperatures of 880°C and 940°C with those calculated under identical temperatures and under conditions as close as possible to the experimental ones. The latter included two sets of results: one obtained by the use of yield stress data determined in the present work and that determined with the aid of Suzuki's data⁽³⁶⁾. Both the experimental and calculated torques increased as the percentage reduction increased, but at any reduction over 30% the calculated results were always greater. This discrepancy was lower when Suzuki's data was used, and in this instance the calculated torques exceeded the measured values from +10% to 25% as the percentage reduction was increased from 30% to 42%. In the case of torques calculated with the aid of the yield stress values determined during the present work the difference between calculated and experimental results varied between -20% to +27% as the percentage reduction was increased from 18% to 42%. Thus, the magnitude of the discrepancies between these calculated values and the measured torques appeared to increase as the percentage reduction was increased.

In Fig.7.6.2 the calculated and measured torques are plotted against the percentage reduction used at an effective temperature of 980°C . Again both torques increased as the percentage reduction increased,

with the two calculated values higher than the corresponding value determined experimentally at any percentage reduction over 30%. Furthermore, the calculated values obtained by the use of the yield stress data determined during the present work gave better agreement with the measured torques in most cases. In this case, at a given percentage reduction under 20%, the calculated torque was on average 10% lower than the experimental value, while at higher reductions the former was 14% to 40% greater than the latter.

At an effective temperature of 1080°C both the Suzuki yield stress data⁽³⁶⁾ and that extrapolated from the yield stress values obtained during the present work, were used. The two sets of calculated torques were either lower or higher than the corresponding experimental torques, depending on the percentage reduction used. Thus, at reductions under 30% both the calculated torques were on average lower than the measured torque, while at 45% reduction the opposite was the case, with the former 10% on average higher than the latter. From the slope of the graphs representing the measured results, it is apparent that the percentage reduction was less significant in these results than in the case of those obtained by calculation.

At 1150°C the only yield stress data available was that due to Suzuki, and the calculated torques obtained with such data were lower than the measured values, as shown in Fig.7.6.4. The discrepancy between both results fell from 34% to 13% as the percentage reduction increased; thus, at 12% reduction the calculated result was 34% lower than the measured one, while at 33% reduction the former was only 13% lower than the latter.

Finally, all the torques calculated with the aid of both Suzuki's data and the yield stress data obtained in the present work have been

plotted as abscissae in Fig.7.6.5 and Fig.7.6.6. respectively, with the corresponding measured values as ordinates. In both cases the data as a whole showed a scatter of $\pm 2\%$ about the line representing total agreement between calculated and measured results, with all the results obtained at temperatures over 1000°C lying above that line.

7.7 Limitations in the accuracy of the measured and calculated forces and torques.

The overall level of agreement between the calculated and experimental roll forces and torques is reasonable in view of the limitation imposed by the accuracy of the experimental technique and the assumptions involved in the mathematical model.

In the case of the experimental results the accuracy of the data was limited by the method by which the roll force was measured and the inability of the rolling power recordings to account for the inertial energy stored in the mill. Since a progressive increase in the roll force occurred as the material passed through the roll gap, the upper chocks tended to move upwards and friction between the chocks and the mill housing created a frictional restraining force. This might result in a reduction in the measured value of the roll force obtained from the load cells placed on the upper chocks. Zeltkans et al.⁽⁶²⁾ found that this frictional restraining force, which depends mainly on the coefficient of friction between the chocks and the mill housing, could vary between 0.2% and 5% of the total roll force. Therefore, measurements from the load cells could underestimate the actual roll force by as much as 5%. The accumulated energy due to inertia of the rotating elements of the mill assisted the motor during a rolling pass. Wusatowski⁽⁴⁸⁾ gave an expression by which the dynamic torque produced by the deceleration of the mill during a rolling pass could be estimated,

viz.,

$$G_d = \frac{\sum GD^2 (n_2 - n_1)}{375 t}$$

It was assumed that the total rotating mass G , was about $3x$ (mass of the rolls) and that the effective diameter of the rotating elements D , was equivalent to roll diameter. Hence, it can be shown that for a typical deceleration of the rolls ($n_1 - n_2$) to about 20% of the idling speed (10 rev/min), the dynamic torque could be as much as 60 N - m, which strictly should be added to the torque measurements.

In the case of the calculated results a source of error might originate from the limitation of the various assumptions made. Thus, at high reductions and temperatures up to 950°C error in the predicted roll torques might have been introduced during the calculation of the deformed roll radius, since roll flattening will cause the centre of the deformed arc of contact to be displaced from the roll centre. Bland's method⁽³²⁾ of successive approximations, by which the elastic distortion of the roll surface could be determined, showed that a depression of the arc of contact appeared in the region of the peak pressure. Although Bland found that the difference between values of roll force obtained using both Hitchcock's formula and the successive approximations method was within the limits of error introduced in the calculation of the elastic distortion of the rolls by the latter method, the effect of a non-circular arc of contact on the roll torque was not investigated. Since an increase in roll pressure increased the degree of roll flattening any error introduced by the assumption of a circular arc of contact will be similarly increased.

In addition it can be noted that at high reductions and temperatures of 880°C and 950°C the discrepancy between calculated and measured torque was higher than that observed in the associated values

of roll force. Since the net area under the frictional stress distribution along the length of contact is a measure of its contribution to the roll torque, any error in the calculated distribution of frictional stresses produced an error in the predicted torque. Experimental evidence (51,51a,51b) showed that the distribution of frictional stresses was such that the coefficient of friction must decrease towards the neutral point. In the present mathematical model the effective coefficient of friction decreased when the frictional stresses reached the shear yield stress of the material, as can be seen in Fig.7.7. where the roll pressure distribution and the associated shear stress/roll pressure ratio are plotted against the angular position at 40% reduction and 1100°C. A cold rolling test conducted by Rooyens (51b) on aluminium, using ground rolls (C.L.A.11µin) without lubrication and at 52% reduction gave a shear stress/radial stress distribution very similar to that shown in Fig. 7.7. Although a variable coefficient of friction could have been incorporated into the calculations, the equipment available did not allow the experimental determination of the variation of the coefficient of friction along the arc of contact. Therefore any such assumed distribution would be arbitrary and of limited value.

During hot rolling the rapid cooling that occurs in the surface layers of the plate gives rise to a variation in yield stress which reaches a maximum as the material approaches the exit plane. This would be expected to increase the frictional forces at the surface so that the associated roll force and torque will also be increased. Although an attempt has been made to take this effect into account, by the use of a mean rolling temperature lower than the nominal one, this approach involved a considerable degree of simplification. The actual

variation in yield stress in the plate was also affected by the presence of inhomogeneous deformation. This condition has been considered in terms of the Orowan analysis but its effect on the variation in yield stress within any section of the plate has not been included.

In general, an increase in the percentage reduction produced an increase in the calculated values of roll force and torque relative to those obtained by experiment. In addition an increase in temperature reduced the level of the former relative to the latter. As a consequence of the combination of these two effects the discrepancies between the calculated and the experimentally determined values shown in Figs. 7.5.1 - 7.6.6 varied in a complex manner. However, the best agreement between these two sets of results was obtained at the lower end of the temperature range with percentage reductions that did not exceed about 20%. The increased percentage reduction was associated with increases in mill load and contact angle which will increase any inaccuracies due to roll flattening and inhomogeneity of deformation respectively. These effects may explain the increase in the calculated values of roll force and torque relative to the experimental values as the percentage reduction increased.

The effect of an increase in temperature on the relative difference in the calculated and experimental roll forces and torques may be explained by a general underestimation of the yield stress data at higher temperatures coupled with low percentage reductions. Under these circumstances the critical strain value at which softening of the material occurred became very low, so that it proved difficult to represent the relationship between yield stress and deformation by a single equation.

Although some doubts existed about the magnitude of the coefficient

of friction associated with small percentage reductions, the values used produced the best fit between calculated and experimental roll forces and torques. Thus, the selection of the rather low coefficients of friction under these circumstances would appear to be justified.

7.8 Conclusions.

1. Values of the coefficient of friction, determined from forward slip measurements associated with percentage reductions between 30 - 45% were within the range 0.2 - 0.45 under dry conditions. The thickness of the scale, the rolling velocity and the temperatures at the interface between the material and the rolls appeared to control the magnitude of the coefficient of friction, but a simple relationship between these parameters was not obtained.
2. On entry to the rolls the peripheral layers of the plates underwent a severe quench, due to the rapid transfer of heat from the plate to the rolls: the magnitude of the associated temperature reduction was increased by an increase in the roll pressure and the contact time.
3. Towards the centre of the plates the deformation process produced an increase in temperature, the magnitude of which increased when either the entry temperature was reduced or the rate of deformation was increased.
4. The experimentally determined relationship between temperature and flow stress indicated that the temperature gradient generated in the plate during rolling produced a significant variation in the yield stress of the material. This variation has been taken into account in the subsequent calculations of roll force and torque by the use of an effective temperature of rolling given by the geometric mean of temperature measurements across the plate thickness mid-way between entry and exit.

5. Roll force values calculated with the aid of the flow stress data determined in the present work were within $\pm 13\%$ of the measured values, while the results obtained by means of Suzuki's data gave better agreement, at temperatures between 880°C and 950°C and reductions of up to 30% . However, when higher temperatures and reductions were considered in conjunction with Suzuki's data the degree of discrepancy increased to $\pm 25\%$.

6. Most of the calculated torque values were within $\pm 25\%$ of the measured values, but the results obtained with the use of Suzuki's flow stress data generally gave slightly better agreement. However, correlations better than $\pm 14\%$ were obtained at 950°C with reductions of up to $\pm 35\%$ in conjunction with the yield stress data produced during the present work.

Consideration of the inherent sources of error in the present mathematical model suggests that a further significant improvement will be difficult to obtain, since several of the difficulties arise from variations in the deformation process within a transverse section. Other methods of calculation, such as finite element techniques, may be more suitable when such effects are considered. The level of agreement between calculation and experiment obtained in the present work is probably sufficiently good for the method to be of practical value. It is not clear that the improvement in accuracy obtained by alternative methods would justify the great increase in the complexity and length of the calculations. Some improvement to the present model might be possible by further consideration of the effect of the rolling parameters (rolling velocity, amount of reduction and temperature) on the coefficient of friction and the yield stress, particularly at the upper end of the hot rolling temperature range.

BIBLIOGRAPHY.

The following abbreviations are used:

Zeitschrift fur angewandte Mathematik
und Mechanik.

Z. angew. Math. Mech.

Mitteilungen aus dem Kaiser Wilhelm
Institut fur Eisenforschung.

Mitt. K.W. Inst. Eisenf.

- | | | | |
|----|------------------------------------|------|---|
| 1 | Karman, T. Von | 1925 | Z. angew. Math. Mech. 5,
pp.139 - 42. 'On the theory
of rolling'. |
| 2 | Siebel, E. | 1925 | Stahl und Eisen, 45,pp.1563-6
'Forces and material flow
during plastic deformation.' |
| 3 | Nadai, A. | 1939 | Jnl. App. Mechanics,6,pp.A55-62
'The forces required for roll-
ing steel strip under tension'. |
| 4 | Orowan, E. | 1943 | Inst. Mech. Eng.,150,p.140
'The calculation of roll
pressure in hot and cold
flat rolling'. |
| 5 | Tselikov, A.
(Trans. Sirk,W.V.) | 1967 | MIR Pub. 'Stress and strain in
metal rolling'. |
| 6 | Ekelund, S. | 1933 | Steel,vol 93,Aug.21 and follow-
ing nos.'Analysis of factors
influencing rolling pressure
and power consumption in the
hot rolling of steel'. Trans.
from, Jern Kon Torals Ann.1927
vol.111,p.39 & 1928,vol.112,p.67. |
| 7 | Siebel, E. & Lueg,W. | 1933 | Mitt.K.W. Inst. Eisenf.vol.15,
p.1. ' |
| 7a | Siebel,E. & Pomp,A. | 1927 | Mitt. K.W. Inst. Eisenf.vol.9
p.157. 'Determination of the
resistance to deformation of
metals by compression'. |
| 8 | Underwood, L.R. | 1952 | The Rolling of Metals, vol.1. |
| 8a | Smith, T.L. | | As given by Underwood,(8). |
| 8b | Trinks, W. | 1937 | Blast Furnace and Steel Plant,
vol.25,pp.617-19.'Pressures and
roll flattening in cold rolling. |

- | | | | |
|-----|----------------------------|------|--|
| 9 | El Waziri | 1963 | Iron and Steel Engineer, p.73
'An up-to-date examination of rolling theory'. |
| 10 | Prandtl, L. | 1923 | Z. angew. Math. Mech., 3, pp. 401-6. |
| 11 | Nadai, A. | 1943 | Theory of flow and fracture of solids. McGraw Hill Book Co. 'Plane strain and stress'. |
| 12 | Bland, D.R. & Ford, H. | 1948 | Procs. Inst. Mech. Eng., 159 p.144. 'The calculation of roll force and torque in cold strip rolling with tensions'. |
| 13 | Bland, D.R. & Sims, R.B. | 1953 | Procs. Inst. Mech. Eng., 167, p.371. 'A note in the theory of rolling with tensions'. |
| 14 | Sims, R.B. | 1954 | Procs. Inst. Mech. Eng., 168, pp.191-200. 'The calculation of roll force and torque in hot rolling mills'. (Research on the rolling of strip). |
| 15 | Orowan, E. & Pascoe, K.J. | 1946 | Iron & Steel Inst. Spec. Rpt. No. 34 pp.124-145. 'A simple method of calculating roll pressure and power consumption in hot, flat rolling'. |
| 16 | El Kalay, A.K. & Sparling. | 1968 | Jnl. of Iron & Steel Inst. 'Factors affecting friction and their effect upon load, torque and spread in hot, flat rolling'. |
| 17 | Denton, B.K. & Crane, F.A. | 1972 | Jnl. of Iron & Steel Inst. 'Roll load and torque in the hot rolling of steel strip'. |
| 18 | Hencky, H. | 1923 | Z. angew. Math. Mech., 3, pp.241-251. (From, Rowe, G.R. 'Principles of Industrial Metal working Processes'.) |
| 18a | Geiringer, H. | 1930 | Proc. 3rd Int. Con. Appl. Mech. Stockholm, 2, pp.185-190. (From Rowe, G.R. see 18.) |
| 19 | Hill, R. | 1950 | Plasticity, Clarendon Press. pp.131-149. |
| 20 | Prager, W. | 1953 | Plane Flow pp.3-26. (Trans. Royal Inst. Tech., Stockholm). |

- | | | | |
|-----|------------------------------------|---------|--|
| 21 | Alexander, J.M. | 1954 | Inst. Mech. Eng. p.1021
'A slip line field for the hot rolling process'. |
| 22 | Ford, H. & Alexander, J.M. | 1963-4 | Jnl. of Inst. of Metals, vol.92
'Simplified hot rolling calculations'. |
| 23 | Green & Wallace | 1962 | Jnl. Mech. Eng. Sci., 4(2),
pp136-42. 'Estimation of load and torque in the hot rolling process'. |
| 24 | Sparling, L.G.M. & Willows, R.A.L. | 1970-71 | Proc. Inst. Mech. Eng. vol.185
'A study of the hot rolling of thick flat slabs'. |
| 25 | Eriksson, R. & Huhtelin, T. | 1972 | Scand. Jnl. Metallurgy. 'Roll force calculations in hot, flat rolling, using a modified upper bound model.' |
| 26 | Weber, K.H. | 1965 | Jnl. of Iron & Steel Inst. p.27
'A hydrodynamic theory of rolling'. |
| 26a | Knetsche, A. | 1957 | Freiburger Forschungsh, 16, pp.5-34. (From Weber, 26). |
| 27 | Ichinoi, J. & Tomisawa, G. | 1972 | Jnl. Japan Soc. Lub. Eng., 17, 5, pp.327-336. 'Theory of cold rolling in consideration of hydrodynamic lubrication'. |
| 28 | Alexander, J.M. | 1972 | Proc. Royal Soc. London, 326, pp.535-563. 'On the theory of rolling'. |
| 29 | Ford, H., Ellis, F. & Bland, D.R. | 1951 | Jnl. of Iron & Steel Inst. p.57
'Cold rolling with strip tension. Pt. I'. |
| 30 | Prescott | 1924 | Applied Elasticity (Longman, Green & Co.) p.638. (From Hitchcock, 31). |
| 31 | Hitchcock, J.H. | 1935 | Rpt. of ASME Special Research. 'Roll Neck Bearings'. 'Elastic deformation of roll during cold rolling'. Appx. 1. |
| 31a | Hitchcock, J.H. | 1931 | Rolling Mill Jnl. vol.5, pp583-6, 659-60. 'Analysis of rolling forces.' |

- 32 Bland,D.R. 1950 Inst. Mech. Eng. vol.162, p.2.'A theoretical investigation of roll flattening'.
- 33 Bland,D.R. & Ford,H. 1952 Jn. of Iron & Steel Inst.pp.245-249.'Cold rolling with strip tension.Pt3'. 'An approximated treatment of the elastic compression of the strip in cold rolling'.
- 34 Cook,P.M. & McCrum,A.W. 1958 B.I.S.R.A. 'The calculation of load and torque in hot,flat rolling'.
- 35 Hill,R. 1950 Proc. Inst.Mech. Eng.,163,p.135. 'Relations between roll force, torque and the applied tensions in strip rolling'.
- 36 Suzuki,H.et al. 1966 Rpt. of Inst. Ind. Sci.Uni. Tokyo.'Studies on the flow stress of metals and alloys'.
- 36a Inohue,K. 1955 Tetu-to-Hagane,vcl.41.(From Suzuki,36).
- 37 Cook,P.M. 1957 Proc. Conf. Props. of Mats.at a high rate of strain. p.86. 'True stress-strain curves for steel in compression at high temperatures and strain rates for application to the calculation of load and torque in hot rolling.'
- 37a Nadai,A & Manjoine 1941 Jnl. App. Mechs.,June, p77. (From Cook,37).
- 37b Fink,K.,Lueg,W. & Burger,G. 1955 Archiv. fur das Eisenhüttenwesen,Nov.p.655.
- 38 Alder,J.F. & Phillips, V.A. 1954 Jnl. Inst. Metals,83,p.80. 'The effect of strain rate and temperature on the resistance of aluminium, copper and steel to compression'.
- 39 Arnold,R.R. & Parker, R.J. 1959-60 Jnl. Inst. Metals,88, 'Resistance to deformation of aluminium and some aluminium alloys.'
- 40 Bailey,J.A. & Singer, A.R.E. 1963-4 Jnl. Inst. Metals,92,p.288. 'A plane strain cam plastometer for use in metal working studies.'
- 41 Sellars,C.M. & Tegart, McG.W.J. 1972 Int. Met. Reviews,vol.17.'Hot workability'.

- | | | | |
|-----|---|---------|--|
| 41a | Sellars,C.M. & Whiteman,
J.A. | 1974 | The Metallurgist and Mat.
Technologist.'A look at the
metallurgy of the hot rolling
of steel.' |
| 42 | Lubahn,J.D. &
Schenectady,N.Y. | 1947 | Jnl. App. Mech. vol.14,p.229.
'Derivation of stress, strain,
temperature, strain rate
relations for plastic deforma-
tion'. |
| 43 | Jonaš,J.J.,Sellars,
C.M. & Tegart,W.J.McG. | 1969 | Metallurgical Reviews,p.1.
'Strength and structure under
hot working conditions.' |
| 44 | Trinks,W. | 1937 | Blast Furnace & Steel Plant.
'Coefficient of friction and
flow in strip rolling.' |
| 45 | Male,A.T. & Cockroft,
M.G. | 1964-5 | Jnl. Inst. Metals,vol.93.
'A method for the determina-
tion of the coefficient of
friction of metals under
conditions of bulk plastic
deformation.' |
| 46 | Gleave,M.R. & Modlen,
G.R. | 1968 | Iron & Steel. 'Simulation
of conditions in hot rolling.' |
| 47 | Pastrnak,Z. & Piontek,
E. | 1977 | Hutnik, Prague.'Application of
slot test to determine the co-
efficient of external friction
when hot rolling.' |
| 48 | Wusatowski | 1969 | Fundamentals of Rolling. |
| 48a | Batchinov | 1948-58 | Symp. of Select. Papers -
Research on the rolling strip.
B.I.S.R.A. London 1960.(From
Wusatowski,48). |
| 49 | Rolling Mill Research
Sub-committee. | 1946 | Iron & Steel Inst. Spec. Rpt.
No.34. |
| 49a | Tafel,W. | 1923 | Rolling and Roll Pass Design.
Dortmund. |
| 49b | Pavlov,I.M. | 1938 | Deformation of Metals during
rolling.(From:Tarnovski &
Pozdeyev,CONTI,1965,'Theory
of rolling and fundamentals
of plastic deformation of
metals'). |

- 50 Roberts, W.L. 1974 Iron & Steel Eng. 'Friction in the hot rolling of steel strip'. Tribological considerations in the hot rolling of low C steels.
- 51 Matsuura, Y. & Motomura, A. 1967 Rpt. of Castings Research Lab. Waseda, no.18. 'Pressure distribution over the arc of contact in cold strip rolling of steel'.
- 51a Zengler, P. 1970 Neue Hutte, pp.274-278.
- 51b Rooyens, G.T. Van & Bachhofen, W.A. 1957 Jnl. of Iron & Steel Inst. 'Friction in cold rolling.'
- 52 Khayyat, F.A. & Lancaster, P.R. 1969 Jnl. of Strain Analysis, vol.4 No.4. 'A photoelastic examination of the stresses in rolls during rolling'.
- 53 Stewartson, R. 1954 Proc. Inst Mech. Eng., 168, pp. 201-208.
- 53a Sims, R.B. & Wright, H. 1963 Jnl. Iron & Steel Inst., March, 'Roll force and torque in hot rolling mills. A comparison between measurement and calculation.'
- 54 Bradley, B.F., Cockett, W.A. & Peel, D.A. 1974 Mathematical process models in iron and steel making. Iron & Steel Inst. 'Transient temperature behaviour of aluminium during rolling and extrusion.' 669.71:629.771-621.777.
- 55 Harding, R.A. 1977 Ph^D Thesis Univ. of Sheffield. 'Temperature and structural changes during hot rolling'. Monitor, June.
- 56 Control & Instrumentation 1975
- 57 Dahlstrom, F.P. 1933 Trans. Am. Soc. Mech. Eng. 15, pp.56-62. 'Morgoil roll neck bearing.' (From: Rolling Mill Research Comm., 49).
- 58 Gregory, B.A. 1977 'An introduction to electrical instrumentation.' Macmillan Pr.
- 59 American Soc. for Met. Metal Handbook, vol.1, 9th ed. 'Properties and selection of iron & steels'.

- 60 Schneider, P.J. 1955 Conduction heat transfer, p.266
Addison-Wesley.
- 61 Jones, A. & Walker, B. 1974 Metals Technology, Jul, pp.310-315.
- 62 Zeltkans, A & Ricciatti, 1977 Iron & Steel Eng., Jan, pp.72-78
R.L. 'Force sensing in rolling mills'.
- 63 Poloukhine, V. 1975 MIR Pub. Technique sovietique.
'Simulation mathematique et
calcul sur ordinateur des
laminoirs a toles.'
- 64 Pawelski, O. & Brun, E. 1976 Stahl und Eisen, 96, (18), pp.864-
869. 'Heat transfer and temper-
ature fields in hot rolling of
steel with special regard to
the influence of scale.' (Trans.
BISITS.)
- 65 Potapkin, V.F. & Bobukh, 1975 Izvestiya vuz Chernaya Metallur.
I.A. (18), pp.670-672. 'Deformation
zone metal flow kinematics
during the rolling of heavy-
gauge strip'.
- 66 Sansome, D.H. 1975 Metals Technology, Nov. pp.522-
31. 'Factors affecting the shape
of strip emerging from a rolling
mill.'
- 67 B.I.S.R.A. Research Rpt. PMT/6622/72/A
'Physical properties for use in
computing temperature and stresses
during heat treatment.'

Appendix I - Case Study.

A steel plate 10cm thick is to be hot rolled to 1cm. In order to produce the minimum grain size it is desirable to make the final reduction when the plate is at a temperature as close as possible to 750°C. At the same time it is necessary to carry out the rolling process as quickly as possible. If all the stands in the mill employ an automatic cut-off when the load applied exceeds 35 MN, determine the optimum rolling programme.

Diameter of the work rolls	450 mm
Width of the strip	1500 mm
Length of the rolls	2200 mm
Coefficient of friction	0.34
Time between passes	5 sec.
Allowable overload on mill	13500 Kw

You should use the data you have obtained for the cooling of a plate during rolling at 900°C to obtain similar information at other rolling temperatures. You should assume that the surface heat transfer coefficient is independent of temperature and the percentage of reduction. You should also assume that the thermal diffusivity and conductivity of the steel are $5.5 \text{ mm}^2/\text{s}$ and $28 \text{ W/m}^2\text{K}$ respectively. Use the yield stress data as given by Cook and McCrum for mild steel.

A method of calculating the temperature of the stock during its passage through a reversing roughing mill is established and modifications to the Cook and McCrum method of calculating roll force and torque are used. A combination of the above elements resulted in a mathematical model which enabled a hot rolling schedule to be established.

The validity of any method used to calculate roll force and torque in hot rolling is closely dependent on the accuracy to which the rolling temperature of the stock is known. Temperature changes inside the stock during a rolling programme were described by Fick's law of transient heat conduction and it was assumed that heat transfers in the thickness direction only and that the heat losses are caused by radiation-convection outside the rolls and conduction between the roll gap. Temperature measurements during an experimental hot rolling test enabled values of surface heat transfer coefficient and the temperature rise associated to the energy of deformation to be established.

1.1 Temperature distributions.

Clearly the amount of heat that can be transferred across the material surface to the relatively cold roll is critically dependent upon the duration of contact. The rolling geometry considered is shown in Fig.2.2.1. The average velocity \bar{V} of a point of the slab surface will be between V_1 and V_2 ; and it has been assumed to be equivalent to the peripheral velocity of the rolls V_r . The time of contact is thus,

$$t_c = \sqrt{R \Delta h} / V_r$$

Similarly, the total time t_0 that the slab and rolls are touching during which the material transfers heat by convection and radiation is given by, $t_0 = L_{in} / V_1$.

where L_{in} is the total length of the ingoing material.

If $T_s = T(x, t)$ denotes the temperature distance x from the surface at time t in the slab, of a thickness $2L$, then,

$$\frac{\partial T}{\partial t} = \alpha \frac{\partial^2 T}{\partial x^2}$$

with the boundary conditions,

$T(x, 0) = T_i$ (uniform), no initial thermal gradient,

$\frac{\partial T(x, t)}{\partial x} = 0$ at the mid-thickness plane,

and $\frac{\partial T(L, t)}{\partial x} + \frac{h_0}{\lambda} [T(L, t) - T_r]$ at the surface.

where T_r represents the roll surface temperature or the surrounding temperature.

The final solution has been given by, ⁽⁶⁰⁾

$$\frac{T - T_r}{T_i - T_r} = 2 \sum_{n=1}^{\infty} \frac{\sin \lambda_n L}{\lambda_n L + \sin(\lambda_n L) \cos(\lambda_n L)} \exp(-\lambda_n^2 \alpha t) \cos(\lambda_n x) \quad (1.1)$$

where the λ_n 's are the roots of the equation,

$$\cot \lambda_n L = \frac{1}{(h_0/\lambda)L} (\lambda_n L)$$

Graphical evaluations of Eq. 1.1 have been presented in charts ⁽⁶⁰⁾

which are given in terms of four dimensionless groups of variables defined as follows;

relative temperature $\equiv (T - T_r) / (T_i - T_r)$

Fourier number (Fo) $\equiv \alpha t / L^2$

Biot number (Bi) $\equiv h_0 L / \lambda$

relative position $\equiv x / L$

Temperature measurements on a mild steel plate 12.5 mm thick preheated to about 900°C, were made with a thermocouple (1.5 mm) inserted in a hole drilled in such a position that the hot junction lay on the mid-width plane < 1.0 mm beneath the surface; a second thermocouple was located on both the mid-width and mid-thickness planes. The thermocouples, (chromel-alumel) encased in stainless steel sheaths with a response time of 0.2 - 0.1 sec. and a standard accuracy of $\pm \frac{3}{4}\%$, ⁽⁵⁶⁾

represented a suitable compromise between response and mechanical strength. Fig.5.5.2 shows the temperature measurements, and the contact of the ingoing material with the rolls is indicated by the jump of the thermocouple voltage.

In order to establish an overall value of surface heat transfer coefficient, from the temperature results, during conduction to the rolls, the time of contact inside the roll gap was assumed of the order of 0.2 sec. and the thickness of the plate $2L$ equivalent to the geometric mean of the entry and exit thickness. Similarly, temperature measurements, before and after rolling, enabled a mean heat transfer coefficient during convective-radiative losses to be established. Hence, using the thermal properties of steel at 900°C and the relevant values of temperature, surface heat transfer coefficients, as given by the graphical solutions of Eq.1.1, were found. Thus,

$$h_c = 1714.3 \text{ W/m}^2\text{ }^{\circ}\text{C} \text{ during conduction}$$

$$h_c = 176.4 \text{ W/m}^2\text{ }^{\circ}\text{C} \text{ during convection-radiation.}$$

In the rolling programme corrections to the total decrease in temperature during the contact time to include the heat due to deformation, was made by assuming that the resulting temperature rise, measured in the experimental test of about $\sim 20^{\circ}\text{C}$, was uniformly distributed over the slab thickness during each pass. Finally, it was assumed that the effective temperature across the slab section, \bar{T}_s , was equivalent to the mean between the temperature at the surface and the centre respectively.

1.2 Modified Cook and McCrum method to calculate roll force and torque.

The Cook and McCrum formula⁽³⁴⁾ to calculate roll force is $P = R C_p J_p$ where C_p is a geometric factor plotted against R/h_2 for a range of reductions up to 50%, and J_p is a function of the mean yield stress

of the material, \bar{K}_p , and plotted against strain rate and reduction at 900, 1000, 1100 and 1200°C. Linear interpolation was used to determine the function J_p at intermediate temperatures, thus,

$$J_p' = \left[\frac{J_p T_1 - J_p T_2}{100} (T - T_1) + J_p T_1 \right]$$

and extrapolations at temperatures below 900°C approximated to,

$$J_p' = \left[J_p 900 + \left(\frac{900 - T}{150} \right) 4.5 \right]$$

The formula to calculate roll torque is $G = 2R'RC_\epsilon J_\epsilon$, where C_ϵ is a geometric factor which is plotted against R'/h_2 for a range of reductions and J_ϵ is a function of the mean yield stress of the material, \bar{K}_ϵ . Temperature corrections for J_ϵ are complicated by the fact that the temperature decrease calculated for the contact time, t_c , will overestimate the effect of temperature drop on the yield stress in the vicinity of entry where the associated lever arms are greatest. Thus, a correction suggested by Denton et al. (17) was expressed in this work as,

$$J_\epsilon' = \frac{J_p'}{J_p} J_\epsilon$$

1.3 Calculation procedure.

A calculation procedure was adopted in order to establish a hot rolling programme complying with the following conditions,

- a minimum reheating temperature
- a minimum scheduled time
- a final high reduction as close to 750°C as possible, in order to produce a minimum grain size.

The initial reheating temperature was limited to 1250°C, as the oxide formed on the slab becomes liquid at 1280°C and this might result in a loss of traction between the material and the rolls. The following steps were taken during the calculations:

1. Assume n equal reductions r to give the selected final thickness,

from the expression, $(1-r)^n = h_f/h_o$.

2. Calculate the mean temperature of front end at exit from the rolls at a minimum rolling velocity ($N = 40 \text{ rev/min}$)
3. Calculate roll force for the front end at mean exit temperature $P_c = R'_c \rho_j \rho_w$. If the value of P_c exceeds the capacity of the stands, iterate until the maximum allowable reduction is achieved.
4. Calculate the associated roll torque allowing 2.5% losses to the back-up rolls^(4e), thus, $G_c = 2.25 R'_c \rho_c \rho_w$
5. Convert the roll torque into output motor power from the formula, $KW = 0.102 G_c N$. If this exceeds the allowable overload, recalculate stages 3 and 4 to find the maximum possible reduction; otherwise increase the rolling velocity until the capacity of the motor is reached.
6. Calculate the pass entry temperature of the back end of the slab $\bar{T}_s = T_s(t)$ where time $t = L_{in} / v_r \left(\frac{h_1 + h_2}{2 h_1} \right)$
7. Repeat stages 3, 4 and 5 until an acceptable reduction for the back end of the slab is achieved.
8. If the reduction given by stage 7 differs from that calculated in stage 1, find the equal reductions required in the remaining passes to give the selected final thickness.
9. Calculate the pass entry temperature of the front end after the time between passes (5 sec.) and repeat stages 3 to 8.
10. If the slab mean temperature during the last pass exceeds significantly 750°C , decrease the initial rolling temperature and repeat the entire procedure.

Roughing Mill Schedule for 10 mm Breakdown Thickness.

Pass No.	N, rpm	h ₂ , mm	r%	l, m	Delay time, s	Pass time, s	Pass temp, °C	P, MN	Power, kW
1	80	60	40	8.3	5	4.4	1200 1165	16.1 17.8	10768.5 11812.0
2	90	36	40	15.0	5	6.5	1113 1084	17.24 18.4	10504.5 11245.6
3	100	20	44	27.0	5	11.5	1031 1005	20.6 21.7	11695.0 12267.3
4	80	10	50	54.0	5	28.6	940 780	25.0 33.5	5868.0 8130.0

The temperature column indicates front/back end entry temperatures.

Mean temperatures between the rolls during the last pass at front/back end - 900/740°C.

/IC GARZALEZ

J30

/ETC

400 MUSIC JOB

```

C PROGRAM FOR ESTIMATING ROLL FORCE AND TORQUE IN FLAT HOT ROLLING
C USING A NUMERICAL METHOD OF INTEGRATION OF VON KARMANS EQUATION
C  $D((H(S-2K+TAU*TAN(PHI)))/DPHI=2.0*RD*(S*SIN(PHI)+TAU*COS(PHI)))$ .
C WHERE TAU=M*AS OR K,WHICHEVER THE SMALLER,AND INCLUDING
C THE VARIATION OF 2K,AND BOTH ELASTIC ARCS OF CONTACT.
C NOTATION
C H = THICKNESS, H1 = ENTRY THICKNESS, H2 = EXIT THICKNESS,
C HM = MEAN THICKNESS, X2K = YIELD STRESS IN PLANE STRAIN,
C X2K1 = X2K AT ENTRY, X2K2 = X2K AT EXIT, XK = YIELD SHEAR STRESS,
C XKM = XK AT NEUTRAL POINT,
C T1 = ENTRY TENSION STRESS, T2 = EXIT TENSION STRESS,
C T1E1 = TENSION STRESS ON THE ENTRY SIDE OF THE PLASTIC ARC OF CONTACT.
C T1E2 = TENSION STRESS ON THE EXIT SIDE OF THE PLASTIC ARC,
C E = YOUNGS MODULUS AND XNU = POISSON'S RATIO OF THE STRIP MATERIAL
C B,G,D,H ARE CONSTANTS IN EQ.  $2K = EXP(B)(STR*G)(ST**((D+H*LN(STR)))$ 
C S(I) = STRAIN,STR(I) = STRAIN RATE,XW = INHOMOGENEITY FACTOR
C R = UNDEFORMED ROLL RADIUS, RD = DEFORMED ROLL RADIUS,
C VR = PERIPHERAL ROLL VELOCITY,XMU = COEFFICIENT OF FRICTION
C PHI = ANGULAR COORDINATE IN ARC OF CONTACT, DPHI = DELTA PHI,
C PHI1 = PHI AT ENTRY, PHIN = PHI AT NEUTRAL POINT,
C PHIE = PHI AT ONSET OF YIELDING,
C PEX(I) = HORIZONTAL PRESSURE CALCULATED FROM THE EXIT PLANE
C PEN(I) = HORIZONTAL PRESSURE CALCULATED FROM THE ENTRY PLANE
C S(I) = ROLL PRESSURE, SPHI(I)= S(I)*PHI
C SEX(I) = S(I) CALCULATED FROM THE EXIT PLANE
C SEN(I) = S(I) CALCULATED FROM THE ENTRY PLANE
C P = ROLL FORCE / UNIT WIDTH, PAP = APPROXIMATE VALUE OF ROLL FORCE
C PE1 = CONTRIBUTION TO THE ROLL FORCE FROM THE ENTRY ELASTIC ARC,
C PE2 = CONTRIBUTION TO THE ROLL FORCE FROM THE EXIT ELASTIC ARC,
C T AND TAP = APPROXIMATE VALUES OF TORQUE,
C G AND GAP = T AND TAP MODIFIED TO ALLOW FOR ROLL FLATTENING,
C GAC = ACCURATE VALUE OF TORQUE FROM THE PLASTIC ARC,
C GE1 = CONTRIBUTION TO THE ROLL TORQUE FROM THE ENTRY ELASTIC ARC,
C GE2 = CONTRIBUTION TO THE ROLL TORQUE FROM THE EXIT ELASTIC ARC,
C GAC12 IS THE BEST ESTIMATE OF THE TORQUE, = GAC+GE1+GE2,
C TAU = SHEAR STRESS AT THE ROLL-MATERIAL SURFACE INTERFACE,
C G1,G2,G3,G4 = FUNCTIONS OF PHI AS DEFINED, J = COUNTER FOR NUMBER
C OF ITERATIONS TO OBTAIN COMPATIBLE ROLL FORCE AND DEFORMED ROLL
C RADIUS.
C M = ODD NUMBER OF ORDINATES IN ROLL PRESSURE DISTRIBUTION.
/LEAD WATFIV
EXTERNAL G1,G2,G3,G4
DIMENSION XK(150),S(150),SEX(150),SEN(150),SPHI(150),TAU(150),SSI
1N(150),GORD(150),TAUSIN(150),SCOS(150),ST(150),STR(150),PEN(150),P
,2FX(150)
COMMON H1,H2,XMU,RD,VR,Z,B,D,G,H,G,PHI1,XW,PHN
READ(5,10)E,XNU,B,D,G,H
10 FURMAT(6F12.5)
READ(5,20)M,XMU,R,VR,H1,H2,T1,T2
20 FURMAT(14,7F9.4)
WRITE(6,40)E,XNU,B,D,H,G,XMU,R,VR,H1,H2
40 FURMAT(F9.1,10F9.3)
Z=2.0/SQRT(3.0)
DRAFT=H1-H2
C SL43 ENTRY CONDITION
H2MIN=H1-2.0*R*(1.0-COS(ATAN(XMU)))

```

```

IF(H2.LT.H2*MIN) H2=H2*MIN
PS=-Z*ALOG(1.0-0.002)
PHI1=ARCOS(1.0-DRAFT/(2.0*R))
PHN=1.0/5.0*PHI1
H1=H2+2.0*R*(1.0-COS(PHN))
XDR=Z*2.0*VR*PHN*COS(PHN)*PHI1/(H2+R*PHI1*2.0)*2.0
X2K1=Z*EXP(B)*XCR**G*PS*(L+H*ALOG(XLR))
X2K2=Z*EXP(B)*0.1*G*(Z*ALOG(H1/H2))**(D+H*ALOG(0.1))
C TENSIONS CONDITIONS
IF(T1.GT.X2K1) T1=X2K1
IF(T2.GT.X2K2) T2=X2K2
WRITE(6,50)
50 FORMAT(/5X, 'H2',10X,'T1',10X,'T2'/)
WRITE(6,60) H2,T1,T2
60 FORMAT(3F18.10)
J=0
N1=N-1
RL=SQRT(2*DRAFT)
HM=(2.0*H2+H1)/3.0
A=XMU*RL/HM
X2KM=(X2K1+2.0*X2K2)/3.0-(T1+T2)/2.0
PAP=X2KM*RL*(EXP(A)-1.0)/A
RD=R*(1.0+0.0024261*PAP/DRAFT)
P1=PAP
TE1=T1
TE2=T2
1 PHI1=ARCOS(1.0-DRAFT/(2.0*RD))
PHIE=ARCOS(COS(PHI1)+0.002*H1/(2.0*RD))
XM=M
DPHI=PHI/(XM-1.0)
XK(M)=.5*X2K2
J3=0
2 PHI=PHIE
DO 11 I=1,M1
XK(I)=.5*Z*w(PHI)
ST(I)=DF(PHI)
STR(I)=DFR(PHI)
11 PHI=PHI-CPHI
S(1)=(2.0*XK(1)-TE1)/(1.0+XMU*TAN(PHIE))
IF(XMU*S(1).GT.XK(1)) S(1)=2.0*XK(1)-TE1-XK(1)*TAN(PHIE)
S(M)=X2K2-TE2
SEX(M)=S(M)
PHI=DPHI/2.0
Q=+1.0
M2=M-2
XW=SQRT(1.0-1.5326*((XMU+SEX(M))/(2.0*XK(M)))**2)
PEX(M)=SEX(M)-2.0*XK(M)*XW
J4=0
C FORWARD INTEGRATION TO DETERMINE PEN(I) AND PEX(I) USING THE
C FOURTH ORDER RUNGE KUTTA METHOD
DO 21 I=1,M2
L=M+1-I
12 IF(XMU*SEX(L).LT.XK(L))CALL RK(PHI,PEX(I),DPHI,DP,G1,G2)
IF(XMU*SEX(L).GE.XK(L))CALL RK(PHI,PEX(I),DPHI,DP,G4,G3)
PEX(L-1)=PEX(L)+DP
SEX(L-1)=SEX(L)+2.0*XK(L-1)*XW
IF(XMU*SEX(L-1).GE.XK(L-1)) GO TO 14
XW1=SQRT(1.0-1.5326*((XMU+SEX(L-1))/(2.0*XK(L-1)))**2)
GO TO 15
14 XW1=0.7854
15 IF(ABS((XW1-XW)/XW1).LE.0E-2.OR.J4.GT.3)GO TO 21
XW=XW1

```

```

J4=J4+1
GO TO 12
21 PHI=PHI+CPHI
SEX(1)=SEX(2)
SEN(1)=S(1)
PHI=PHIE
Q=-1.0
XW= SQRT(1.0-1.5326*((XMU*SEN(1)/(2.0*XK(1)))**2))
PEN(1)=SEN(1)-2.0*XK(1)*XW
J5=0
DO 31 I=1,M2
13 IF(XMU*SEN(I).LT.XK(I))CALL RK(PHI,PEN(I),DPHI,DP,G1,G2)
IF(XMU*SEN(I).GE.XK(I))CALL RK(PHI,PEN(I),DPHI,DP,G4,G3)
PEN(I+1)=PEN(I)+DP
SEN(I+1)=PEN(I+1)+2.0*XK(I+1)*XW
IF(XMU*SEN(I+1).GE.XK(I+1)) GO TO 16
XW1=SQRT(1.0-1.5326*((XMU*SEN(I+1)/(2.0*XK(I+1)))**2))
GO TO 18
16 XW1=0.7854
18 IF(ABS((XW1-XW)/XW1).LE.0E-2.OR.J5.GT.3)GO TO 31
XW=XW1
J5=J5+1
GO TO 13
31 PHI=PHI-DPHI
SEN(M)=SEN(M1)
DO 41 I=1,M
IF(SEX(I).LE.SEN(I)) S(I)=SEX(I)
IF(SEN(I).LE.SEX(I)) S(I)=SEN(I)
41 CONTINUE
DO 51 I=1,M1
IF(SEX(I).GE.SEN(I).AND.SEN(I+1).GE.SEX(I+1)) GO TO 61
51 CONTINUE
GO TO 24
61 X=DPHI/(1.0+(SEX(I)-SEN(I))/(SEN(I+1)-SEX(I+1)))
X11=I+1
PHIN=(X-X11)*DPHI+X
IF(ABS((PHIN-PHN)/PHN).LE.0E-1.OR.J3.GT.12)GO TO 81
PHN=PHIN
C ITERATE J3 TIMES TO FIND CONSISTENT PHIN
J3=J3+1
GO TO 2
81 Y=(SEN(I+1)-SEN(I))*(1.0-X/DPHI)
SN=SEN(I)+Y
IN=I
XKN=.5*Z*W(PHIN)
IF(XMU*SN.LT.XKN) TAU=AMU*SN
IF(XMU*SN.GE.XKN) TAU=XKN
PHI=PHIE
DO 71 I=1,M
ARG=PHI-0.5*PHIE
XS=SIN(ARG)
XC=COS(ARG)
SPHI(I)=S(I)*PHI
SSIN(I)=S(I)*XS
SCOS(I)=S(I)*XC
IF(XMU*S(I).LT.XK(I)) TAU(I)=XMU*S(I)
IF(XMU*S(I).GE.XK(I)) TAU(I)=XK(I)
TAUSIN(I)=TAU(I)*XS
GORC(I)=TAU(I)*(RD-(RD-R)*XC)
71 PHI=PHI-CPHI
C INTEGRATE ROLL PRESSURE BY TRAPEZOIDAL RULE TO FIND THE ROLL FORCE
C INCLUDING THE CONTRIBUTIONS OF THE SHEAR STRESSES

```

```

TAUNSN=TAUN*SIN(PHIN-PHI1+0.5)
DAEN=(TAUSIN(IN)+TAUNSN)*(DPHI-X)*0.5
DAEX=(TAUSIN(IN+1)+TAUNSN)*X*0.5
CALL TRAPEZ(TAUSIN,DPHI,2,IN-1,AREA)
AREAEN=AREA+DAEN
CALL TRAPEZ(TAUSIN,DPHI,IN+2,M-1,AREA)
AREAEX=AREA+DAEX
CALL SIMPSN(SCOS,DPHI,2,M-3,AREAP)
P=RD*(AREAP+AREAEN-AREAEX)
C ITERATE J1 TIMES TO FIND PE1 AND TE1
J1=0
PE1=(1.0-XNU**2)*H1*(X2K1-T1)**2*SQRT(RD/DRAFT)/(4.0*E)
44 TE1=T1-2.0*XMU*PE1/H1
PE1=(1.0-XNU**2)*H1*(X2K1-TE1)**2*SQRT(RD/DRAFT)/(4.0*E)
IF(ABS((PE1-PE11)/PE1).LT.1.0E-4.OR.J1.GT.12) GO TO 45
PE11=PE1
J1=J1+1
GO TO 44
45 A1=(2.0/3.0)*SQRT(RD*H2*(1.0-XNU**2)/E)
C ITERATE J2 TIMES TO FIND PE2 AND T2
J2=0
PE2=A1*(X2K2-T2)**1.5
59 TE2=T2-2.0*XMU*PE2/H2
PE2=A1*(X2K2-TE2)**1.5
IF(ABS((PE2-PE21)/PE2).LT.1.0E-4.OR.J2.GT.10) GO TO 46
PE21=PE2
J2=J2+1
GO TO 39
46 P=P+PE1+PE2
DRAFTT=XNU*(1.0+XNU)*(H2*T2-H1*T1)/E
DRAFTE=(1.0-XNU**2)*(X2K2-TE2)*H2/E
A2=.00024261/(SQRT(DRAFT+DRAFTE+DRAFTT)+SQRT(DRAFTE))**2
RD=R*(1.0+A2*P)
IF(ABS((P-P1)/P1).LT.1.0E-5.OR.J.GT.30) GO TO 17
P1=P
C ITERATE J TIMES TO FIND COMPATIBLE P AND RD
J=J+1
GO TO 1
17 GE1=XMU*R*PE1
GE2=-XMU*R*PE2
C INTEGRATE SHEAR STRESSES TO DETERMINE THE TORQUE APPROXIMATELY
DAEXT=(TAUN+TAU(IN+1))*X/2.0
DAENT=(TAUN+TAU(IN))*(DPHI-X)/2.0
CALL TRAPEZ(TAU,DPHI,2,IN-1,AREA)
AREANT=AREA+DAENT
CALL TRAPEZ(TAU,DPHI,IN+2,M-1,AREA)
AREAXT=AREA+DAEXT
TAP=R*RD*(AREANT-AREAXT)
GAP=RD**2*(AREANT-AREAXT)-0.5*(RD-R)*(P*PHI1+T1*H1-T2*H2)
CALL SIMPSN(SPHI,DPHI,2,M-3,AREAT)
T=R*RL*AREAT+(R/2.0)*(T1*H1-T2*H2)
G=RD**2*AREAT+(R/2.0)*(T1*H1-T2*H2)-P*(RD-R)*PHI1/2.0
C INTEGRATE EQUATION FOR ACCURATE TORQUE GAC
GURDN=TAUN*(RD-(RD-R)*COS(PHIN-PHI1+0.5))
DAEXG=(GURDN+GURD(IN+1))*X*0.5
DAENG=(GURDN+GURD(IN))*(DPHI-X)*0.5
CALL TRAPEZ(GURD,DPHI,2,IN-1,AREA)
AREANG=AREA+DAENG
CALL TRAPEZ(GURD,DPHI,IN+2,M-1,AREA)
AREAXG=AREA+DAEXG
CALL SIMPSN(SSIN,DPHI,2,M-3,AREAG)
GAC=RD*(RD-R)*AREAG+RD*(AREANG-AREAXG)

```

```

GAC12=GAC+GE1+GE2
WRITE(6,52)(S(I),XK(I),I=1,M)
52 FURMAT(10F10.4)
WRITE(6,53)(ST(I),STR(I),I=1,M1)
53 FURMAT(10F10.4)
WKITE(6,100)P,P1,PAP,T,TAP,RC,G,GAC,GAC12,PHI1,PHIN,SN,J
100 FURMAT(///12F9.3,I3)
GO TO 26
24 WRITE(6,25)
25 FURMAT(//'NO NEUTRAL POINT CAN BE FOUND'/)
26 CALL EXIT
END
FUNCTION DF(PHI)
COMMON H1,H2,XMU,RD,VR,Z,B,D,G,H,Q,PHI1,XW,PHN
XH=H1-2.0*RD*(COS(PHI)-COS(PHI1))
DF=Z*ALOG(H1/XH)
RETURN
END
FUNCTION DFR(PHI)
COMMON H1,H2,XMU,RD,VR,Z,B,D,G,H,Q,PHI1,XW,PHN
XCN=COS(PHN)
HN=H2+2.0*RD*(1.0-XCN)
XH=H1-2.0*RD*(COS(PHI)-COS(PHI1))
DFR=2.0*VR*HN*XCN*PHI/XH**2.0*Z
RETURN
END
FUNCTION W(PHI)
COMMON H1,H2,XMU,RD,VR,Z,B,D,G,H,Q,PHI1,XW,PHN
W=EXP(B)*DFR(PHI)**G*DF(PHI)**(D+H*ALOG(DFR(PHI)))
RETURN
END
FUNCTION G1(PHI)
COMMON H1,H2,XMU,RD,VR,Z,B,D,G,H,Q,PHI1,XW,PHN
XC=COS(PHI)
XH=H1-2.0*RD*(COS(PHI)-COS(PHI1))
G1=2.0*RD*(Q*XMU*XC)/XH
RETURN
END
FUNCTION G2(PHI)
COMMON H1,H2,XMU,RD,VR,Z,B,D,G,H,Q,PHI1,XW,PHN
XS=SIN(PHI)
XC=COS(PHI)
XH=H1-2.0*RD*(COS(PHI)-COS(PHI1))
ST=Z*ALOG(H1/XH)
XCN=COS(PHN)
HN=H2+2.0*RD*(1.0-XCN)
STR=2.0*VR*HN*XCN*PHI/XH**2.0*Z
X2K=Z*EXP(B)*STR**G*ST**(D+H*ALOG(STR))
G2=2.0*RD*X2K*(XS+Q*XMU*XC)*XW/XH
RETURN
END
FUNCTION G3(PHI)
COMMON H1,H2,XMU,RD,VR,Z,B,D,G,H,Q,PHI1,XW,PHN
XS=SIN(PHI)
XC=COS(PHI)
XH=H1-2.0*RD*(COS(PHI)-COS(PHI1))
ST=Z*ALOG(H1/XH)
XCN=COS(PHN)
HN=H2+2.0*RD*(1.0-XCN)
STR=2.0*VR*HN*XCN*PHI/XH**2.0*Z
X2K=Z*EXP(B)*STR**G*ST**(D+H*ALOG(STR))
G3=2.0*RD*X2K*(0.7854-Q*0.5*(1.0/PHI-1.0/TAN(PHI)))*XS+Q*0.5*XC/

```

```

1 XH
RETURN
END
FUNCTION C4(PHI)
COMMON H1,H2,XMU,FC,VR,Z,B,C,C,H,Q,PHI1,XW,PHN
G4=J.0
RETURN
END
SUBROUTINE RK(X,Y,DX,DY,FA,FB)
COMMON H1,H2,XMU,RD,VR,Z,B,L,G,H,C,PHI1,XW,PHN
FO=FA(X)*Y+FB(X)
A=FA(X+0.5*Q*DX)
C=FB(X+0.5*Q*DX)
F1=A*(Y+C.5*Q*DX*FO)+C
F2=A*(Y+0.5*Q*DX*F1)+C
F3=FA(X+Q*DX)*(Y+C.5*Q*DX*F2)+FB(X+Q*DX)
DY=DX*(FO+2.0*(F1+F2)+F3)*Q/6.0
RETURN
END
SUBROUTINE TRAPEZ(Y,DX,N1,N2,A)
DIMENSION Y(1)
SUM=0.0
DO 1 I=N1,N2
1 SUM=SUM+Y(I)
A=(DX/2.0)*(Y(N1-1)+2.0*SUM+Y(N2+1))
RETURN
END
SUBROUTINE SIMPSN(Y,DX,N1,N2,A)
DIMENSION Y(1)
ODD=0.0
EVEN=0.0
DO 1 I=N1,N2,2
EVEN=EVEN+Y(I)
1 ODD=ODD+Y(I+1)
A=(DX/3.0)*(Y(N1-1)+4.0*(EVEN+Y(N2+2))+2.0*ODD+Y(N2+3))
RETURN
END

```

END OF JOB GONZALEZ
345 CARDS READ

AT 20H13M WED JAN 07, 1961 EXECUTE TIME
348 LINES PRINTED

3
0 CARDS PUNCHED 0 TAPE MUO

Appendix III Calculation of temperature distributions.

The temperature distributions at all stages of the contact time during the rolling process may be determined by the use of a finite-difference solution to Fick's law of transient heat conduction⁽¹⁾;

$$\frac{\partial \theta}{\partial t} = \alpha \frac{\partial^2 \theta}{\partial x^2}$$

This allows the magnitude of the surface heat transfer coefficient to be established by a continual inspection between measured and calculated temperature distributions.

It is assumed that the only significant temperature gradient lies perpendicular to the longitudinal plane of the plate and that no appreciable heat generation occurs inside the material. For purposes of calculation, half the plate is sub-divided into a set of elements the two largest dimensions of which are identical to the two dimensions of the contact surface between the plate and the rolls. However, in the direction of the temperature gradient (through the thickness of the plate), the element dimension Δx is 0.5×10^{-3} . The positions of the element boundaries at which the temperatures are calculated are shown in Fig.1. It will be noted that the surface plane of the plate coincides with the mid-plane of the first element and that the temperatures are calculated at a boundary (1) which lies outside the surface of the plate.

Provided that⁽¹⁾,

$$\frac{\alpha \Delta t}{\Delta x^2} = \frac{1}{2} \quad (\text{Eq.1})$$

then

$$\theta_{t+1}^n = \frac{\theta_t^{n+1} + \theta_t^n}{2} \quad n=2, \dots, J \quad (\text{Eq.2})$$

where J identifies the penultimate element boundary (see Fig.1).

At the surface,
$$h_s(\theta^s - \theta^\infty) = \lambda \left(\frac{\partial \theta}{\partial x} \right)^s$$

If it is assumed that $(\partial \theta / \partial x)$ remains constant between the surface and the point at which $\theta - \theta^\infty$ (Fig.1), then,

$$h_s(\theta^\infty - \theta^s) = \frac{2\lambda(\theta_1^s - \theta_0^s)}{\Delta x} \quad (\text{Eq.3})$$

This allows the temperature θ_0^1 to be calculated, which in turn may be used to calculate θ_1^2 using Eq.1. θ_0^s is the only surface temperature known and for all positive values of t a modification of Eq.3 must be made. In the present calculation Eq.3 has been replaced for all values of t greater than 0, in accordance with the method used by Aparci⁽²⁾,

$$\theta_{t+\Delta t}^1 = \left[(\theta_t^2 - \theta^\infty) \left(\frac{\lambda}{h_0} - \frac{\Delta x}{2} \right) / \left(\frac{\lambda}{h_0} + \frac{\Delta x}{2} \right) \right] + \theta^\infty$$

This equation assumed that $(d\theta/dx)^s$ remains constant between λ/h_0 and $\Delta x/2$ (Fig.1). The minimum possible number of elements used is determined by the stability criterion $\lambda/h_0 > \Delta x$. For the values of h_0 used in this calculation the number of elements taken in the half section is 14. The magnitude of Δx in turn determines the magnitude of Δt (Eq.1), which is very small in relation to the total contact time. Hence temperature distributions at most stages during deformation can be established.

The values of α, λ , are included in Fig.1, together with the initial temperature of the plate, the temperature of the rolls and the plate thickness.

References.

- 1 Dusinberre, G.H. 1961 'Heat transfer calculations by finite differences' 8: Scranton, Pa. Inter.
- 2 Aparci, V.S. 1966 'Conduction heat transfer', 509, Reading, Mass, Addison-Wesley.

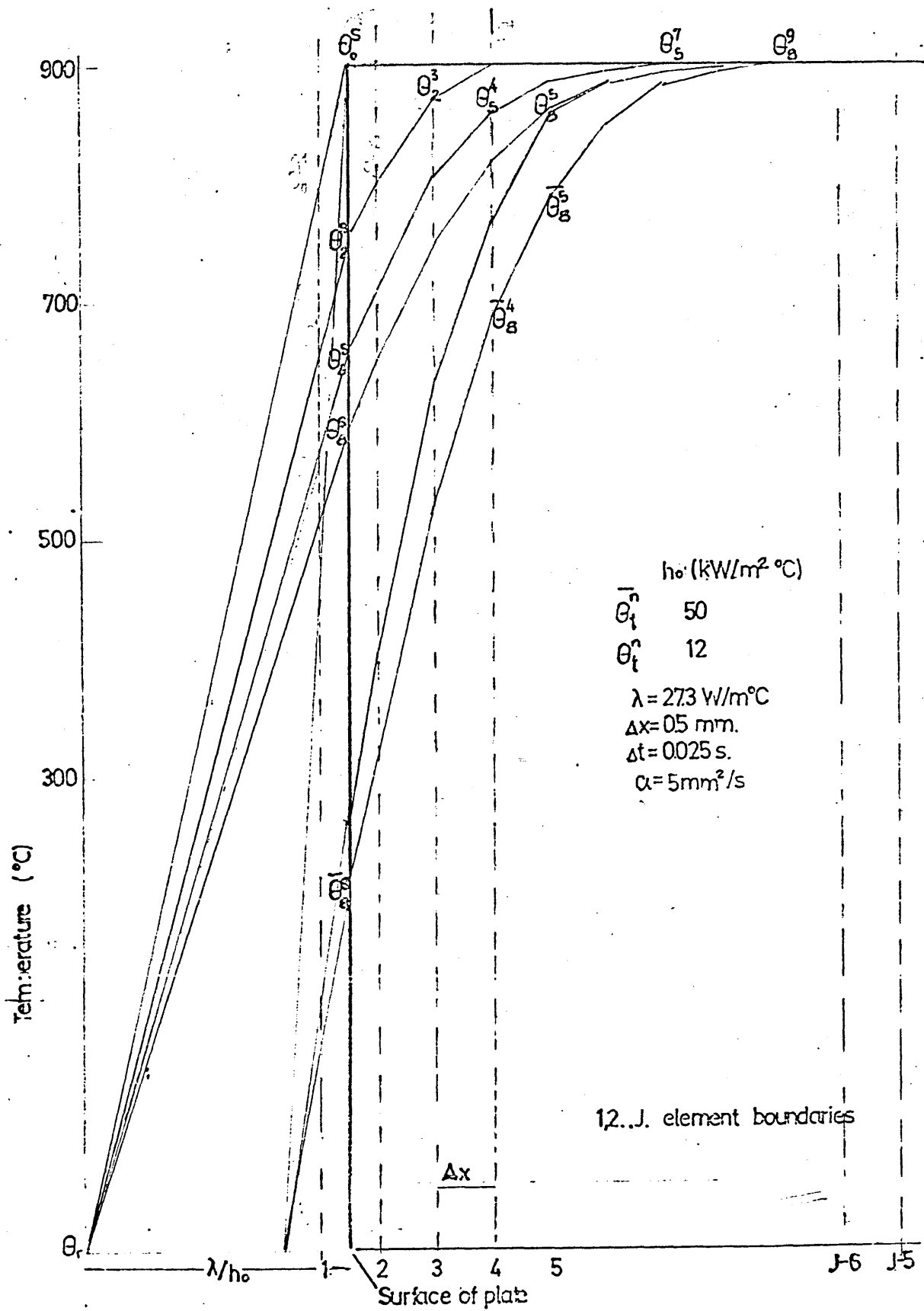


Fig. 1 Temperature distribution through the thickness of the plate.

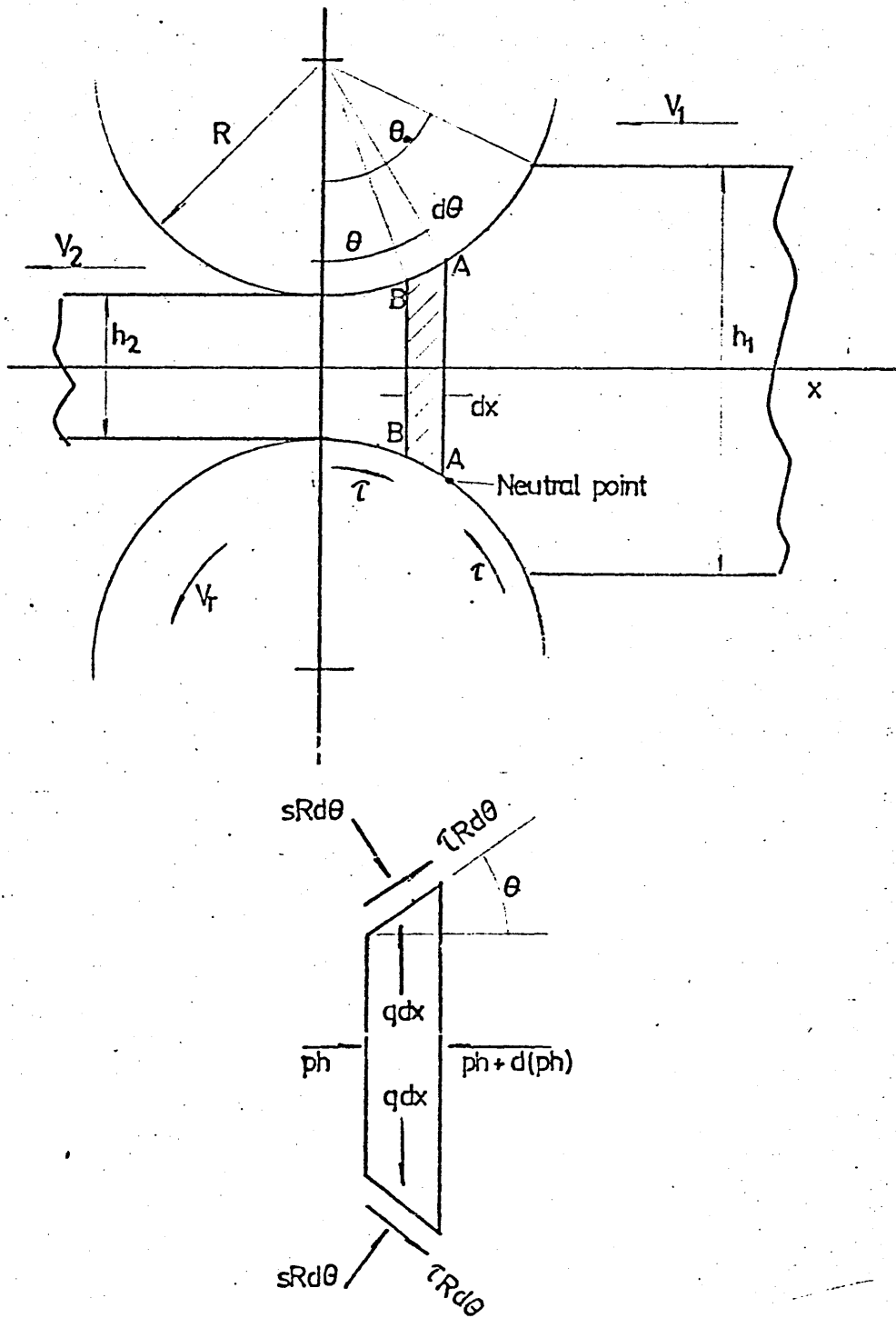


Fig 221 Roll gap geometry and forces applied to a vertical section

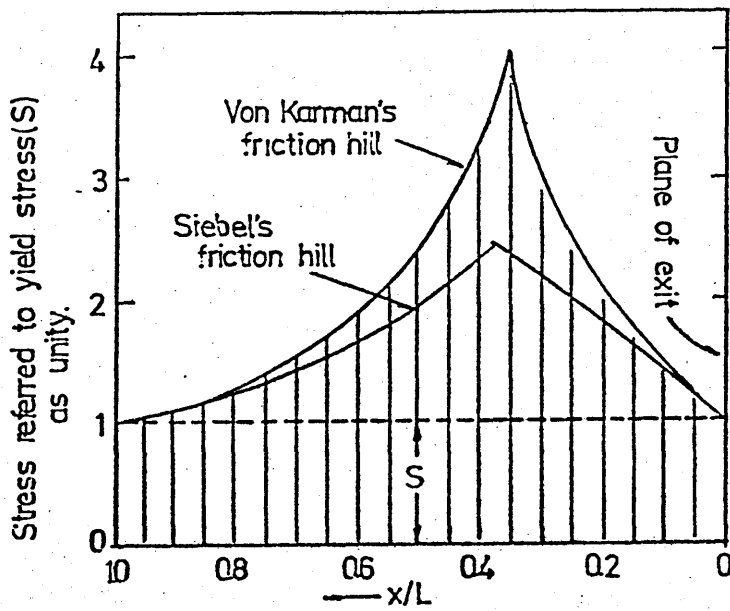


Fig. 2.31 Comparison of Siebel's and von Karman's Roll-pressure distributions.

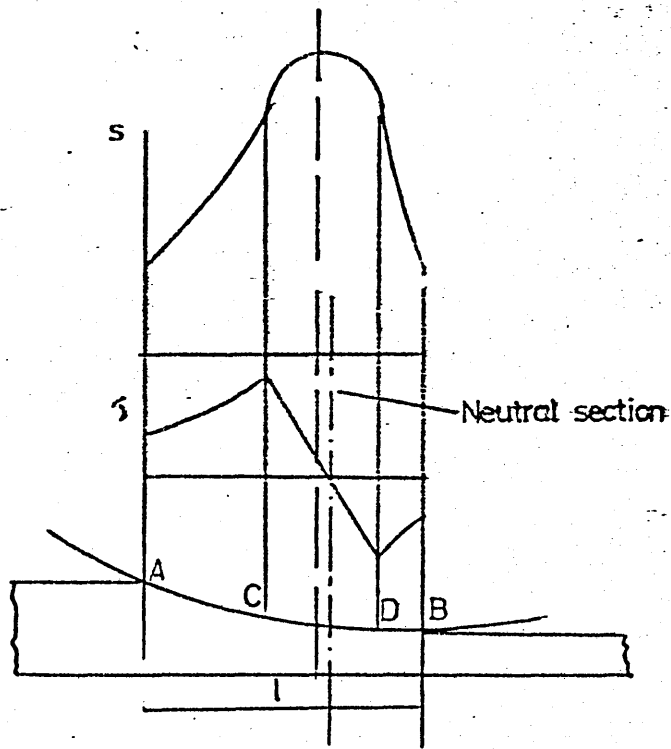


Fig. 2.32 Variation of the radial pressure and shear stresses along the arc of contact.

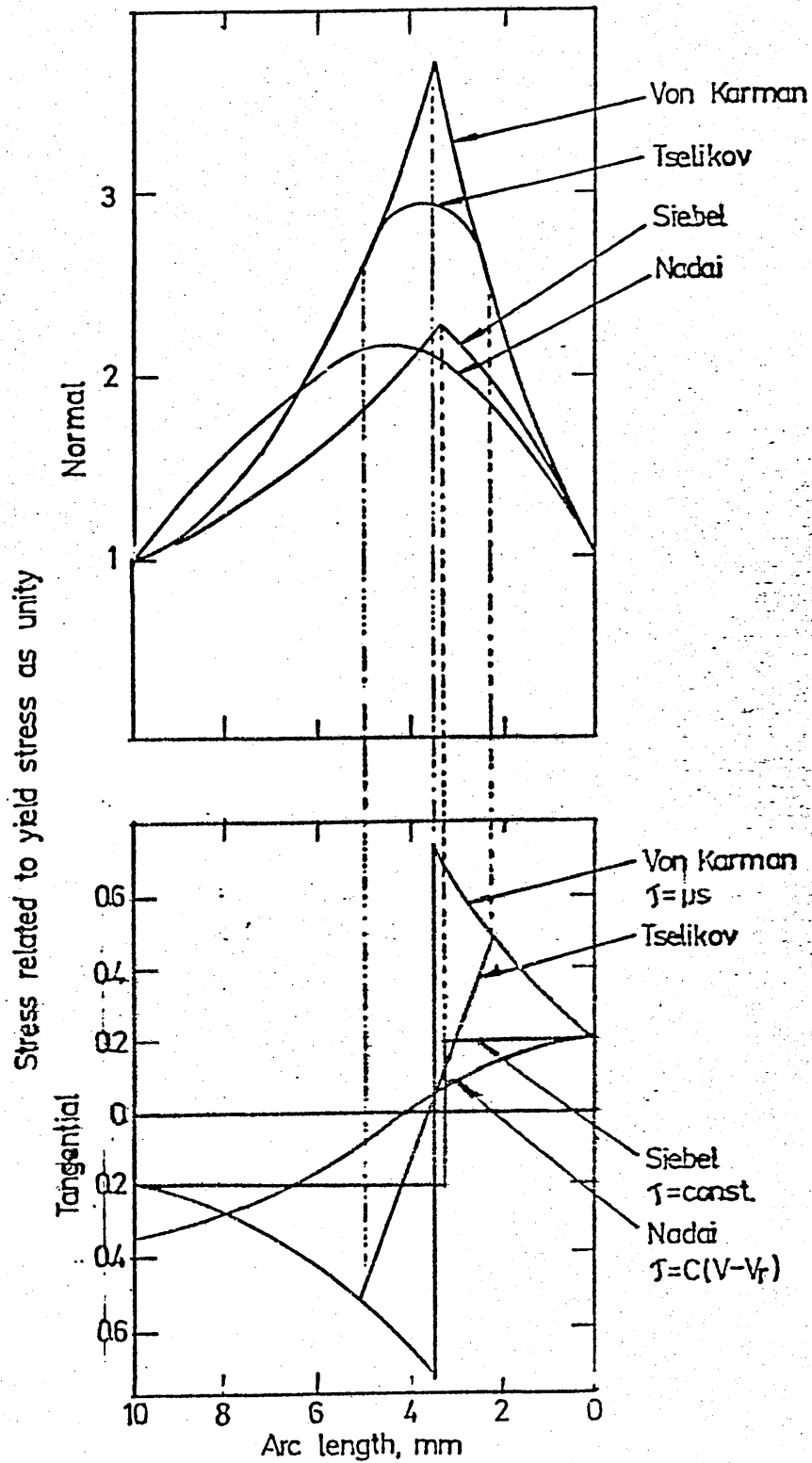


Fig.2.3.3 Distribution of normal and tangential pressures along the arc of contact according to the theories shown.

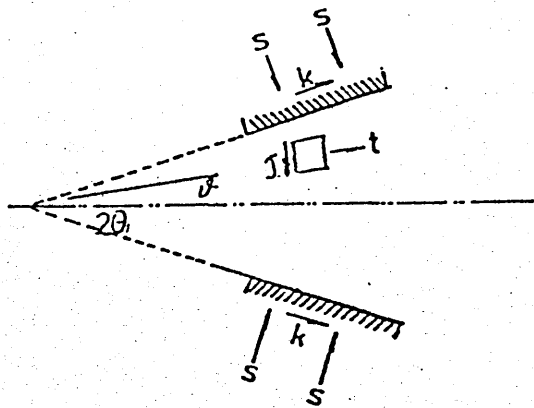


Fig. 2.41. Compression between two rough inclined platens.

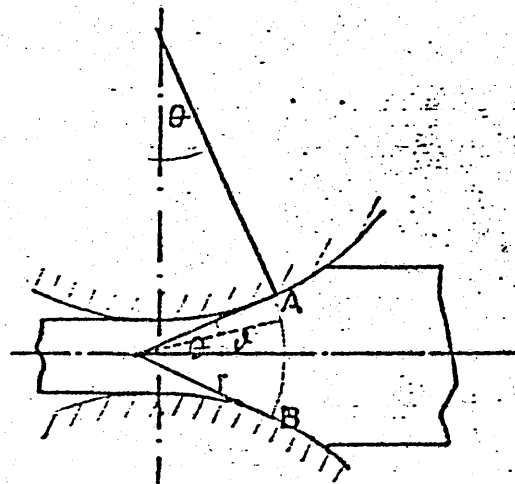


Fig. 2.42 Illustrating the calculation of horizontal force in the strip between the rolls (Orowan)

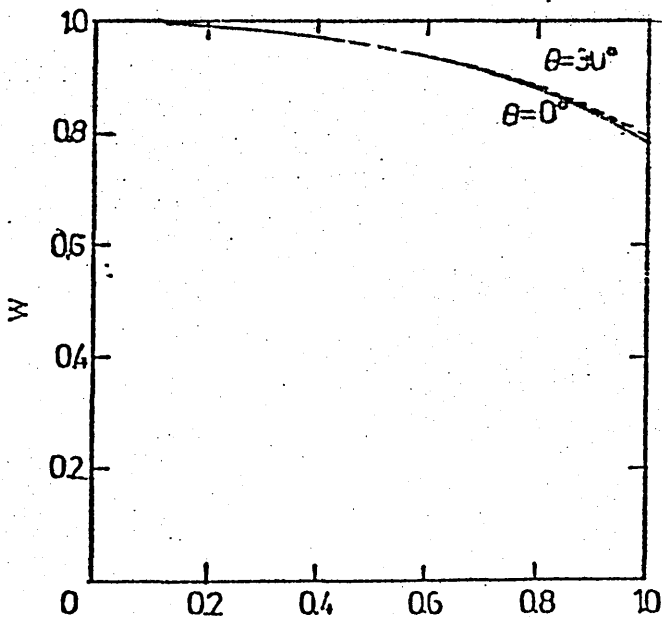


Fig. 2.43. Variation of w with α for various values of θ

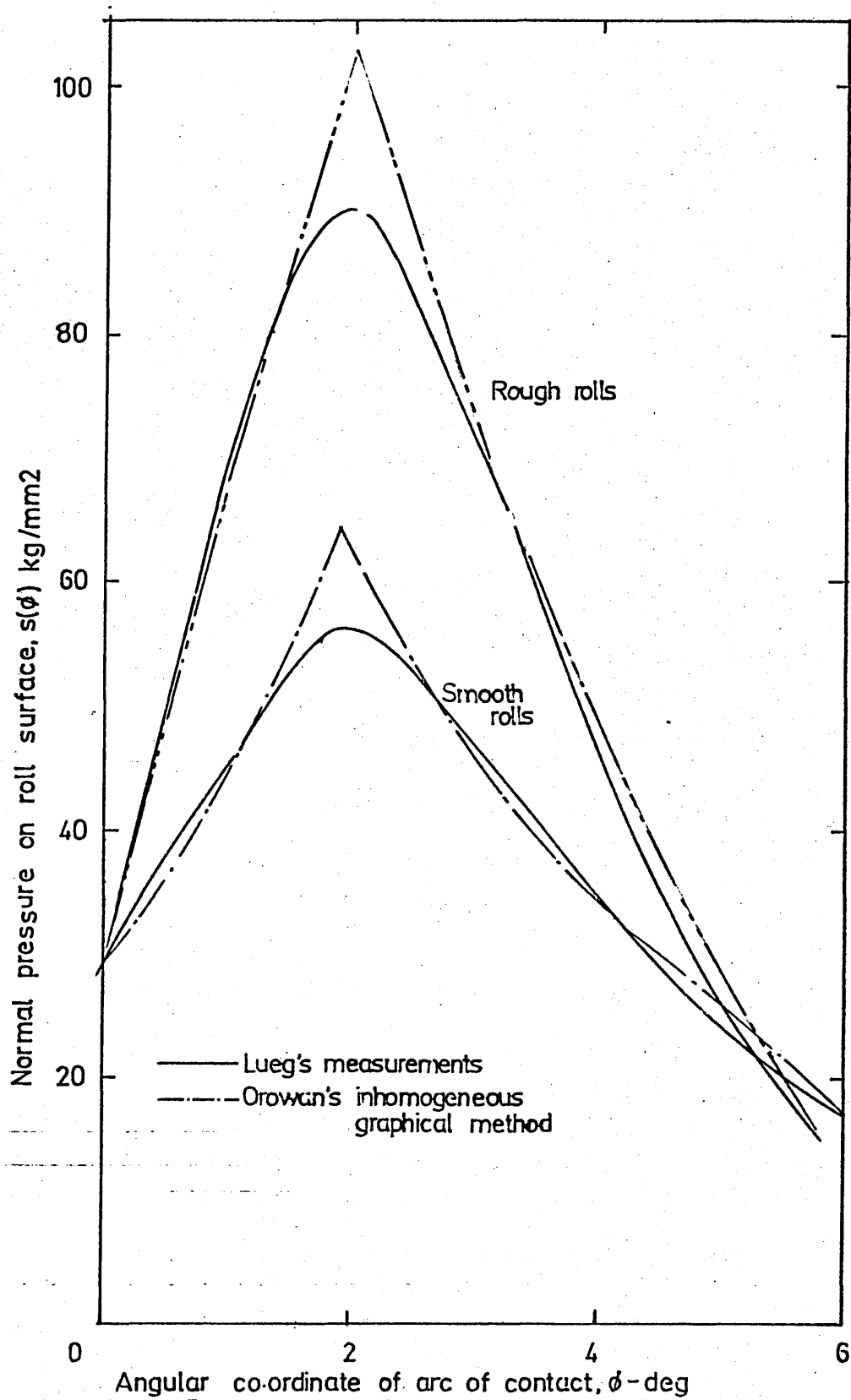


Fig. 2.44. Comparison of measured and calculated roll pressure distributions for smooth ($\mu=0.14$) and rough ($\mu=0.4$) rolls - after Orowan⁴.

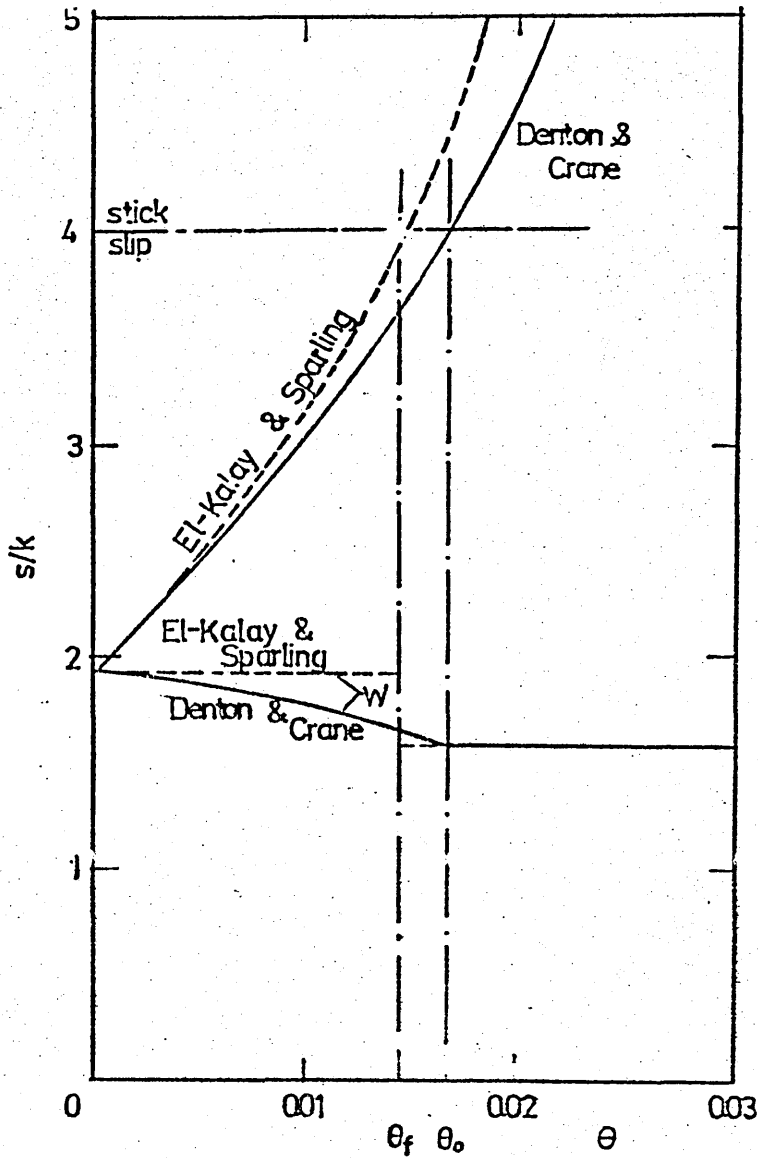


Fig. 2.51 Exit side of a typical friction hill, showing the difference between the Denton & Crane method and that of El-Kalay & Sparling.

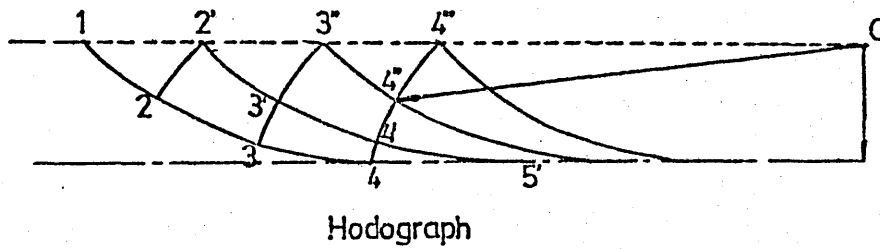
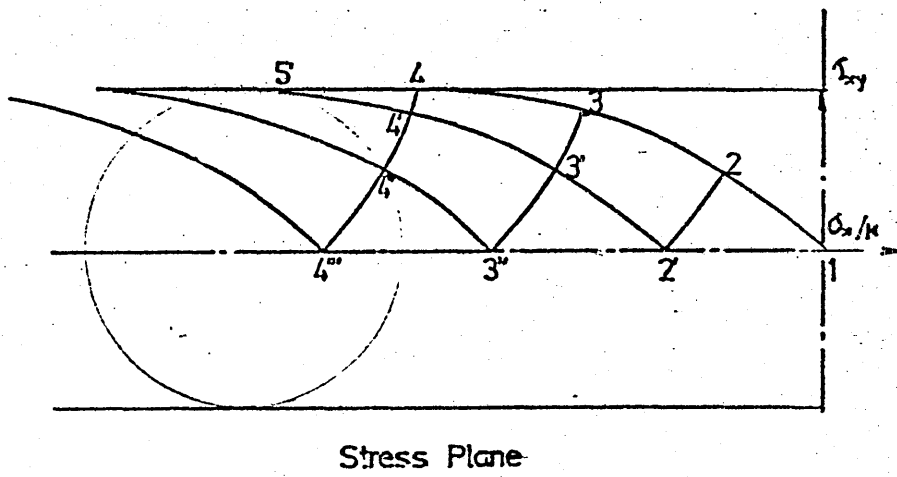
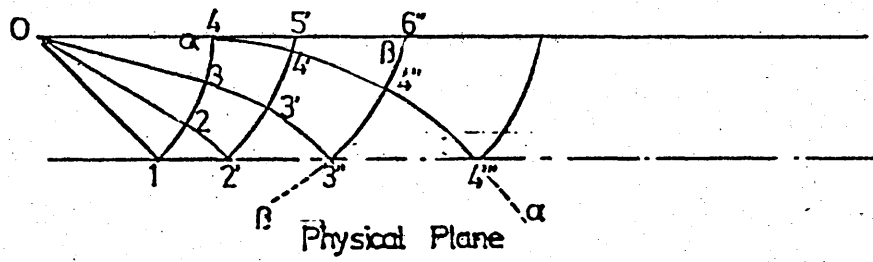


Fig. 261. Geometrical construction of the slip line field solution - after Alexander²¹

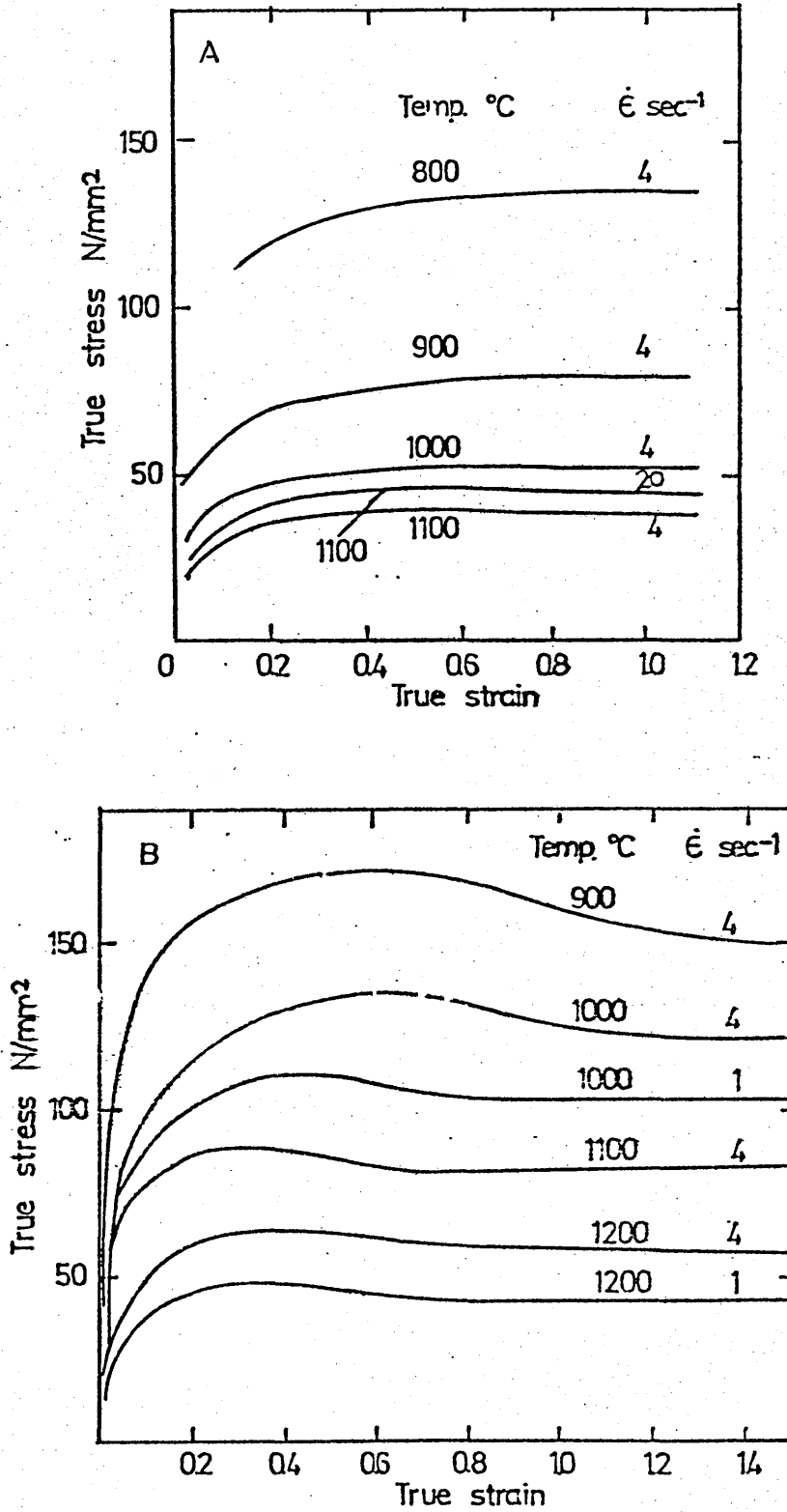


Fig. 29.1. True stress-true strain curves in the hot working temperature range: (A) 3% silicon steel, (B) mild steel.

(after Sellars^{4(a)})

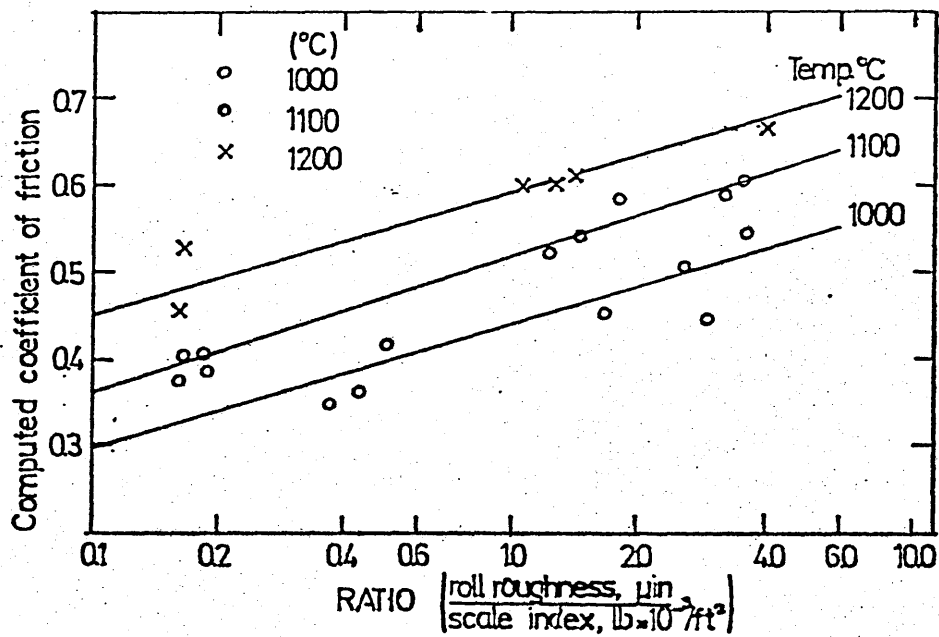


Fig. 2.101. Variation of the coefficient of friction in unlubricated hot rolling conditions - after Roberts⁵⁰

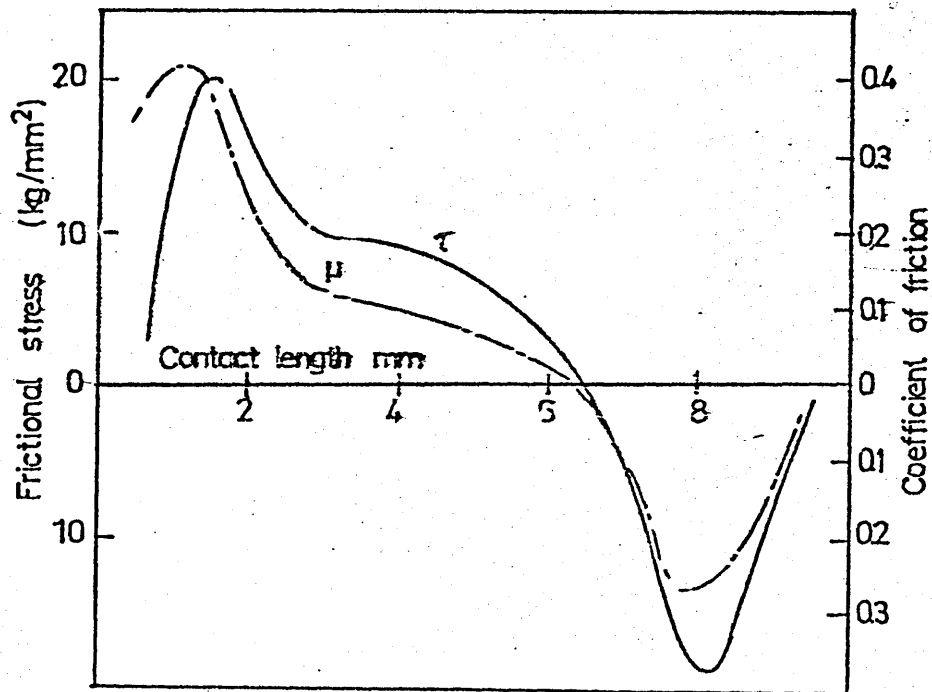


Fig. 2.102. Distributions of shear stress and coefficient of friction along the arc of contact - after Matsuura et al.⁵¹

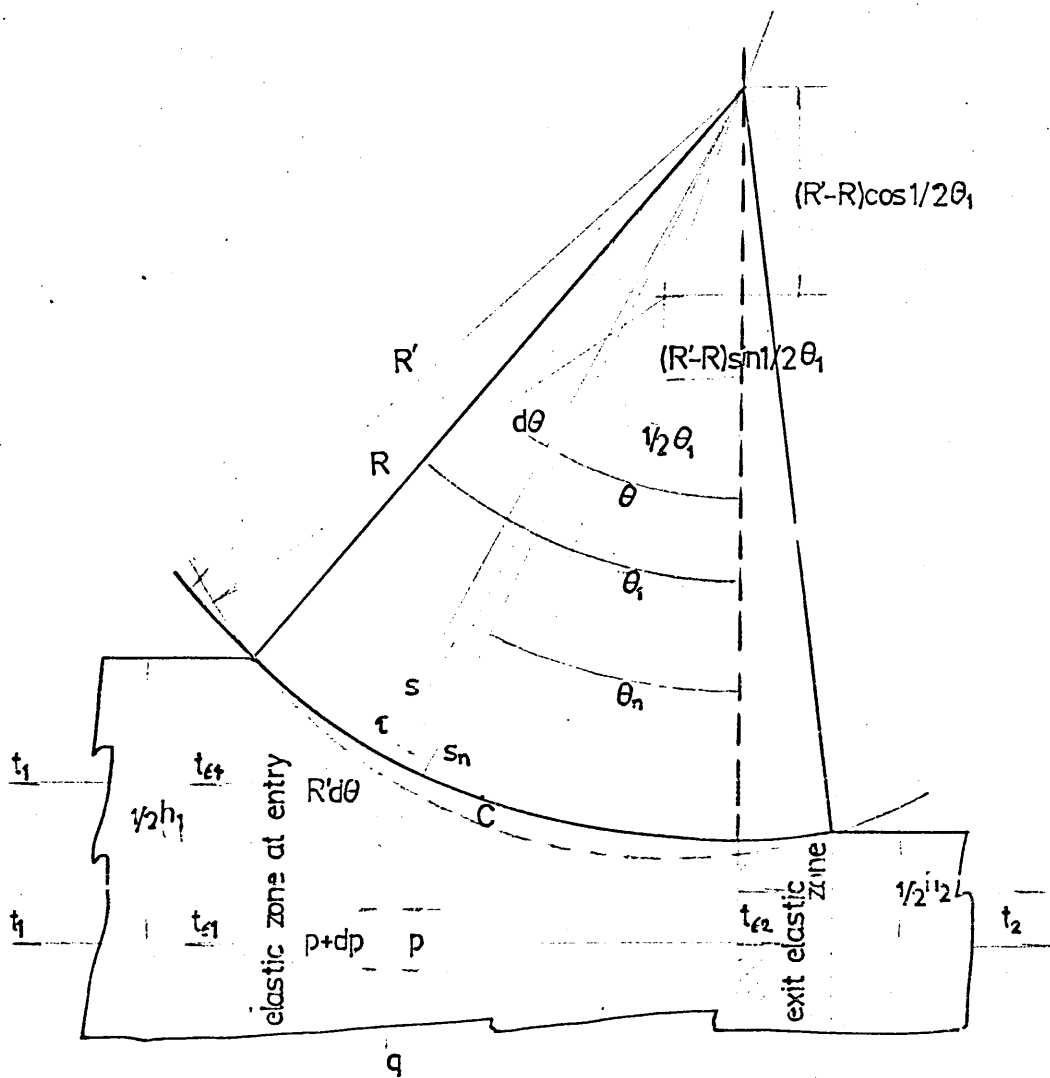


Fig.3.2.1 Longitudinal section of a strip between two rolls.

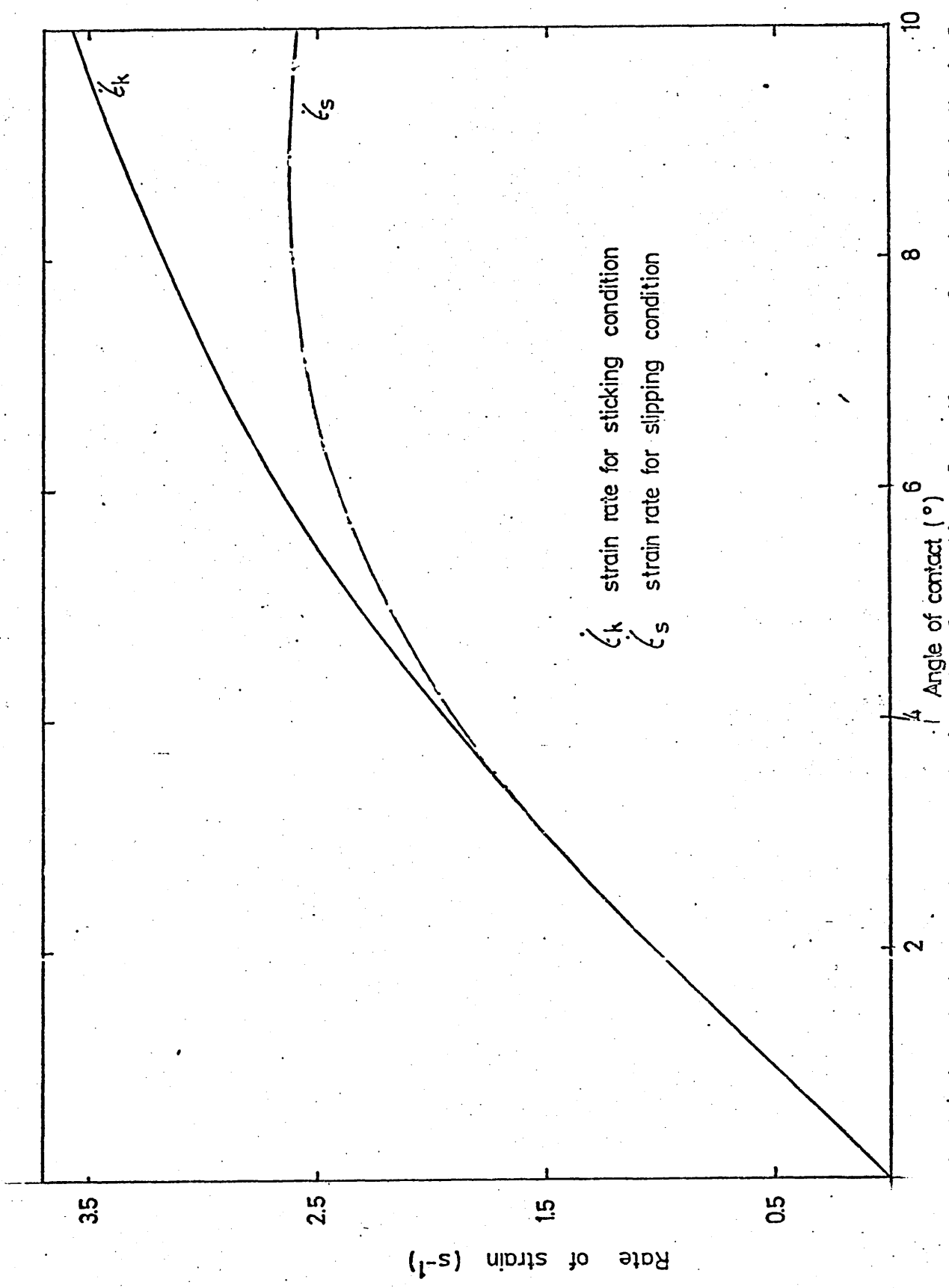


Fig.3.4.1 Variation of the mean strain rate of a section along the arc of contact for a typical rolling pass.

Table A - Flow stress constants of 0.17% C steel at different temperatures.

Temp. (°C)	Equation to fit experimental data. $\Delta = C \dot{\epsilon}^m (D + H \dot{\epsilon})^n$ (N/mm ²)				
	C	G	D	H	
Present flow stress data	900	192.024	0.1307	0.2326	0.0238
	950	172.632	0.1139	0.2534	-0.0061
	1000	147.151	0.0888	0.2846	-0.0509
	1050	130.663	0.1342	0.3019	-0.052
Suzuki's flow stress data	800	227.035	0.1313	0.2231	0.0148
	900	200.783	0.0664	0.2333	0.0228
	1000	153.344	0.0293	0.2421	0.0105
	1100	119.391	0.0751	0.2755	0.022
1200	86.082	0.1629	0.2090	0.0164	

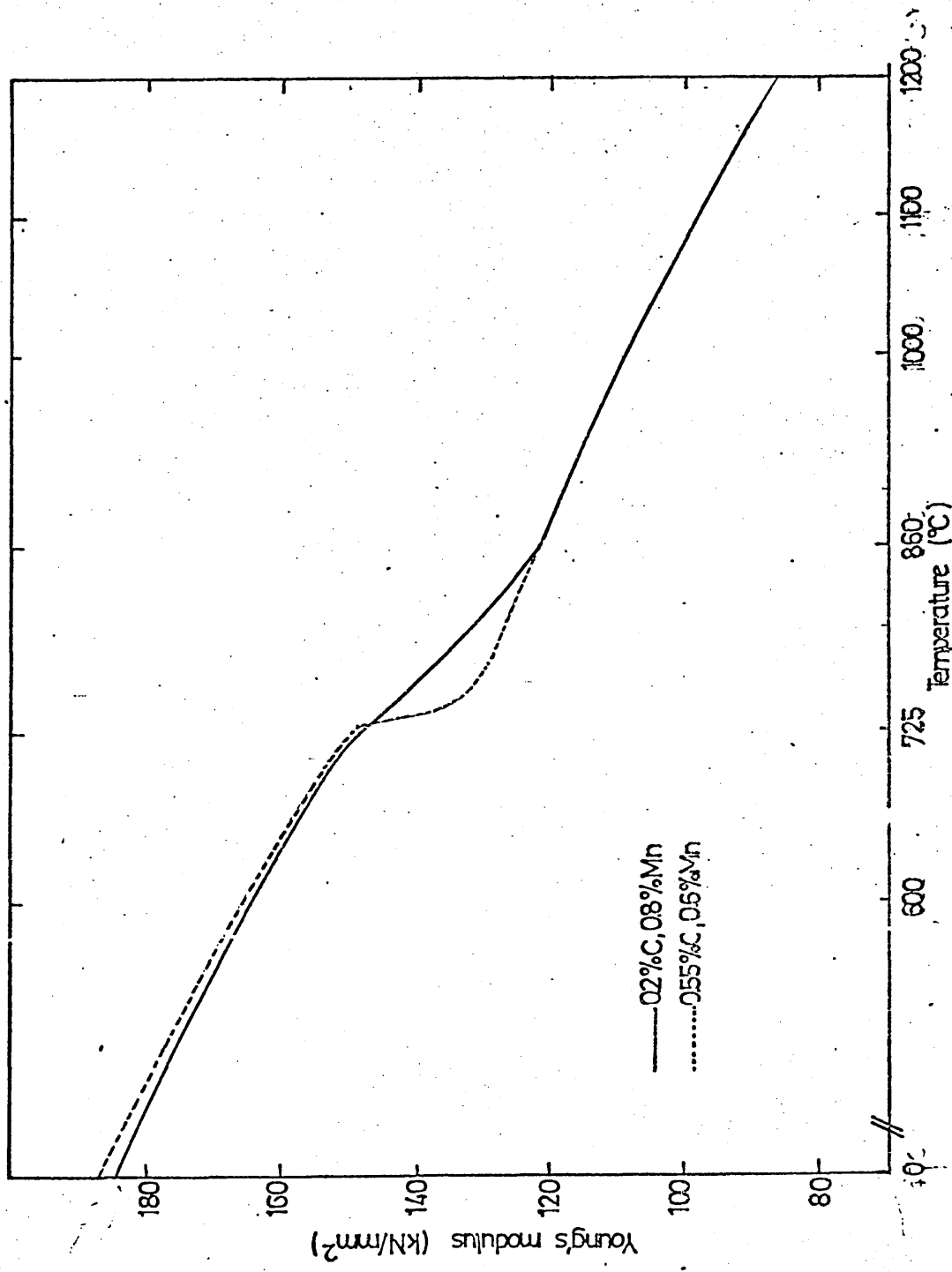


Fig.3.10.1 Variation of Young's modulus with temperature for two steel compositions - after B.I.S.R.A Research Report(67).

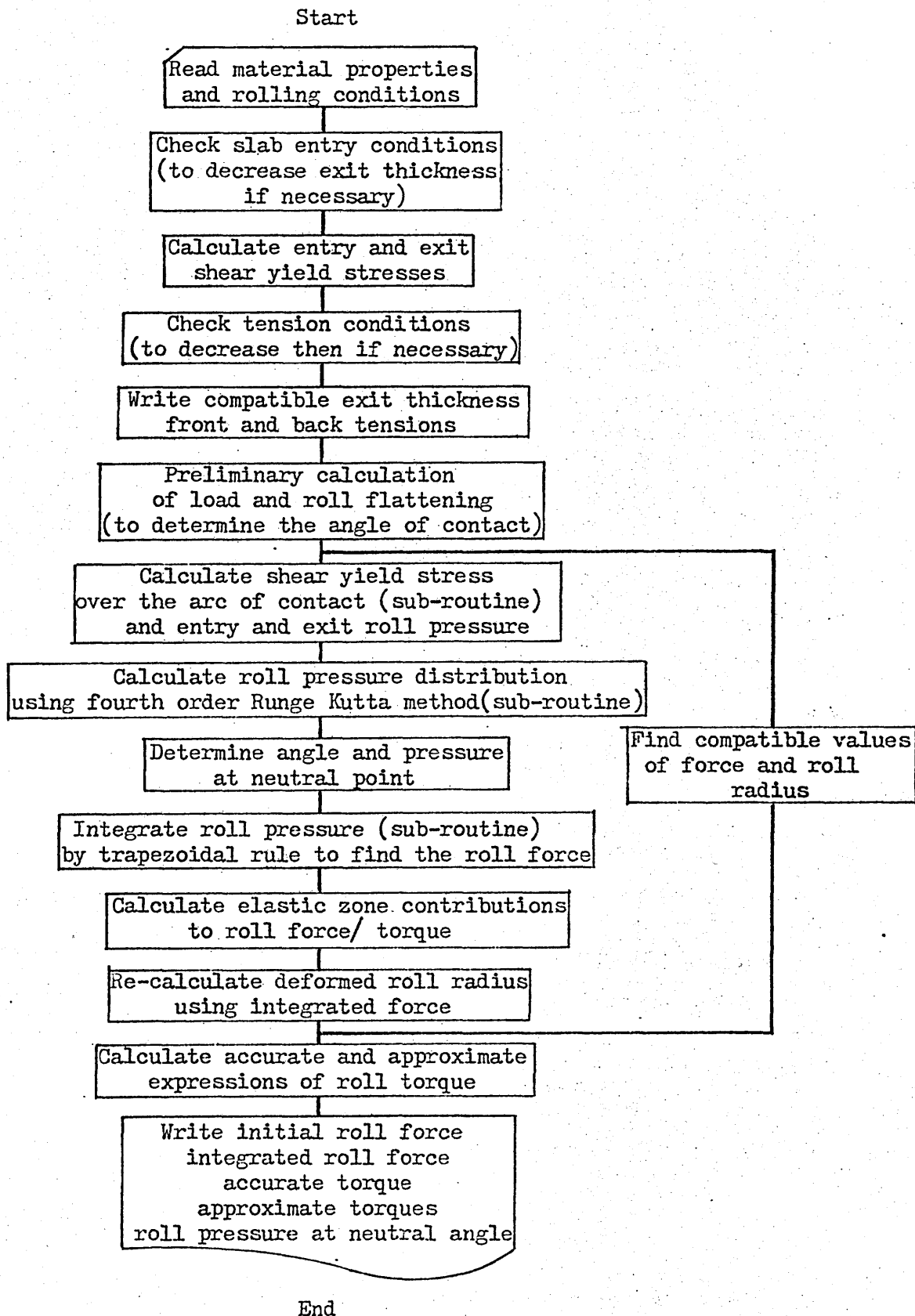
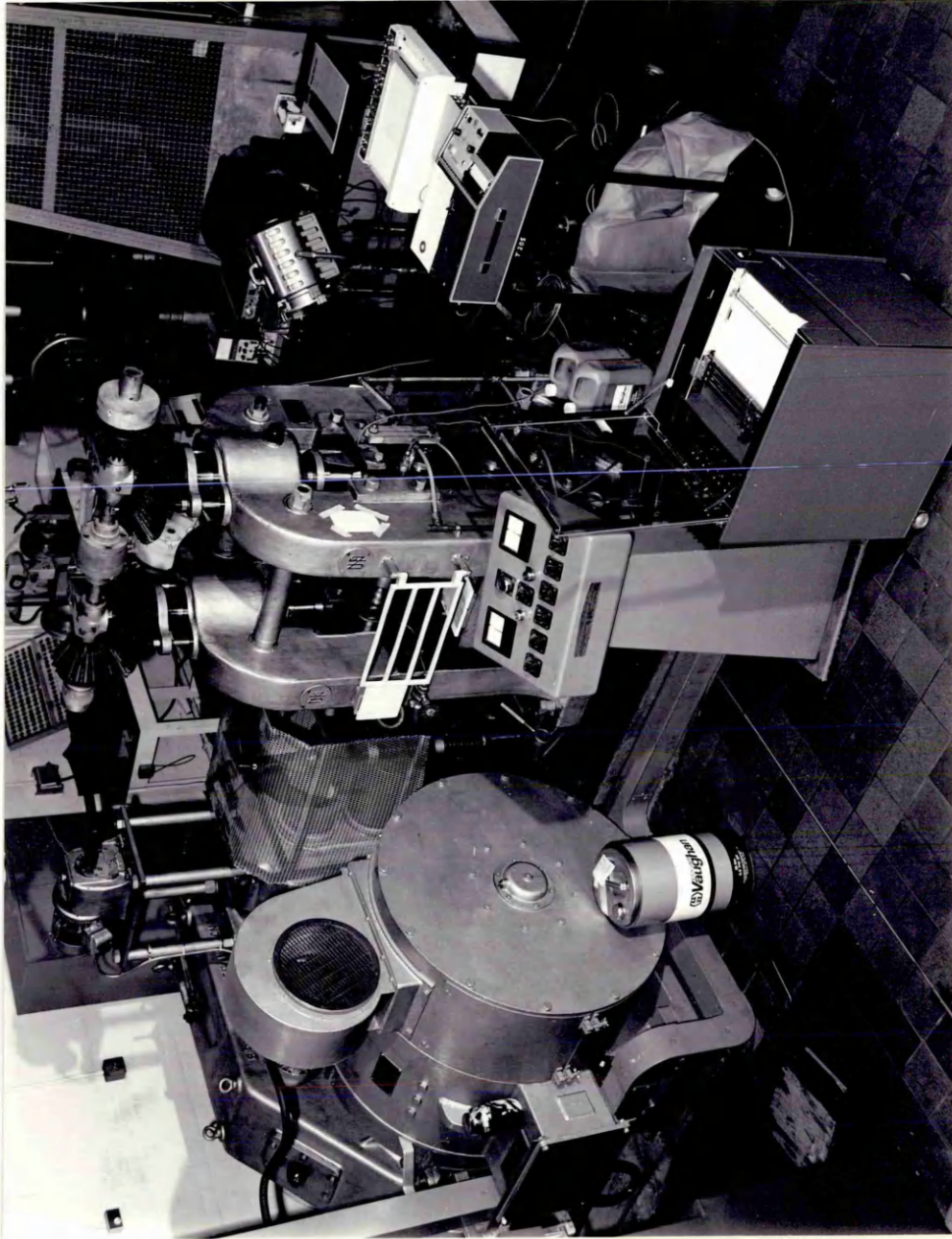


Fig.3.11.1 Flow chart for the numerical solution to the Von Karman Equation to predict roll force and torque per unit width.



411. The Rolling mill and ancillary equipment

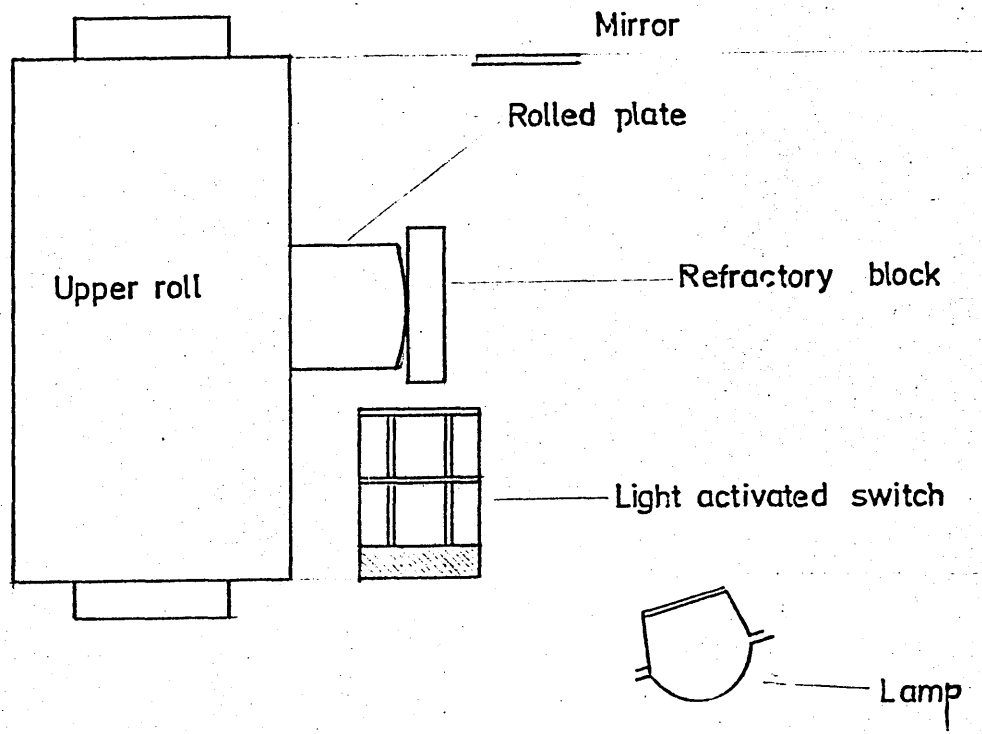
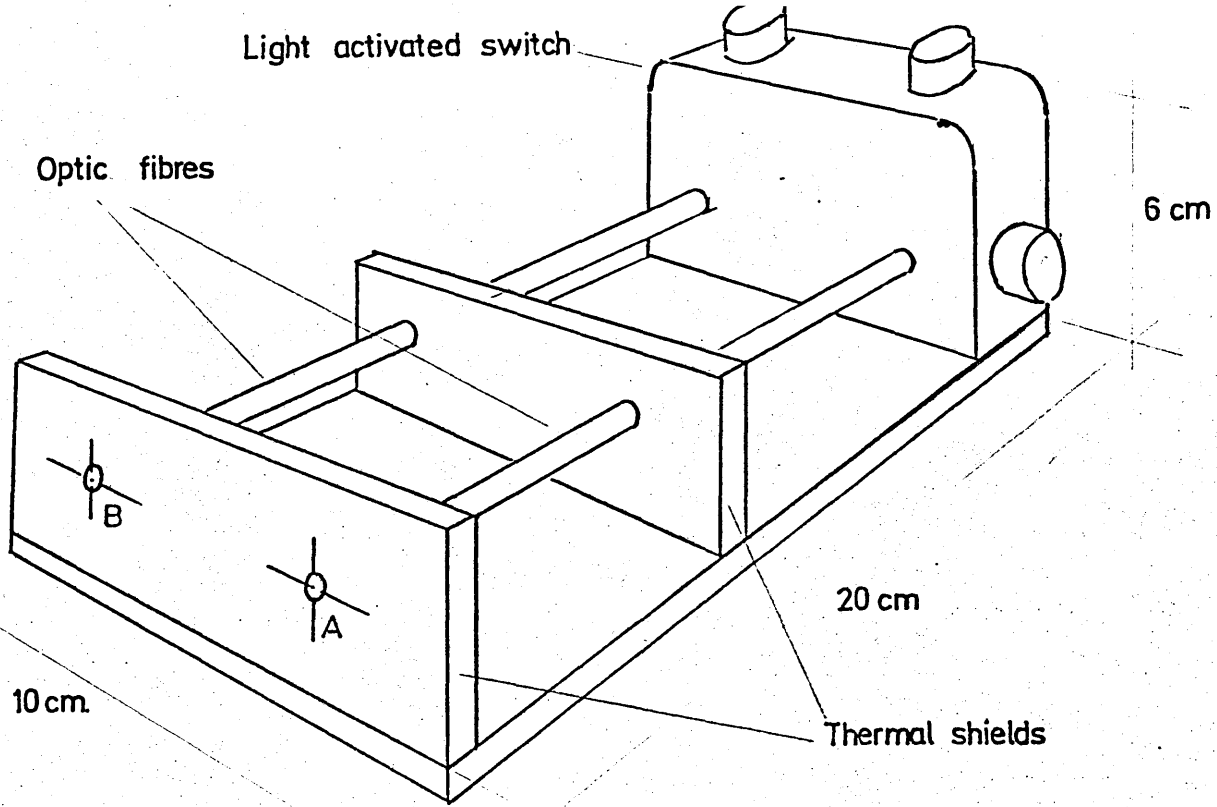
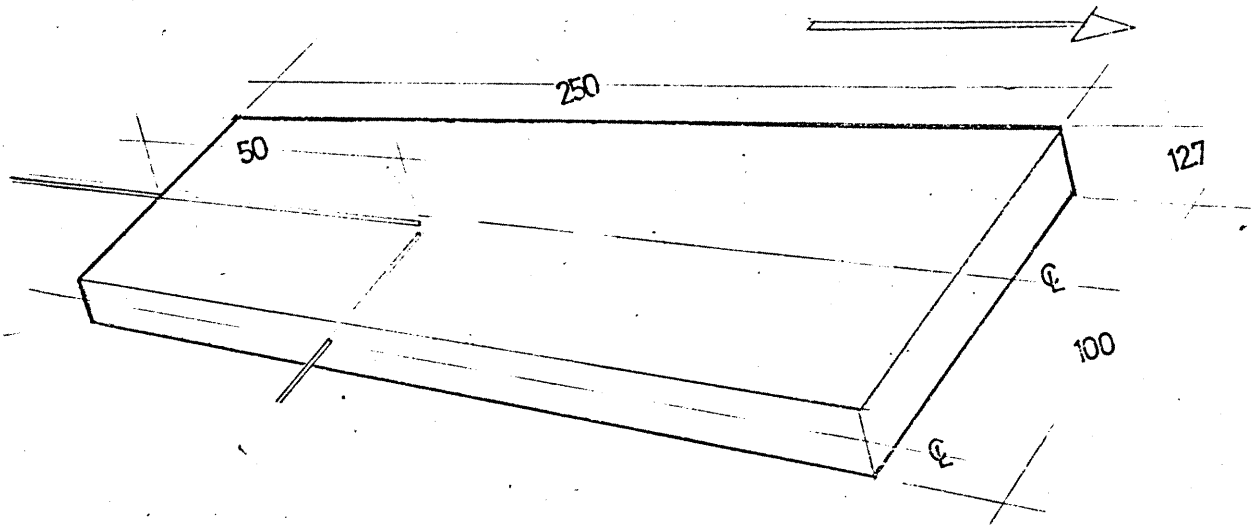
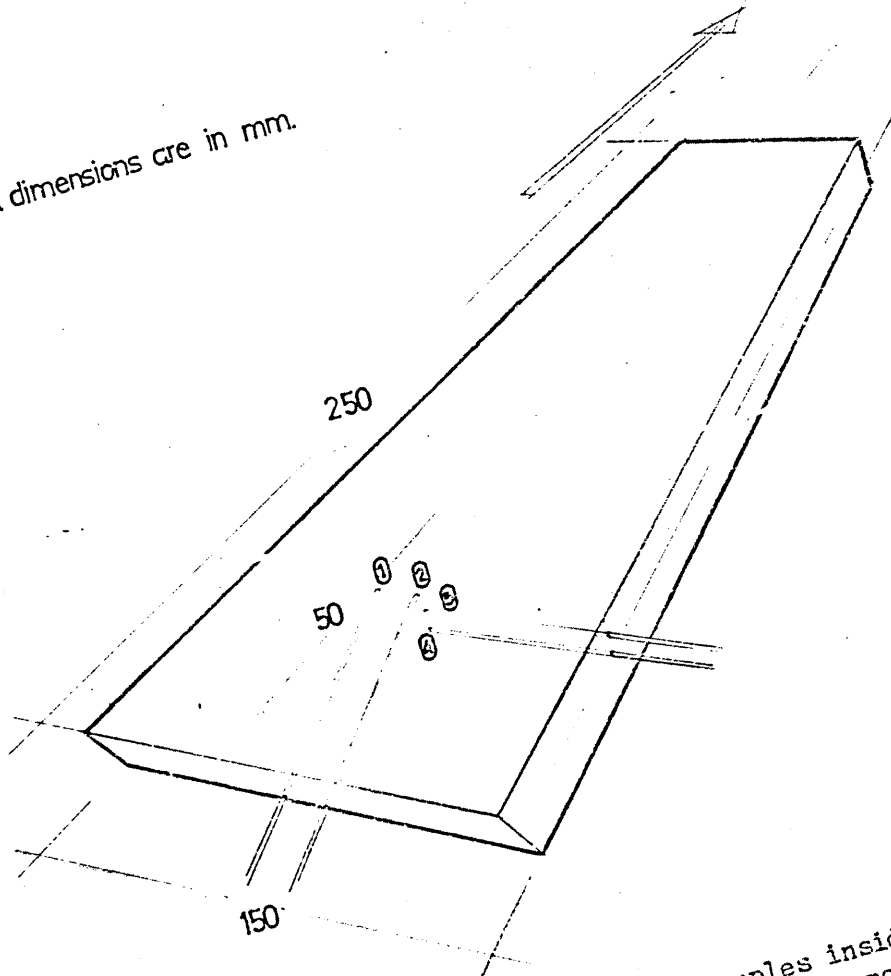


Fig.4.2.2 Light-activated switch and its location on the exit table of the rolling mill.



a.
All dimensions are in mm.



b.

Fig.4.2.3 Location of thermocouples inside a plate, (a) two thermocouples, (b) four thermocouples.

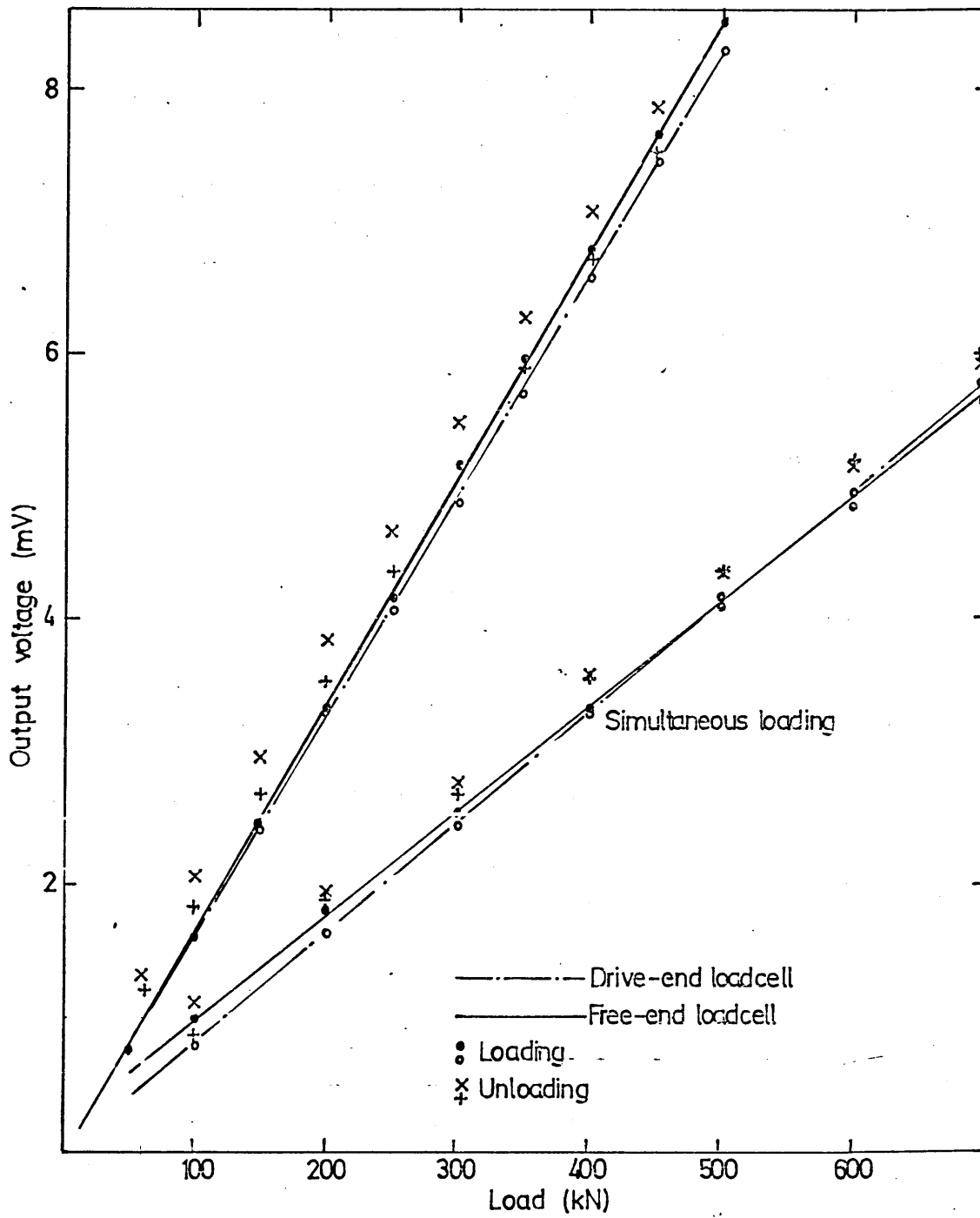


Fig.4.2.4 Calibration curves of the load cells.

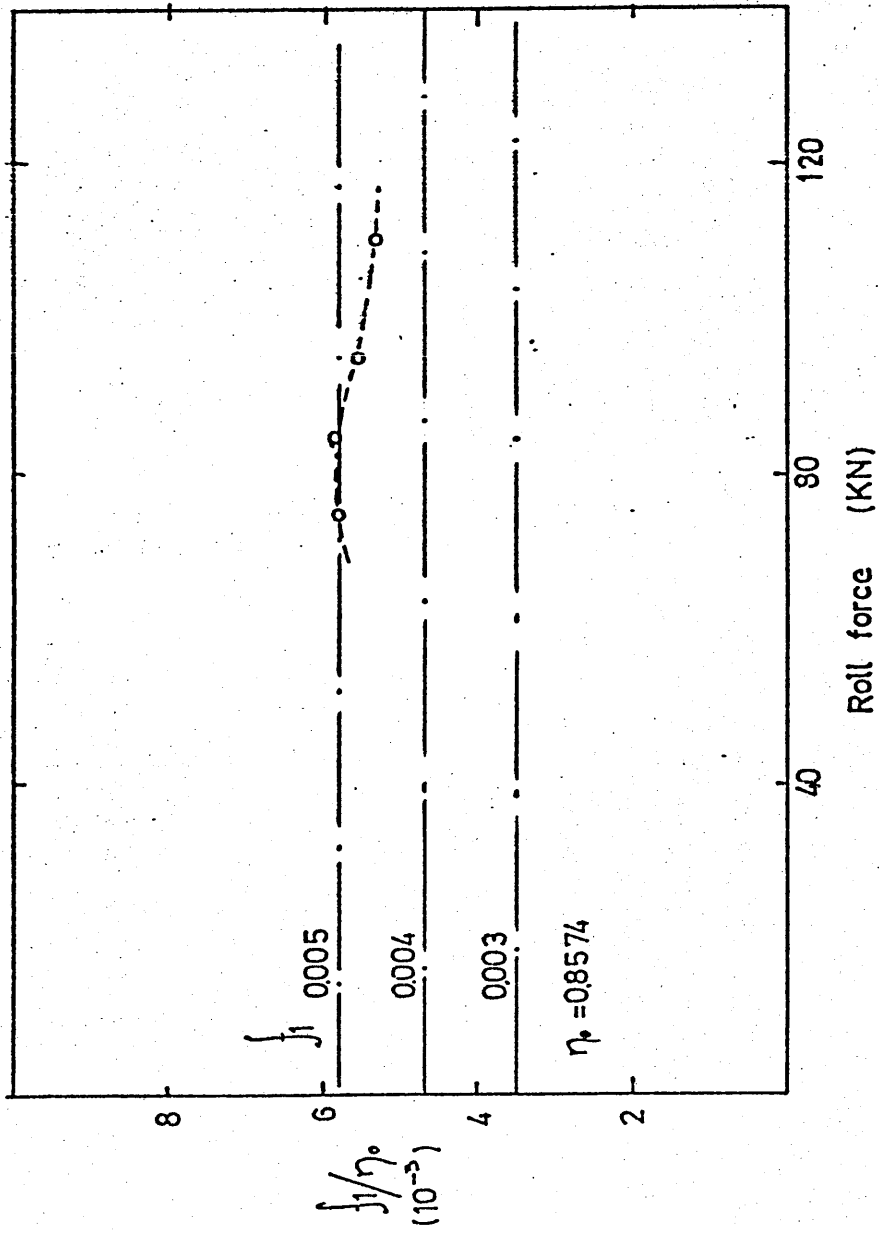


Fig.4.3.5 Experimental values of the roll neck friction coefficient/
drive efficiency ratio at various loads.

- 1,2 Cams
- 3 Clutch plate
- 4 Flywheel
- 5 Cam roller follower
- 6 Cam shaft
- 7 Clutch activation arm
- 8 Piston and piston guide block
- 9 Die assembly

- 10 Adjustable spacer
- 11 Linear potentiometer
- 12 Main frame
- 13 Load cell

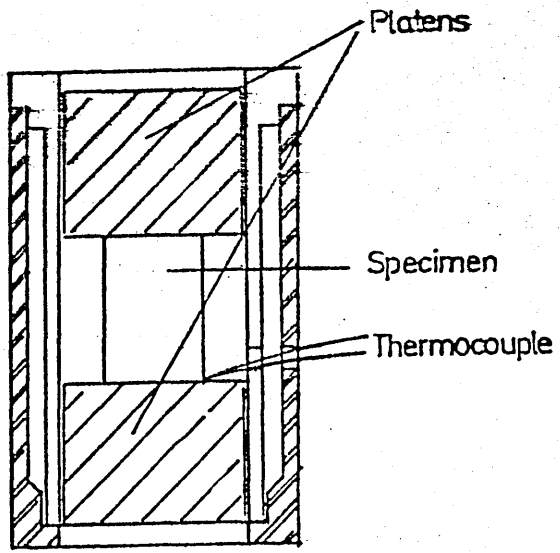
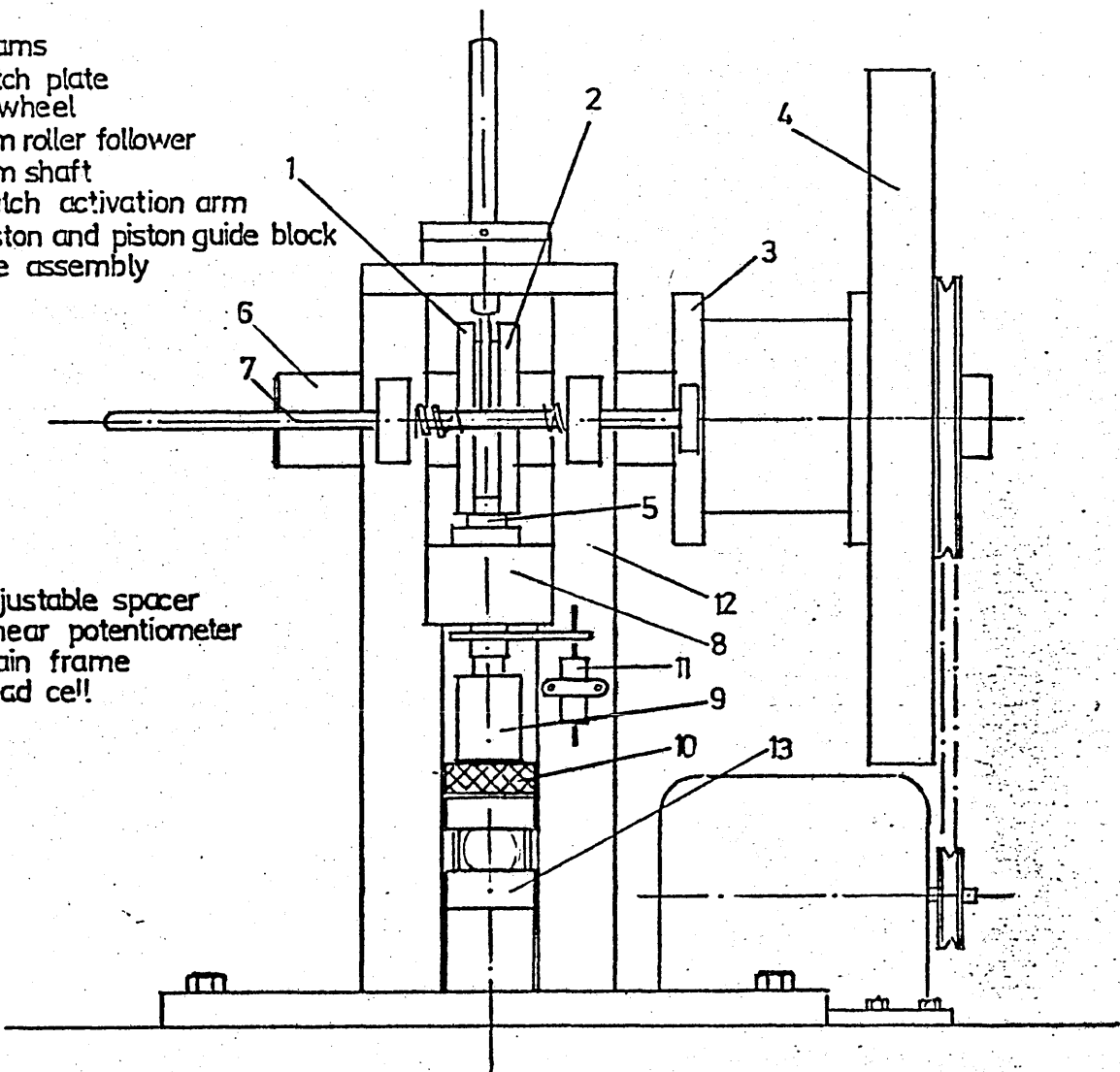


Fig.4.6 Cam plastometer and enlarged section of the die assembly.

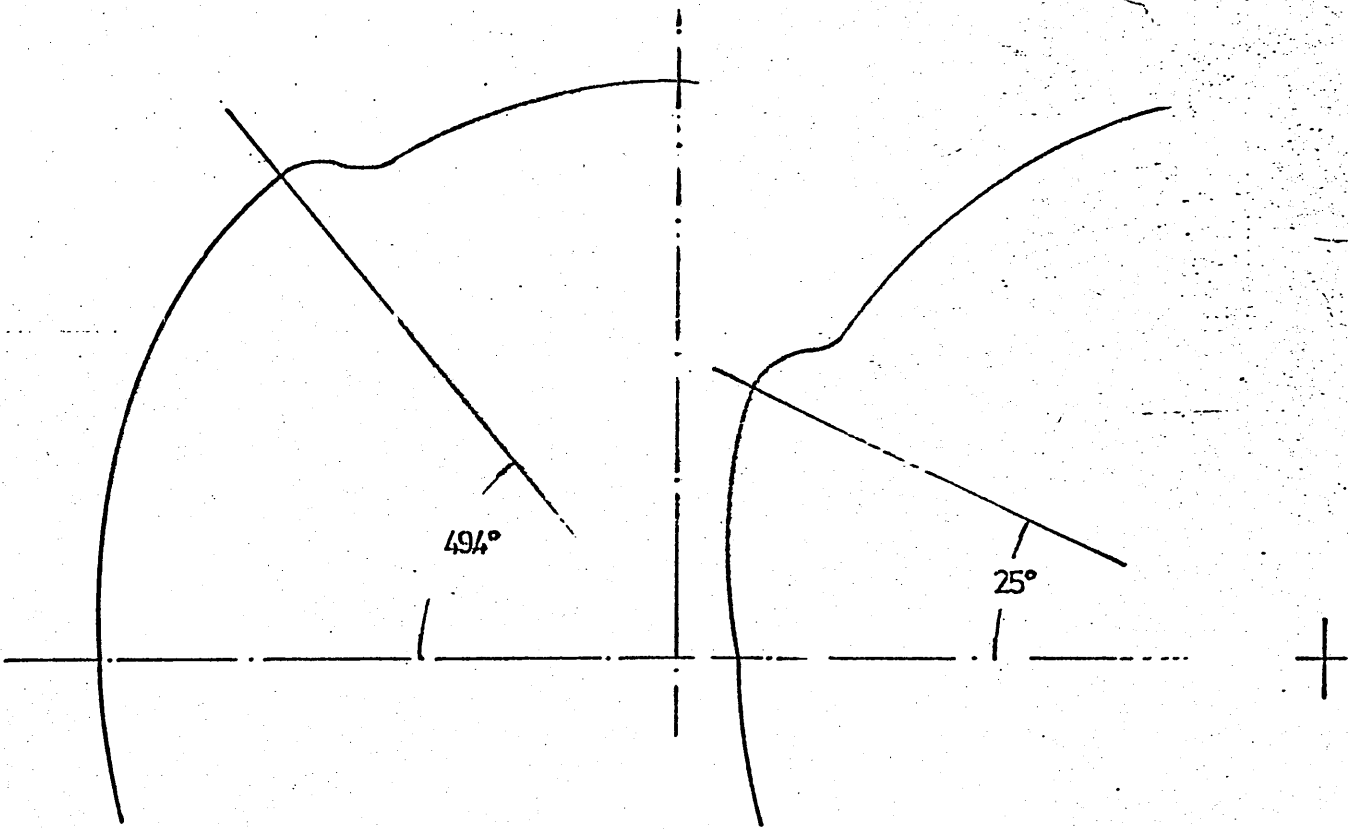
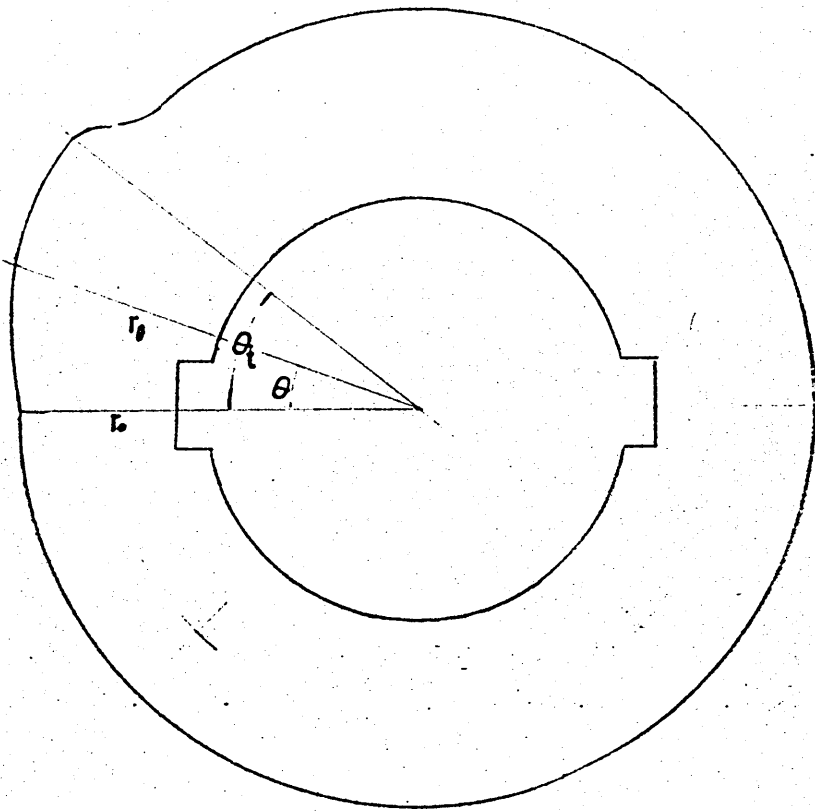


Fig.4.6.1 Cam profiles.

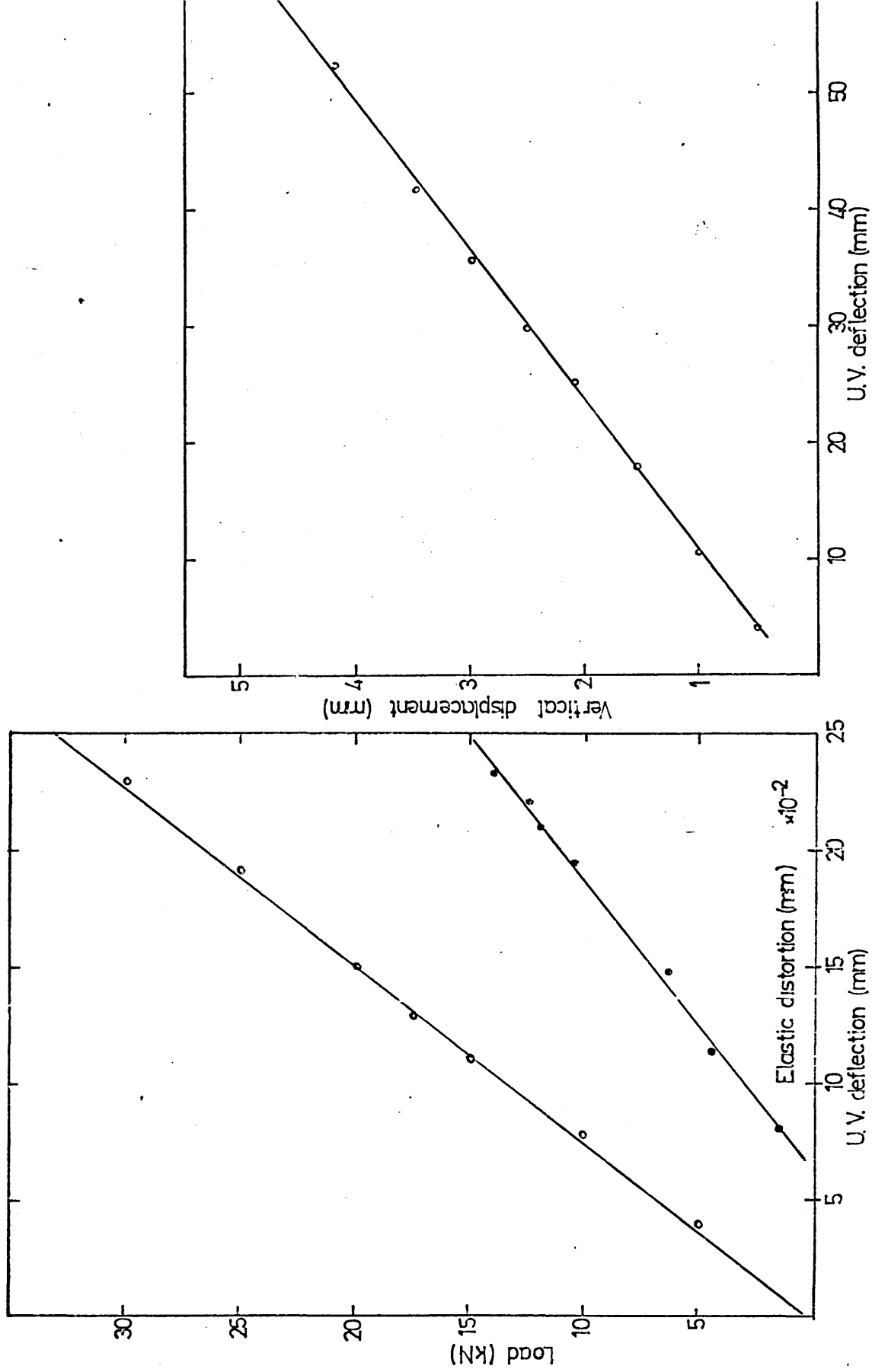


Fig.4.6.2 Calibration curves of the instrumentation of the cam plastometer.

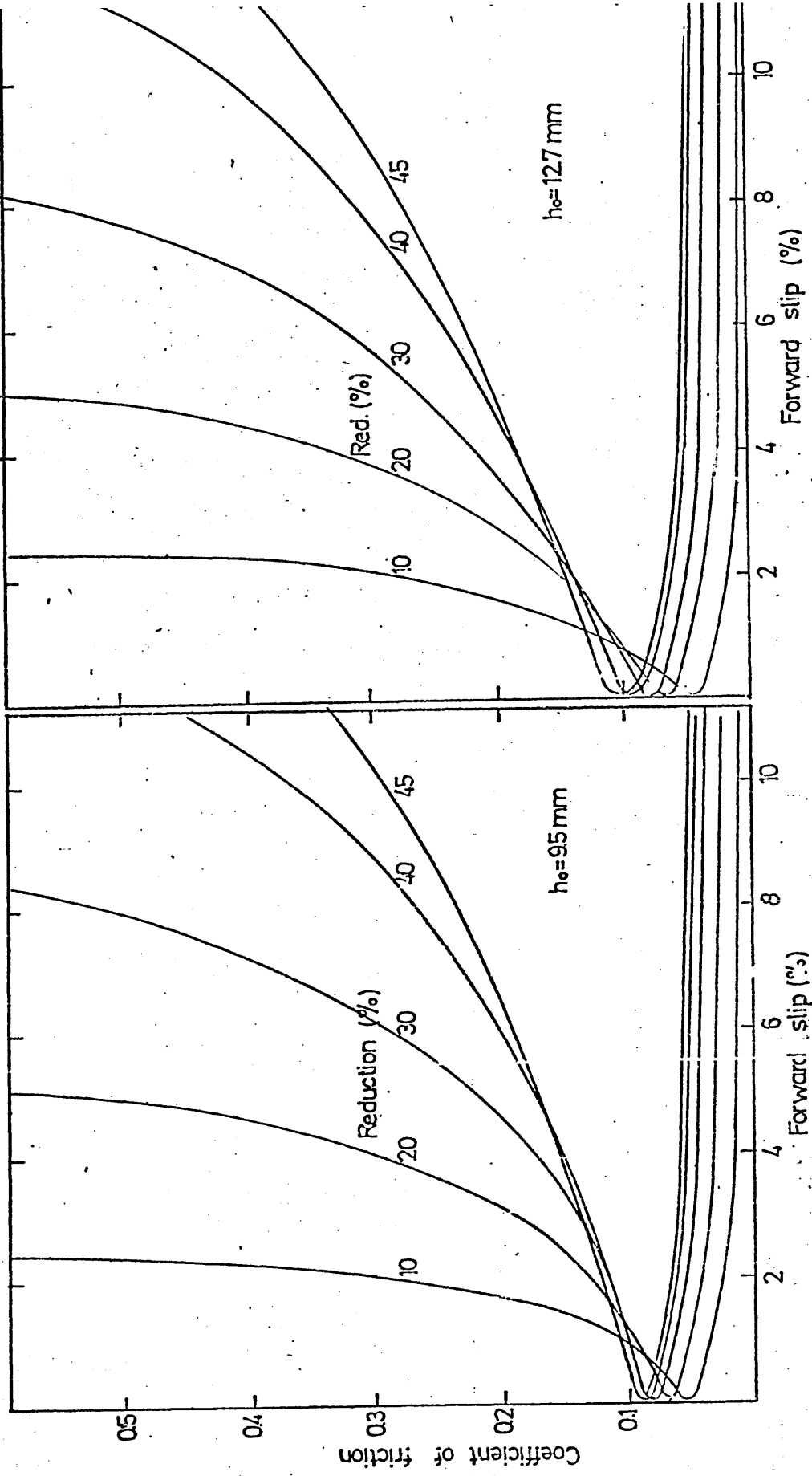


Fig.4.8.1 Relation between the coefficient of friction and the forward slip at various reductions and entry thicknesses, (a) $h = 9.5 \text{ mm}$ (b) $h = 12.7 \text{ mm}$.

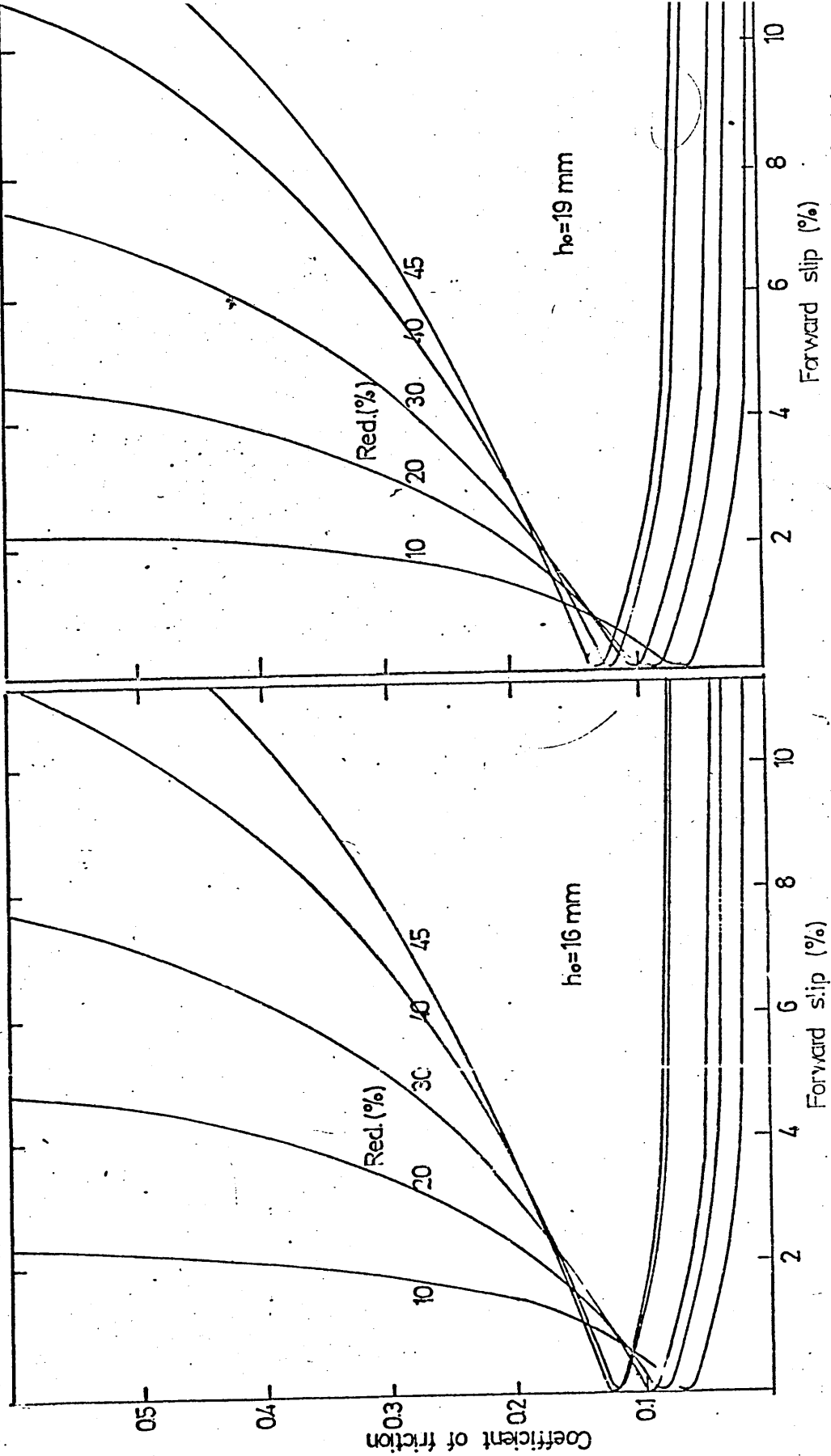


Fig.4.8.1 Relation between the coefficient of friction and the forward slip at various reductions and entry thicknesses, (c) $h = 16 \text{ mm}$ (d) $h = 19 \text{ mm}$

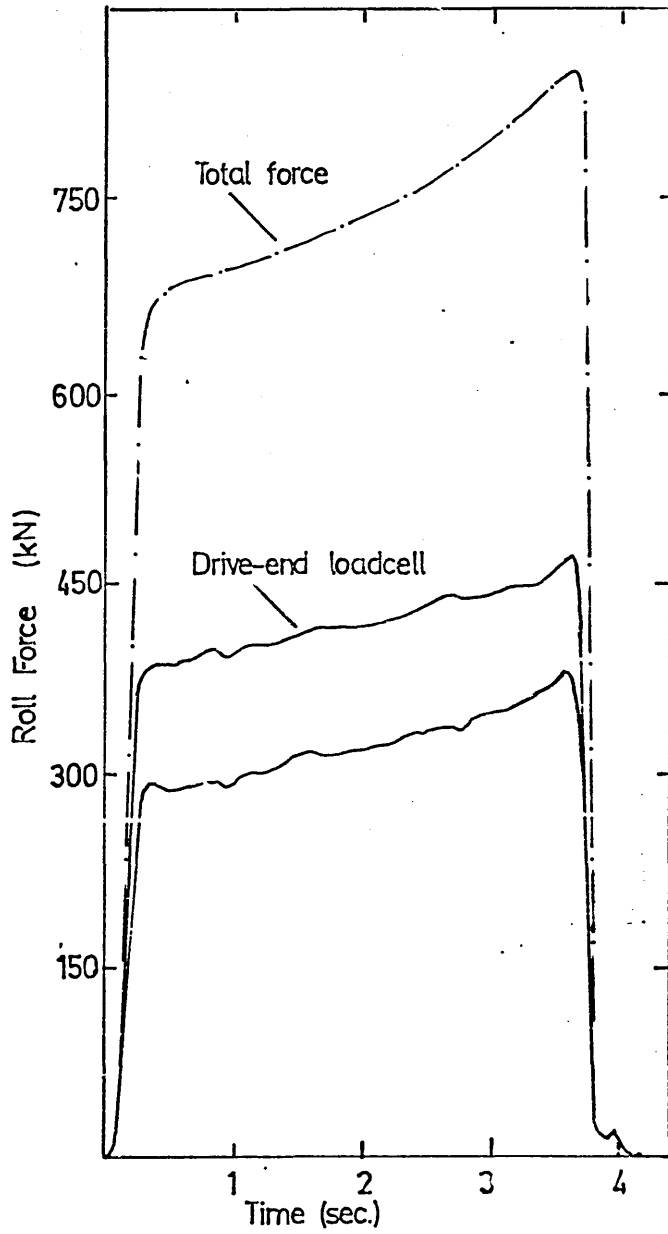


Fig.5.2 Typical recording of the load cells.

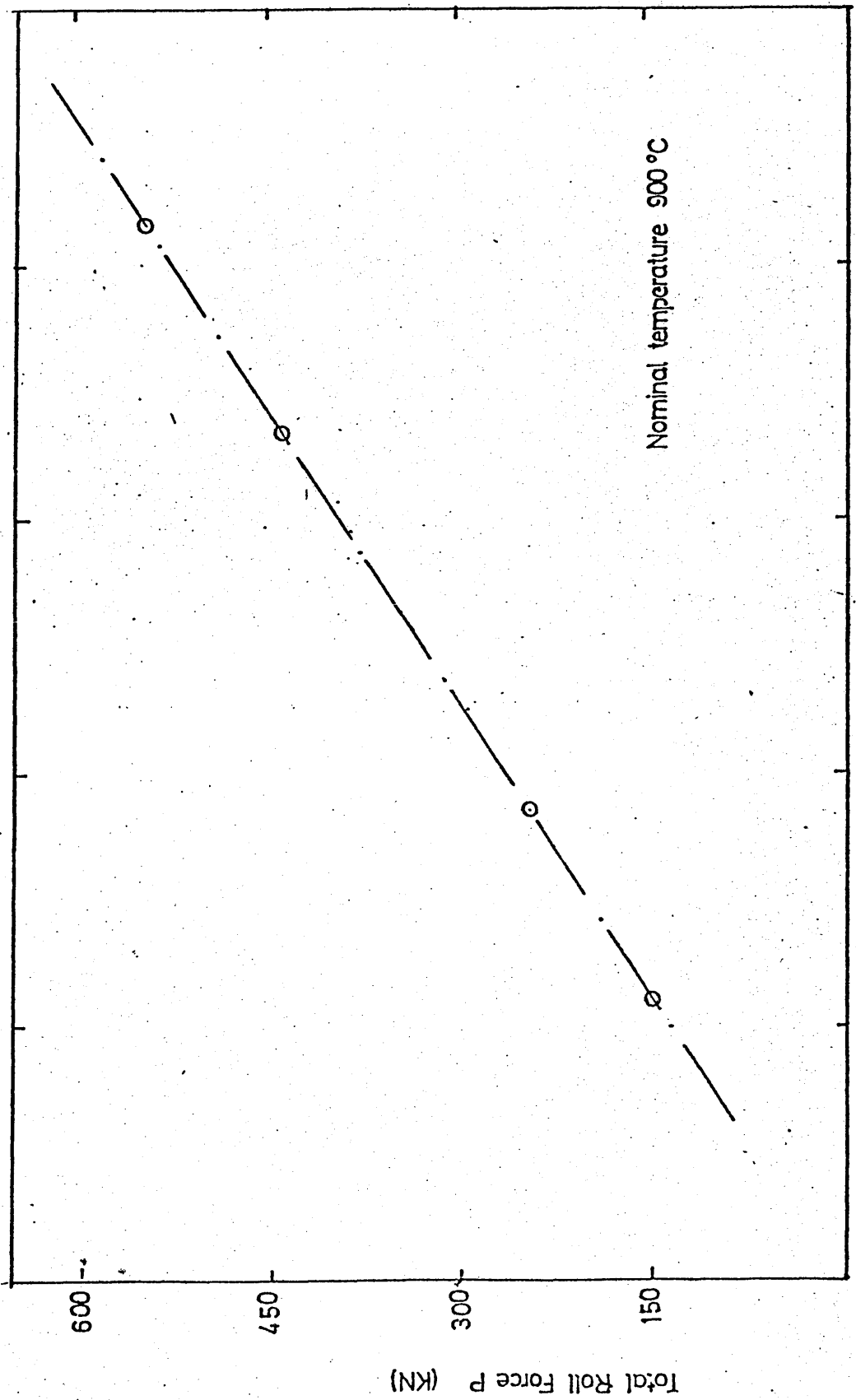


Fig.5.2.1 Relation between mean roll force and reduction measured at 900°C.

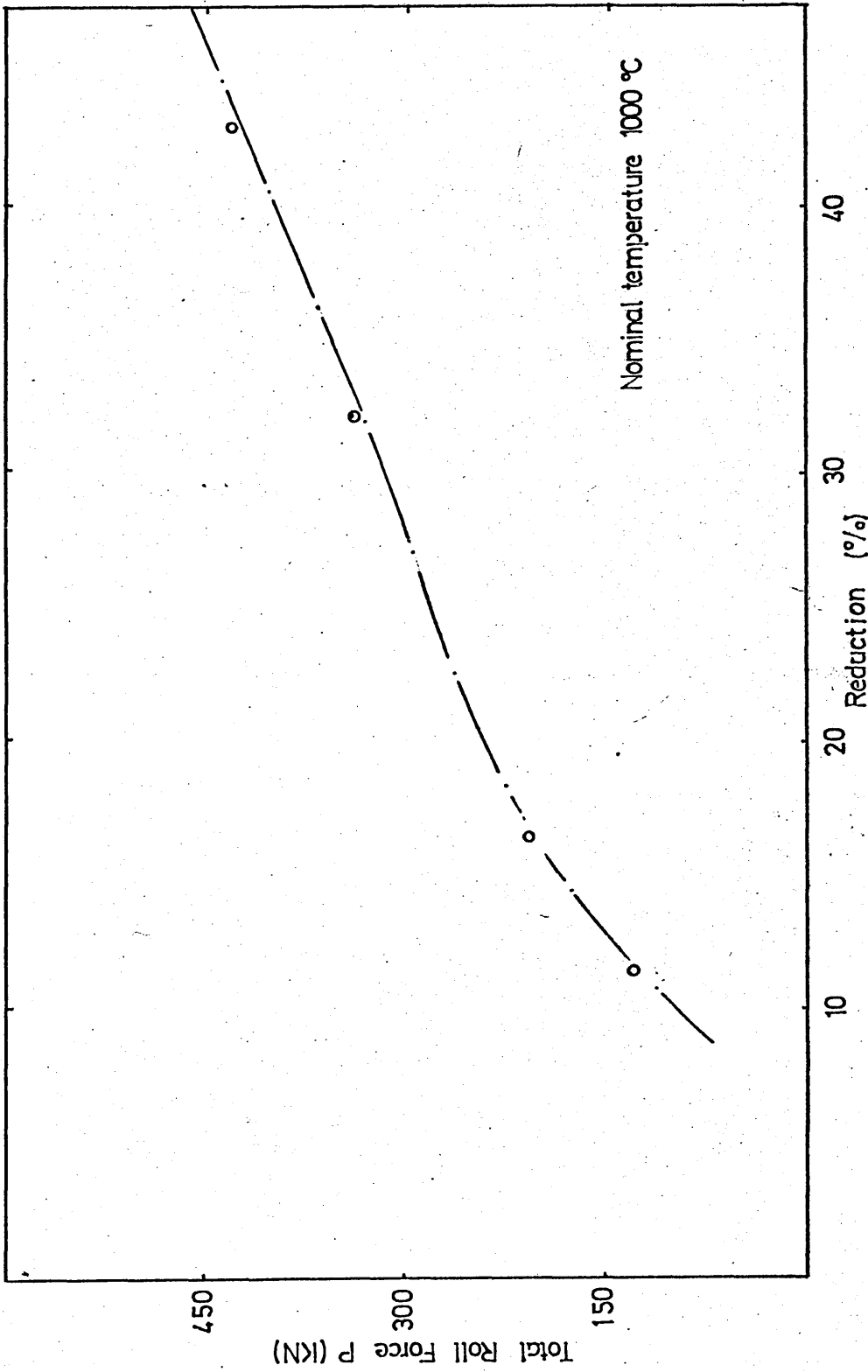


Fig.5.2.2 Relation between mean roll force and reduction measured at 1000 °C.

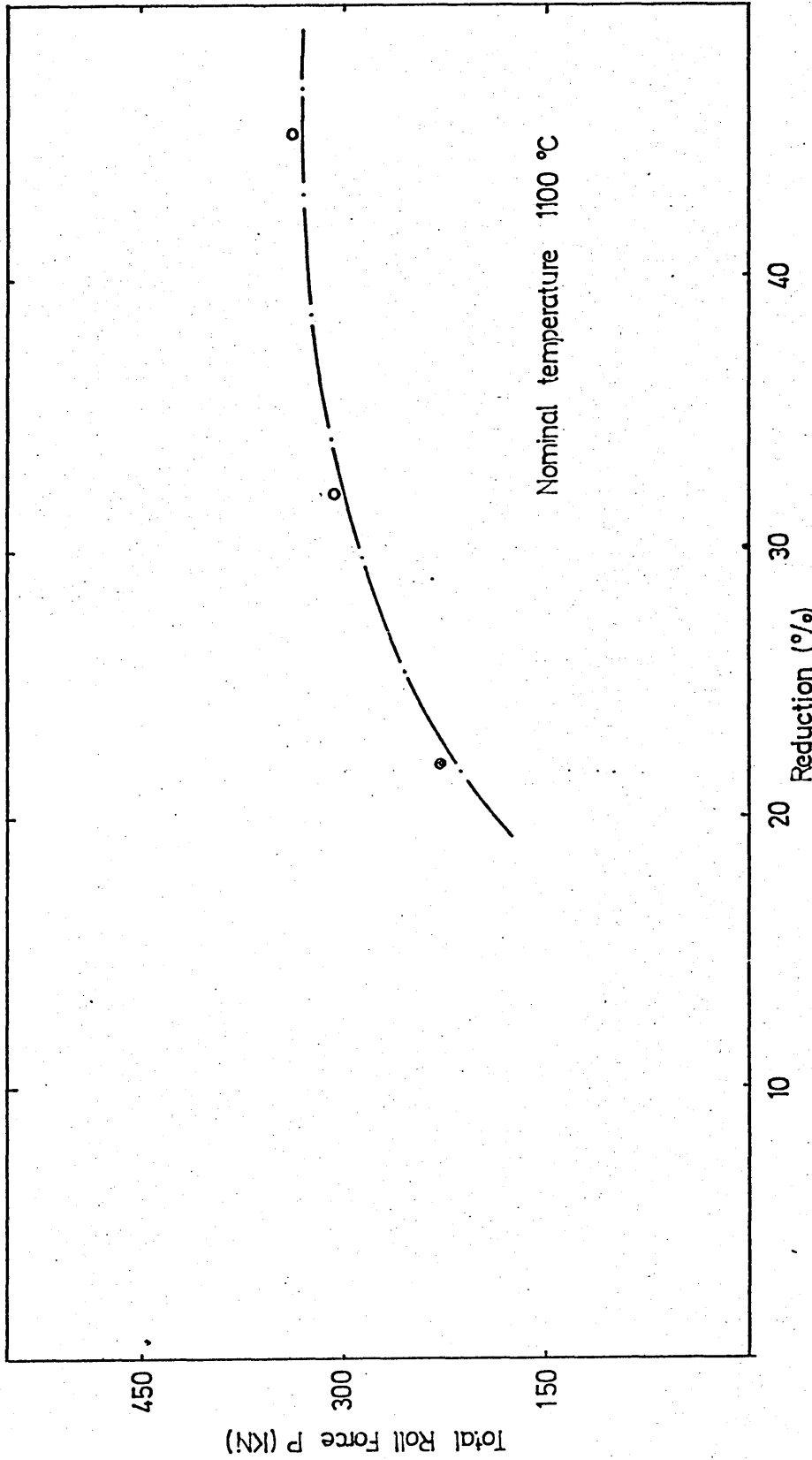


Fig. 5.2.3 Relation between mean roll force and reduction measured at 1100 °C.

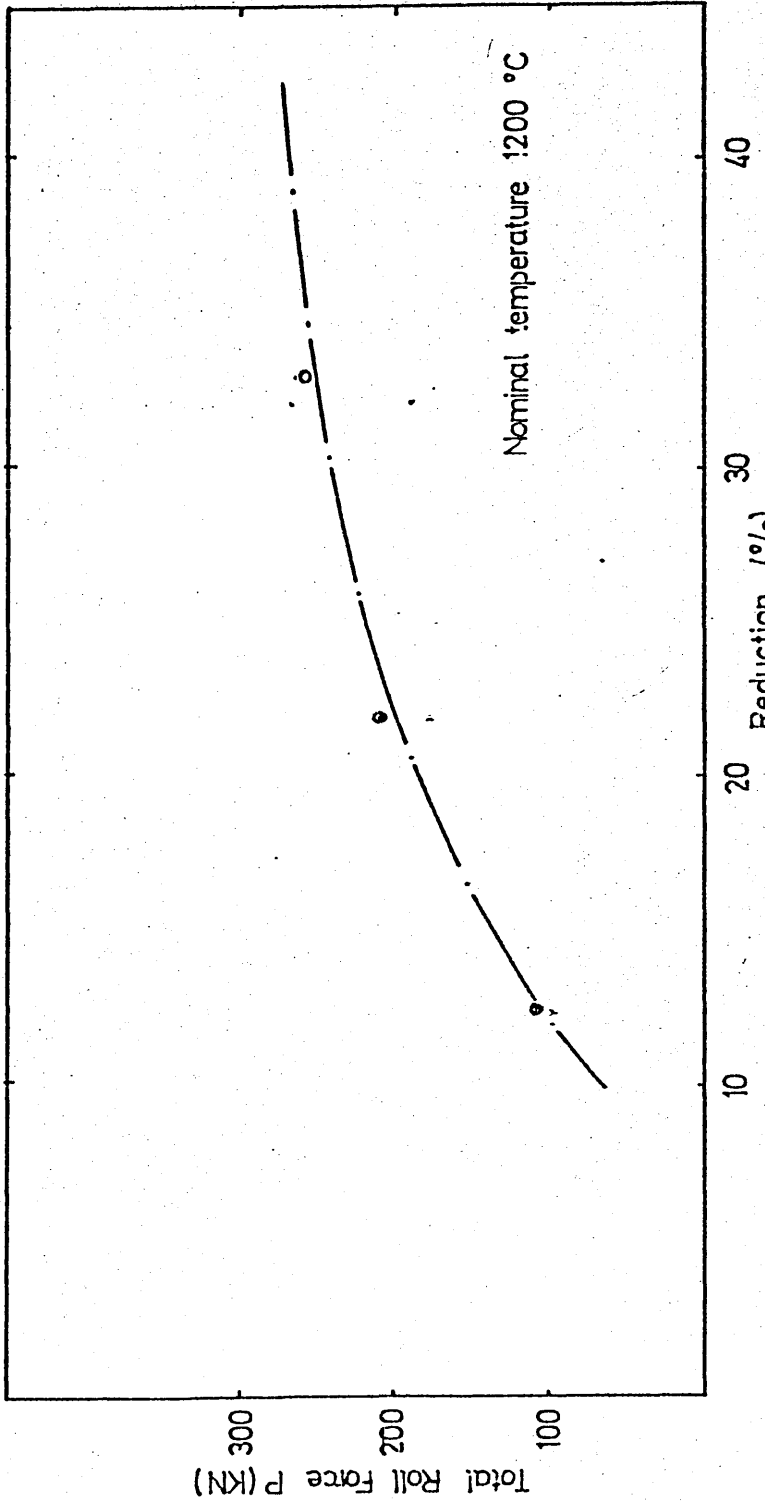


Fig. 5.2.4 Relation between mean roll force and reduction measured at 1200 °C.

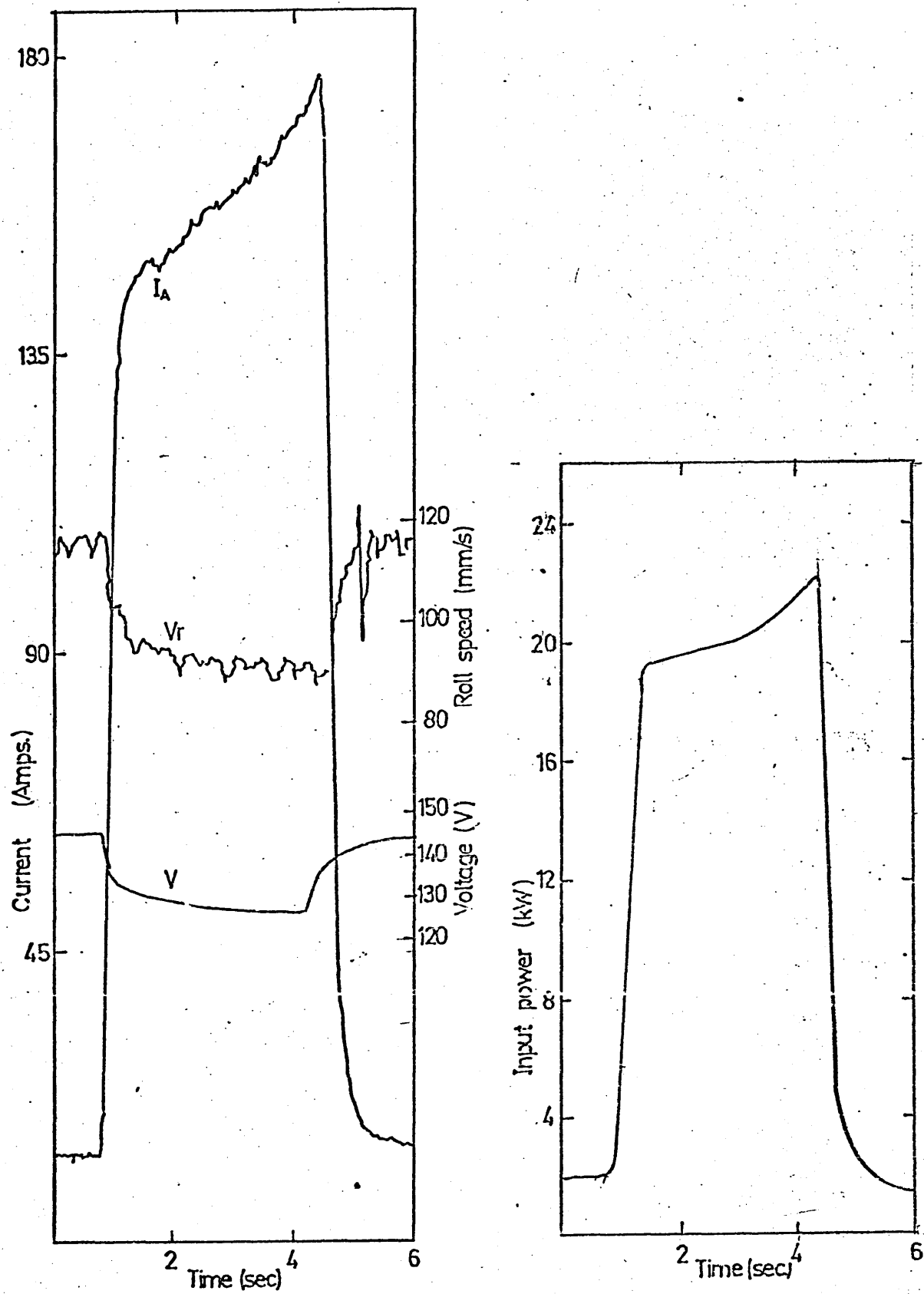


Fig.5.3.1 Simultaneous recordings of voltage, current and angular velocity of the rolls during a test at 900°C and 40% reduction, (a) associated roll power consumption.

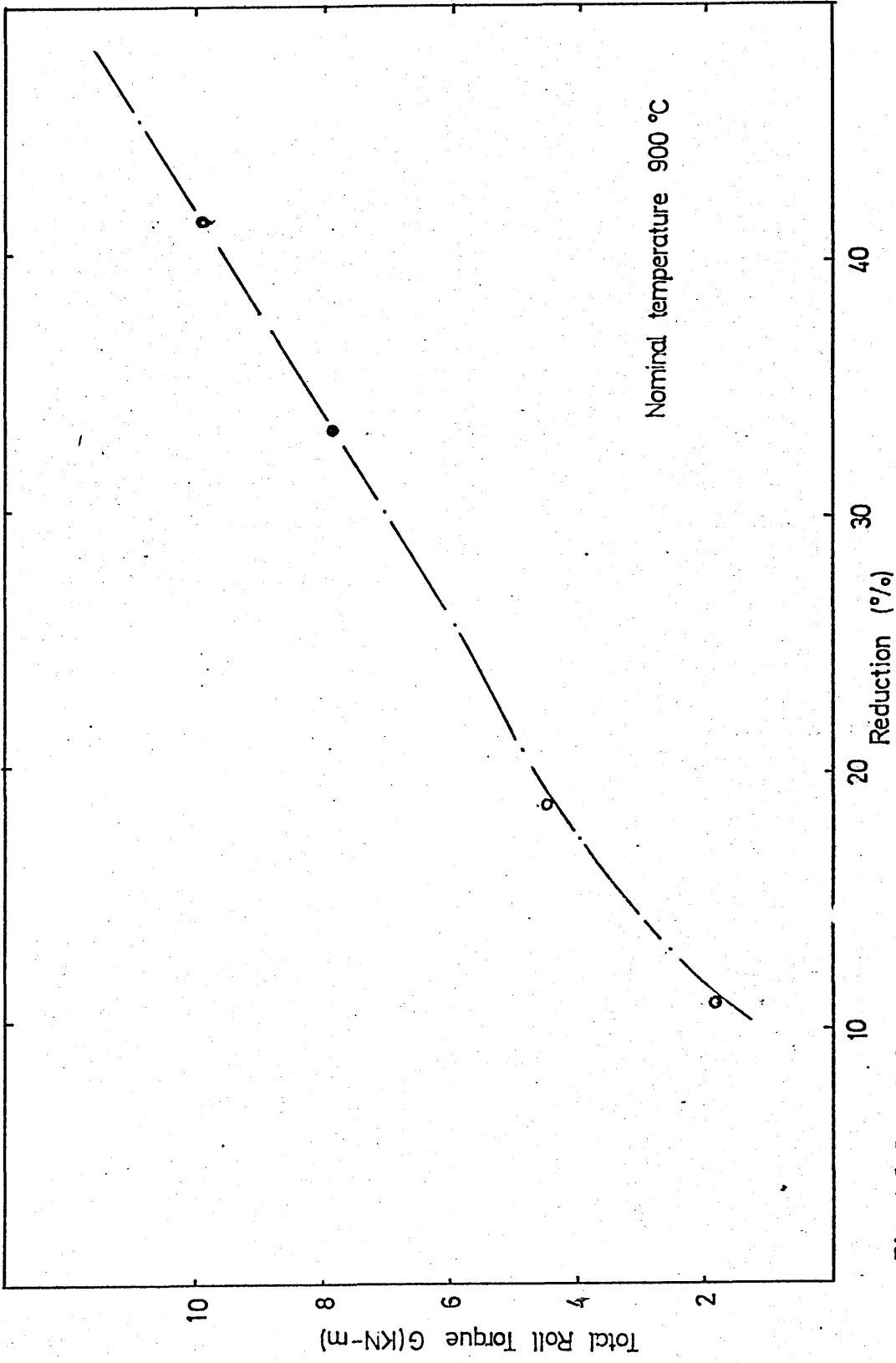


Fig. 5.3.2 Relation between mean roll torque and reduction measured at 900 °C.

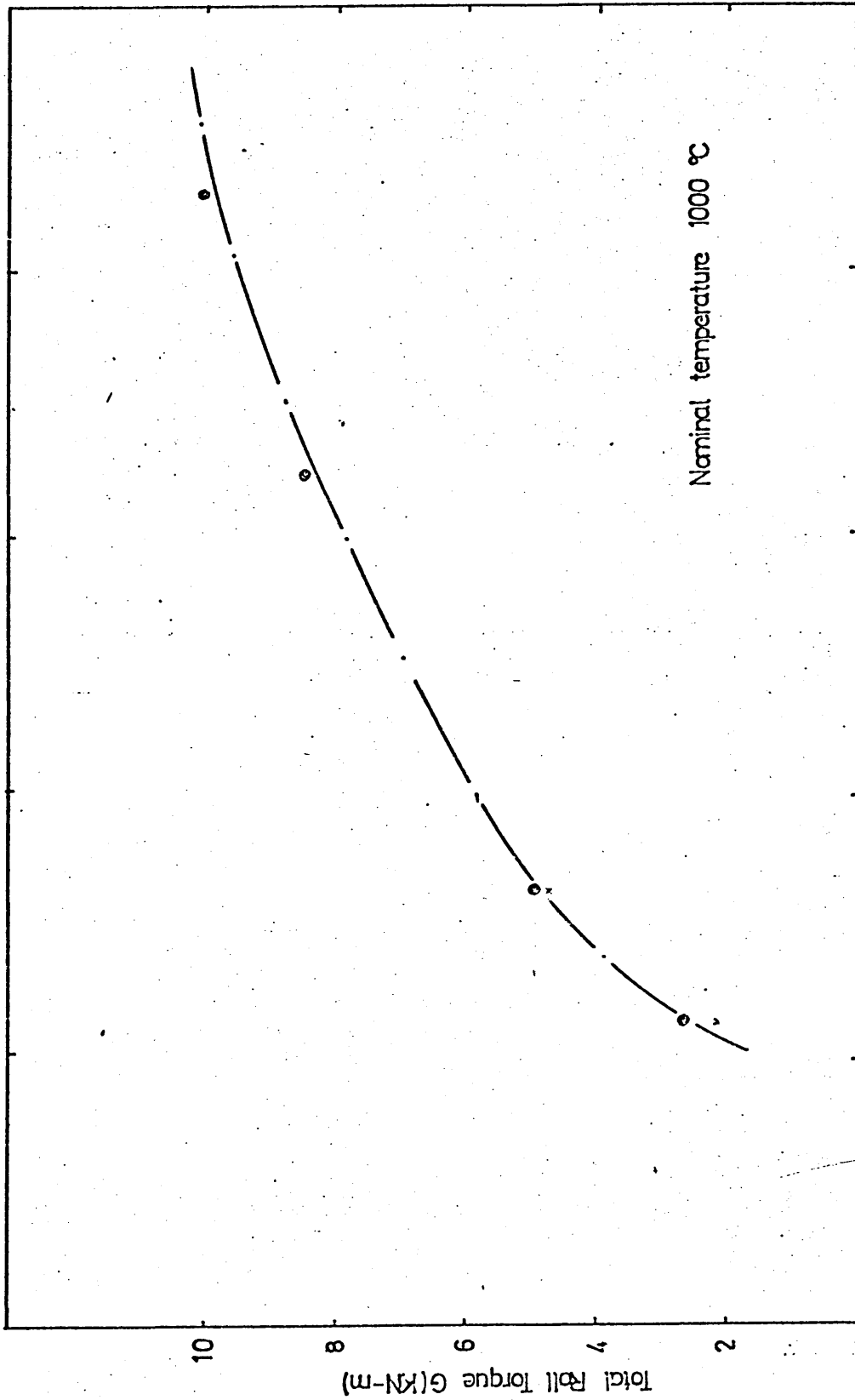


Fig.5.3.3. Relation between mean roll torque and reduction measured at 1000 °C.

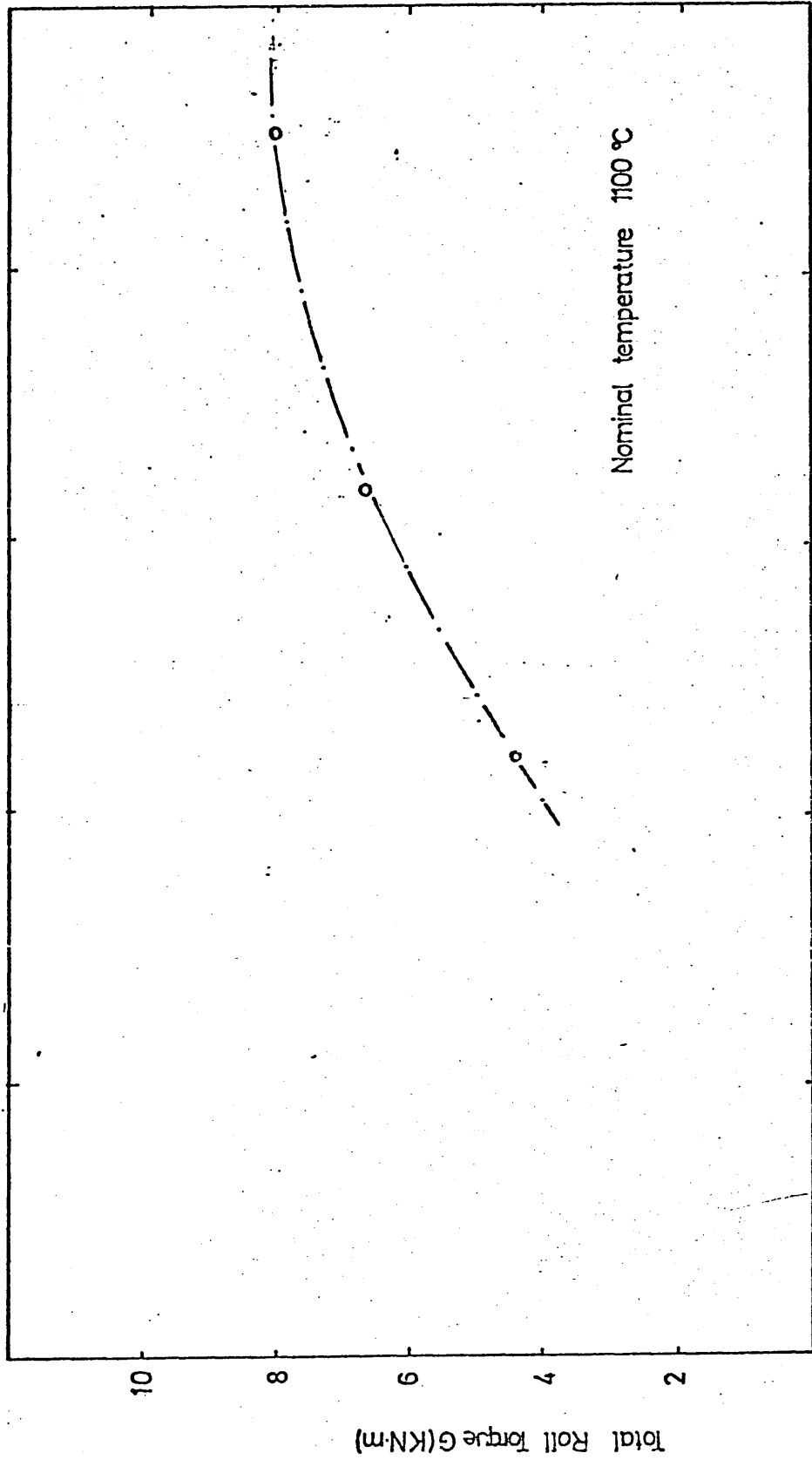


Fig.5.3.4 Relation between mean roll torque and reduction measured at 1100°C.

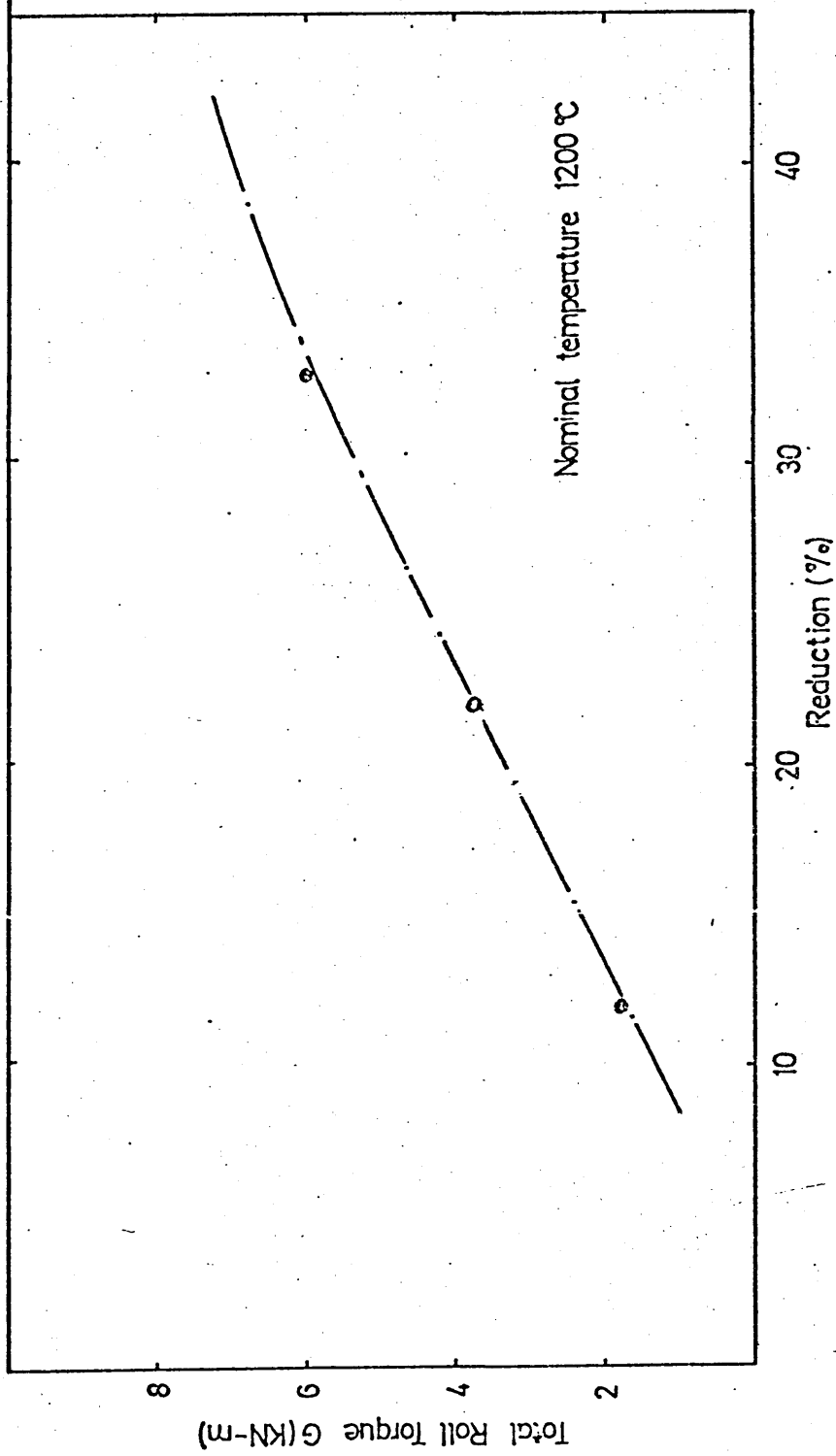


Fig.5.3.5 Relation between mean roll torque and reduction measured at 1200°C.

Table 1 Rolling parameters determined in experimental work.

Preliminary experiments	Nominal temp(°C)	Mean entry temp(°C)	R/h ₁	r(%)	V _r (mm/s)	V ₂ (mm/s)	Φ(%)	μ	P(kN)	G(kN-m)	Ė(s ⁻¹)	ΔW/W ₁ (%)	Scale thickness (mm)
Preliminary experiments	900	885	10.123	34	123.7	133.6	8.0	0.43	730	-	-	2.3	
	800	770	10.12	34	140.6	-	-	-	780	12.3	2.4	2.4	
	900	880	10.12	34	148.0	163.56	10.4	0.6	760	10.7	2.5	2.5	
Series A	Nominal temp(°C)	Mean entry temp(°C)	R/h ₁	r(%)	V _r (mm/s)	V ₂ (mm/s)	Φ(%)	μ	Ė(s ⁻¹)	W ₁ (mm)	ΔW/W ₁ (%)	Scale thickness (mm)	
	900	950	10.12	11	105.3	107.7	2.32	0.4	0.9	115.0	0.7	0.36	
				18	97.6	102.4	4.9	>0.6	1.14	115.4	1.3		
				33	88.8	91.7	3.35	0.18	1.5	116.6	2.1		
				41	77.7	82.9	8.0	0.257	1.6	117.5	2.8		
	1000	870	6.75	11	107.2	117.9	10.1	-	0.77	94	13.7	0.44	
				16	99.6	109.5	10.2	-	0.9	96.6	14.6	0.3	
				32	90.0	100.8	12.0	-	1.23	104.2	4.3	0.4	
				43	82.3	90.3	9.7	0.45	1.4	102.6	5.2	0.44	
	1100	960	10.12	22	96.2	105.2	9.3	-	1.25	102.4	1.56	1.15	
				32	88.4	98.8	11.7	-	1.5	103.2	3.12	0.85	
				45	84.6	93.0	10.0	0.35	1.86	104.2	5.08	0.7	
1200	1190	10.12	12.5	101.5	109.5	7.86	-	0.95	116	1.1	1.0		
			22	95.7	102.9	7.54	-	1.24	107.5	0.6	1.13		
			33	94.8	100.76	6.3	0.32	1.6	117.2	2.0	1.21		
960			13.72	20	96.7	100.5	3.8	0.3					
				30	95	101.3	6.6	0.3					
				40	91	96.9	6.5	0.2					
960			8.0	10.6	110.1	115.7	5.1	-					
				20.7	98.4	106.7	8.4	-					
				30	93.4	99.6	6.5	0.38					
				38	54.4	56.7	4.1	0.2					

Series B
Lubricated
Dry
rolls

R/h₁ Roll radius/entry thickness.
r Percentage reduction.
V_r, V₂ Rolls and emerging material velocities
Φ Forward slip
μ Coefficient of friction
P, G Total roll force and torque.
Ė Mean strain rate.
W Mean width of plate.
ΔW/W₁ Lateral spread.

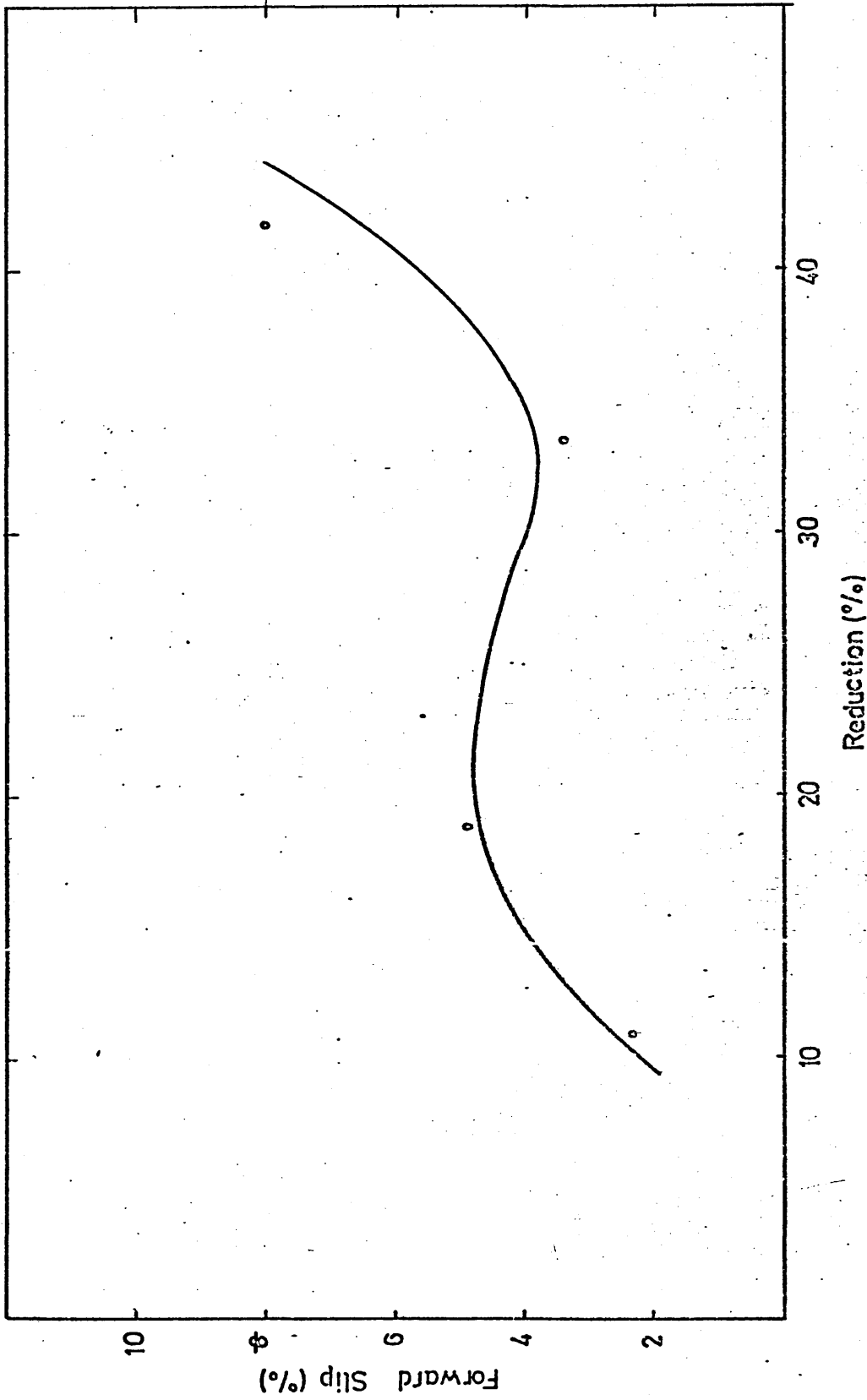


Fig.5.4.4.1 Forward slip variation with the percentage reduction measured at 900 °C.
(Series A)

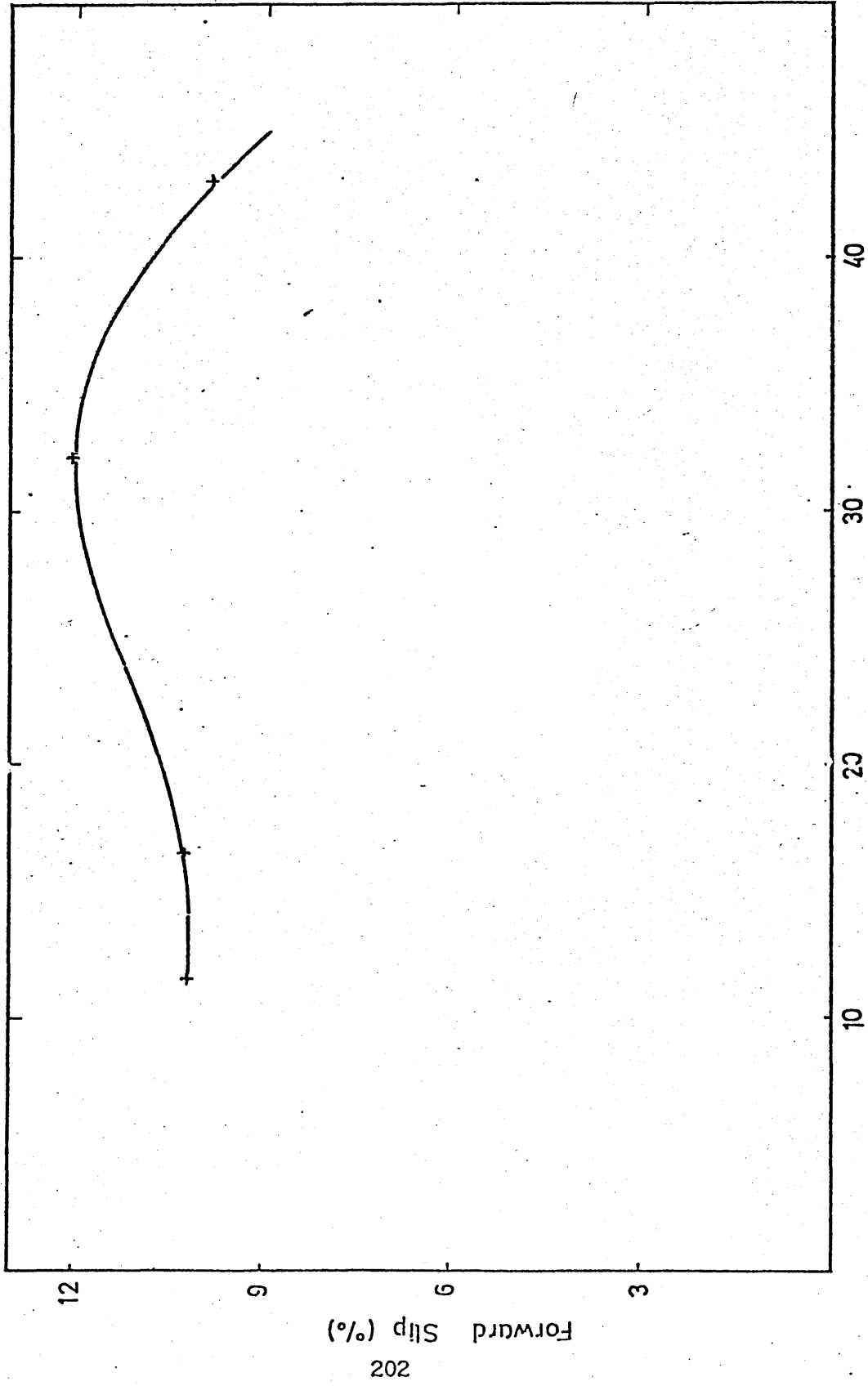


Fig. 5.4.2 Forward slip variation with the percentage reduction measured at 1000 °C. (Series A)

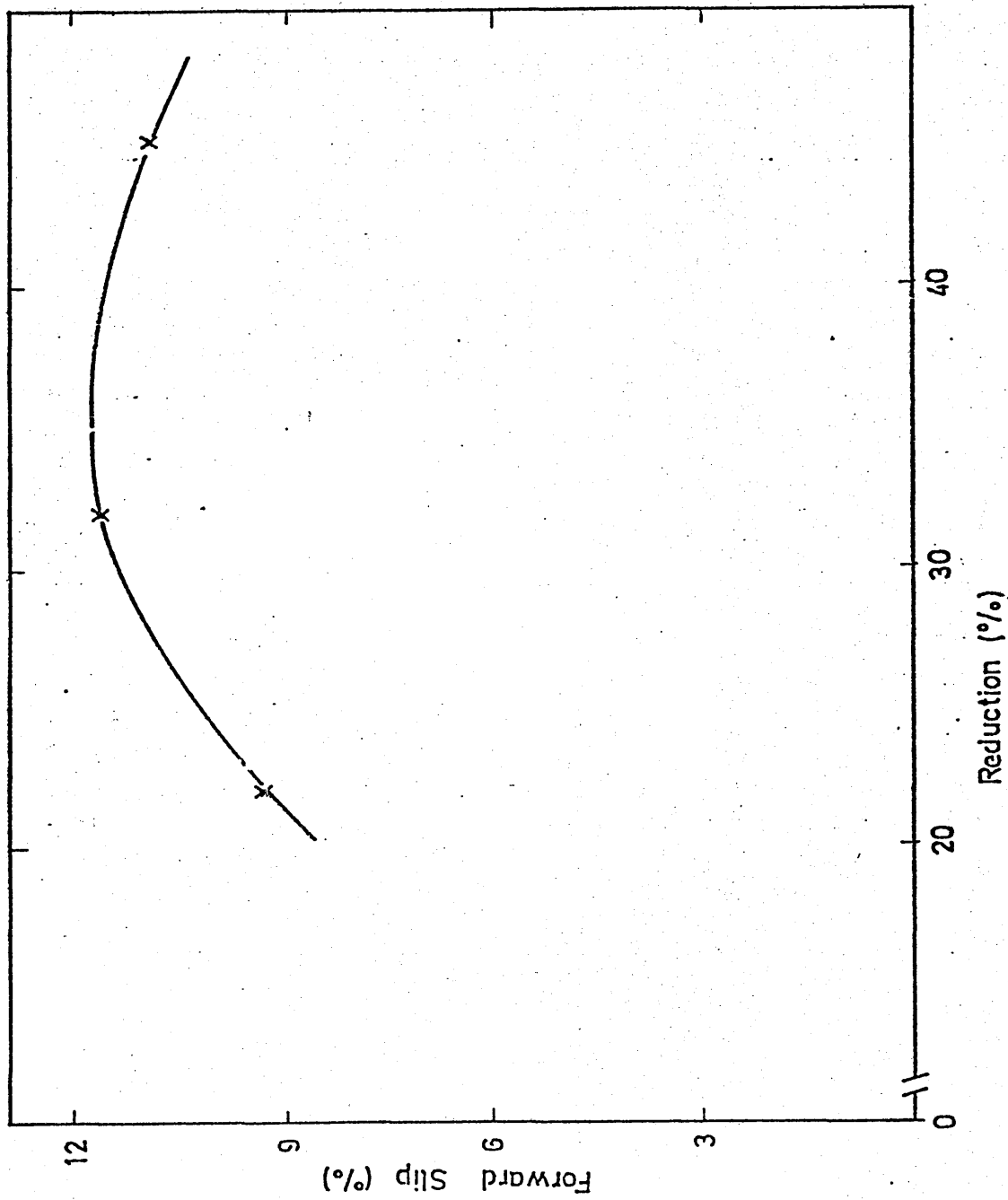


Fig.5.4.3 Forward slip variation with the percentage reduction measured at 1100°C.
(Series A)

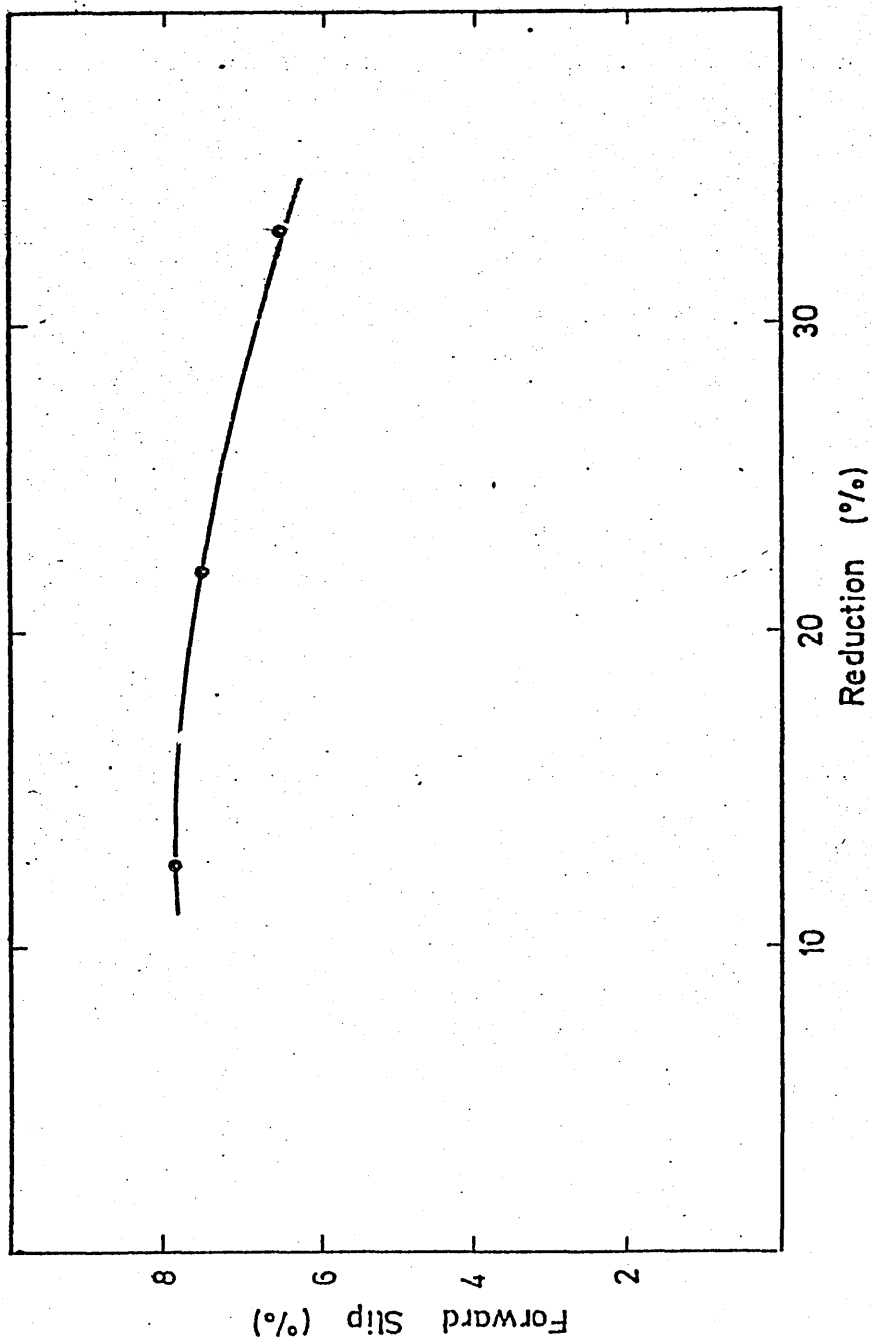


Fig.5.4.4 Forward slip variation with the percentage reduction measured at 1200°C.
(Series A)

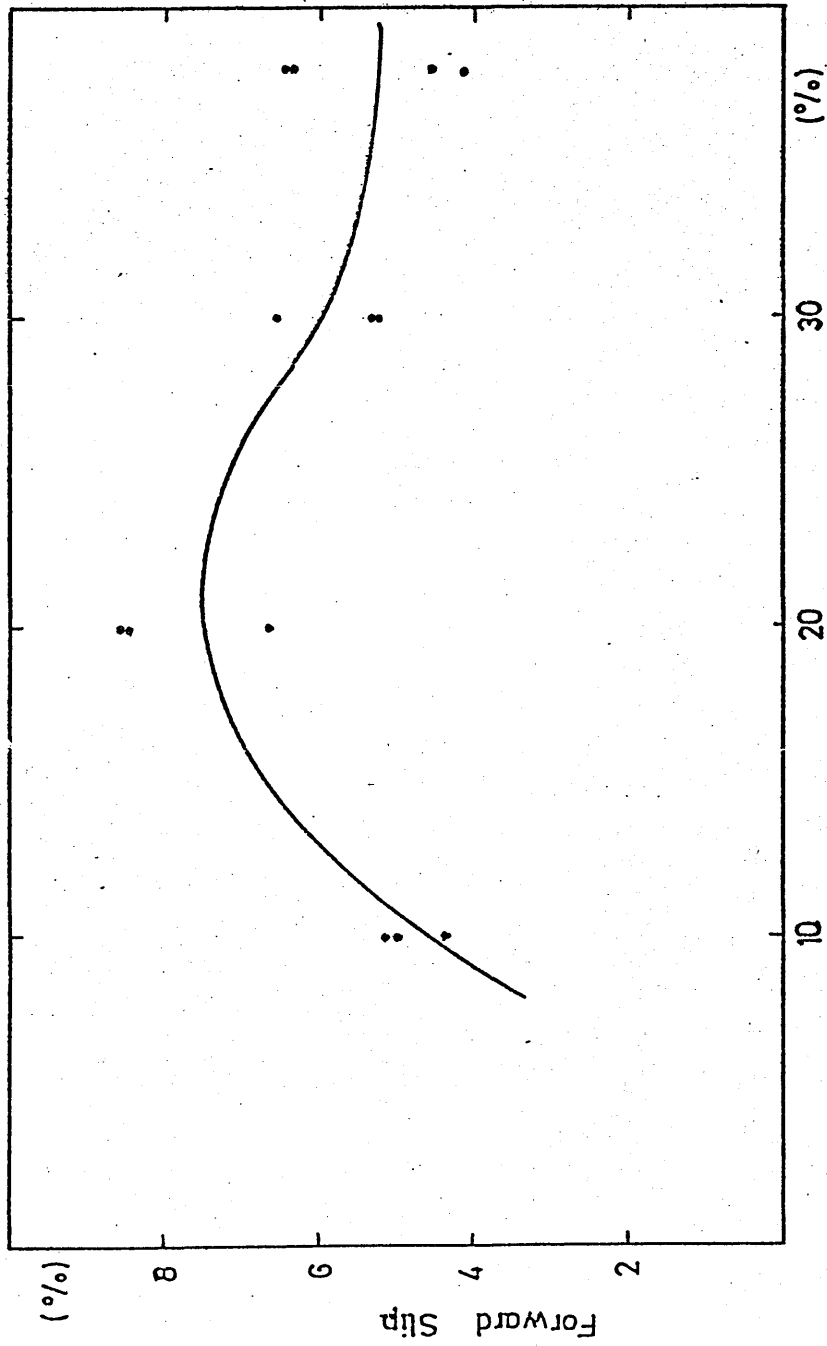


Fig. 5.4.5 Forward slip variation with percentage reduction under lubricated conditions at 960°C. (Series B)

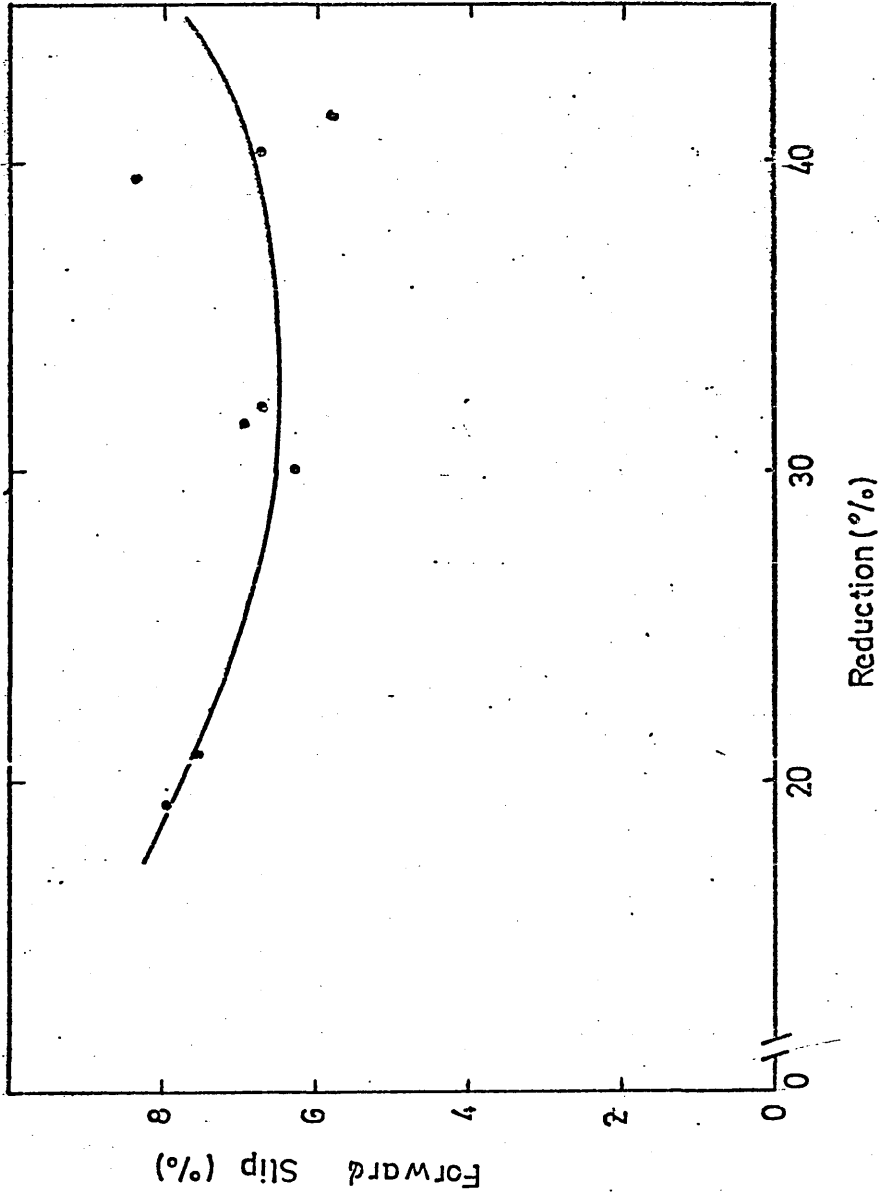


Fig. 5.4.6 Forward slip variation with percentage reduction under unlubricated conditions at 960°C. (Series B)

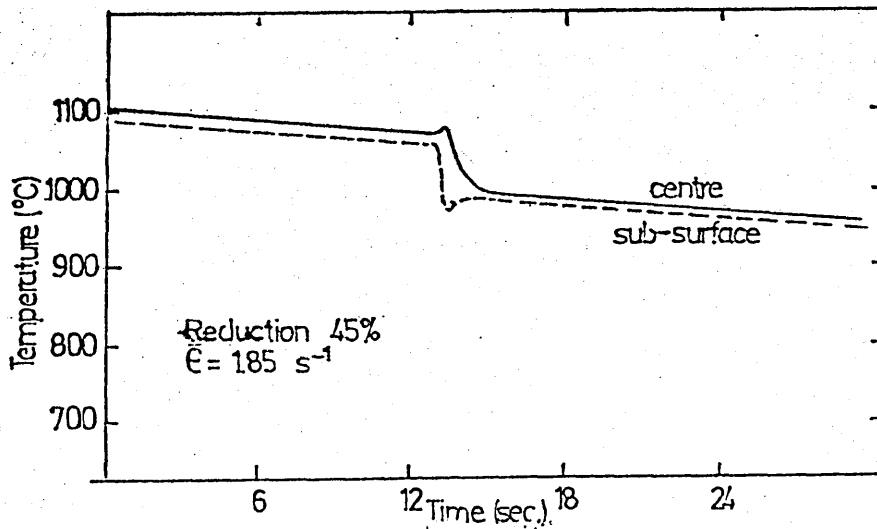
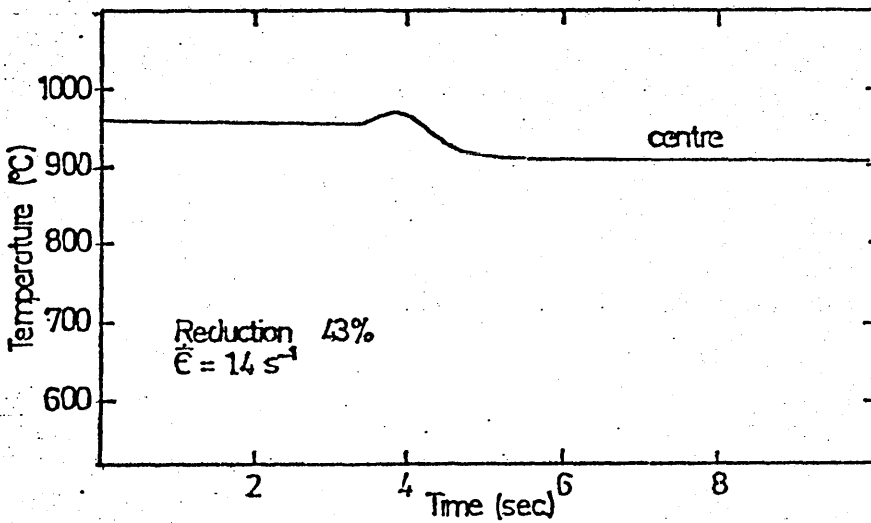
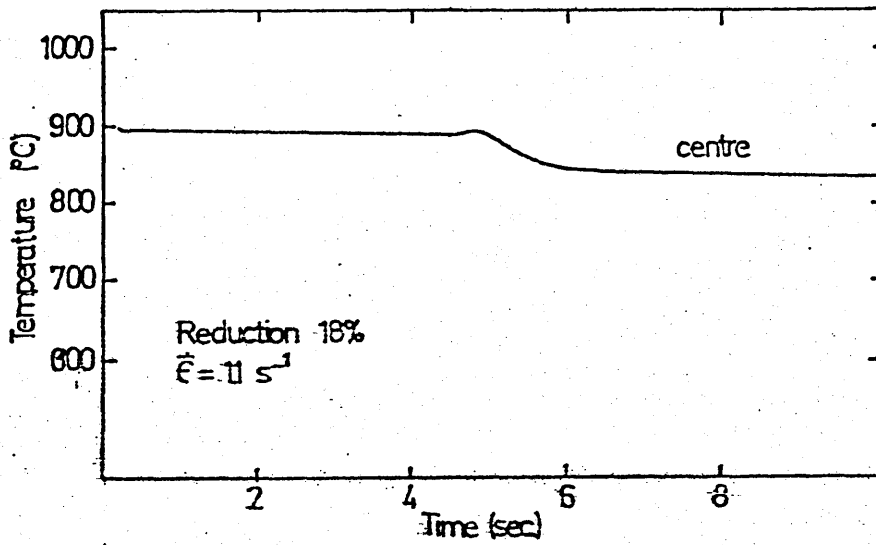


Fig.5.5.1 Temperature variations at the centre and sub-surface of a plate before and during rolling for various reductions, 18-45% and mean entry temperatures, 900-1100 °C.

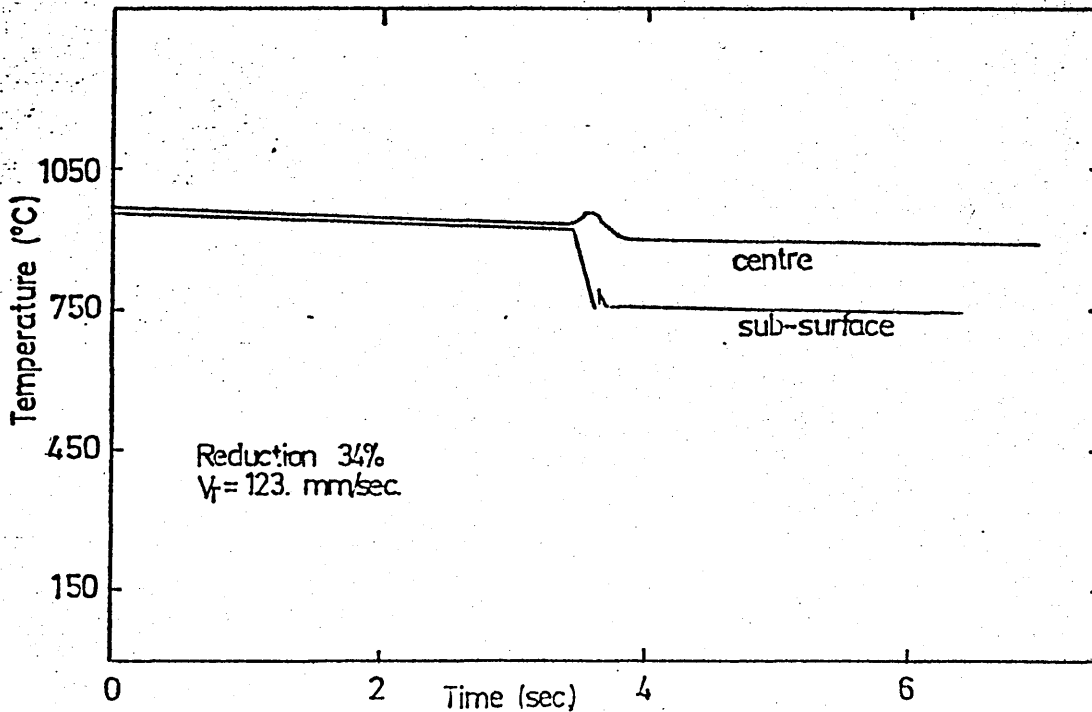
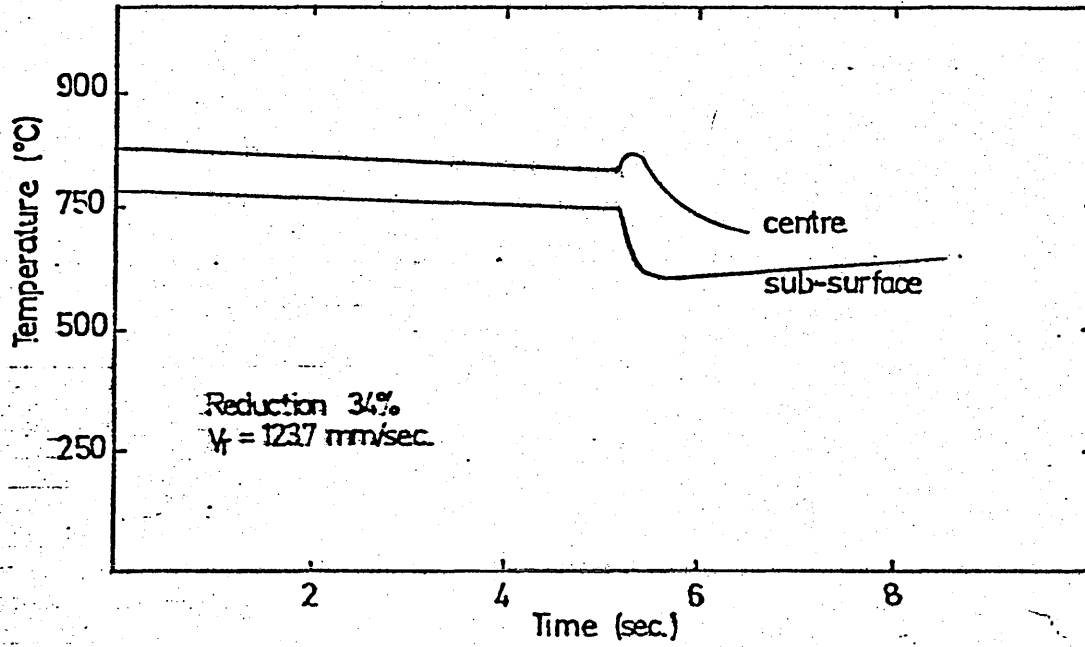


Fig.5.5.2 Temperature variations at the centre and sub-surface of a plate before and during rolling for a reduction of 34% and mean entry temperatures of 800-950°C.

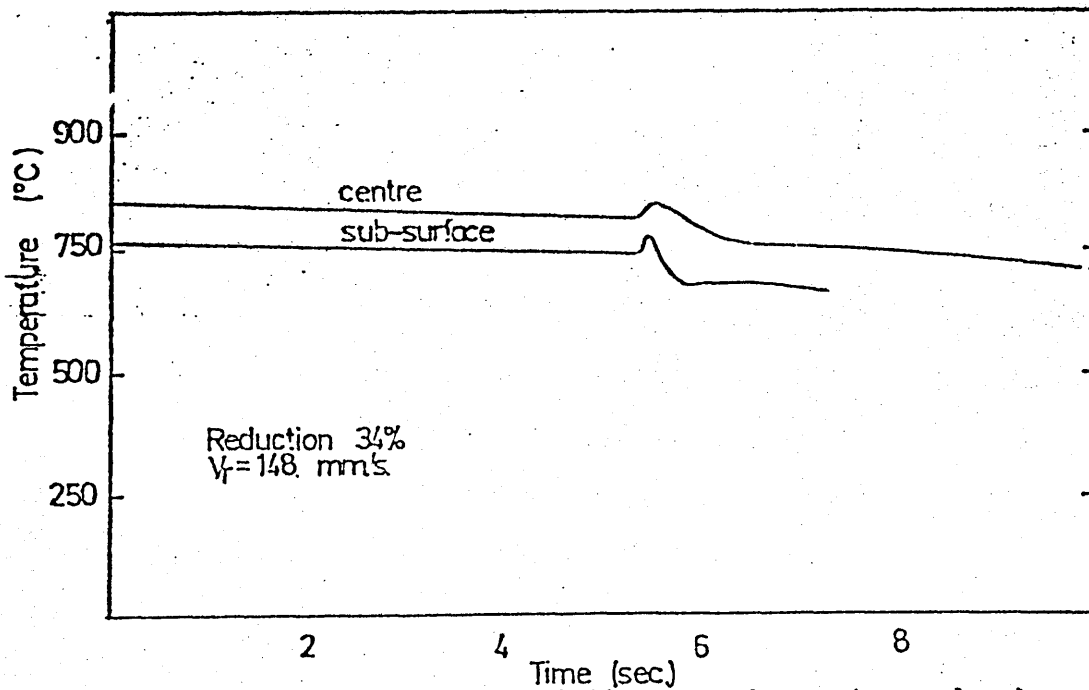
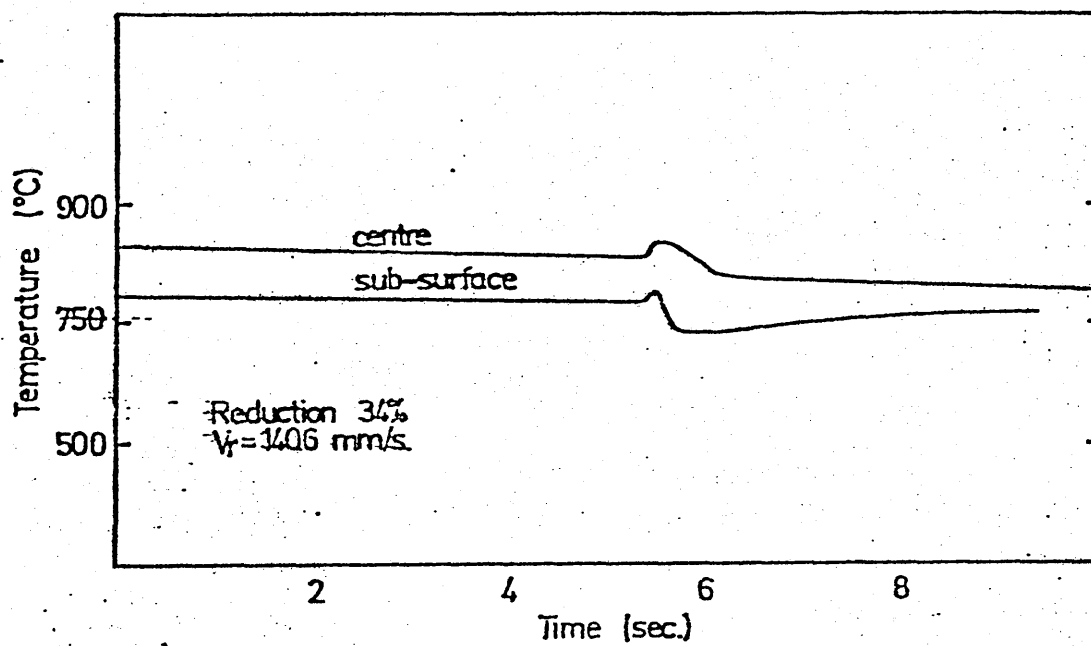
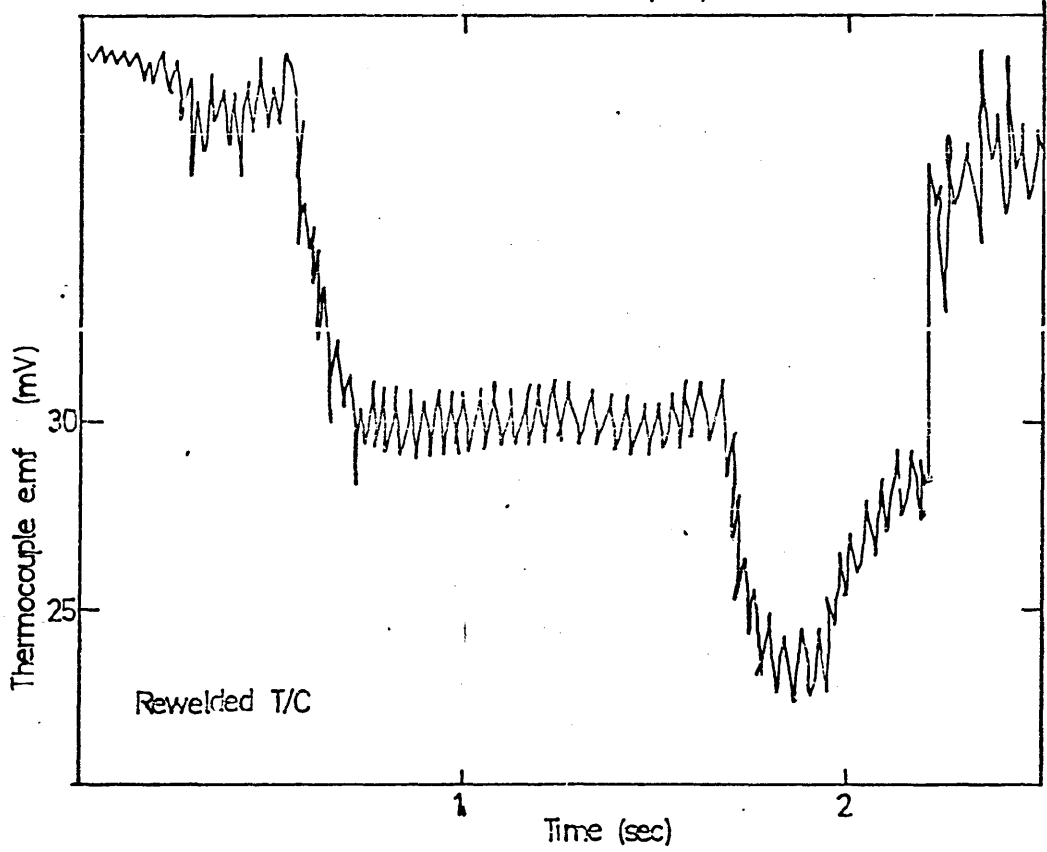
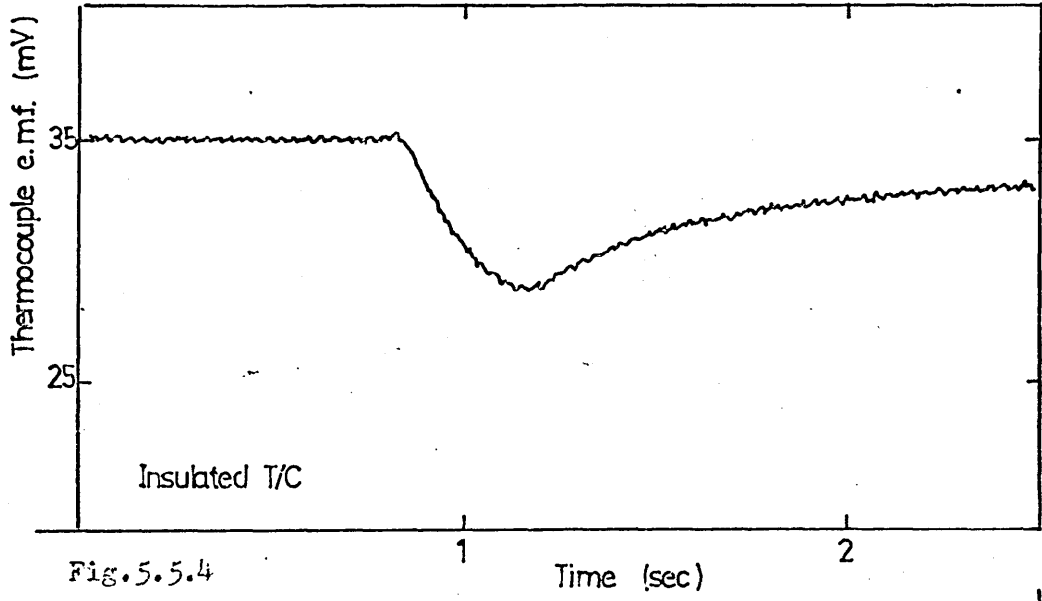


Fig.5.5.3 Temperature variations at the centre and sub-surface of a plate before and during rolling for a reduction of 34% and a mean entry temperature of 850°C.

Fig.5.5.4 Typical recording from an insulated thermocouple inserted in a plate being deformed.

Fig.5.5.5 Correction to allow voltage interference in a re-welded thermocouple.



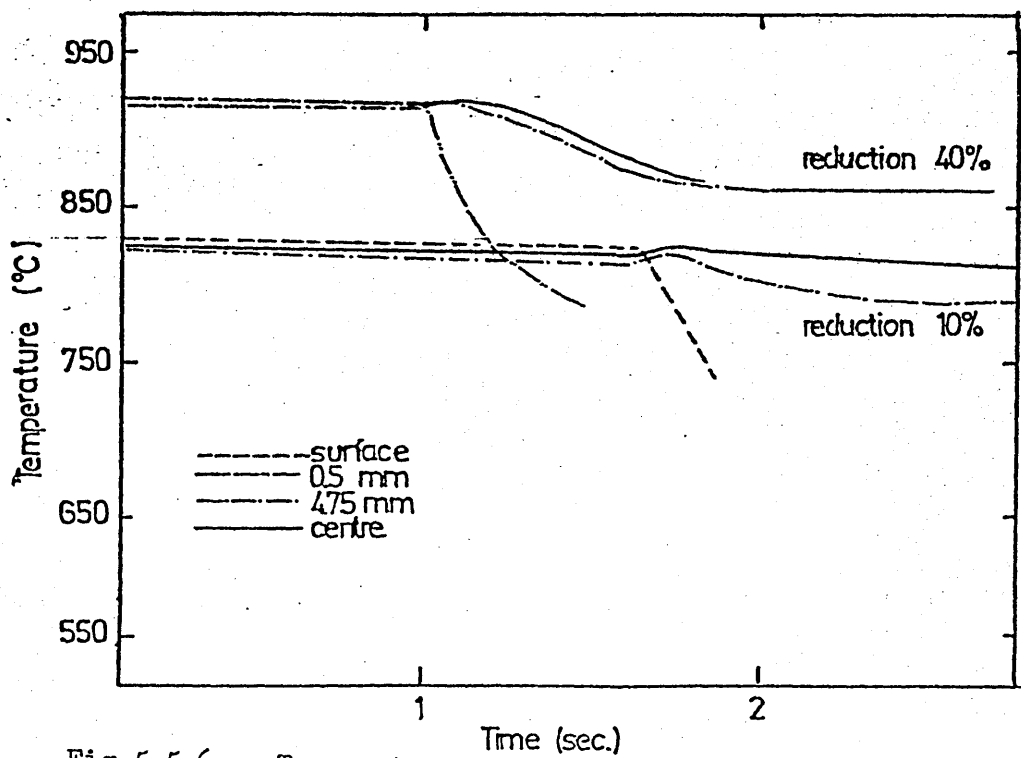
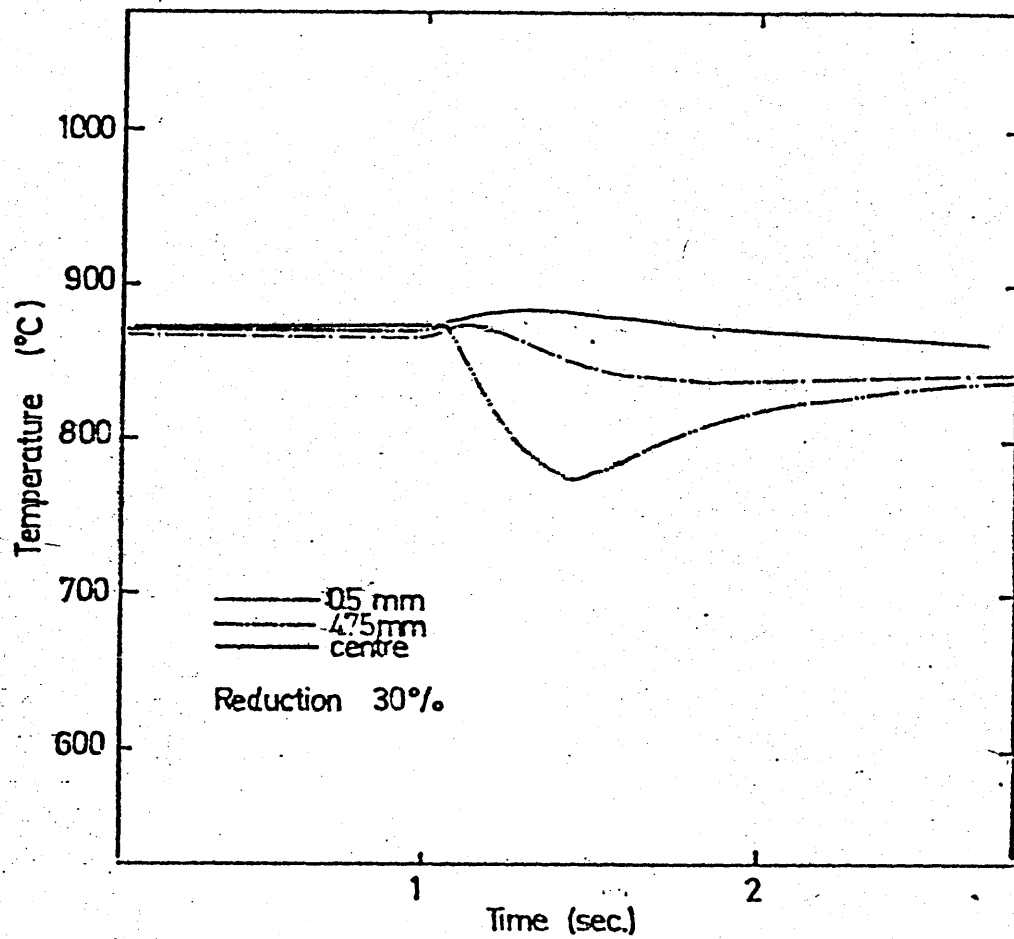


Fig.5.5.6 Temperature variation at several depths of a plate during contact time using insulated thermocouples.

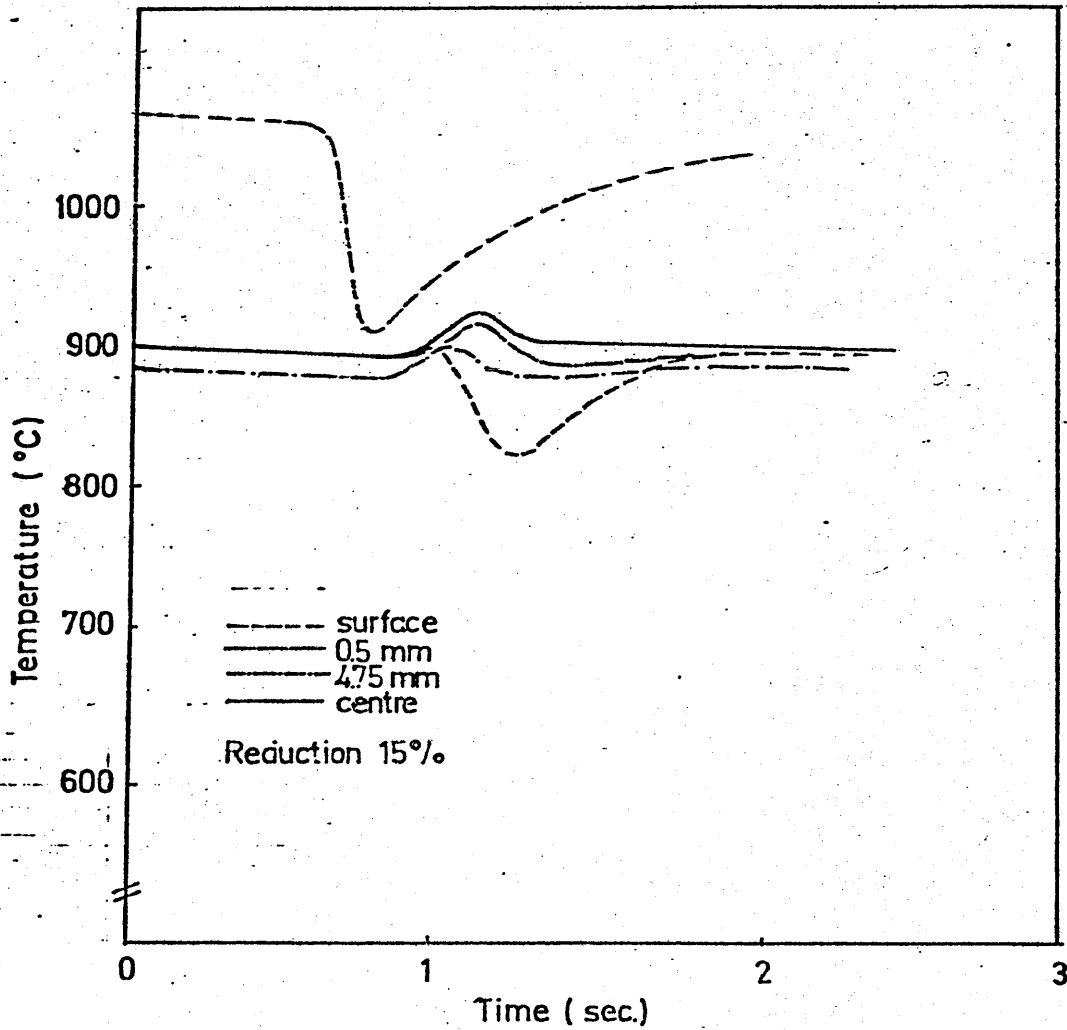


Fig. 5.5.7(a) Temperature variation at several depths of a plate during contact time using re-welded thermocouples with mean entry temperatures of 900-1050°C and 15% reduction.

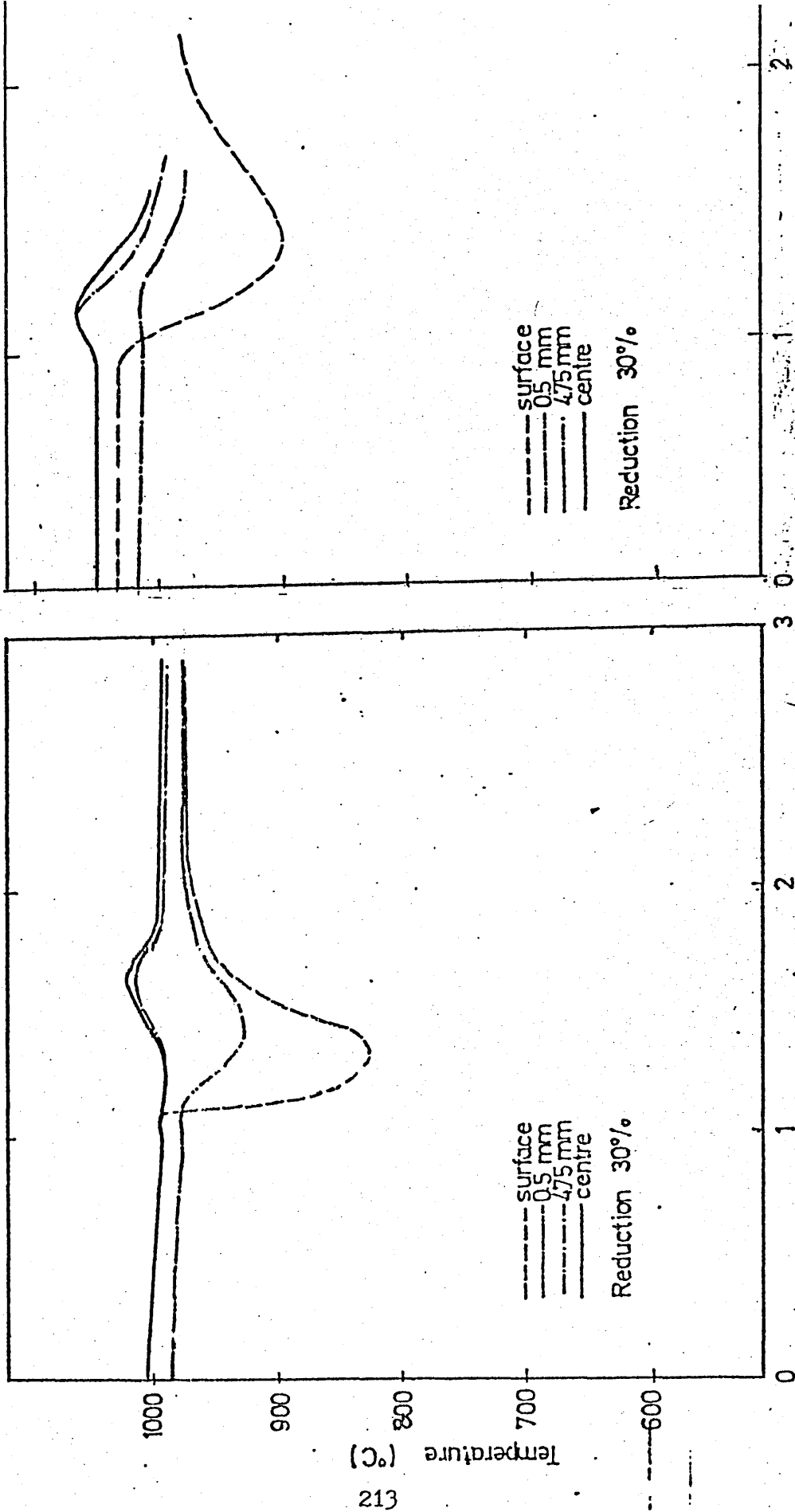


Fig. 5.5.7(b) & (c) Temperature variation at several depths of a plate during contact time using re-welded thermocouples at 1000 °C and 1050 °C and a reduction of

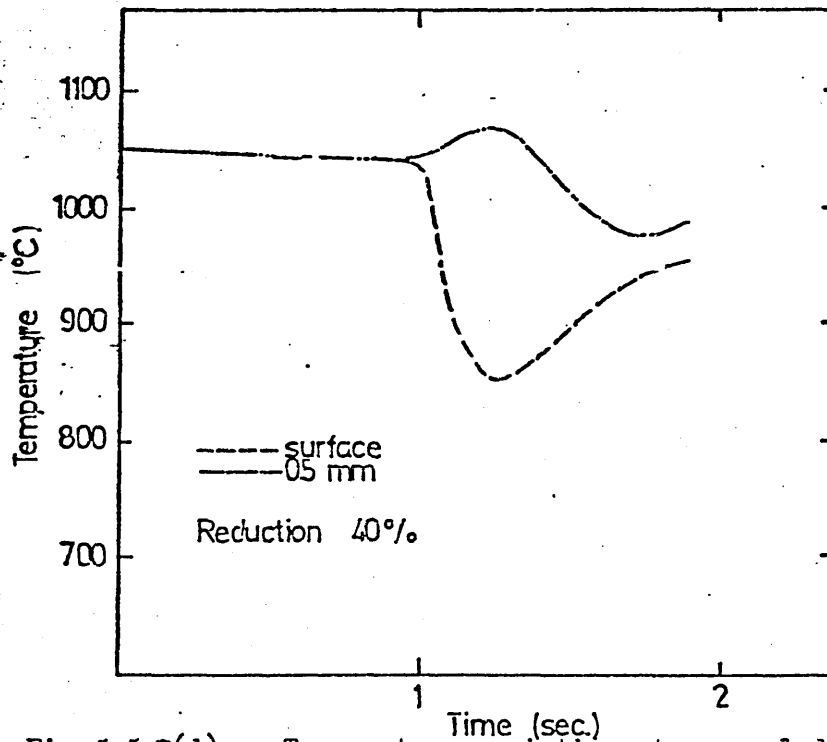
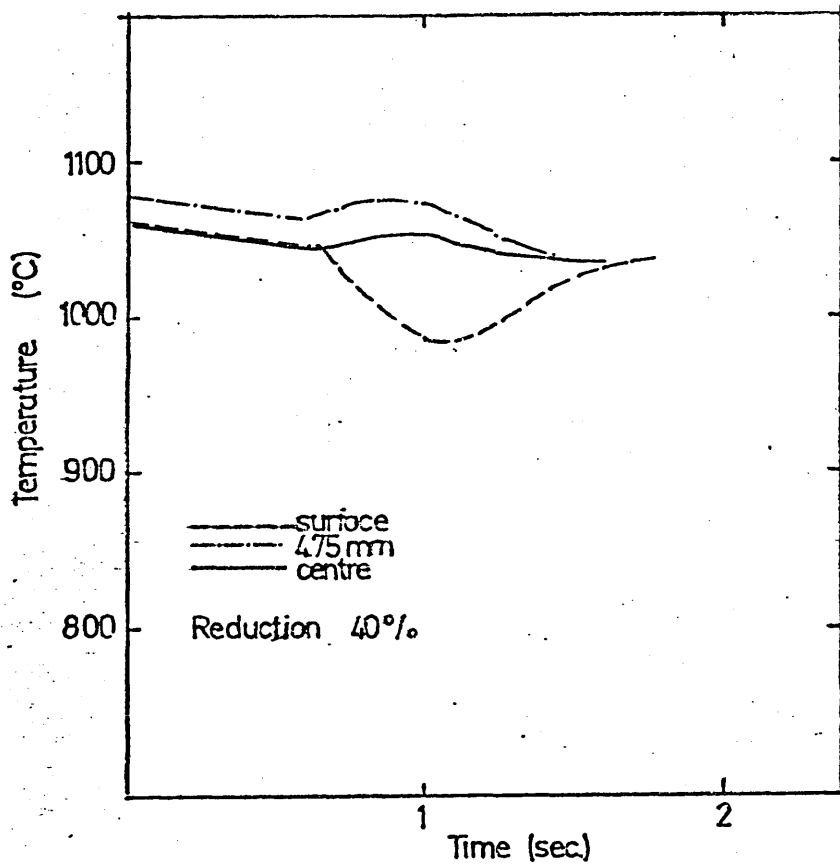


Fig. 5.5.7(d)

Temperature variation at several depths of a plate during contact time using re-welded thermocouples with a mean entry temperature of 1050°C and 40% reduction.

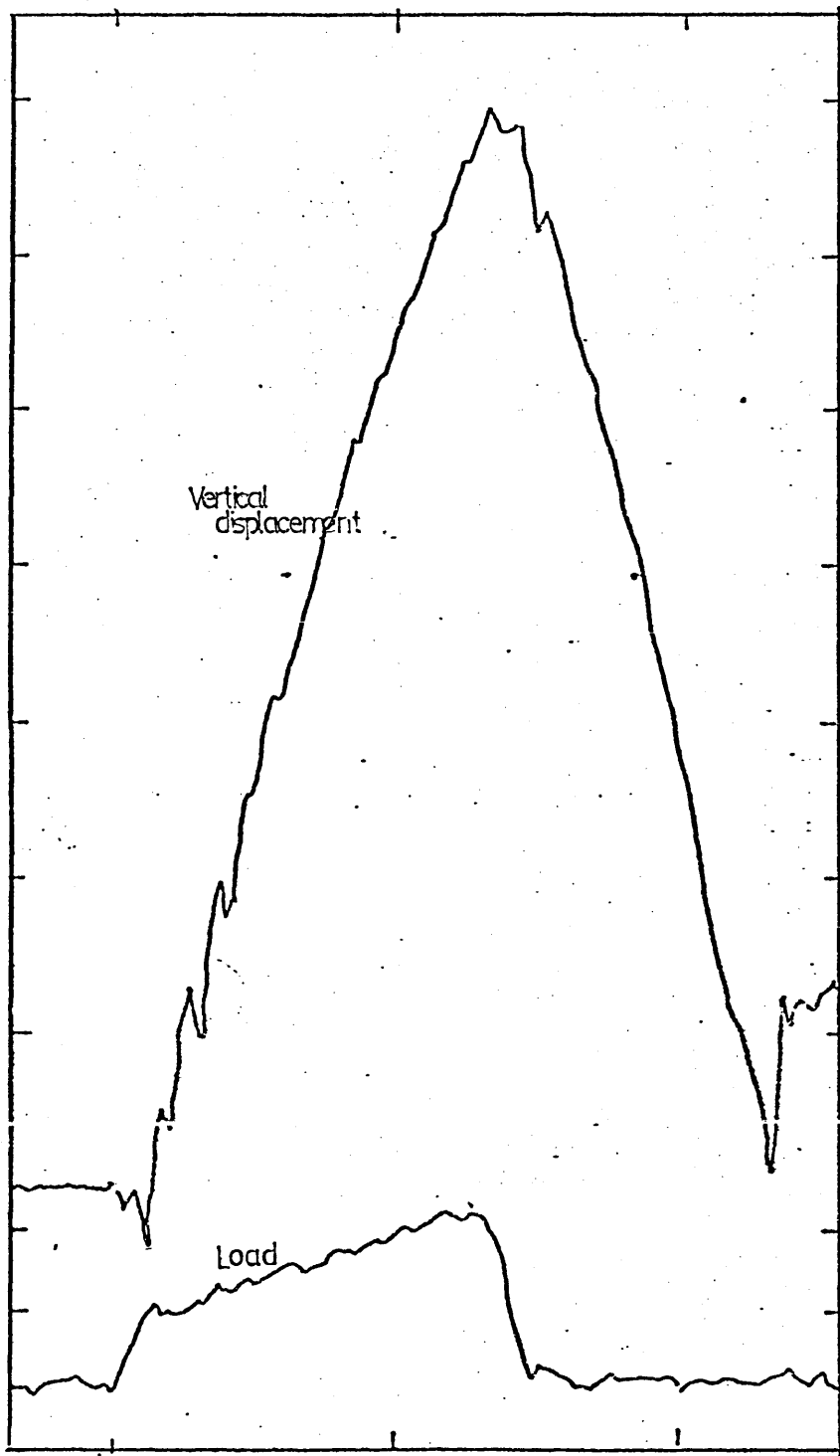


Fig.5.6.1 Typical traces of the load/time and displacement/time recorded in a cam plastometer.

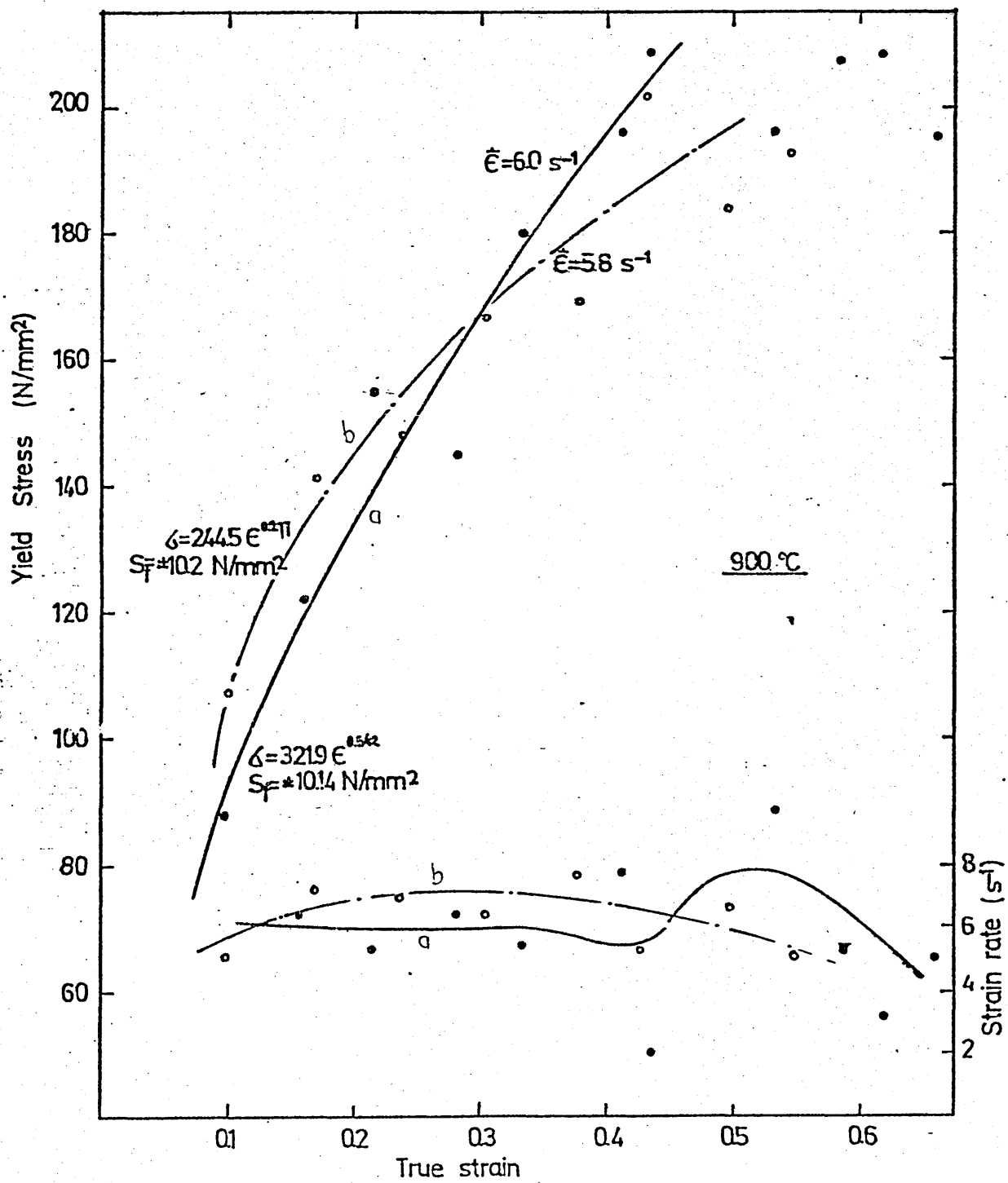


Fig.5.6.2ab Uniaxial yield stress/strain curves of 0.17% C steel at 900 °C.

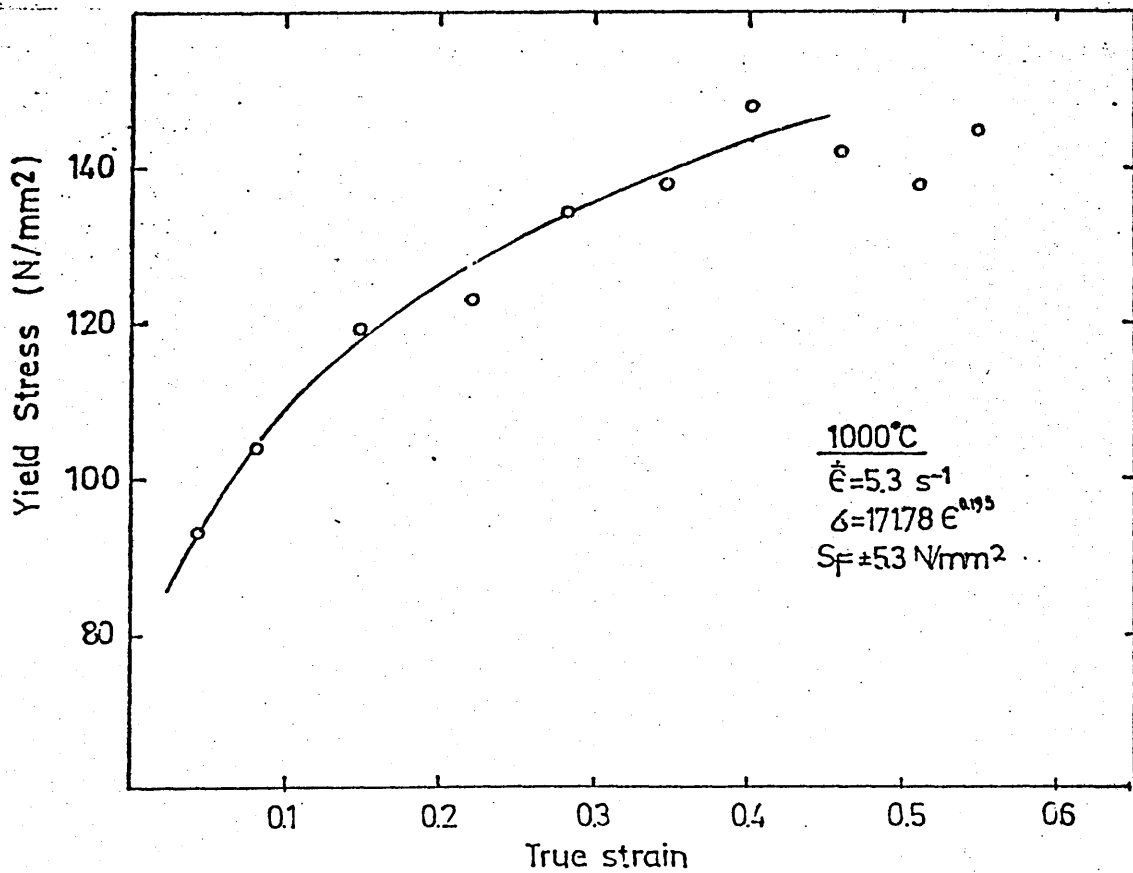
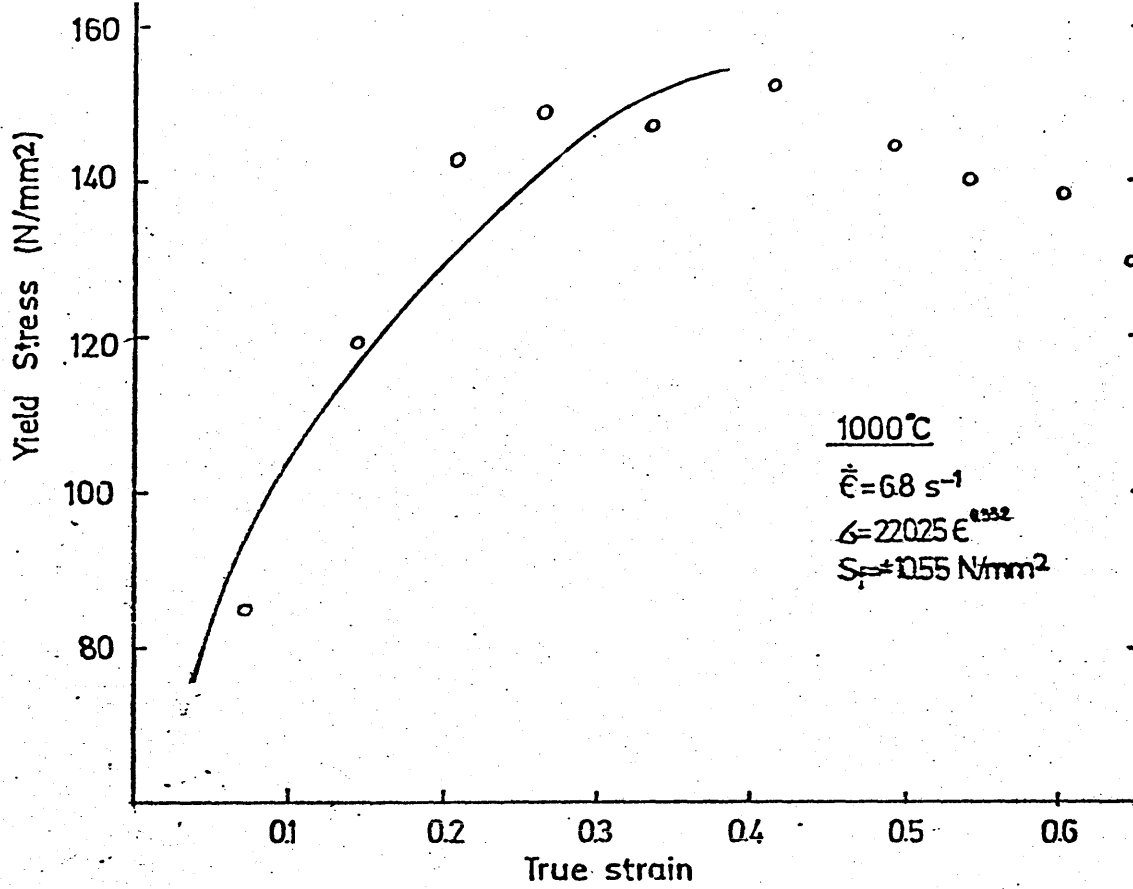


Fig.5.6.3 Uniaxial yield stress/strain curves of 0.17% C steel at 1000°C.

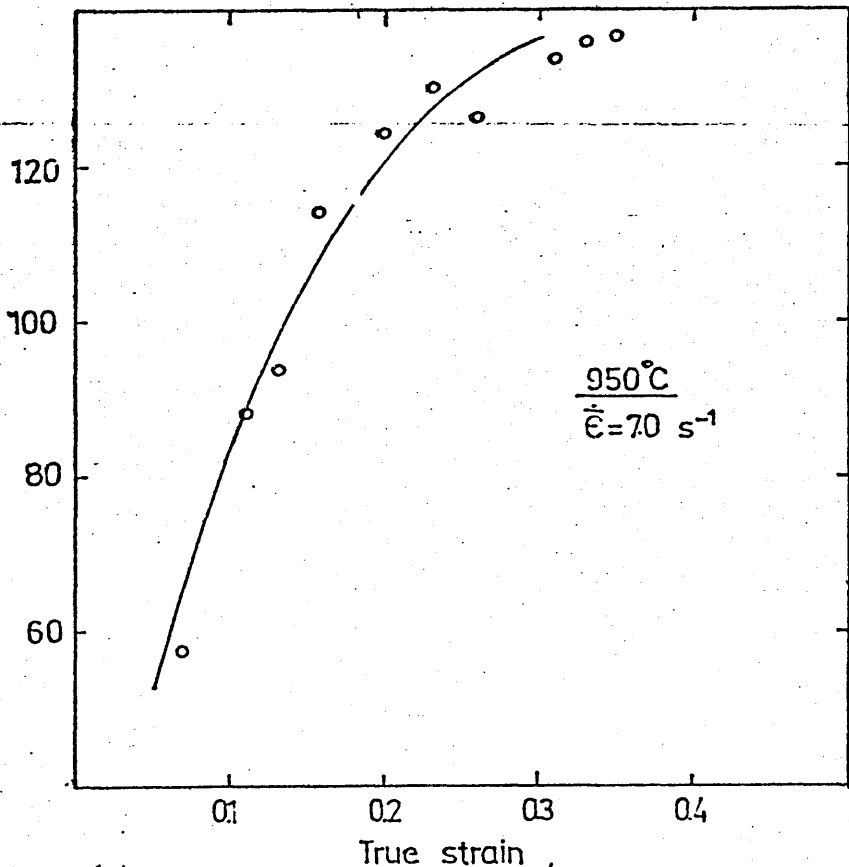
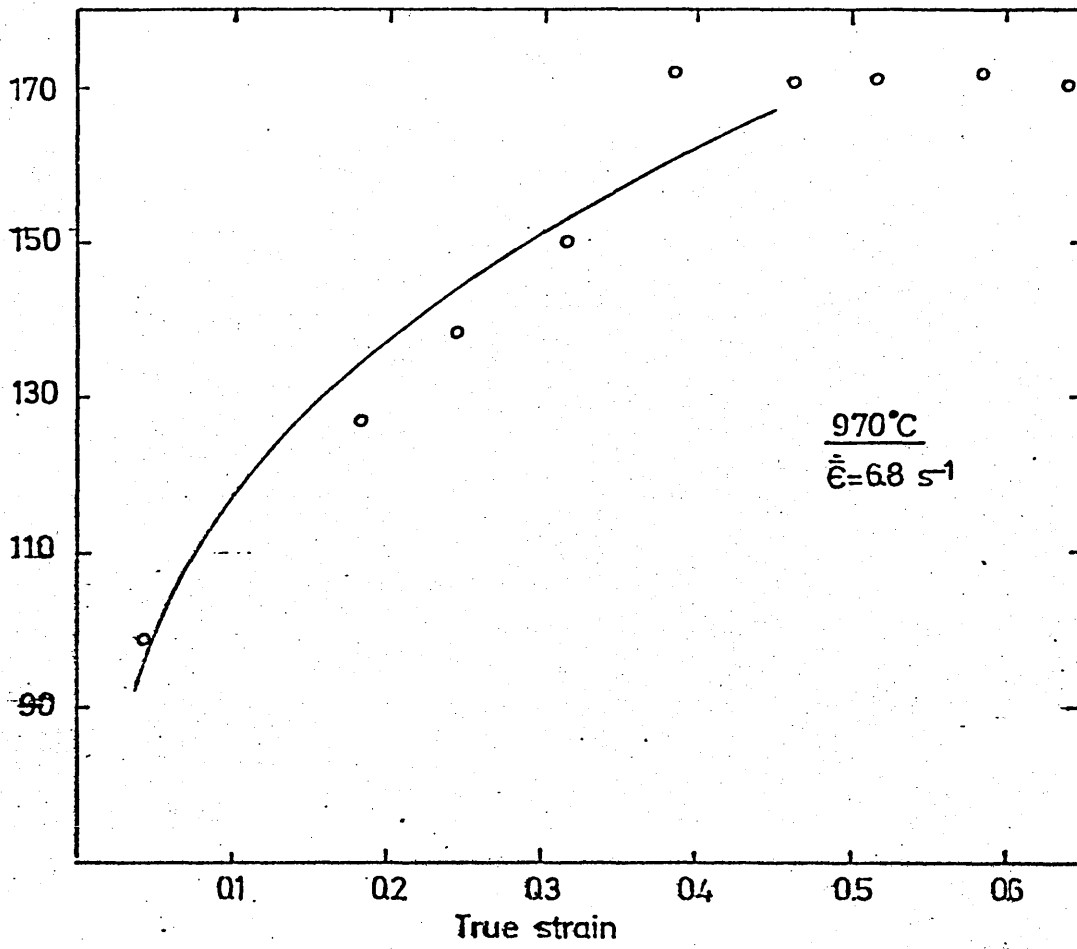


Fig. 5.6.4 Uniaxial yield stress/strain curves of 0.17% C steel at 950-970°C.

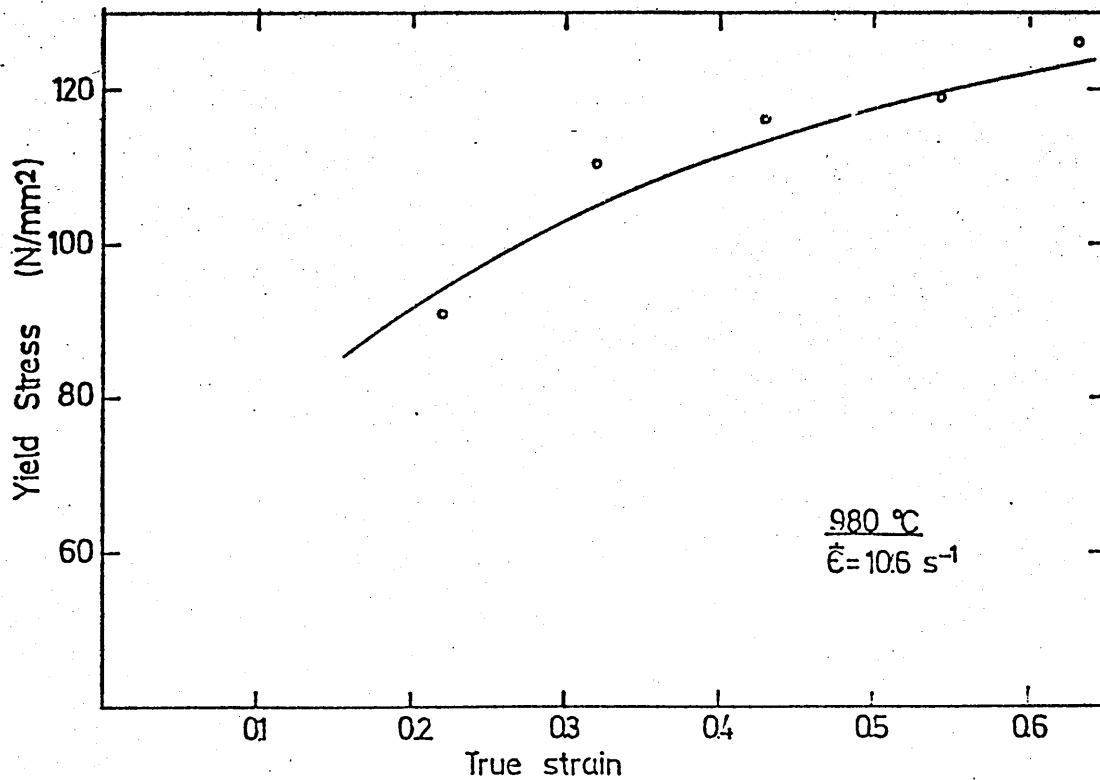
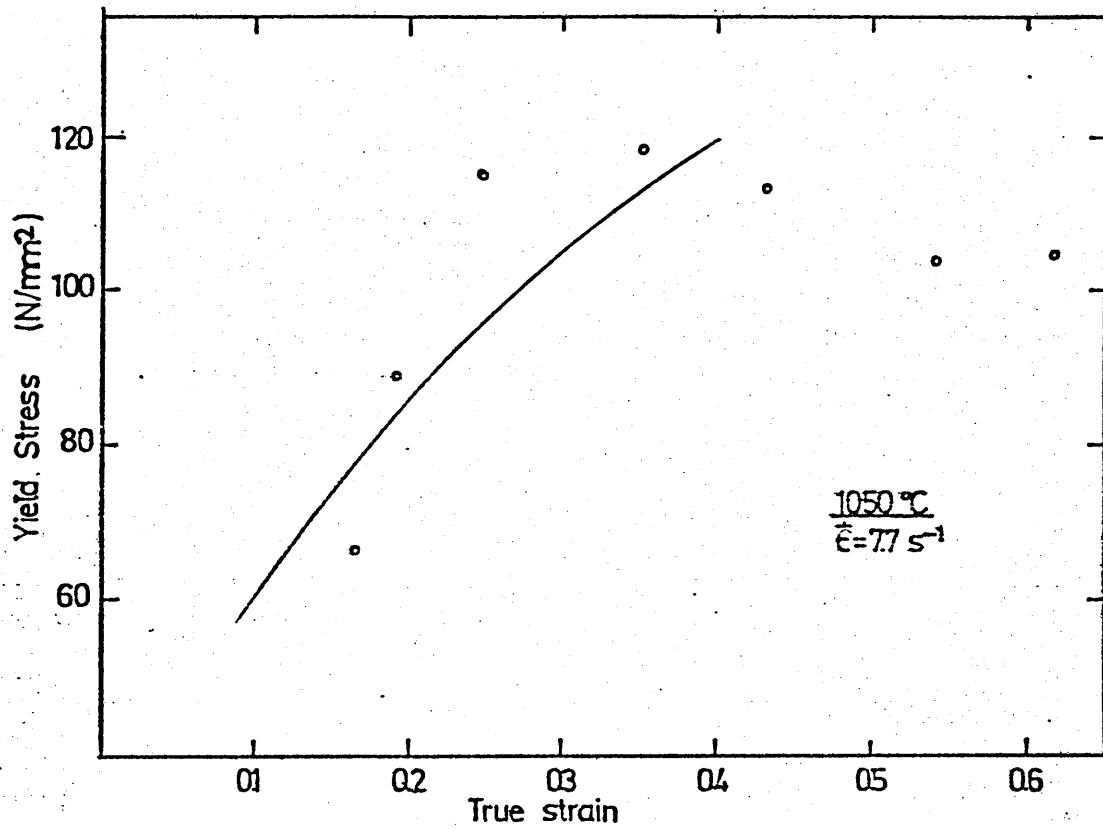


Fig.5.6.5 Uniaxial yield stress/strain curves of 0.17% C steel at 980-1050 °C.

Fig.6.2.2.1 Relation between calculated roll force and reduction under homogeneous deformation and using published flow stress data ($\mu=0.2-0.6$) at 900°C.

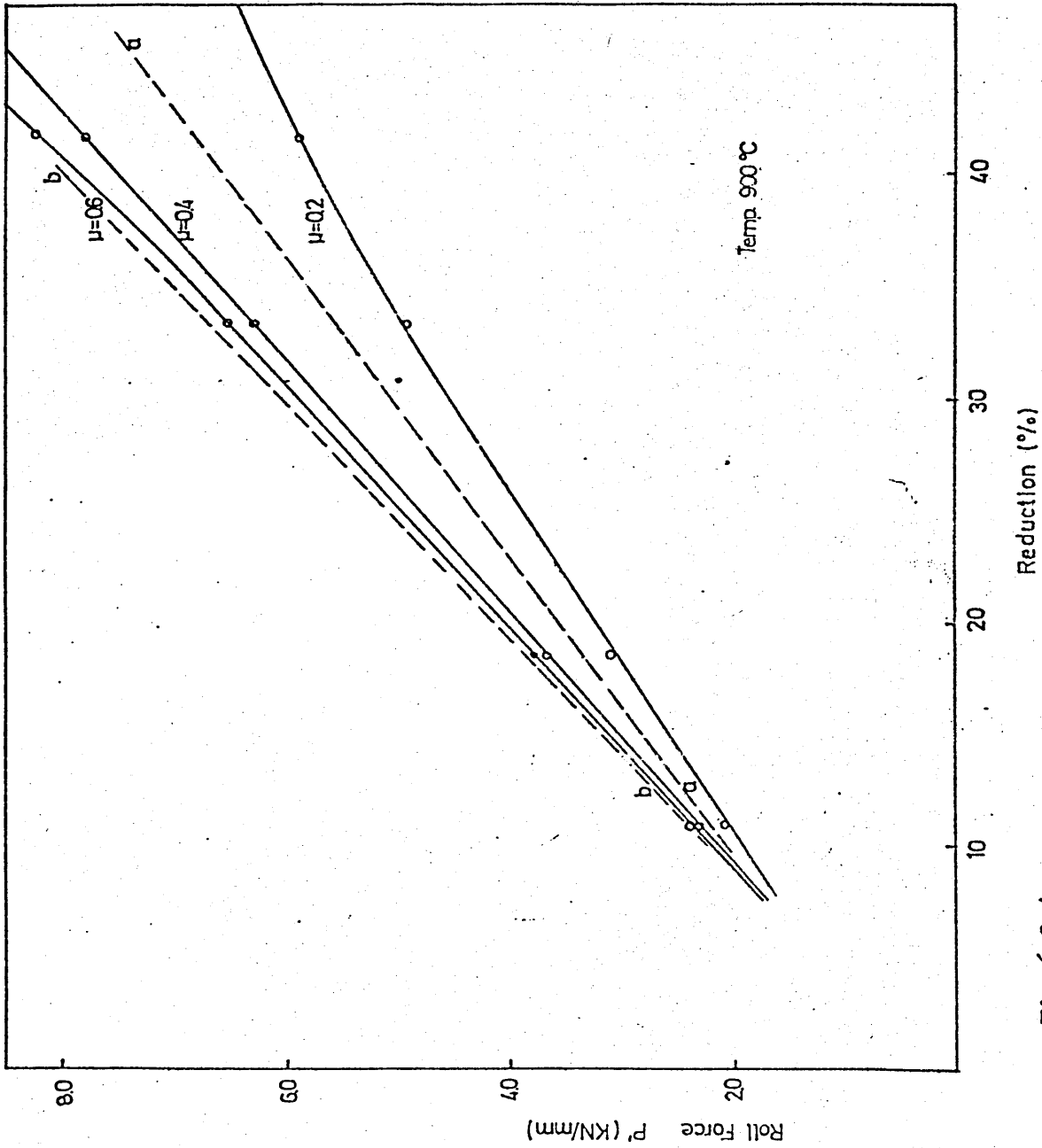


Fig.6.2.1

Fig.6.2.2 Relation between calculated roll force and reduction under homogeneous deformation and using published flow stress data ($\mu=0.2-0.6$) at 1000 °C.

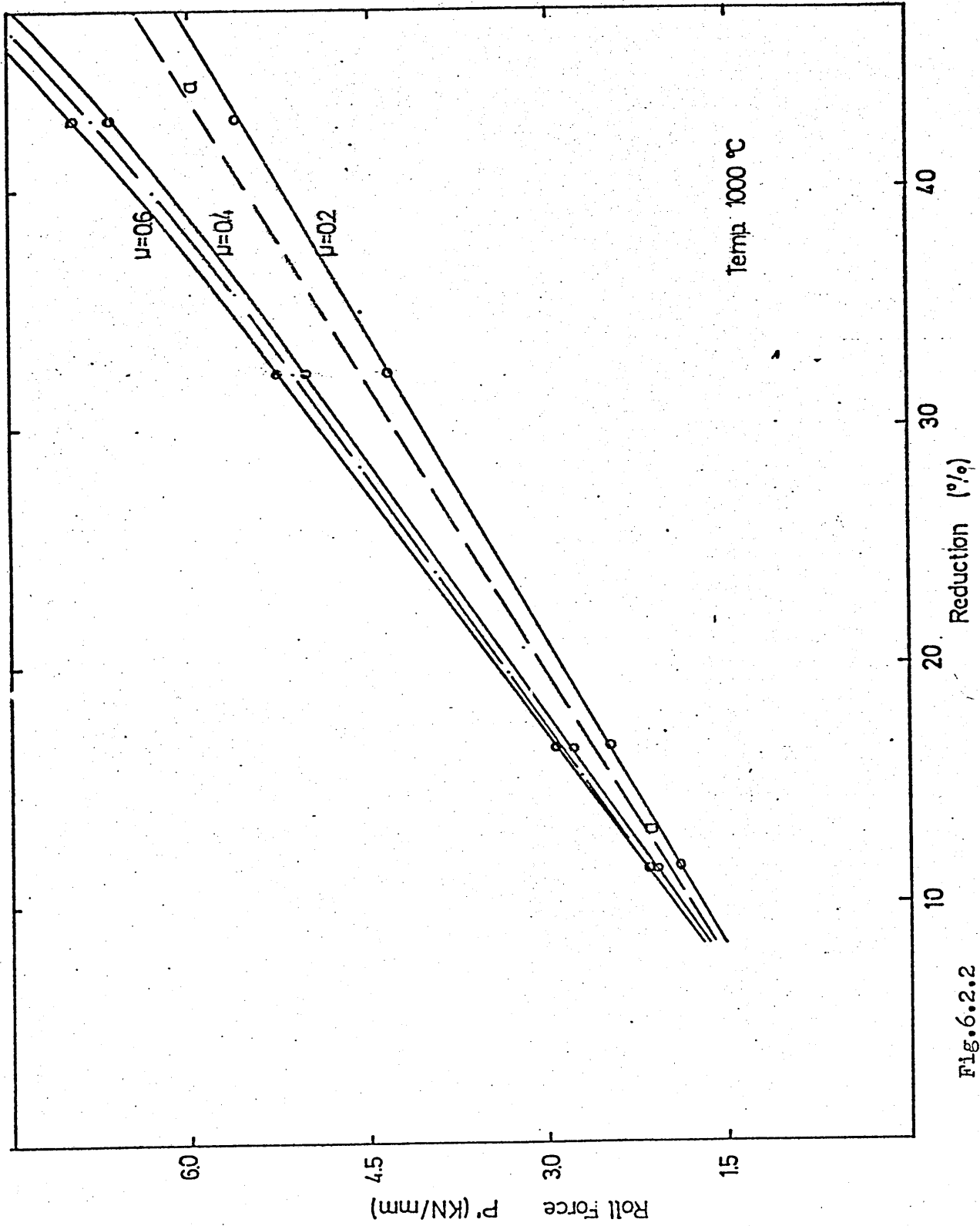


Fig.6.2.2

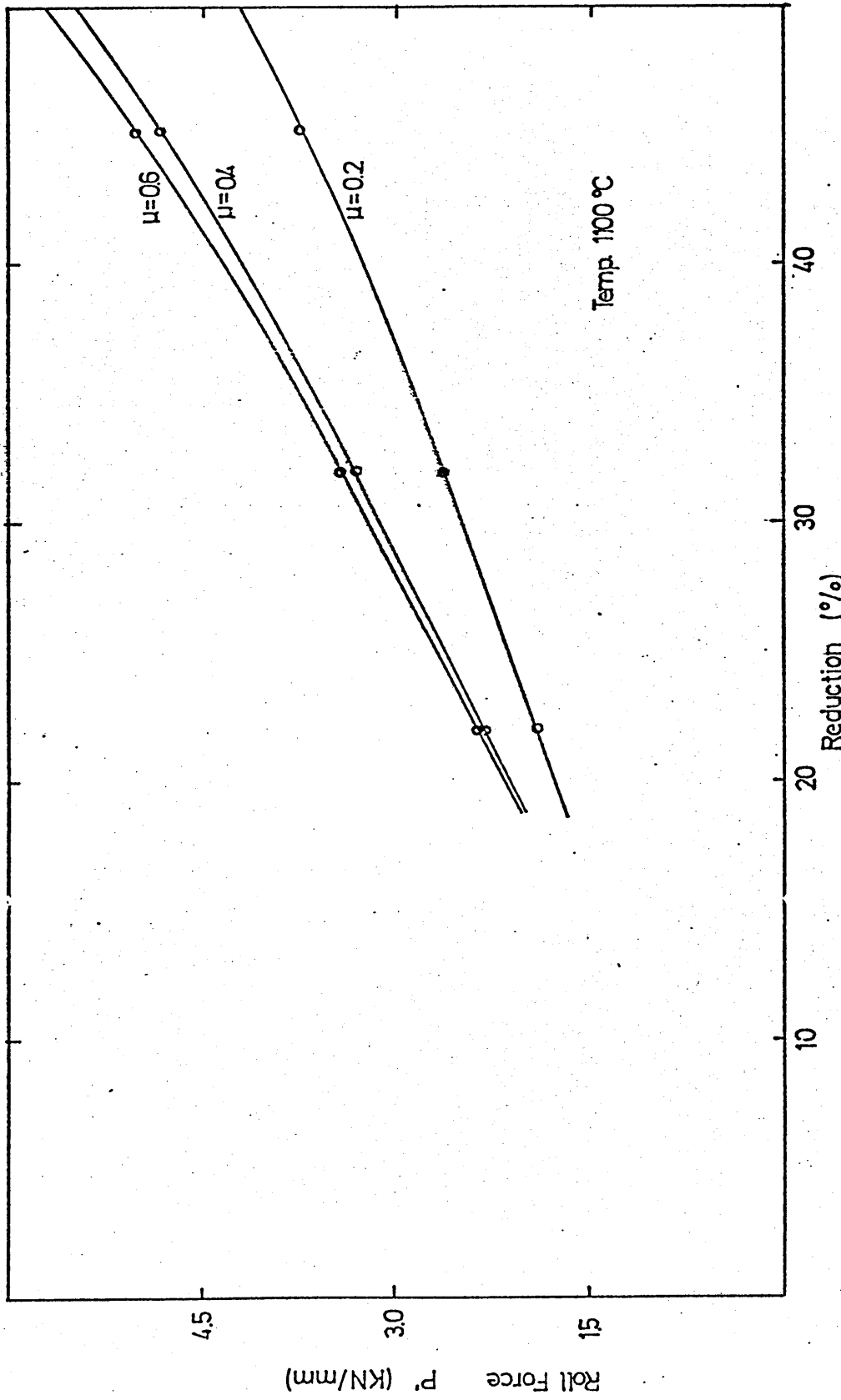


Fig.6.2.3 Relation between calculated roll force and reduction under homogeneous deformation and using published flow stress data ($\mu=0.2-0.6$) at 1100°C.

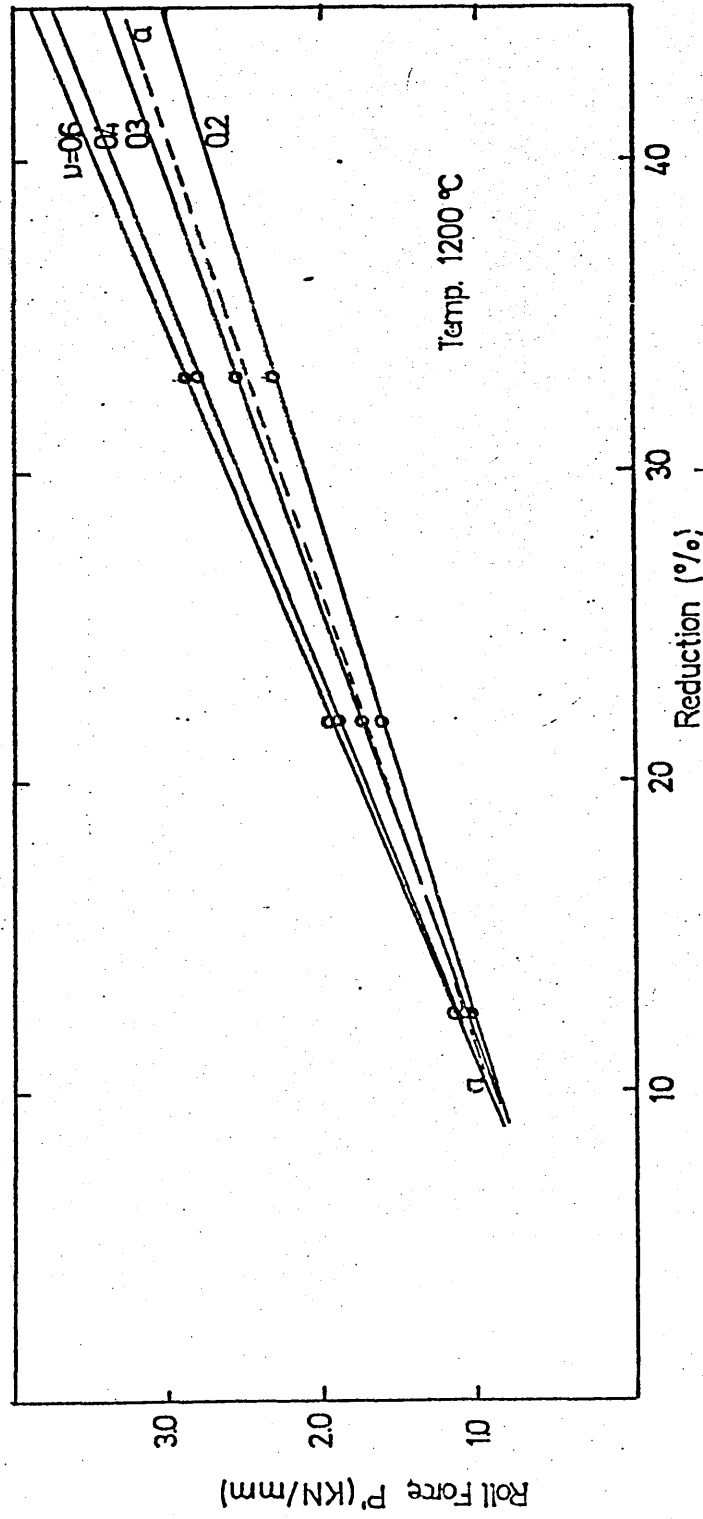


Fig.6.2.4 Relation between calculated roll force and reduction under homogeneous deformation and using published flow stress data ($\mu=0.2-0.6$) at 1200°C.

Fig.6.2.5 Relation between calculated roll force and reduction -
under homogeneous deformation and using flow stress
data determined in the present work ($\mu=0.2-0.6$) at 900°C.

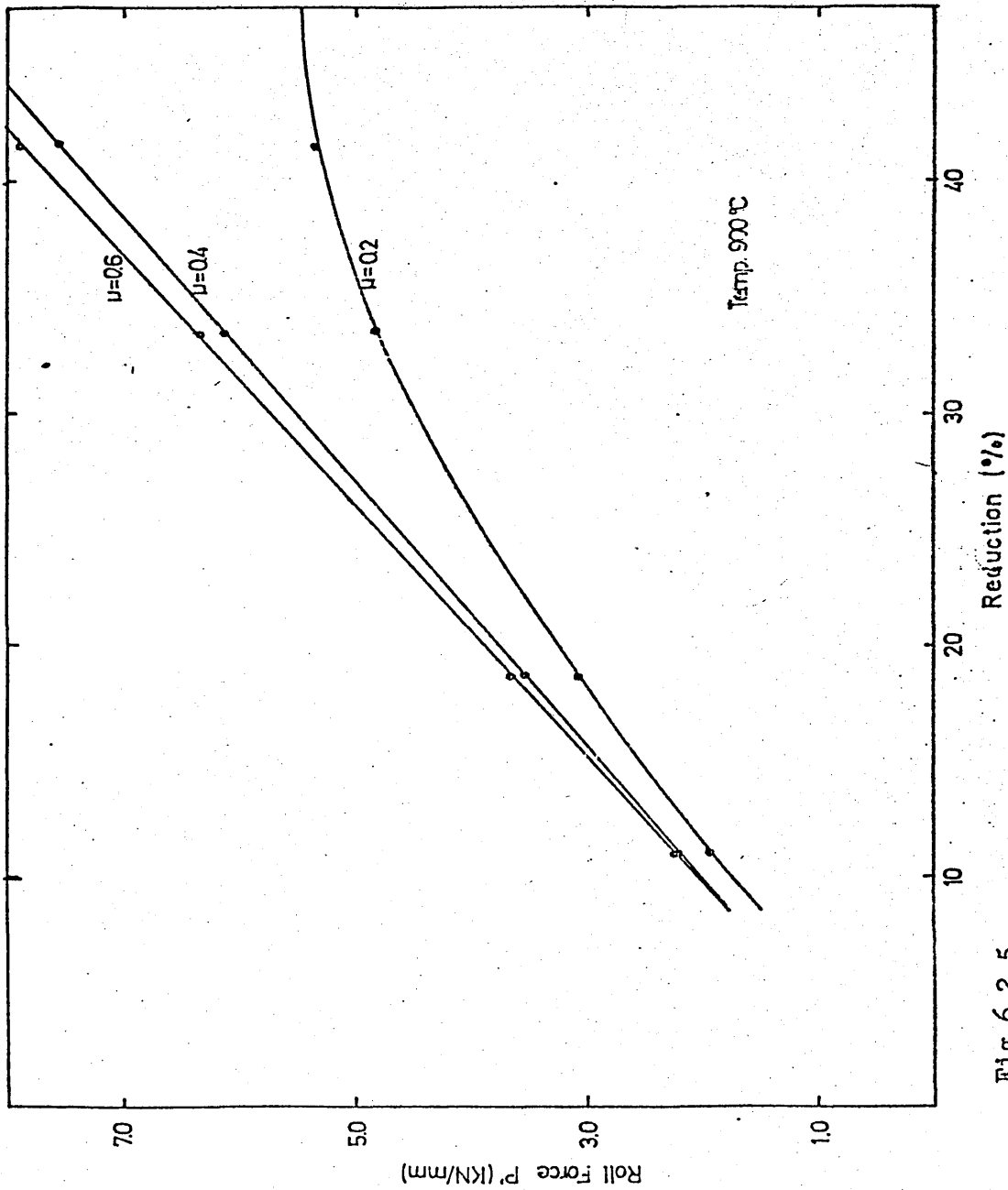


Fig.6.2.5

Fig.6.2.6 Relation between calculated roll force and reduction under homogeneous deformation and using flow stress data determined in the present work ($\mu=0.2-0.6$) at 1000°C.

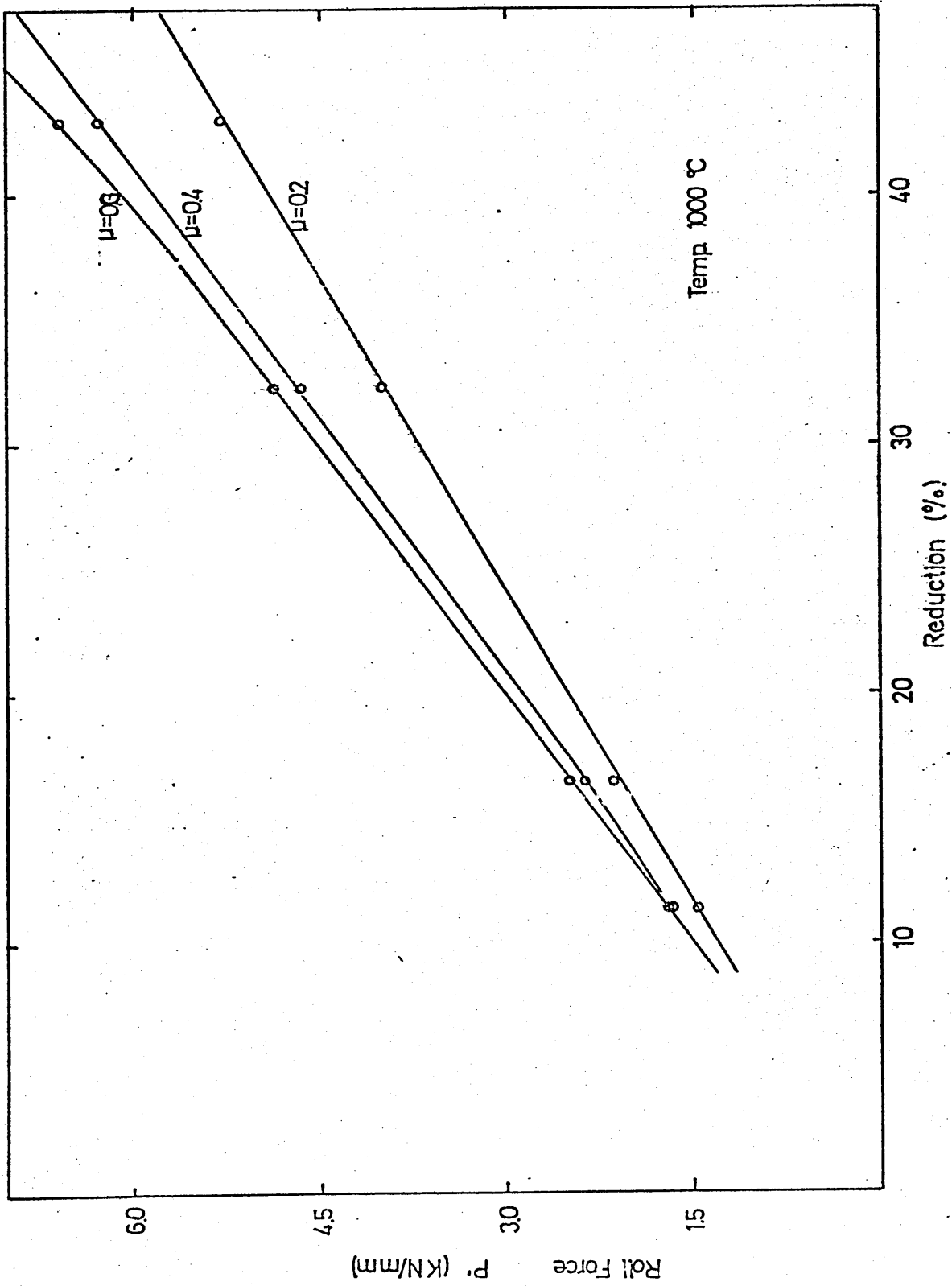


Fig.6.2.6

Fig.6.2.7 Relation between calculated roll force and reduction
under inhomogeneous deformation and using published
flow stress data ($\mu=0.2-0.6$) at 900°C.

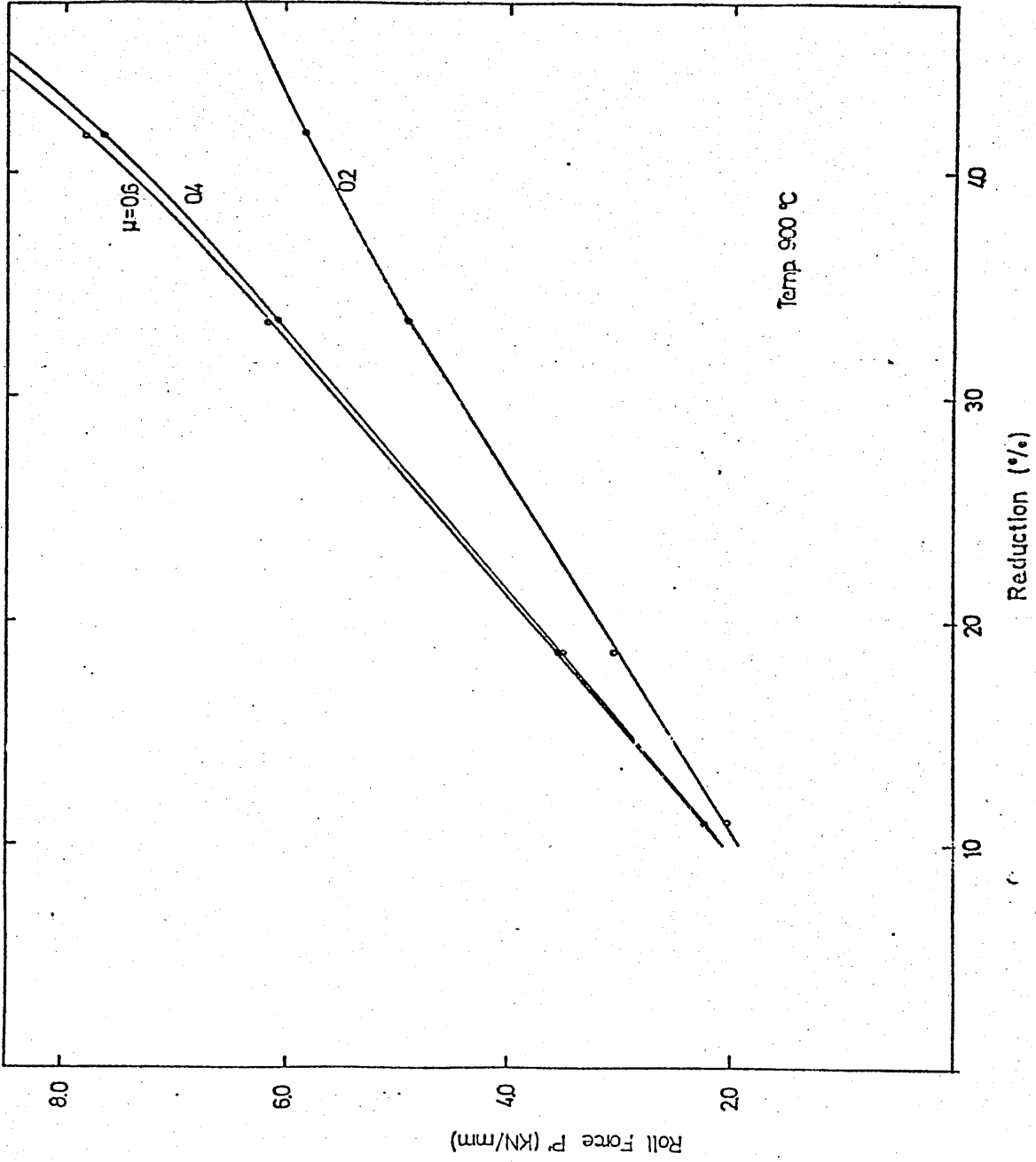


Fig.6.2.7

Fig.6.2.8 Relation between calculated roll force and reduction
under inhomogeneous deformation and using published
flow stress data ($\mu=0.2-0.6$) at 1000°C.

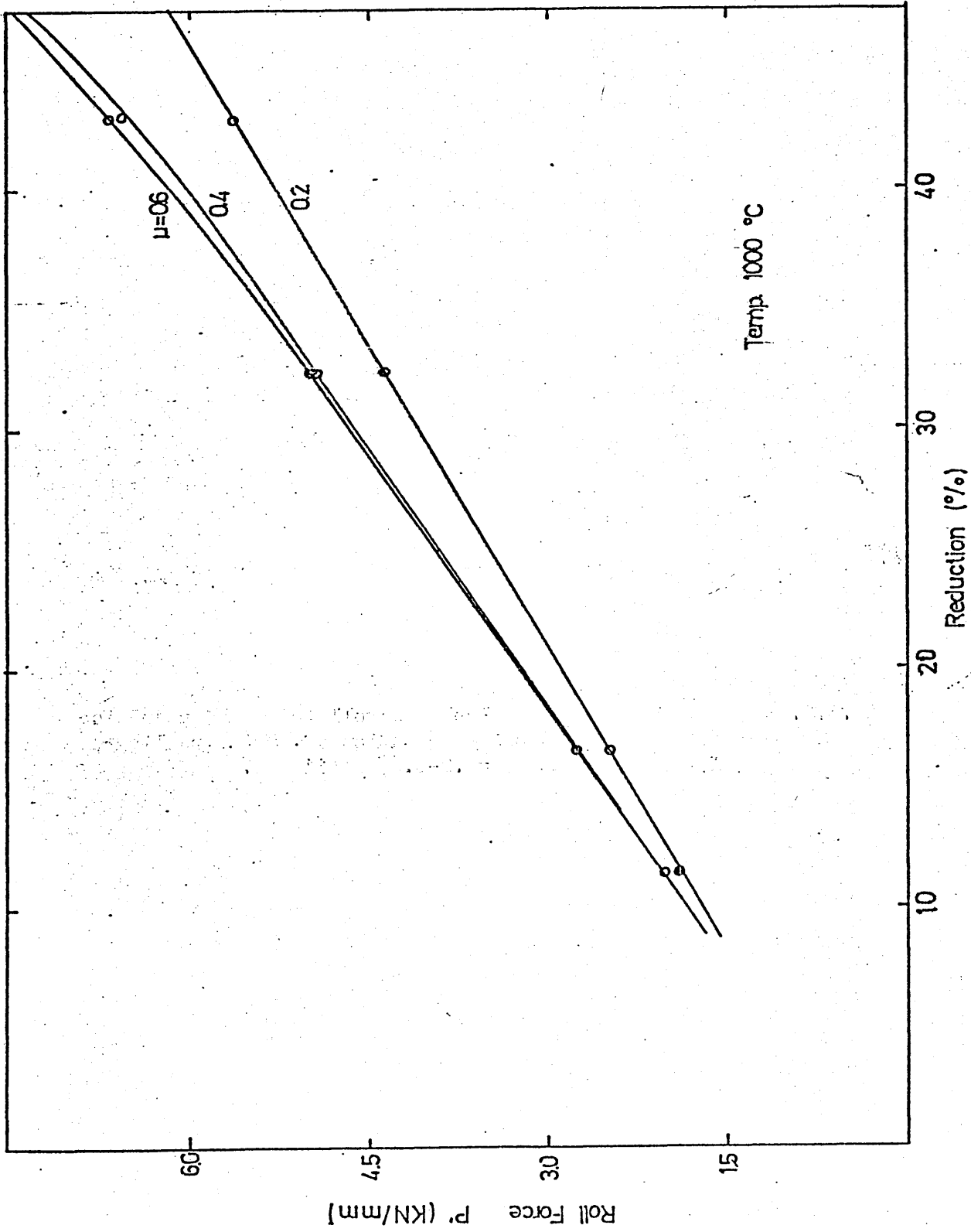


Fig.6.2.8

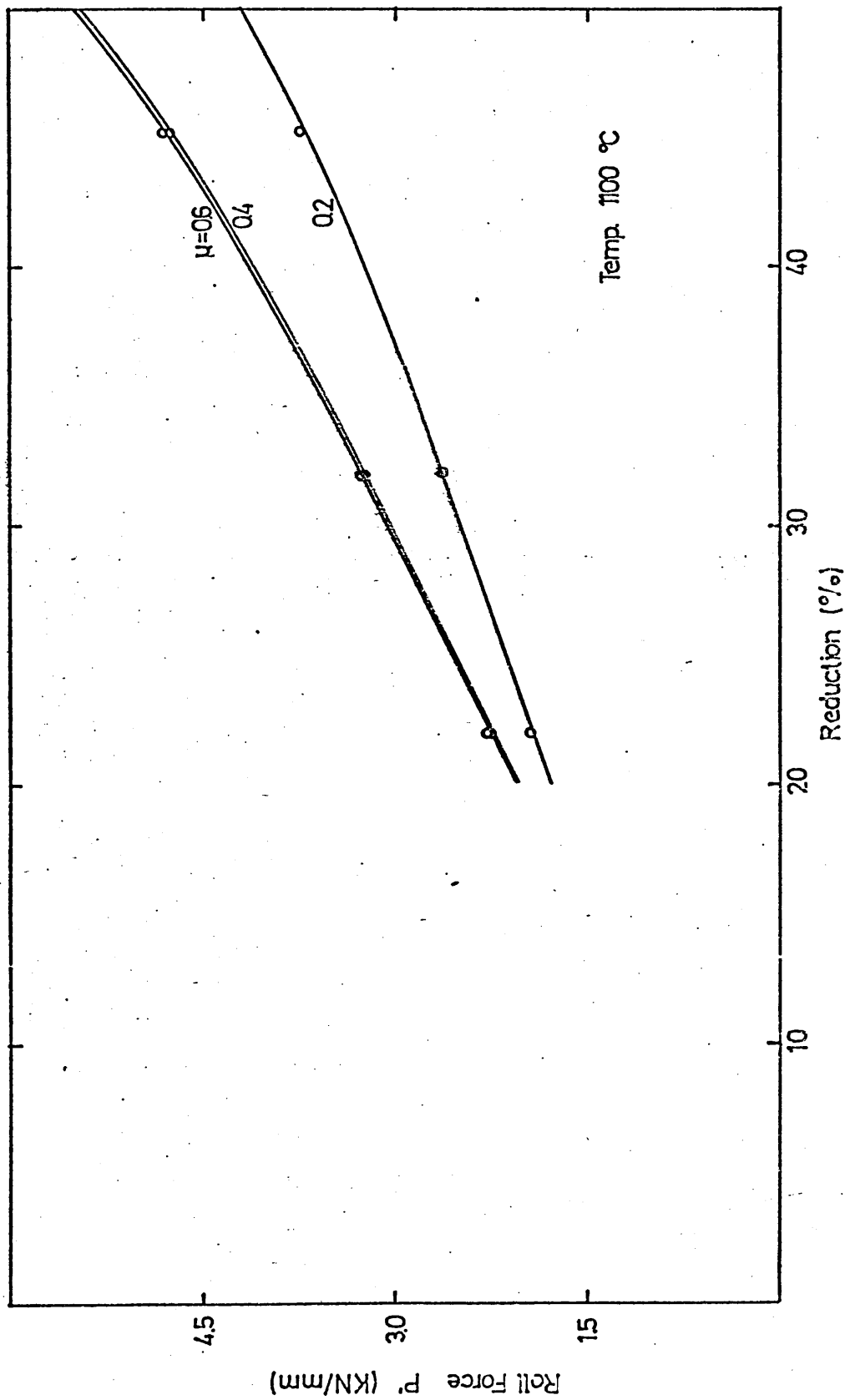


Fig.6.2.9 Relation between calculated roll force and reduction under inhomogeneous deformation and using published flow stress data ($\mu=0.2-0.6$) at 1100°C.

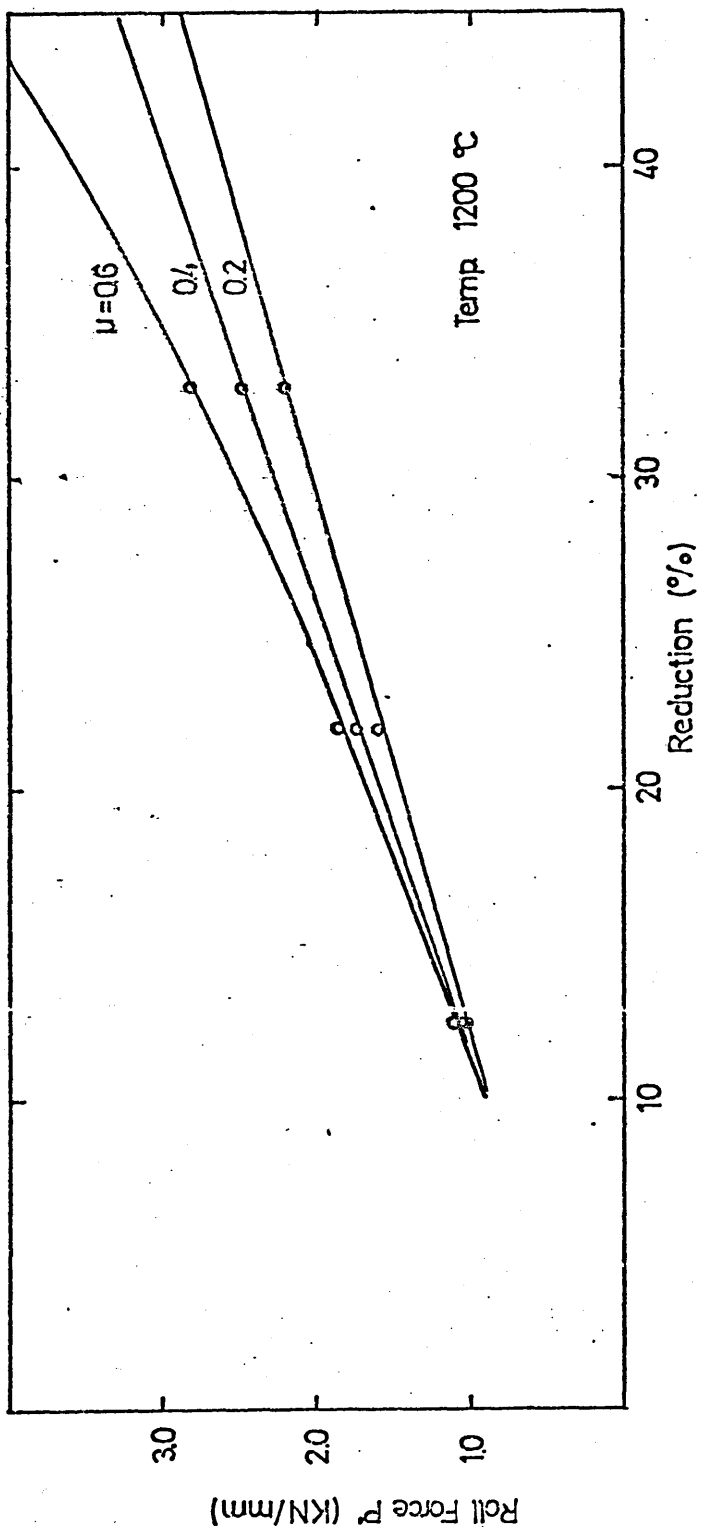


Fig.6.2.10 Relation between calculated roll force and reduction under inhomogeneous deformation and using published flow stress data ($\mu=0.2-0.6$) at 1200 °C.

Fig.6.2.11 Relation between calculated roll force and reduction
under inhomogeneous deformation and using flow stress
data determined in the present work ($\mu=0.2-0.6$) at 900°C .

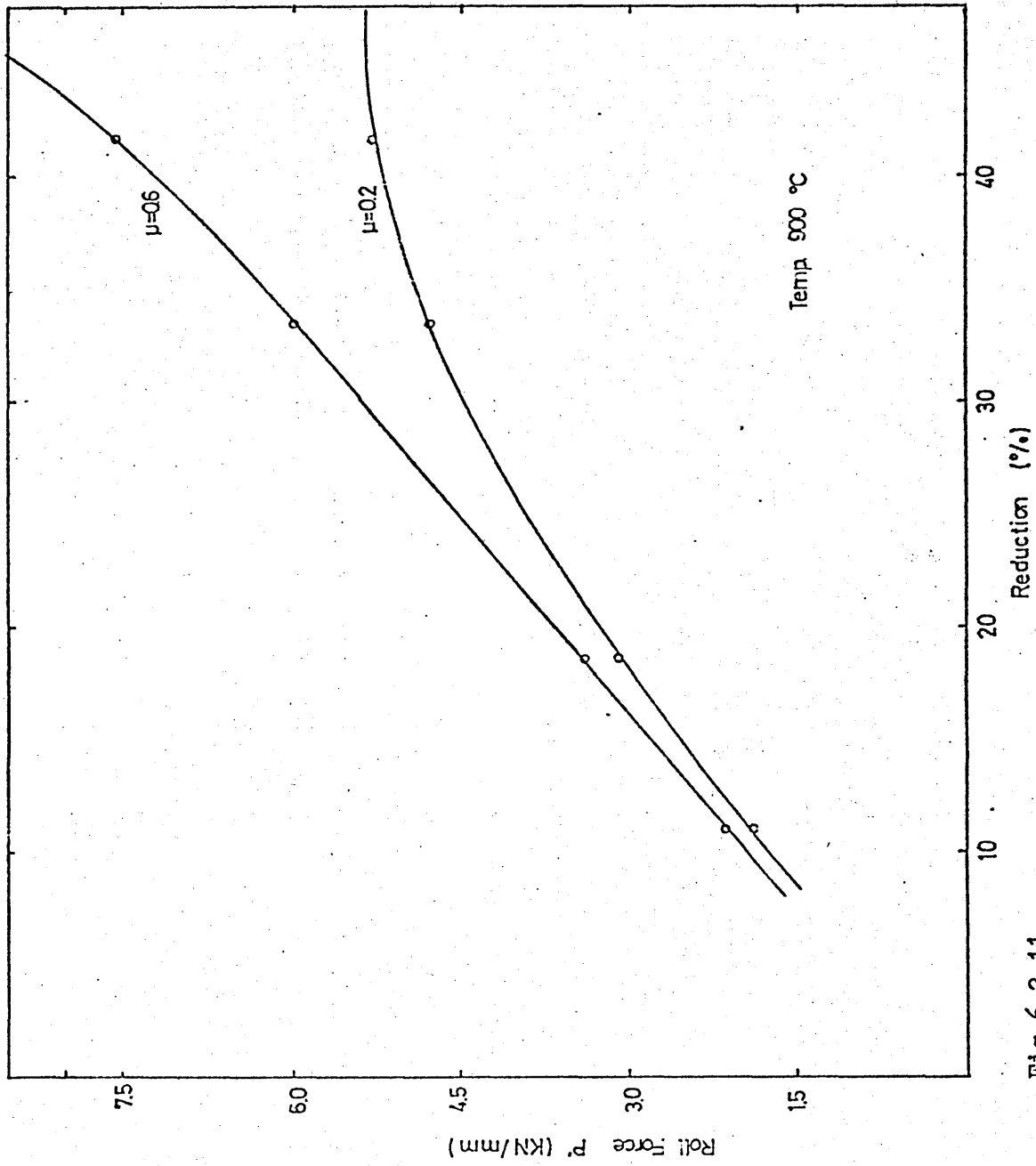


Fig.6.2.11

Fig.6.2.2.12 Relation between calculated roll force and reduction
under inhomogeneous deformation and using flow stress
data determined in the present work ($\mu=0.2-0.6$) at 1000°C.

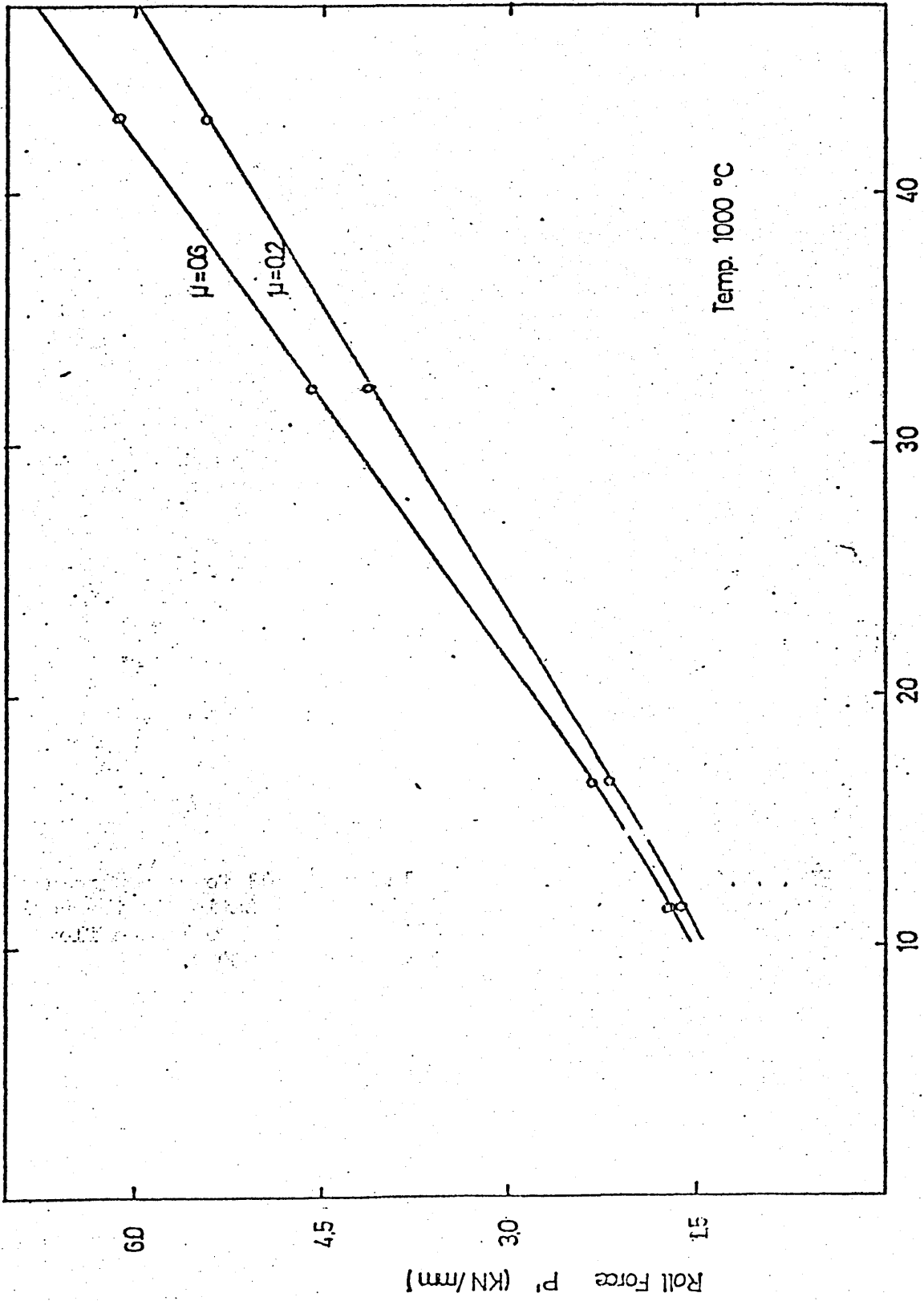


Fig.6.2.12

Fig.6.3.1 Relation between calculated roll force and reduction showing the effect of a $\pm 5\%$ variation in the nominal temperature of rolling and using published flow stress data ($\mu=0.4$) - nominal temperature 900 °C.

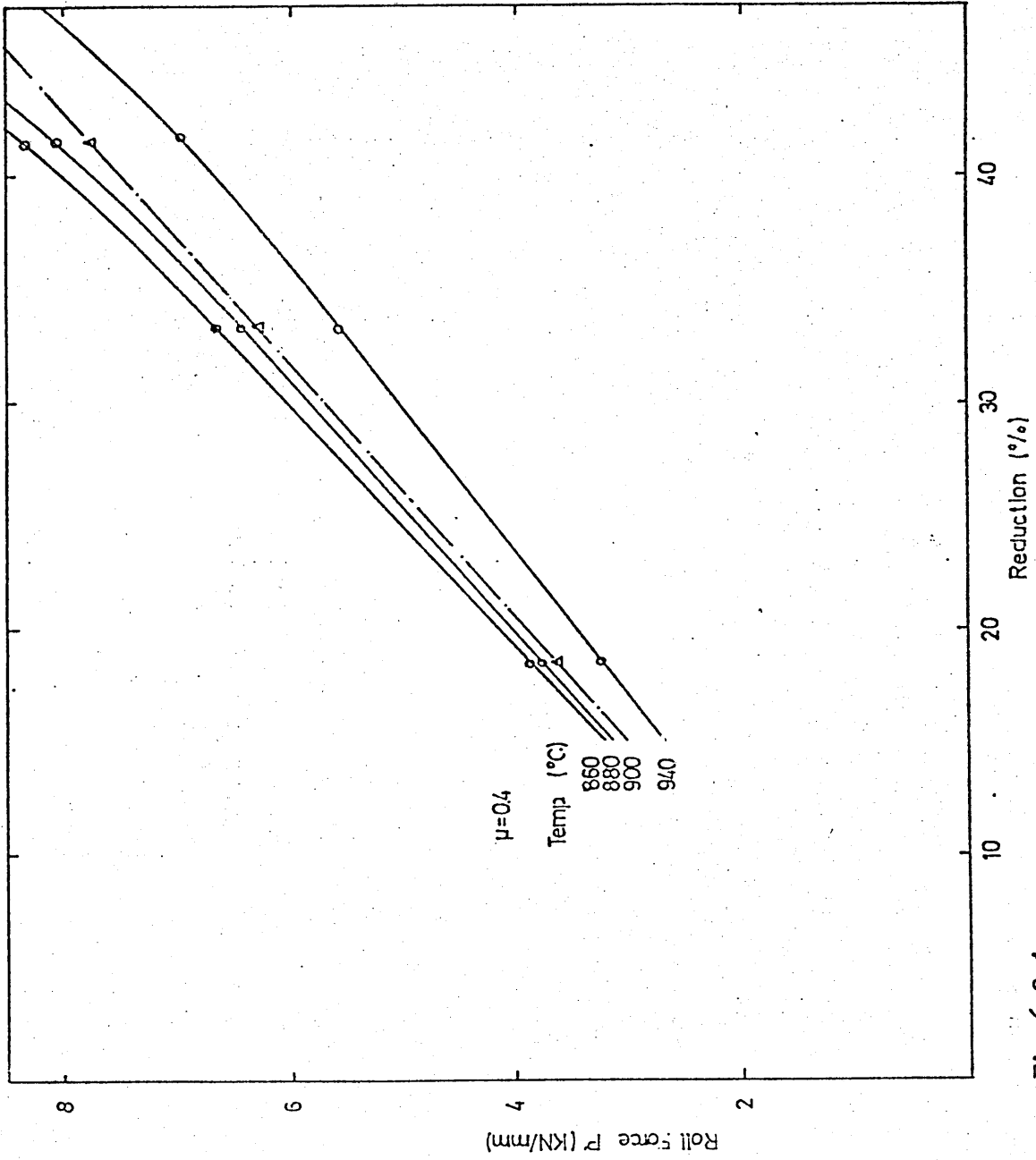


Fig.6.3.1

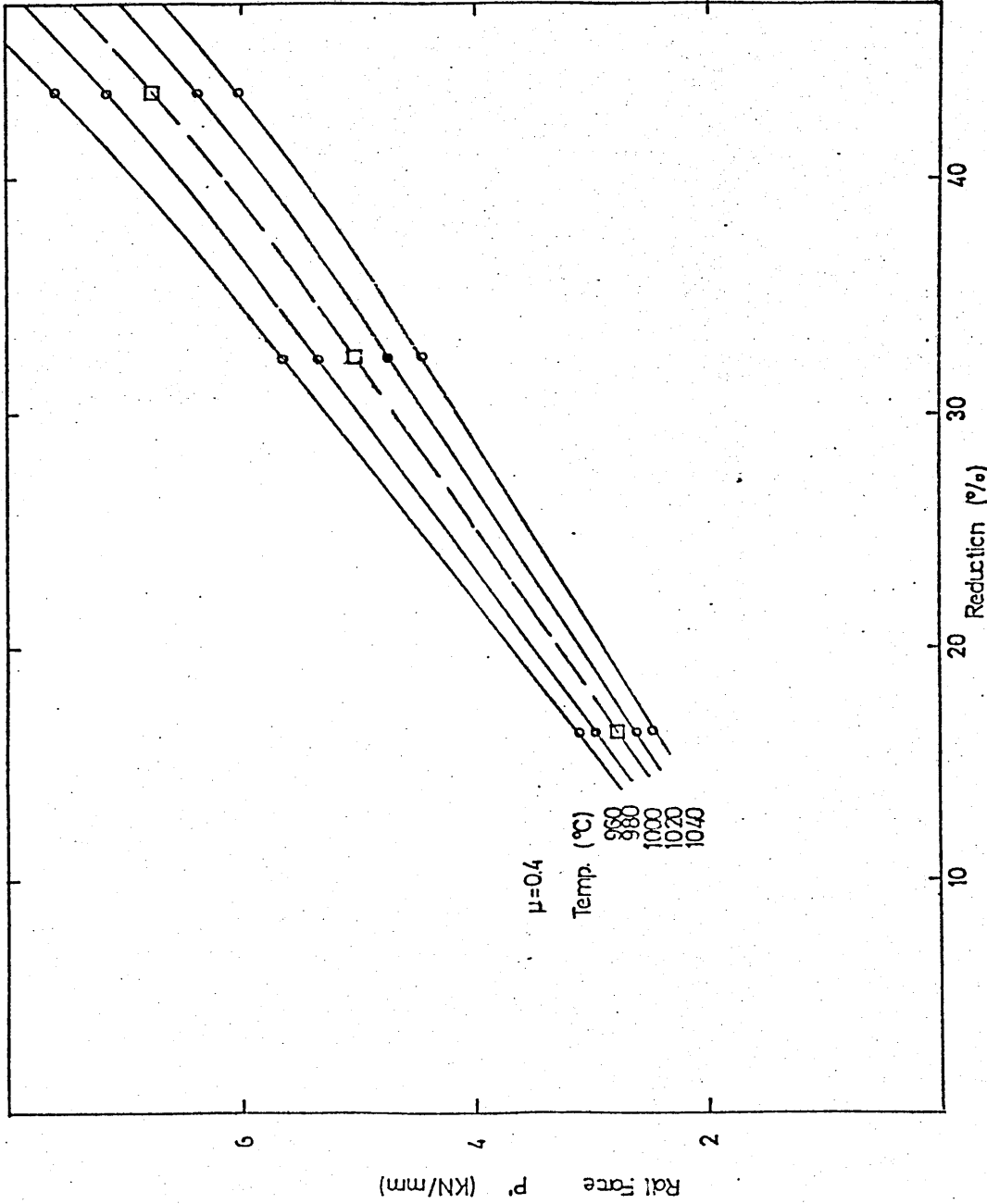


Fig.6.3.2 Relation between calculated roll force and reduction showing the effect of a $\pm 5\%$ variation in the nominal temperature of rolling and using published flow stress data ($\mu=0.4$) - nominal temperature 1000°C.

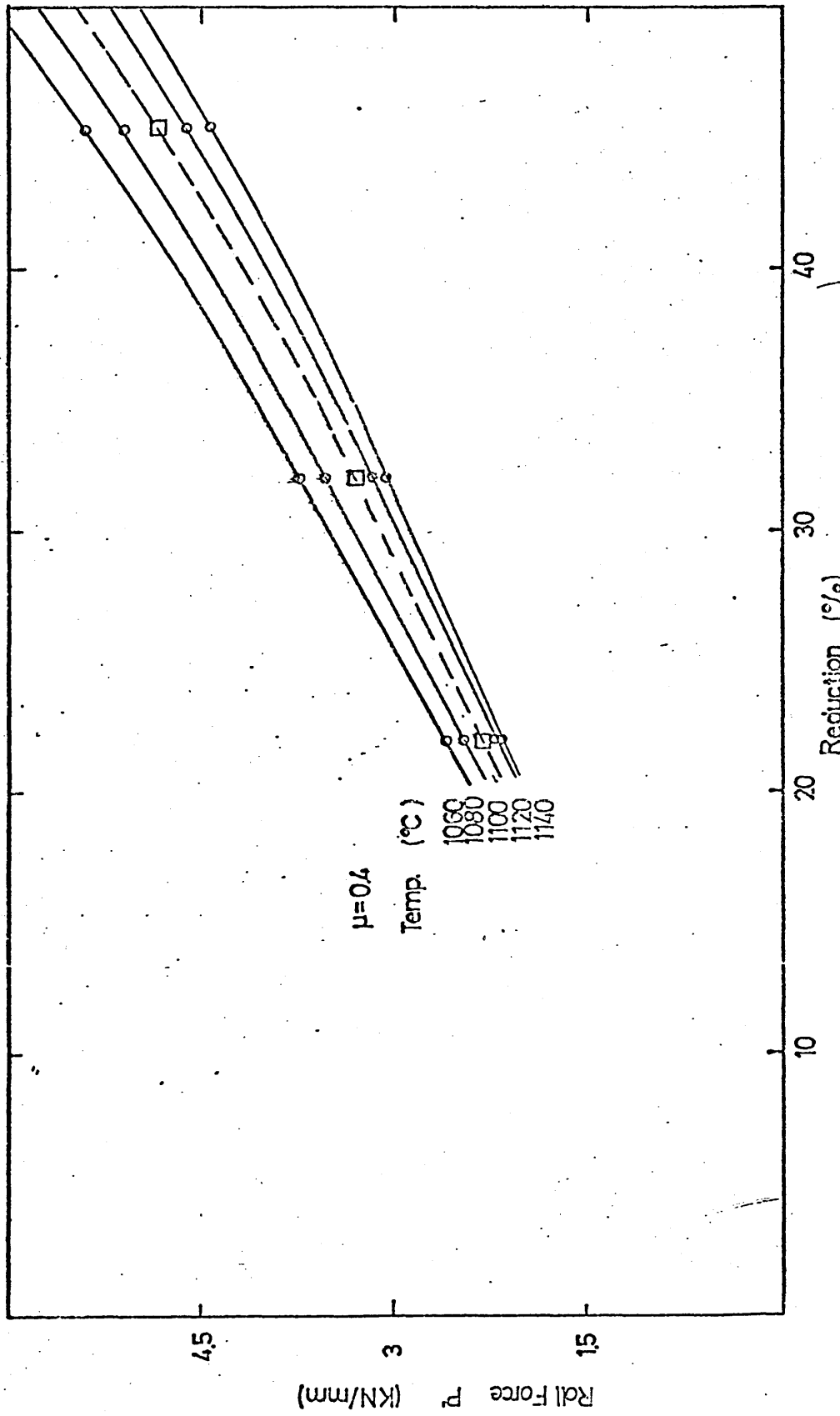


Fig.6.3.3 Relation between calculated roll force and reduction showing the effect of a $\pm 5\%$ variation in the nominal temperature of rolling using published flow stress data ($\mu=0.4$) - nominal temperature 1100 $^{\circ}\text{C}$.

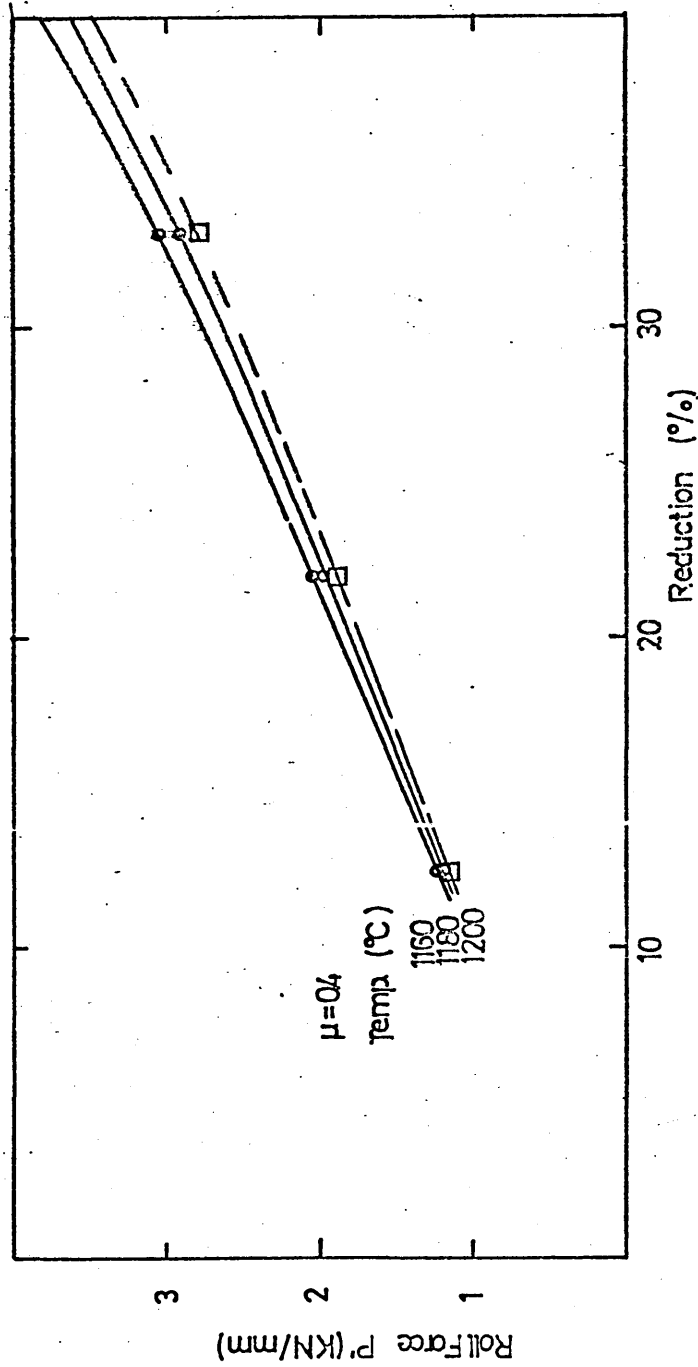


Fig.6.3.4 Relation between calculated roll force and reduction showing the effect of a $\pm 5\%$ variation in the nominal temperature of rolling and using published flow stress data ($\mu=0.4$) - nominal temperature 1200 °C.

Fig.6.4.1 Relation between calculated roll torque and reduction
under homogeneous deformation using published flow
stress data ($\mu=0.2-0.6$) at 900 °C.

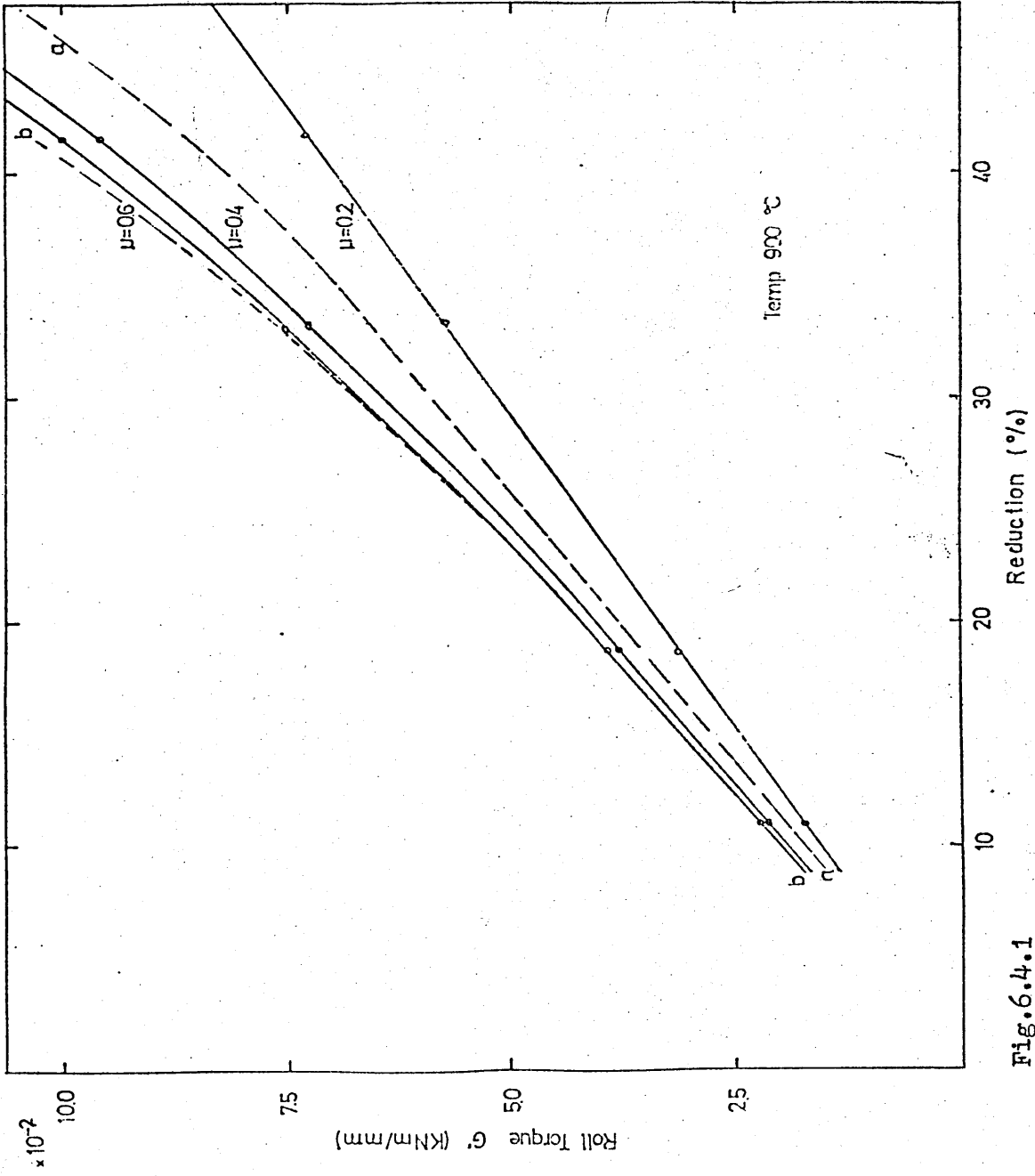


Fig.6.4.1

Fig.6.4.2 Relation between calculated roll torque and reduction
under homogeneous deformation using published flow
stress data ($\mu=0.2-0.6$) at 1000 °C.

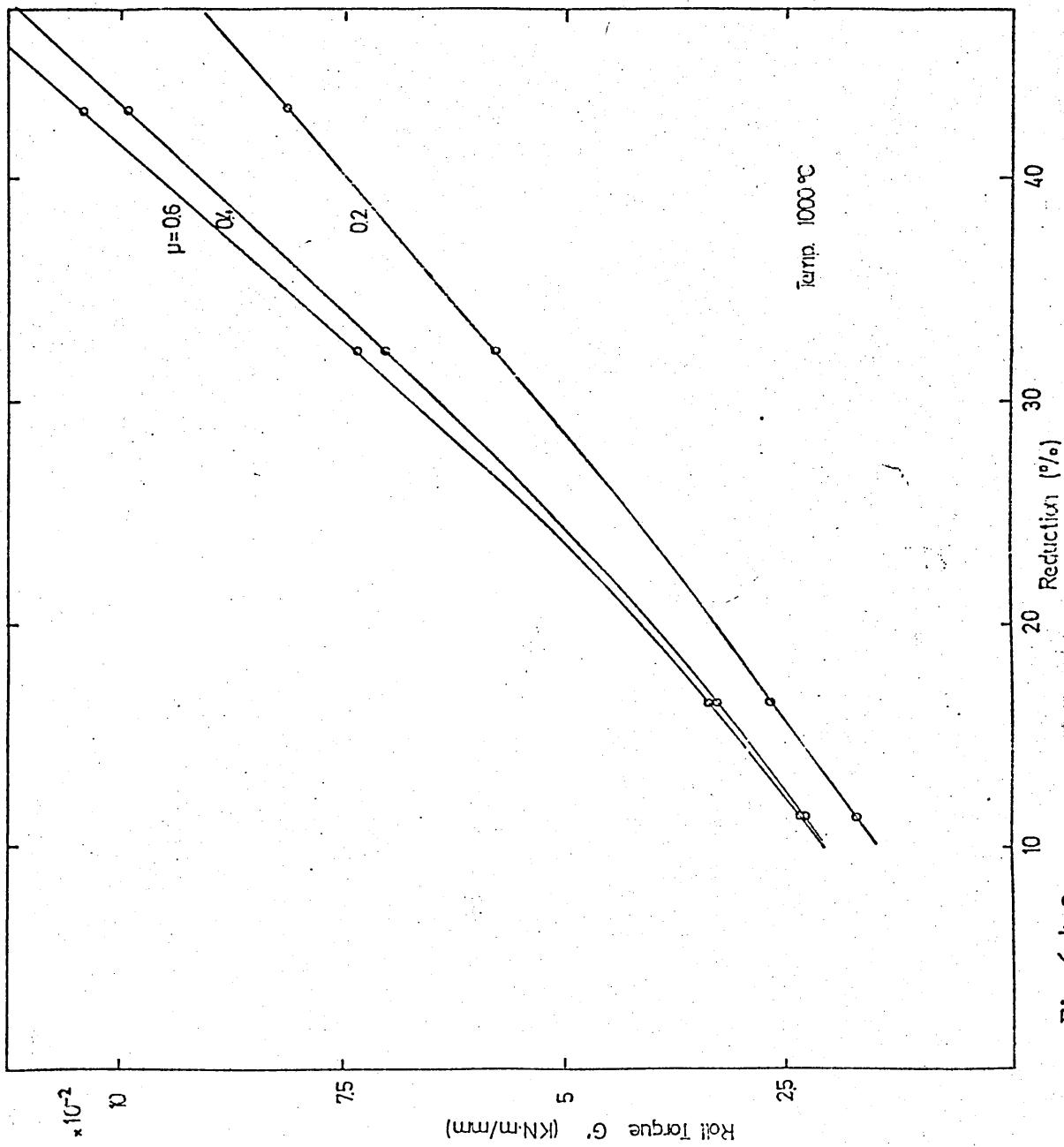


Fig.6.4.2.

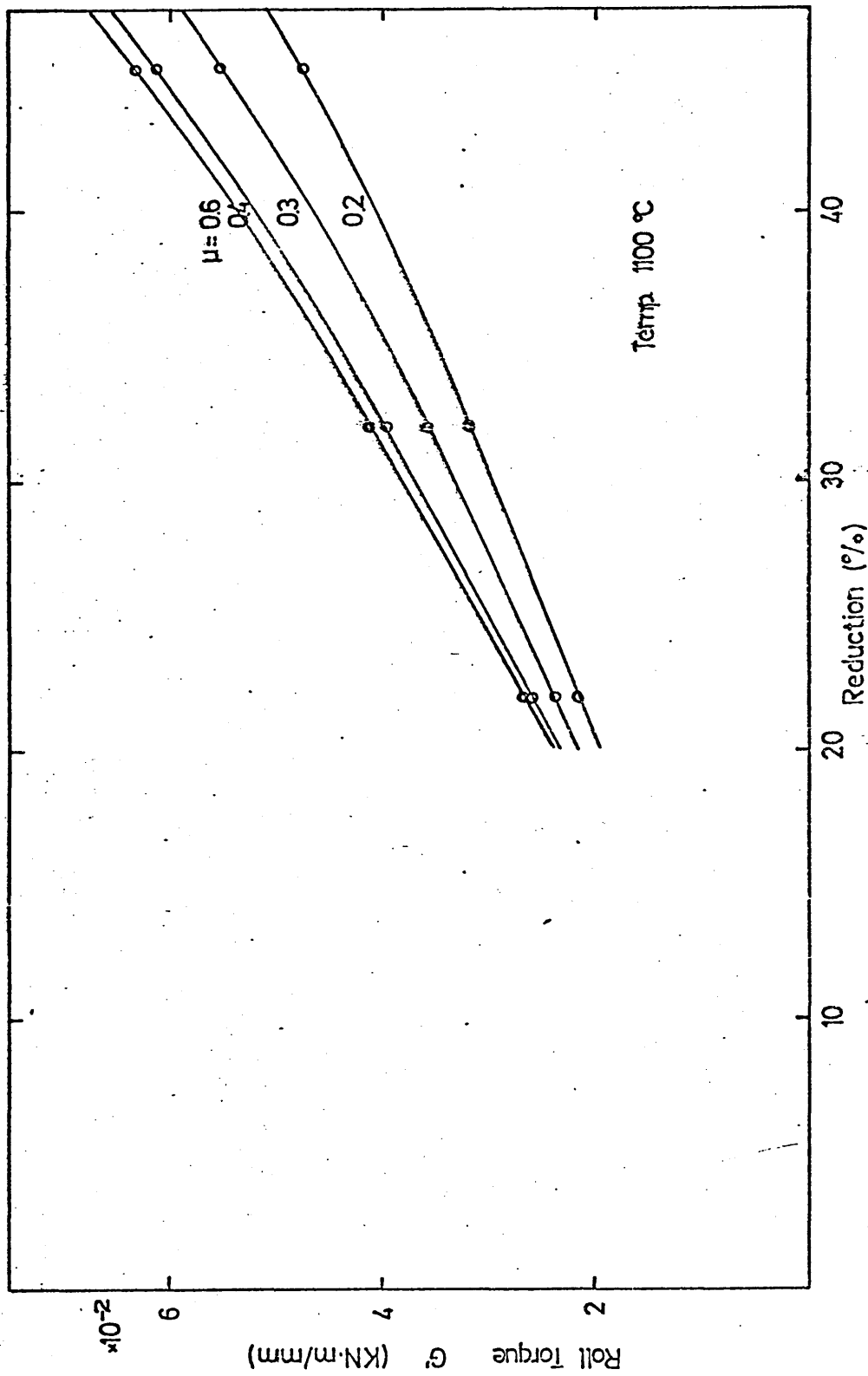
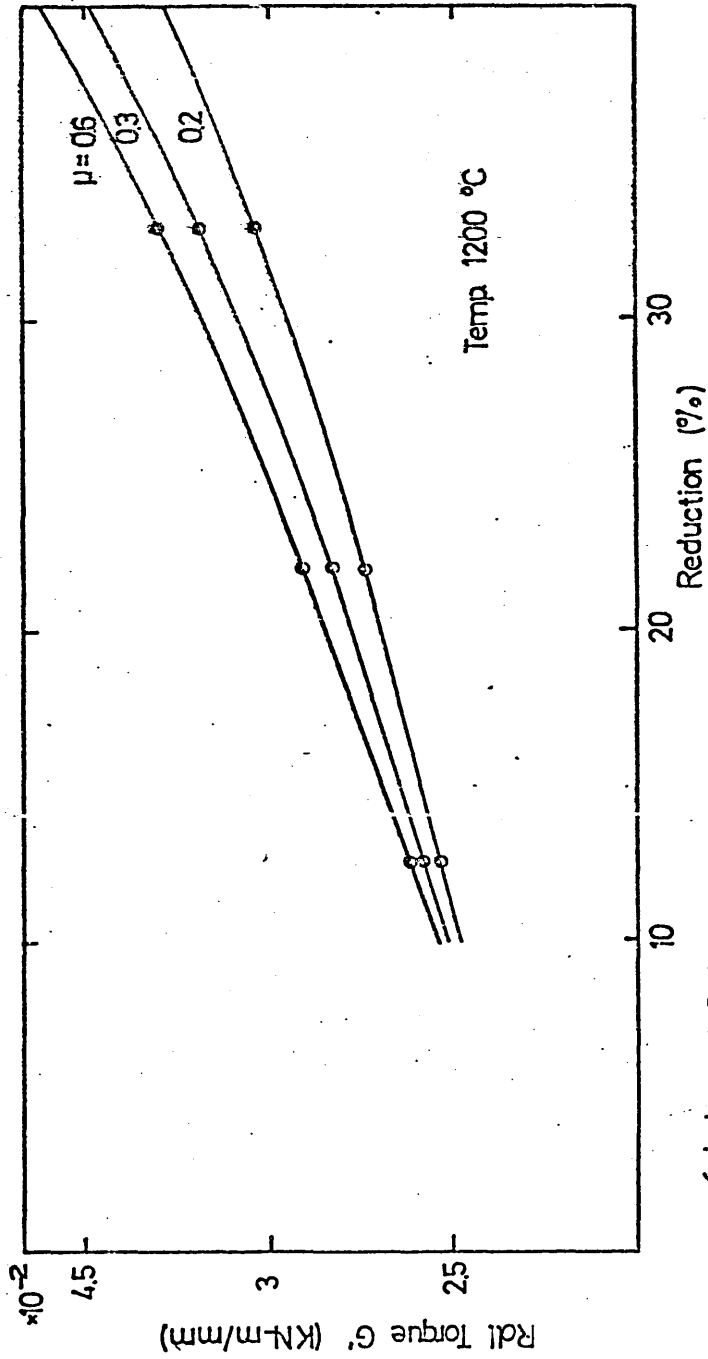


Fig.6.4.3 Relation between calculated roll torque and reduction under homogeneous deformation using published flow stress data ($\mu=0.2-0.6$) at 1100 °C.



6.4.4 Relation between calculated roll torque and reduction under homogeneous deformation using published flow stress data ($\mu=0.2-0.6$) at 1200 °C.

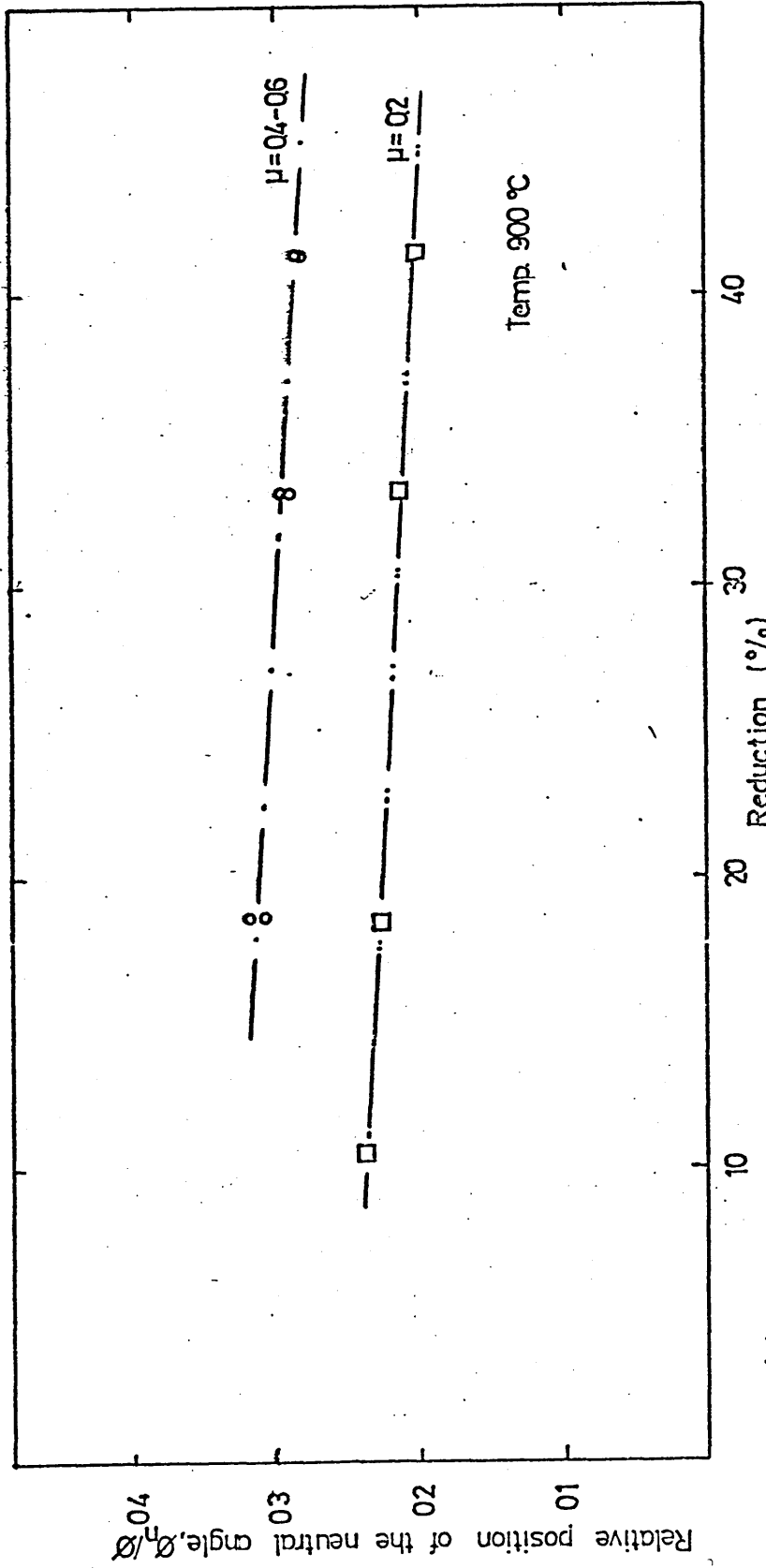


Fig.6.4.5 Variation of the relative position of the neutral angle with the percentage reduction ($\mu=0.2-0.6$) at 900 °C.

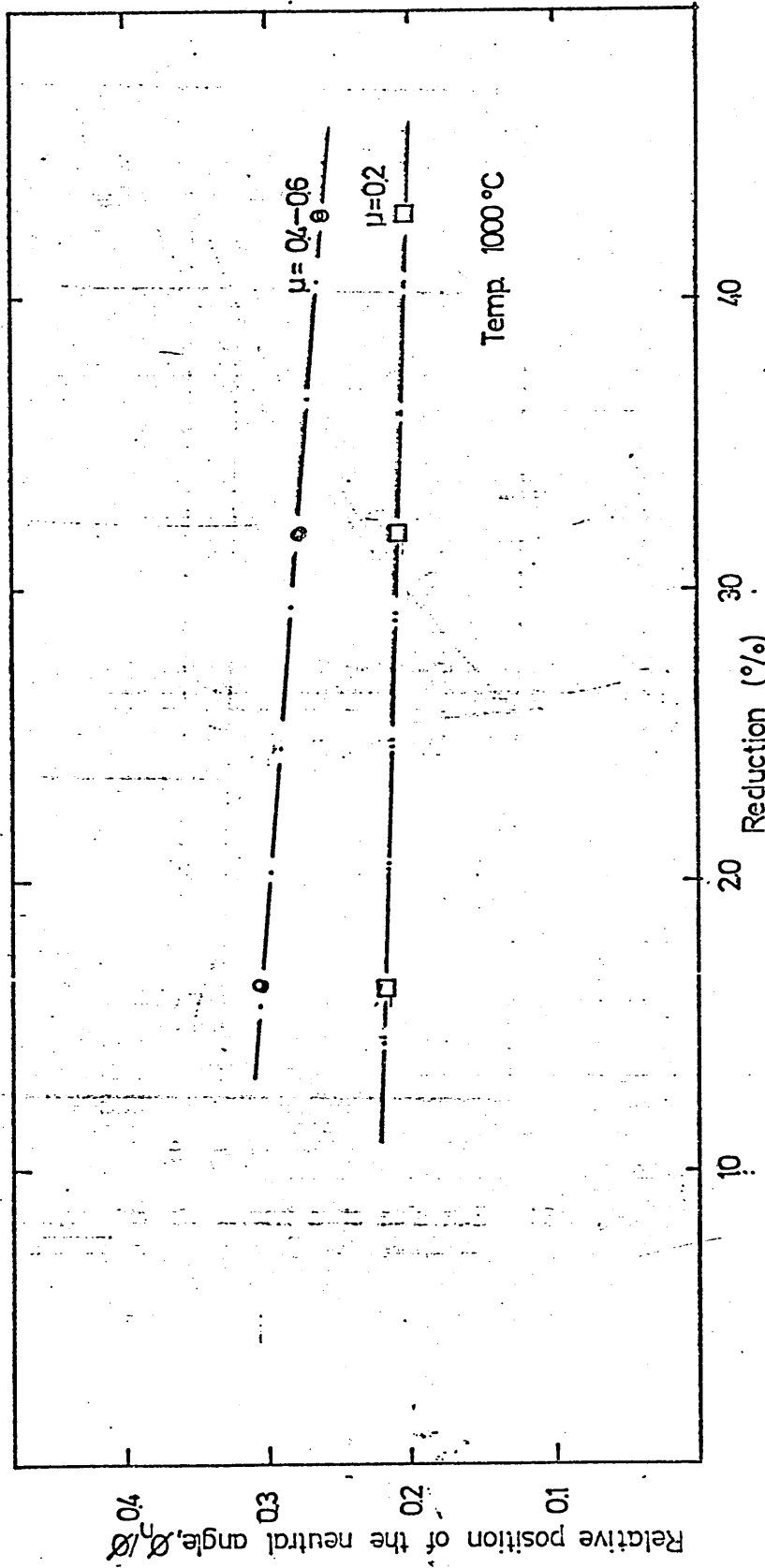


Fig.6.4.6 Variation of the relative position of the neutral angle with the percentage reduction ($\mu=0.2-0.6$) at 1000°C.

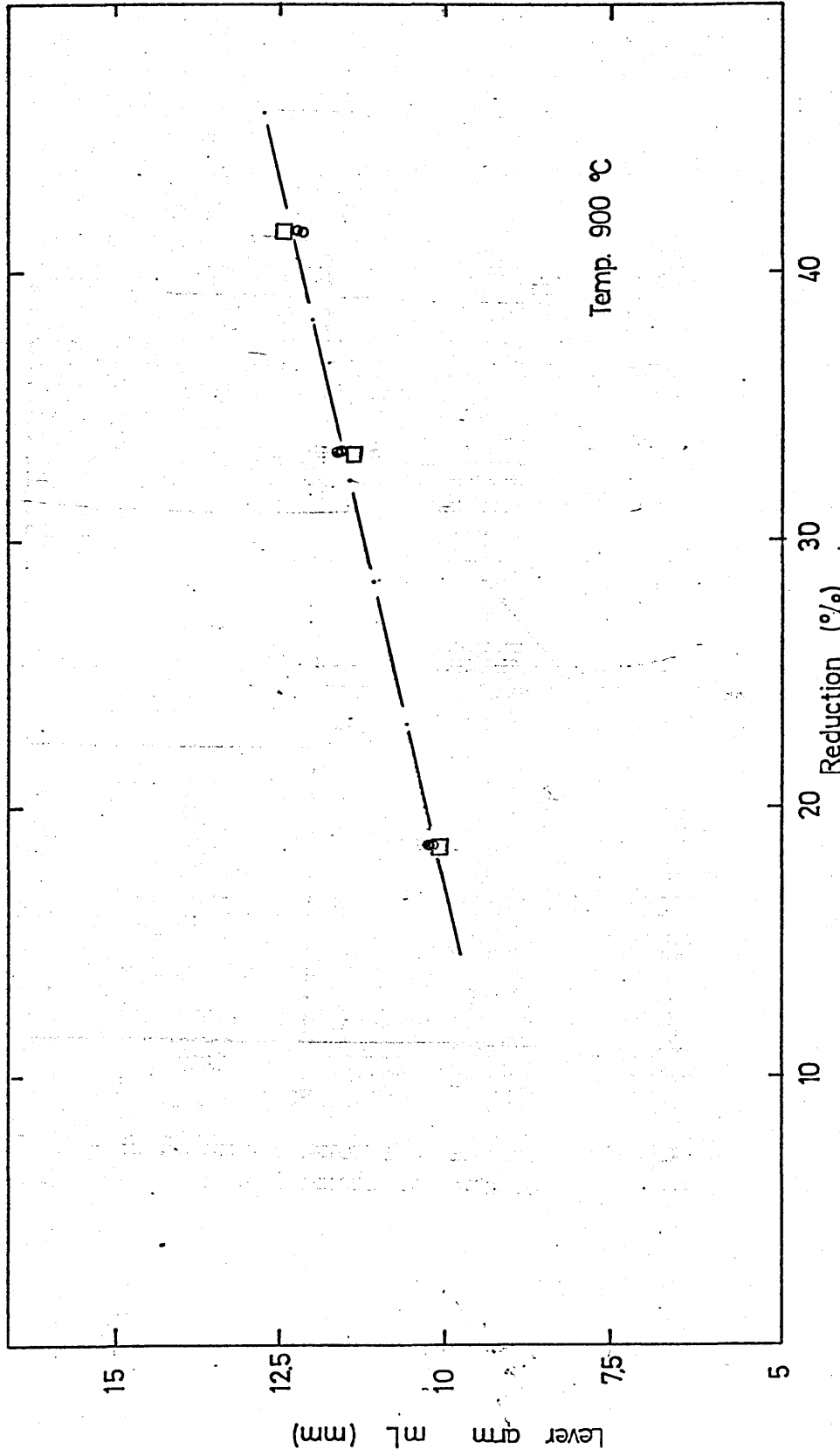


Fig.6.4.7 Variation of the lever arm with percentage reduction at 1000 °C.

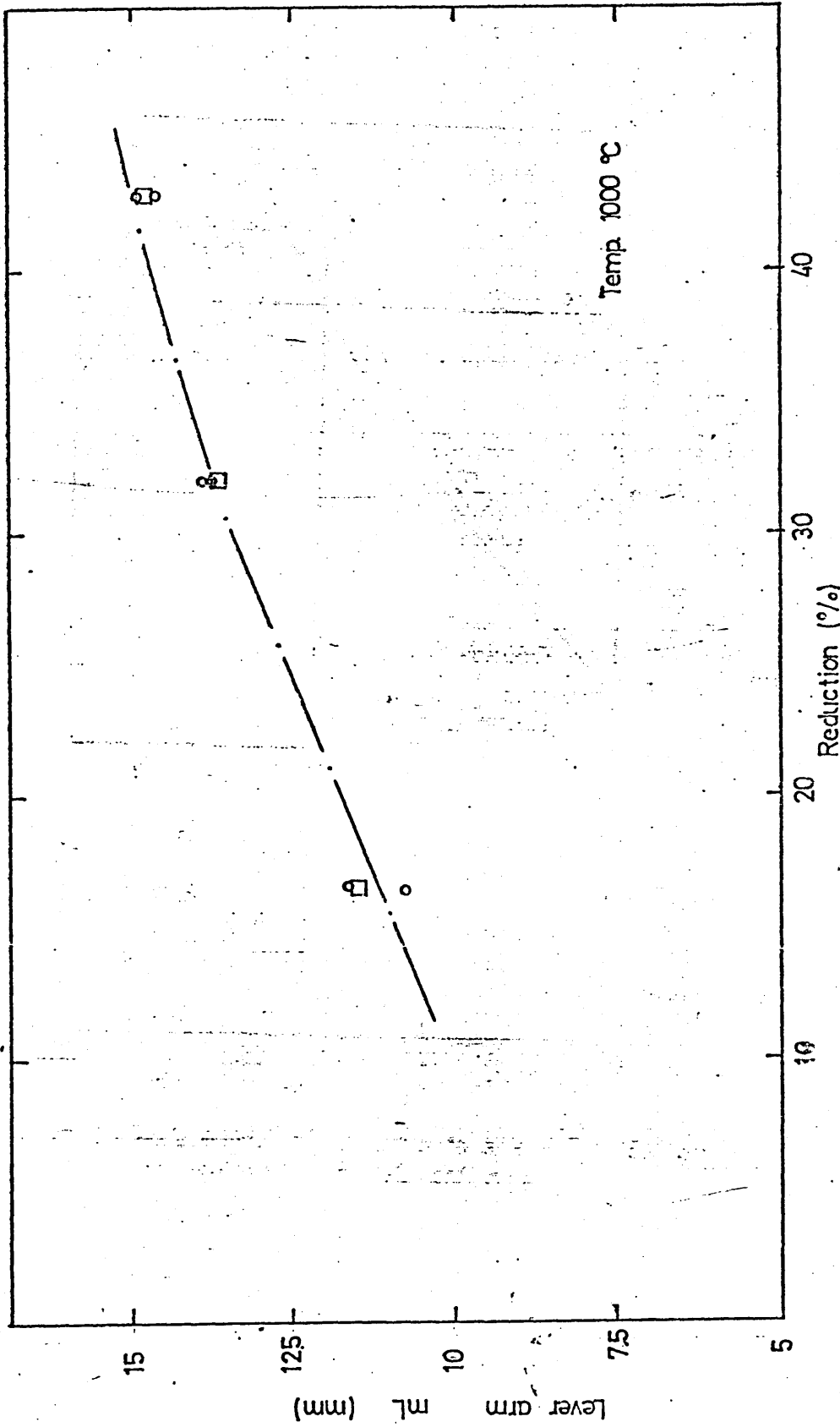


Fig.6.4.8 Variation of the lever arm with percentage reduction at 1000 °C.

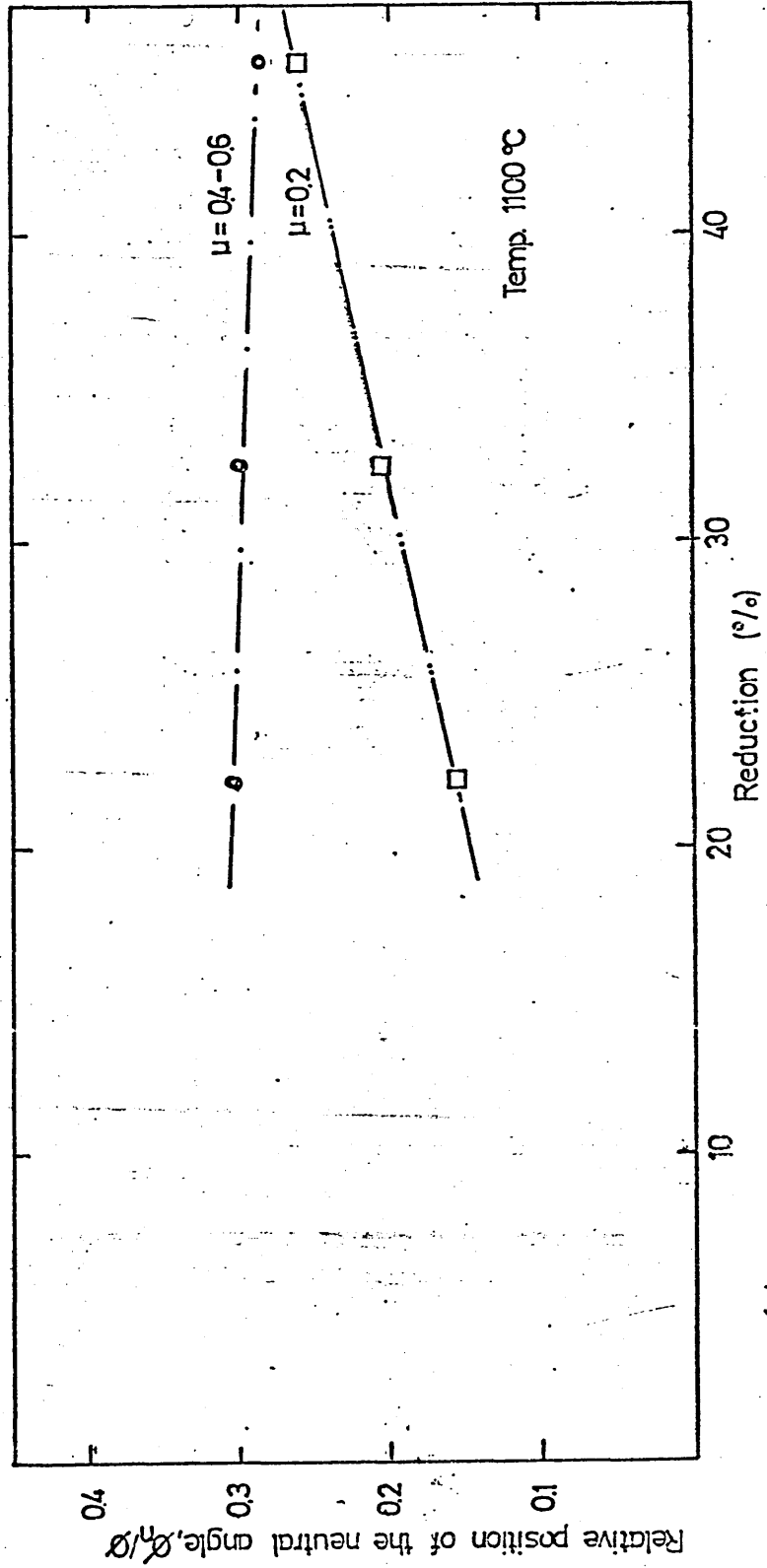


Fig.6.4.9 Variation of the relative position of the neutral angle with the percentage reduction ($\mu=0.2-0.6$) at 1100 °C.

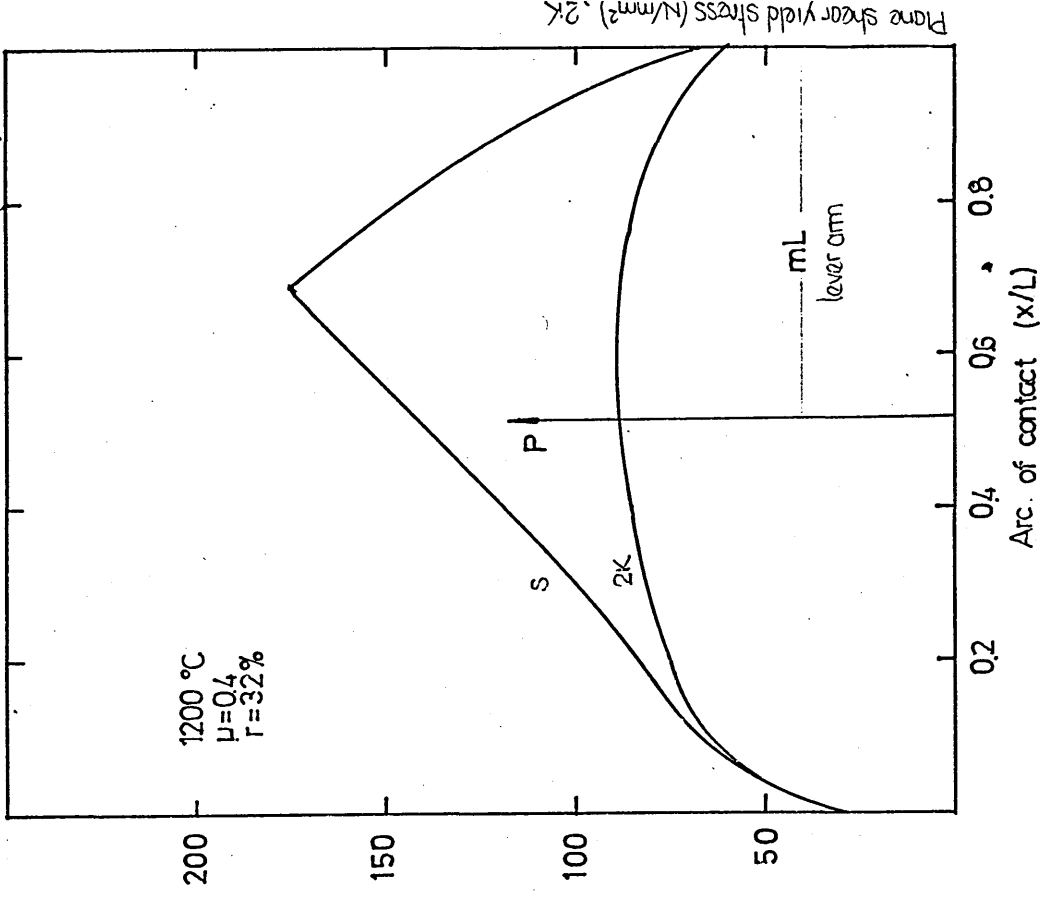
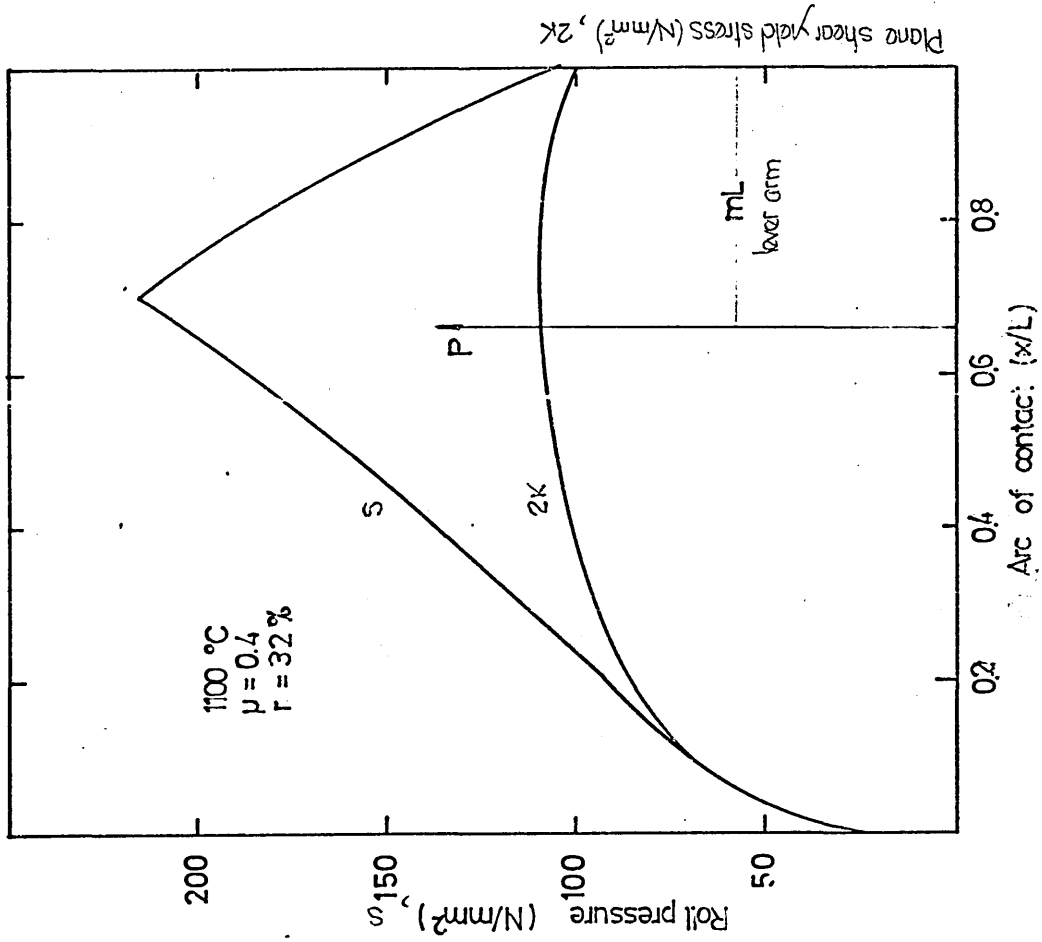


Fig.6.4.10 Roll pressure and yield stress distribution along the arc of contact under homogeneous deformation and using published yield stress data at 1100°C and 1200°C ($\mu=0.4$, reduction 30%).

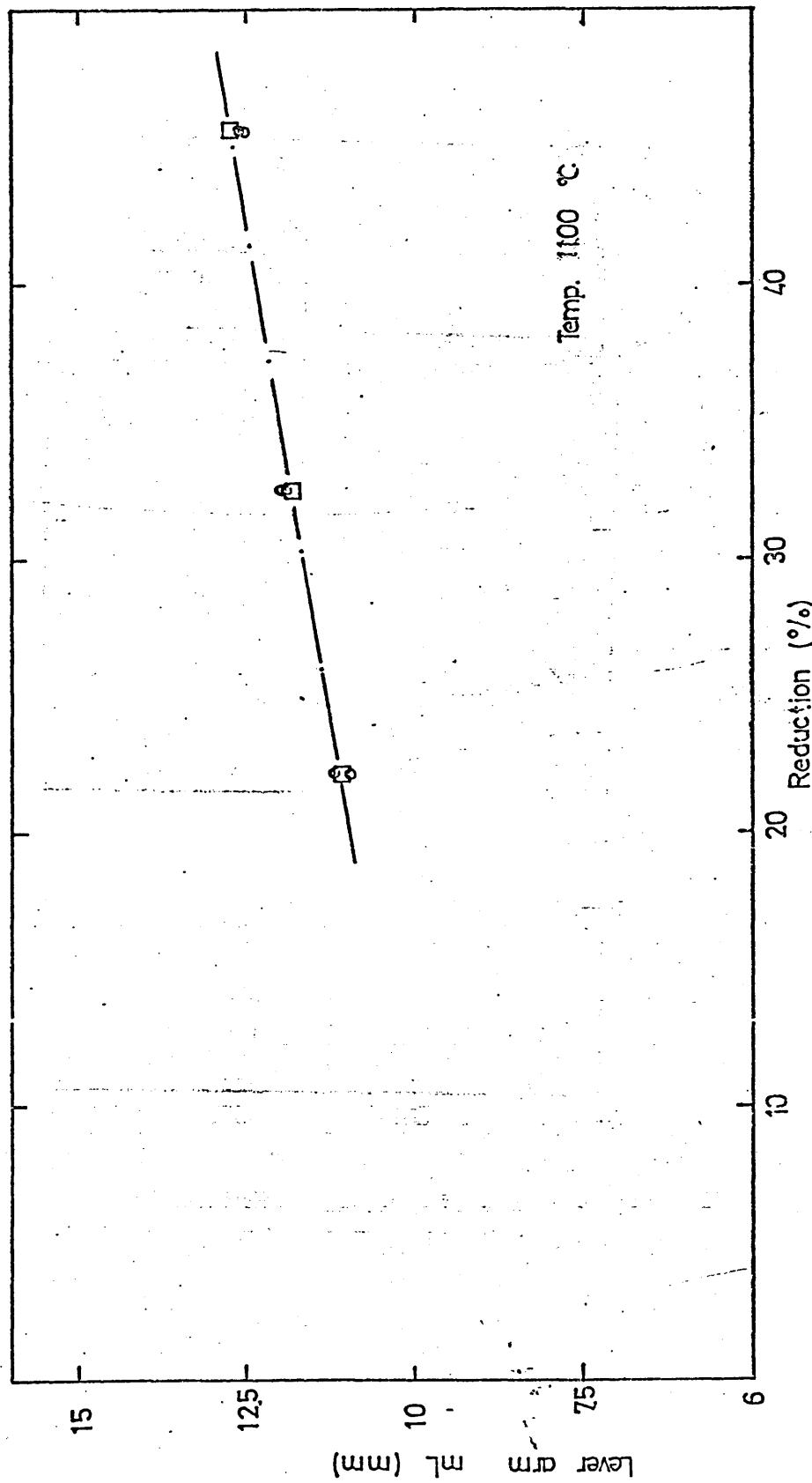


Fig.6.4.11 Variation of the lever arm with percentage reduction at 1100 °C.

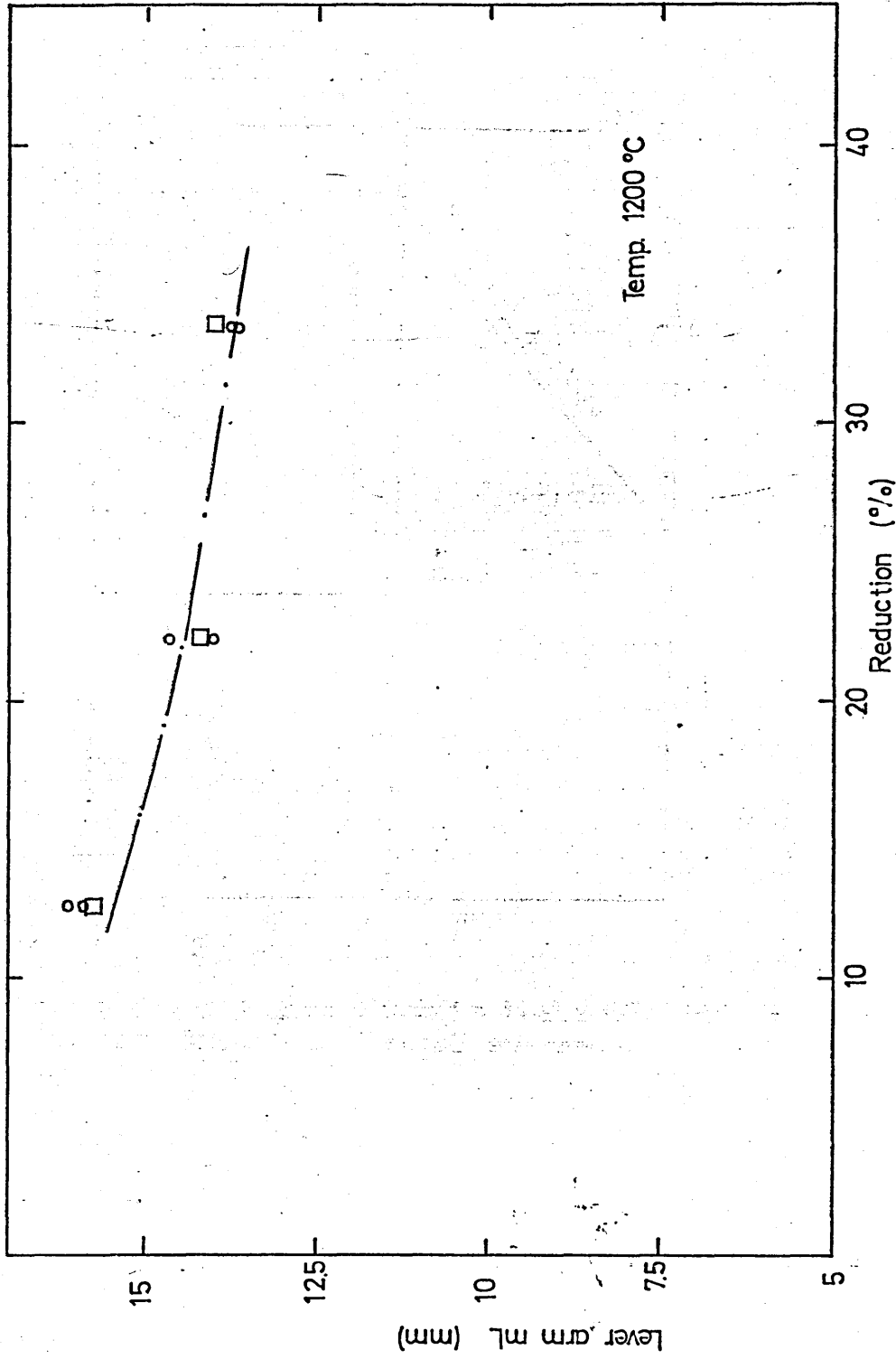


Fig.6.4.12 Variation of the lever arm with percentage reduction at 1200 °C.

Fig.6.4.1) Relation between calculated roll torque and reduction under homogeneous deformation using flow stress data determined in the present work ($\mu=0.2-0.6$) at 900 °C.

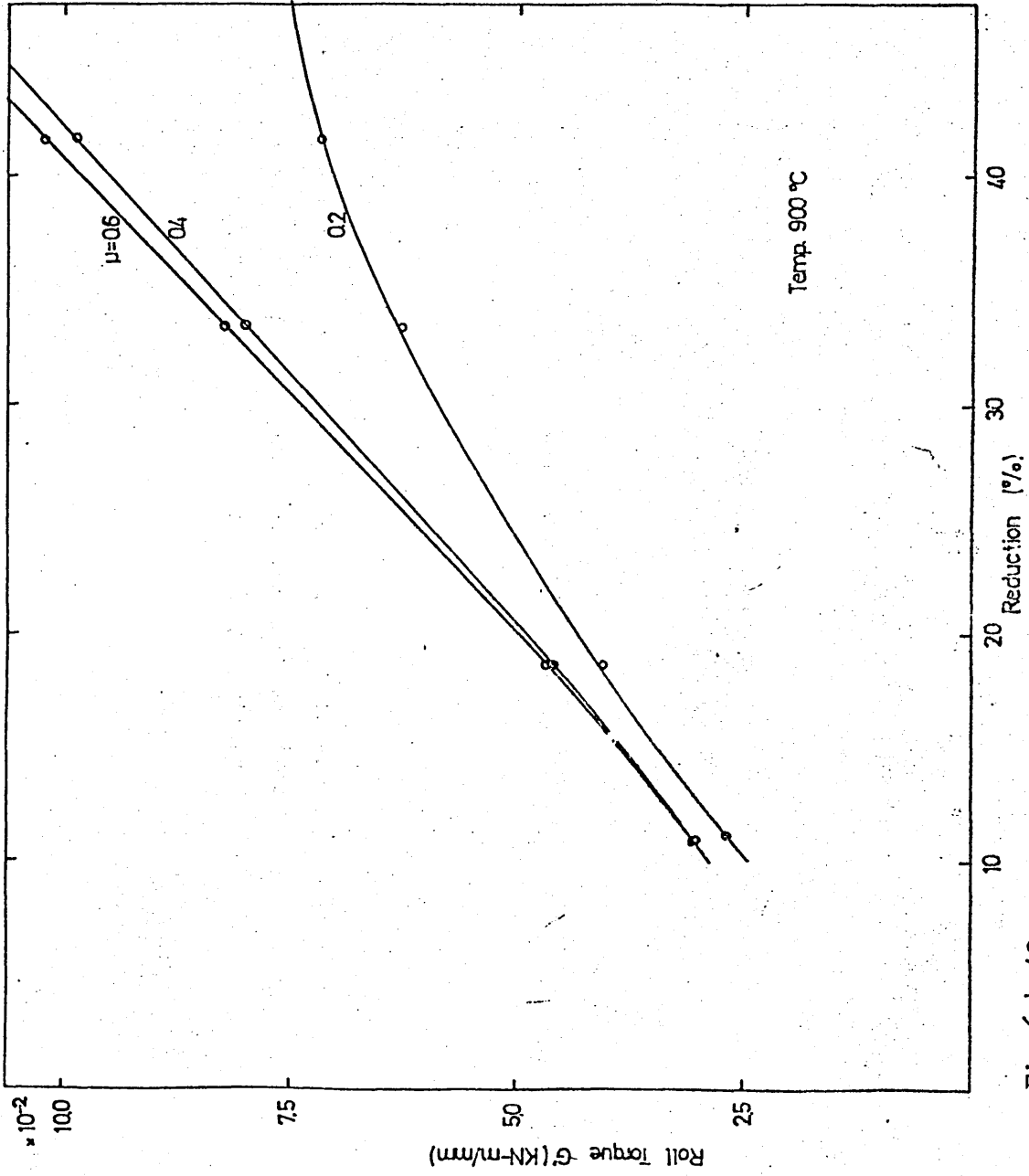


Fig.6.4.13

Fig. 6.4.14 Relation between calculated roll torque and reduction under homogeneous deformation using flow stress data determined in the present work ($\mu=0.2-0.6$) at 1000 °C.

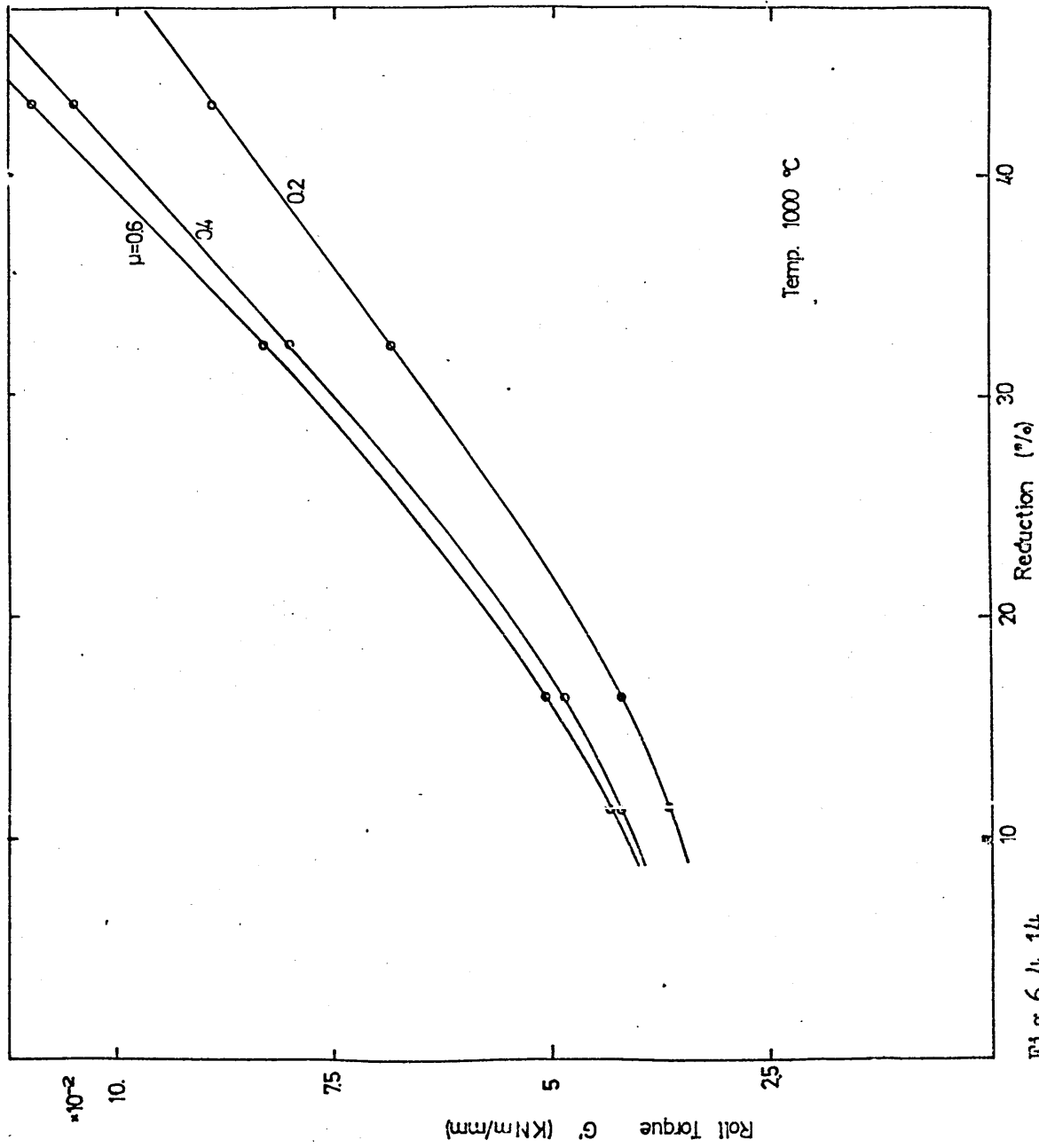


Fig.6.4.14

Fig.6.4.15 Calculated roll pressure distributions under homogeneous deformation using both published flow stress data and that determined in the present work, (900 °C, $\mu=0.2$, $r=33\%$).

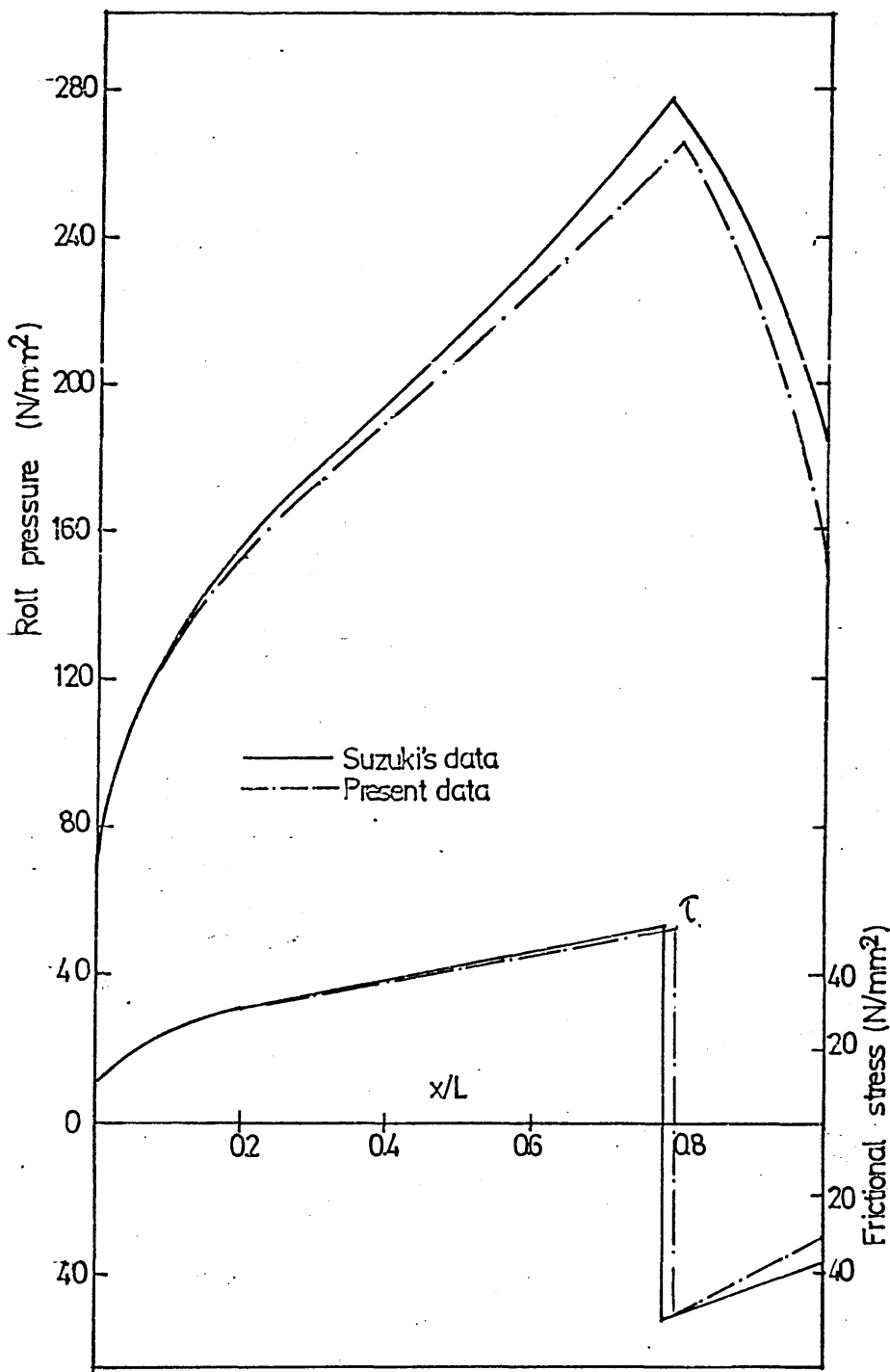


Fig.6.4.15 Calculated roll pressure distributions under homogeneous deformation using both published flow stress data and that determined in the present work (900°C , $\mu=0.2$, $r=33\%$).

Fig.6.4.16 Relation between roll torque and reduction under in-homogeneous deformation using published flow stress data ($\mu=0.2-0.6$) at 900 °C.

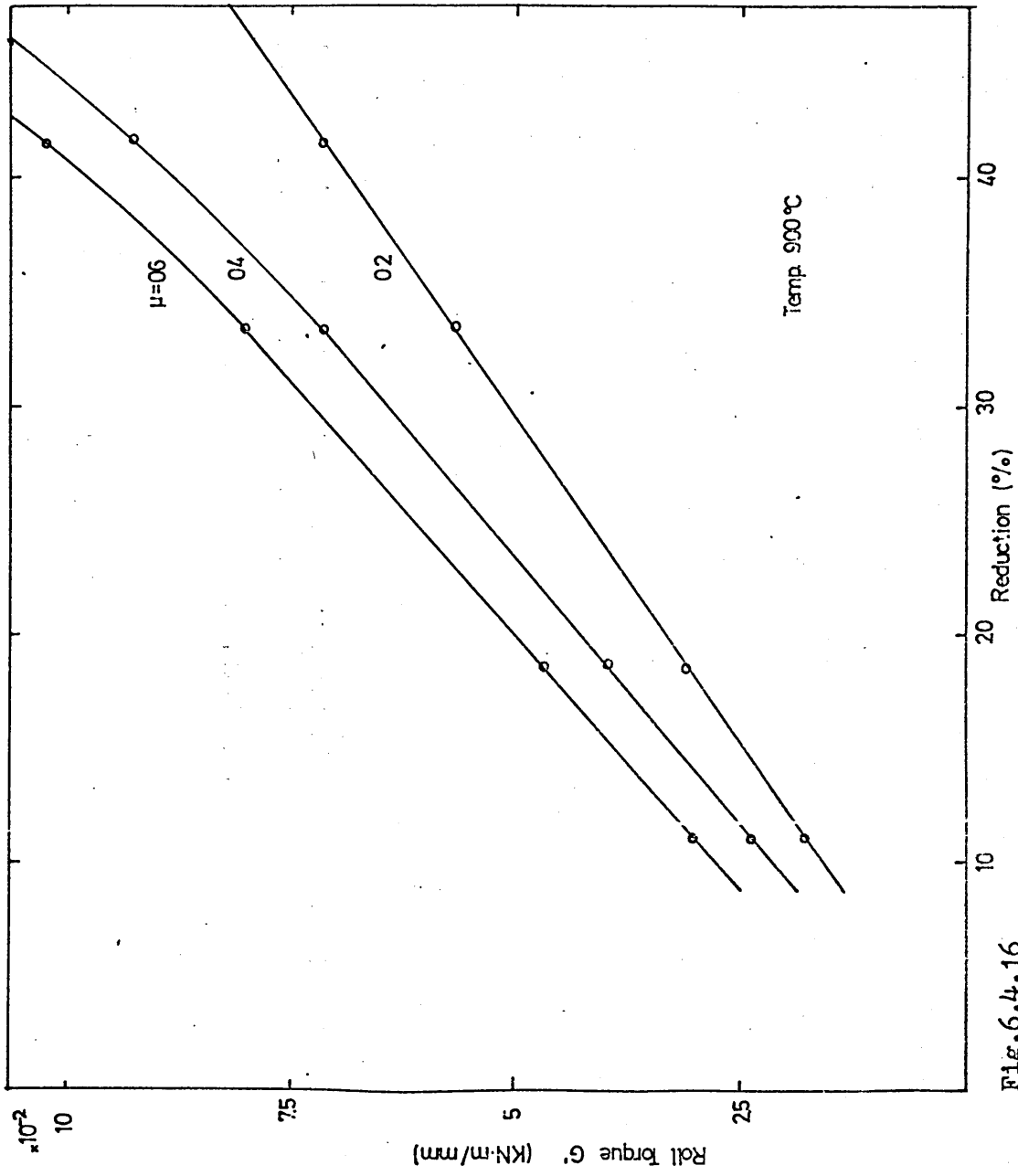


Fig. 6.4.16

Fig.6.4.4.17 Relation between roll torque and reduction under in-homogeneous deformation using published flow stress data ($\mu=0.2-0.6$) at 1000 °C.

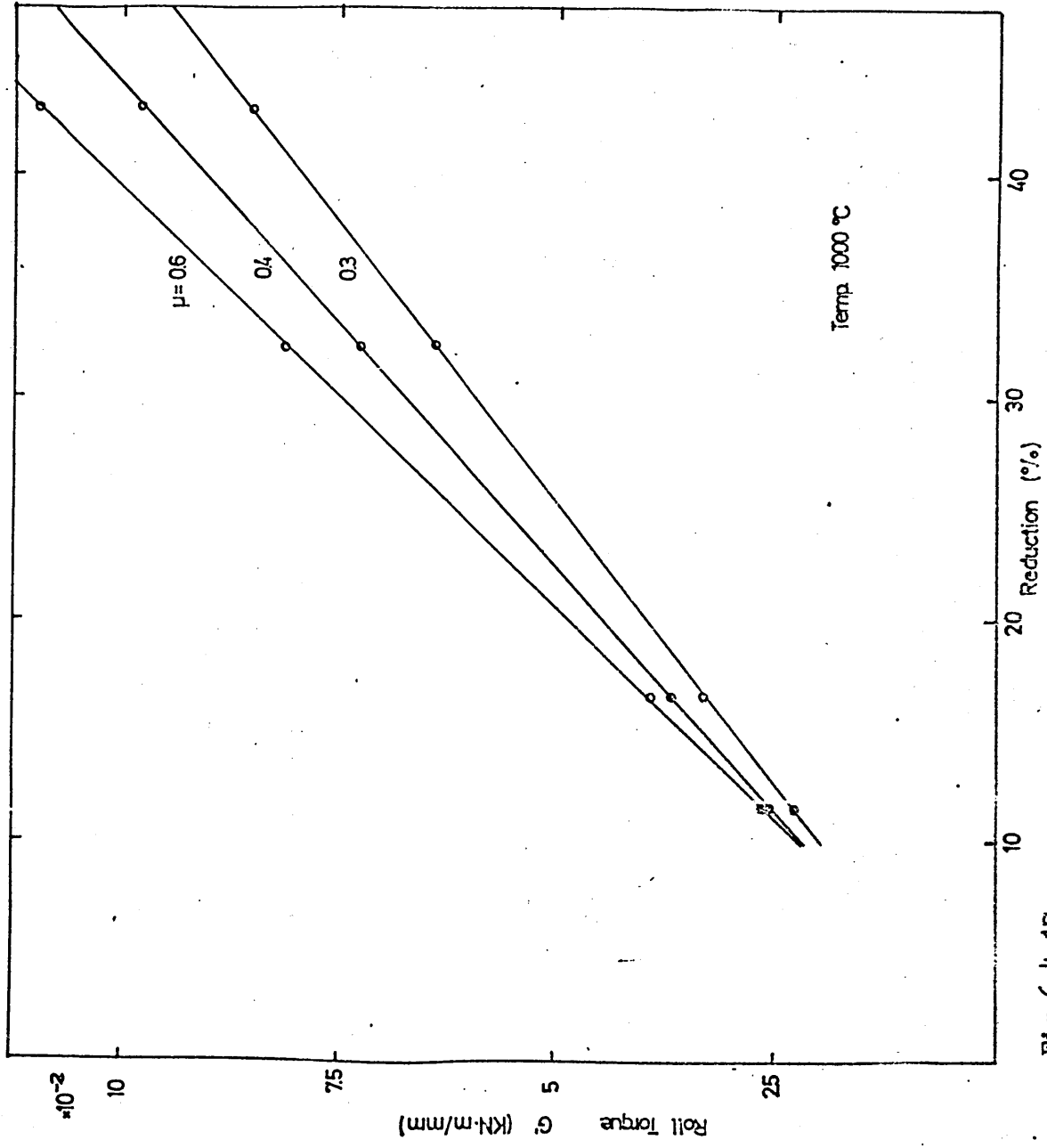


Fig.6.4.17

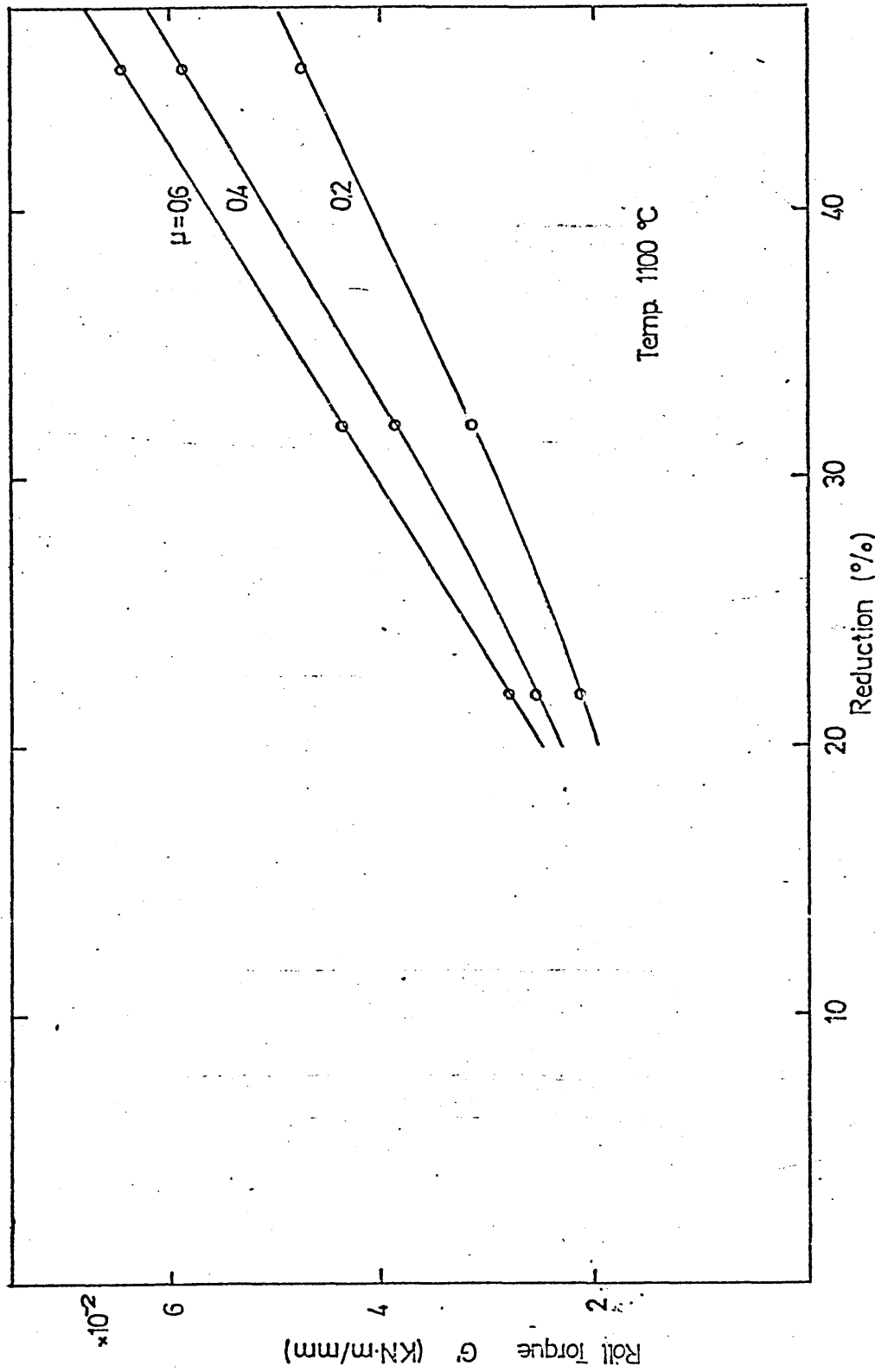


Fig.6.4.18 Relation between roll torque and reduction under inhomogeneous deformation using published flow stress data ($\mu=0.2-0.6$) at 1100°C.

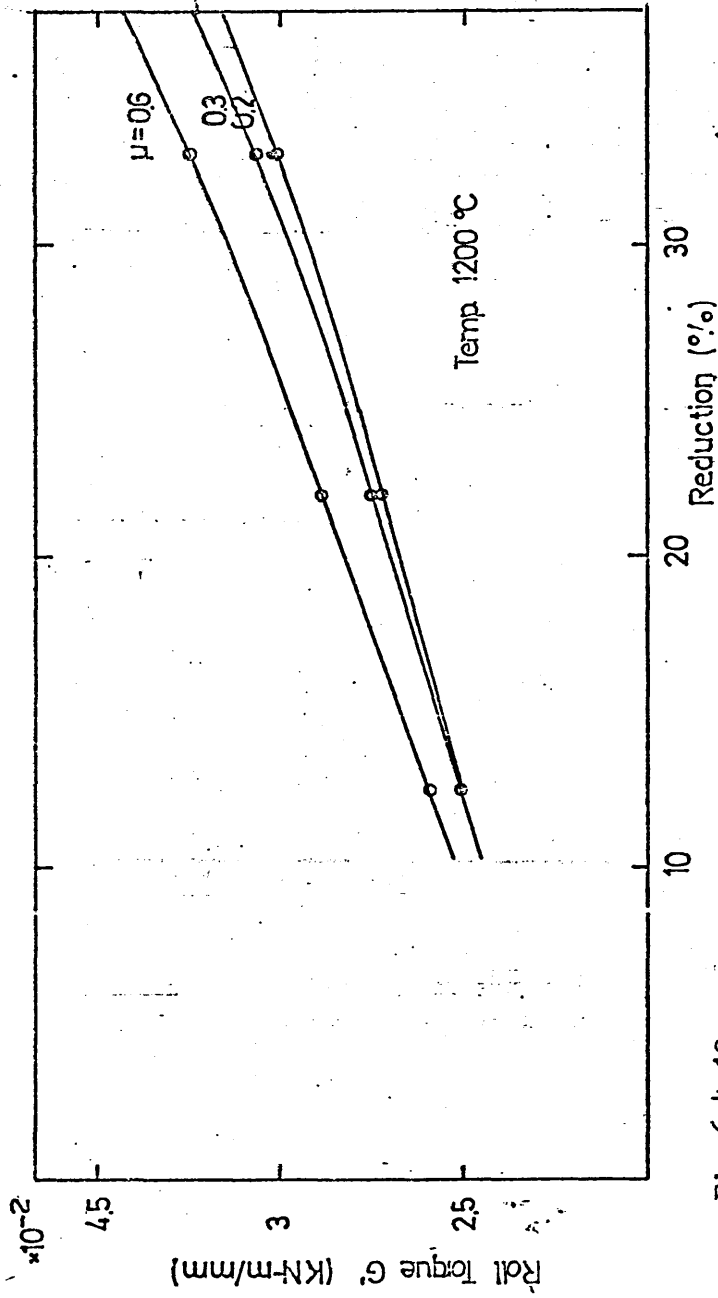


Fig.6.4.19

Relation between roll torque and reduction under inhomogeneous deformation using published flow stress data ($\mu=0.2-0.6$) at 1200 °C.

Fig.6.4.20 Roll pressure distribution assuming both homogeneous and inhomogeneous deformation and using published flow stress data (900°C , $\mu=0.6$, $r=18\%$).

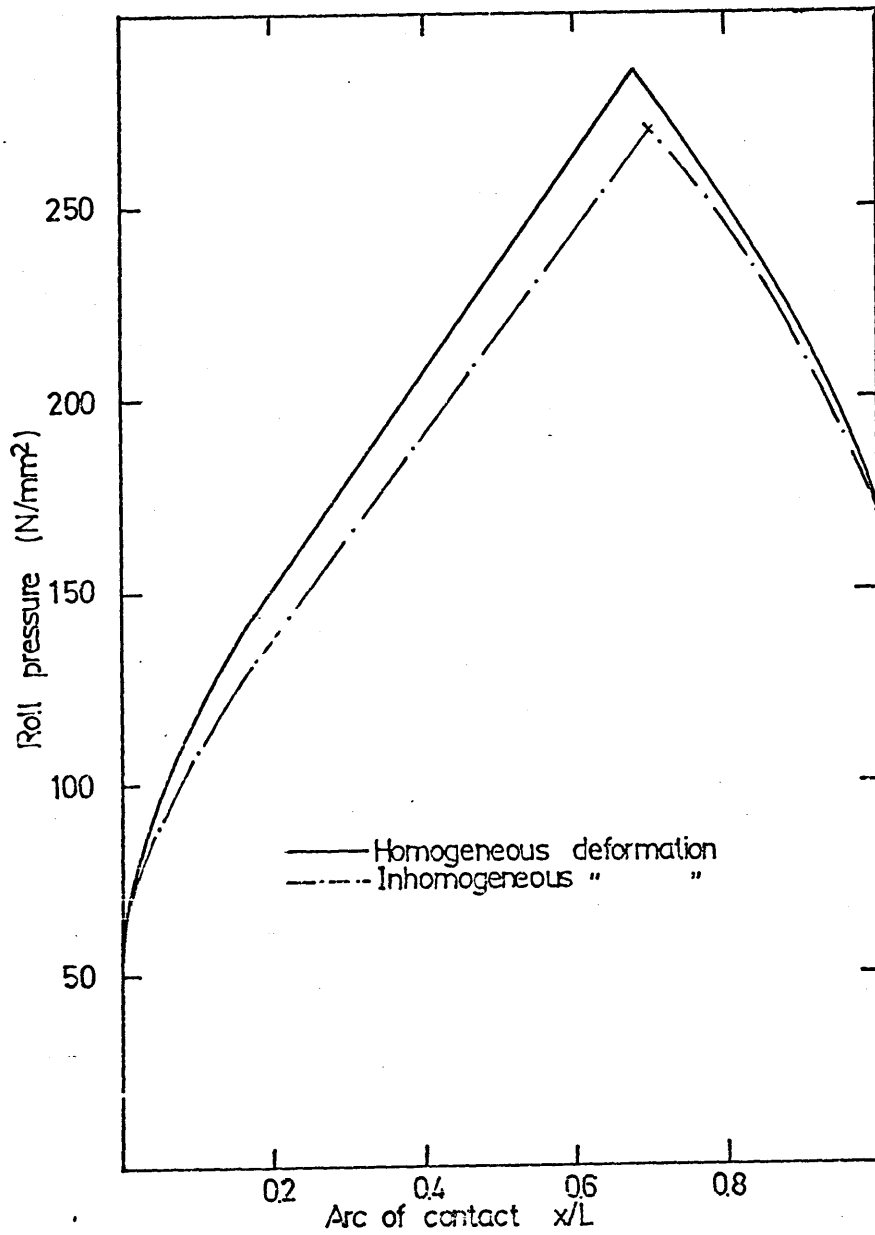


Fig.6.4.20 Roll pressure distribution assuming both homogeneous and inhomogeneous deformation and using published flow stress data (900°C , $\mu=0.6$, $r=18\%$).

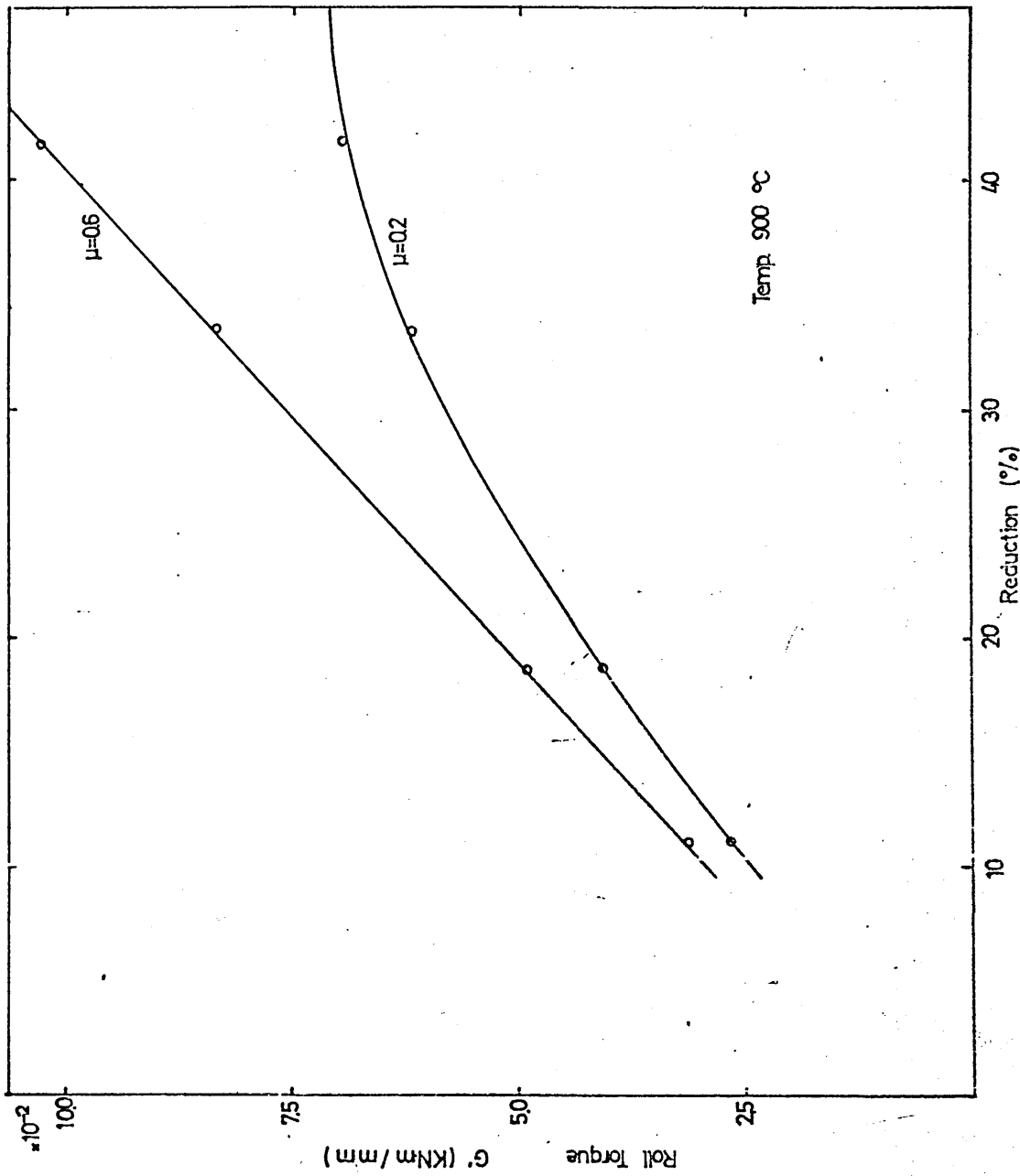


Fig.6.4.4.21 Relation between roll torque and reduction under inhomogeneous deformation using flow stress data determined in the present work ($\mu=0.2-0.6$) at 900°C.

6.4.22 Relation between roll torque and reduction under
 inhomogeneous deformation using flow stress data
 determined in the present work ($\mu=0.3-0.6$) at 1000°C.

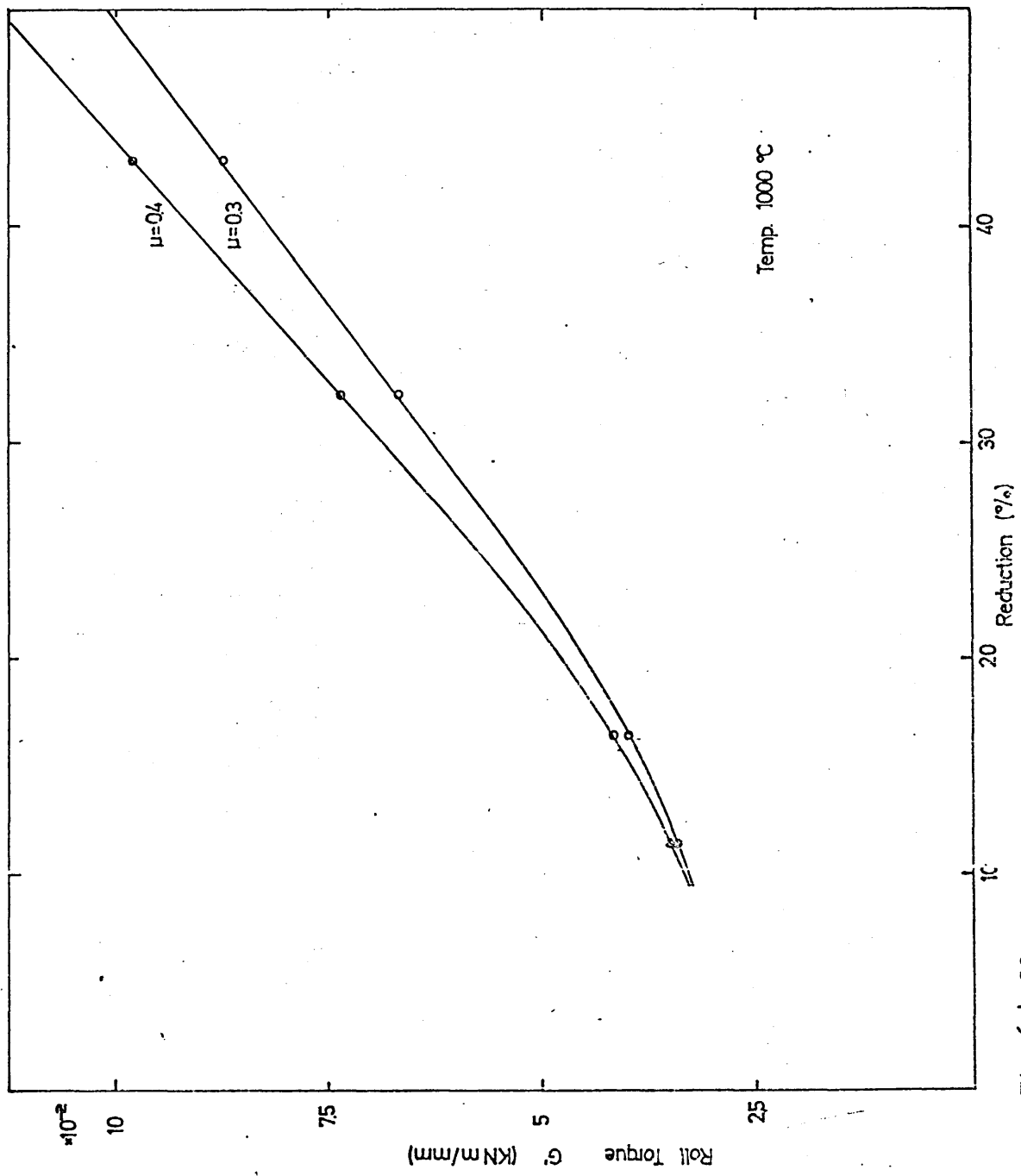


Fig.6.4.22

Fig.6.5.1 Relation between calculated roll torque and reduction showing the effect of a $\pm 5\%$ variation in the nominal temperature of rolling and using published flow stress data ($\mu=0.4$) - nominal temperature 900 °C.

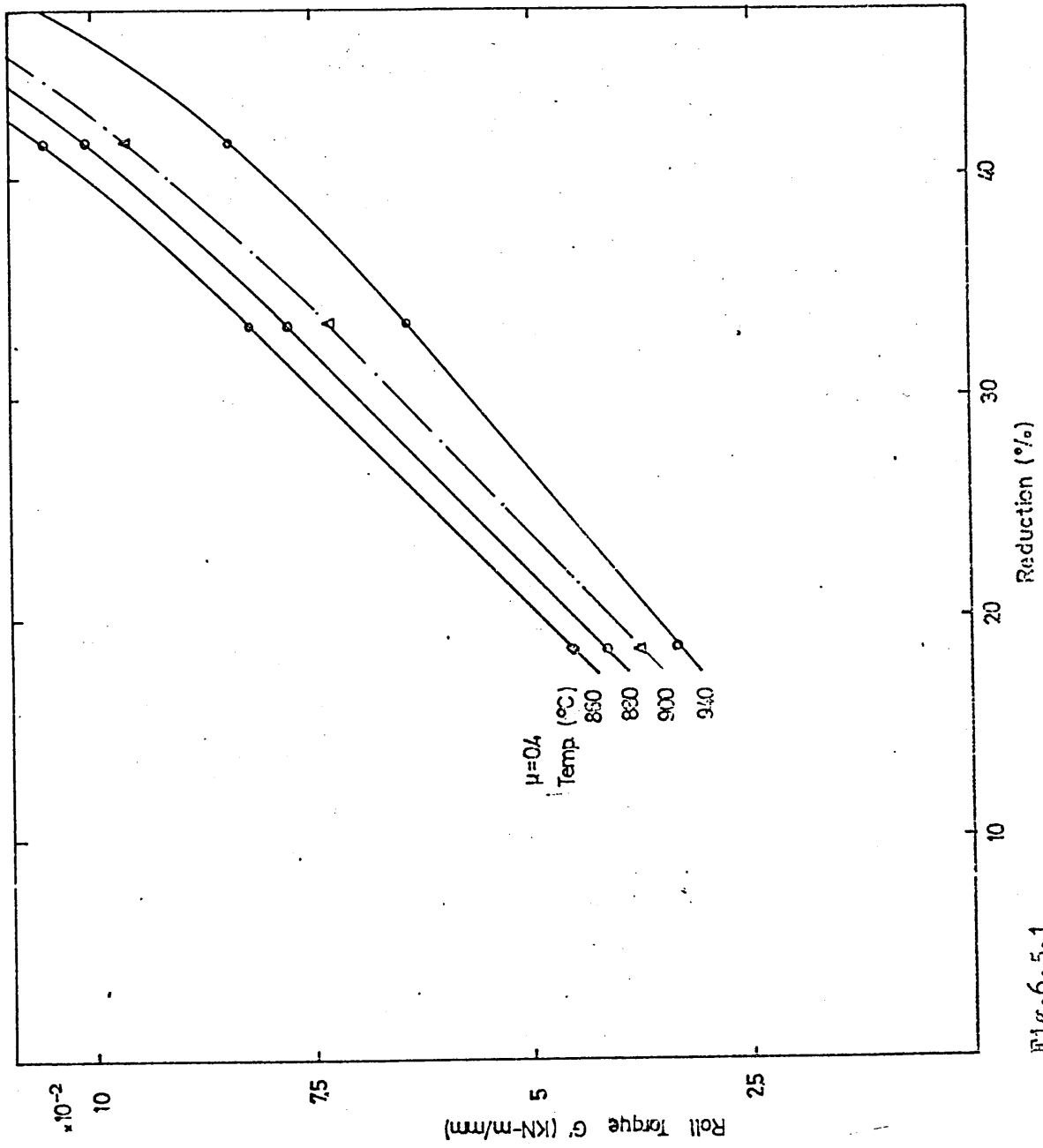


Fig.6.5.1

Fig.6.5.2 Relation between calculated roll torque and reduction showing the effect of a $\pm 5\%$ variation in the nominal temperature of rolling and using published flow stress data ($\mu=0.4$) - nominal temperature 1000°C.

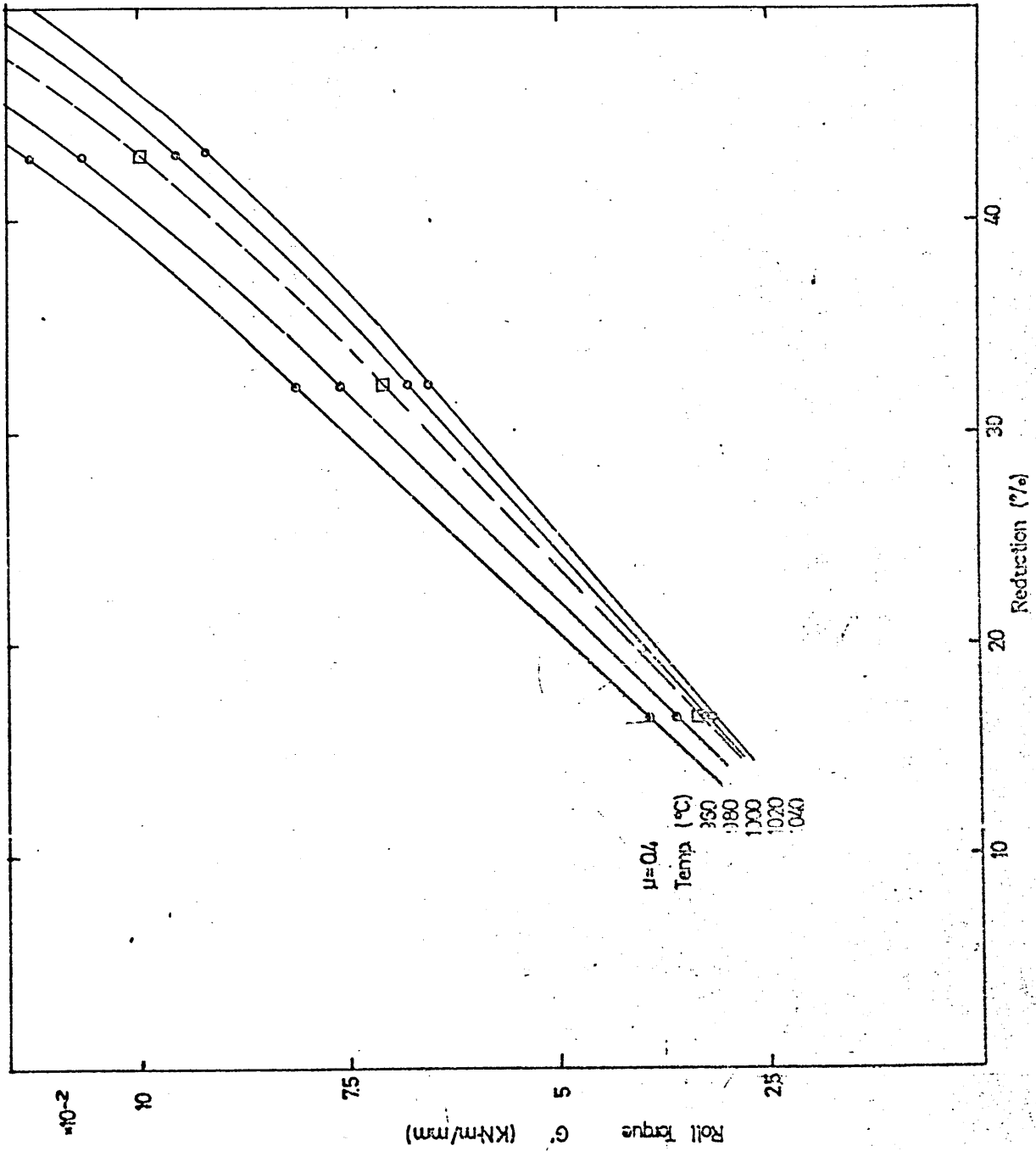


Fig.6.5.2

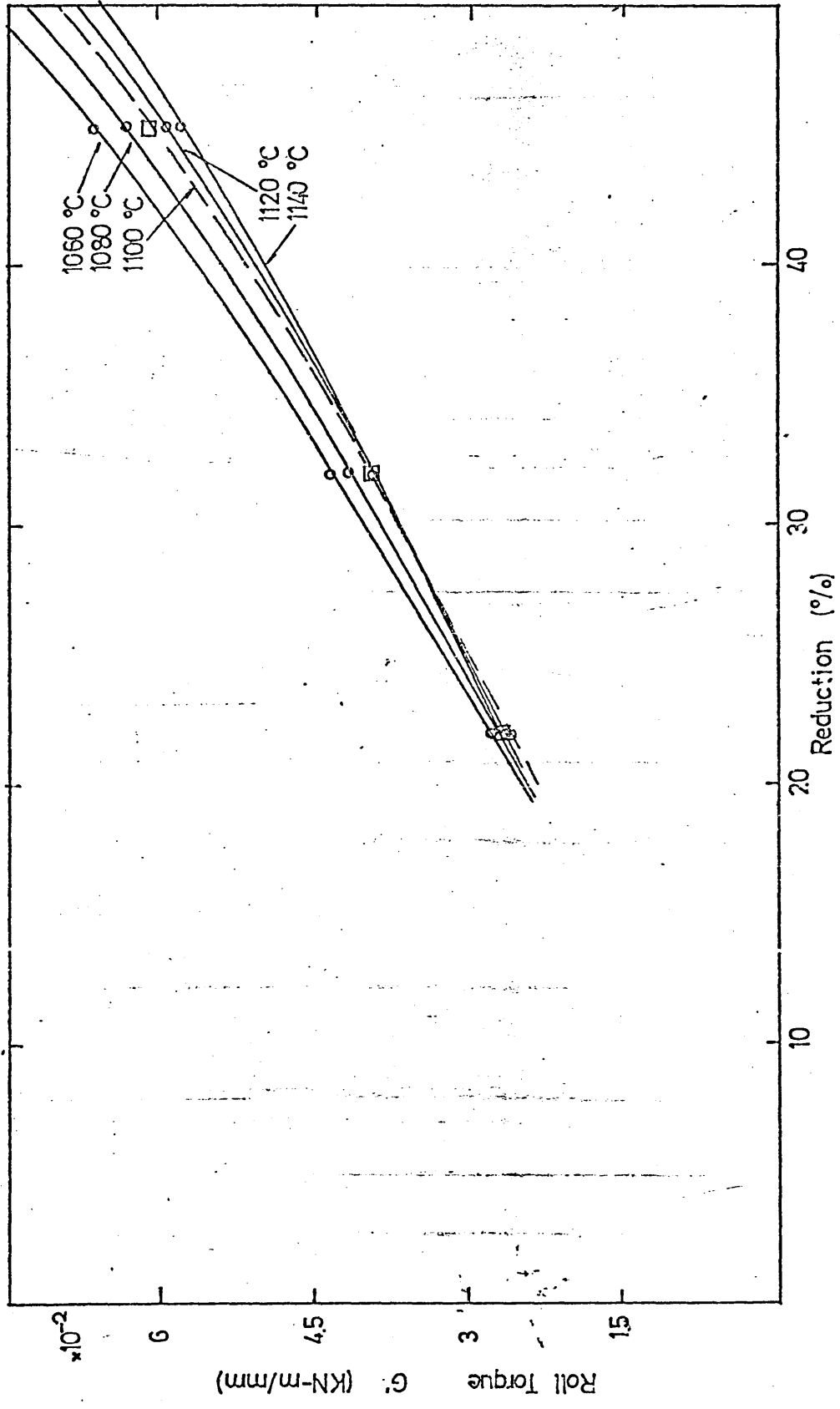


Fig.6.5.3 Relation between calculated roll torque and reduction showing the effect of a $\pm 5\%$ variation in the nominal temperature of rolling and using published flow stress data ($\mu=0.4$) - nominal temperature 1100 °C.

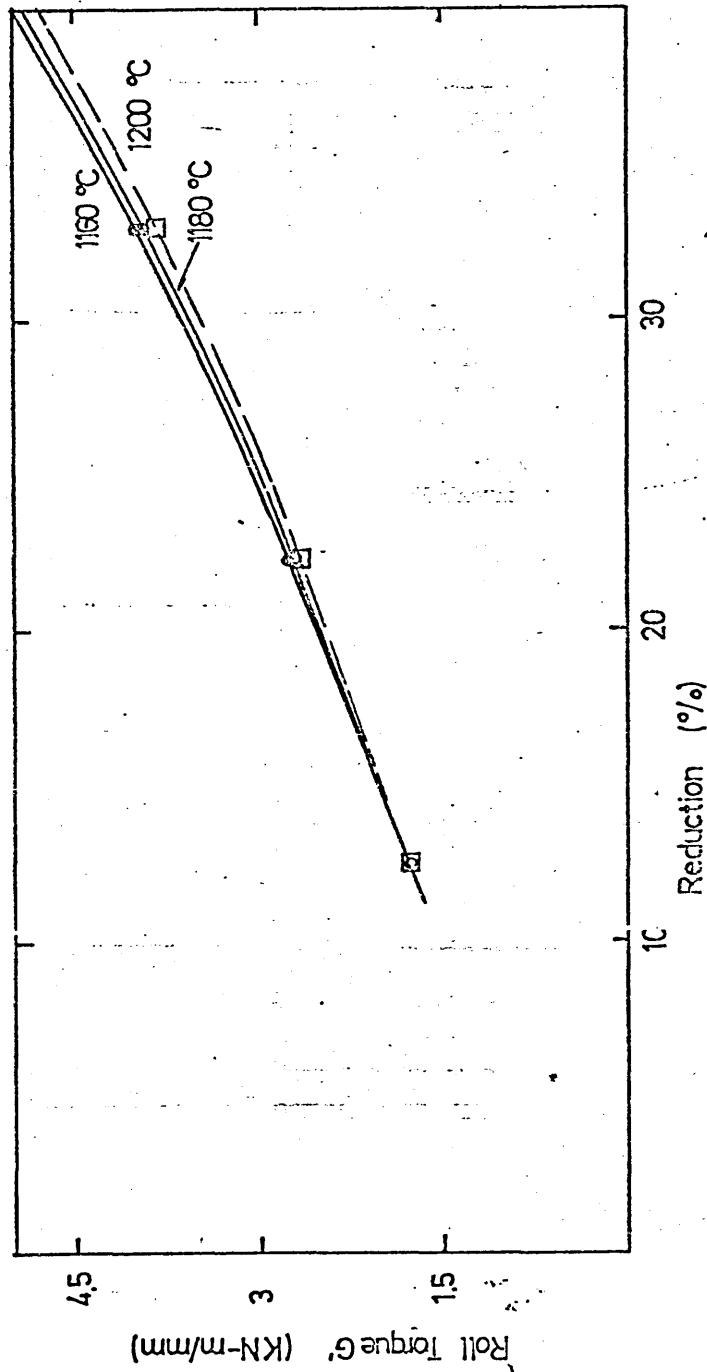


Fig.6.5.4. Relation between calculated roll torque and reduction showing the effect of a $\pm 4\%$ variation in the nominal temperature of rolling and using published flow stress data ($\mu=0.4$) - nominal temperature 1200°C.

Fig.6.6.1 Distribution of stresses across roll
gap mid-way between exit and entry
planes - after Sansome (66).

Fig.6.6.2 Transversal distribution of peak roll
pressures for various cross sectional
shapes of the material between the
rolls - after Polukhine (63).

Fig.6.6.3 Roll force distribution across strip
width - after Matsuura et al. (51).

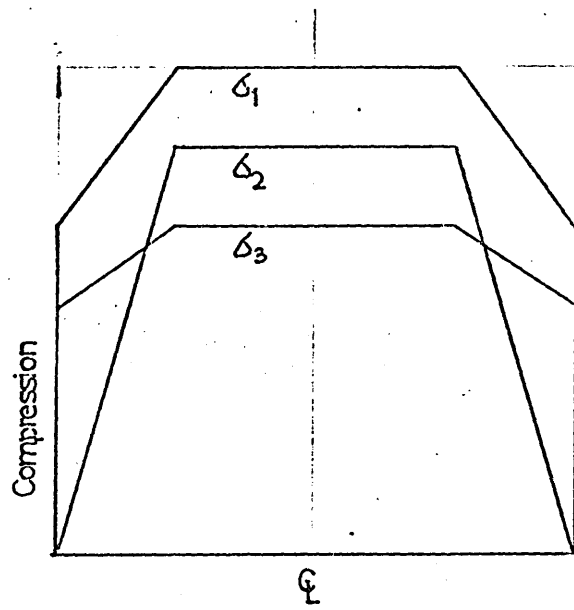


Fig.6.6.1

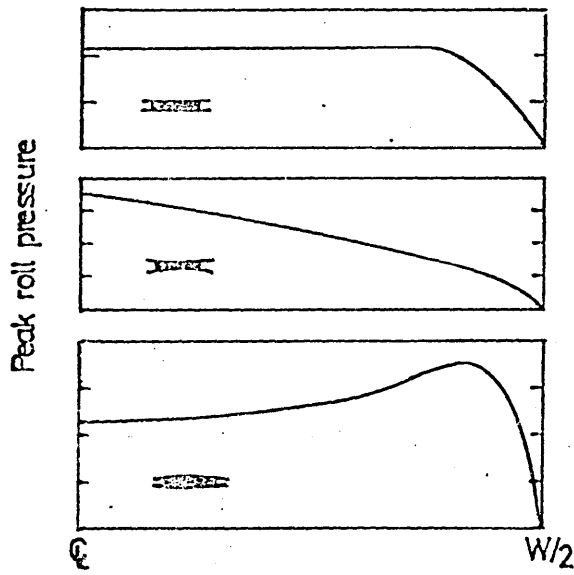


Fig.6.6.2

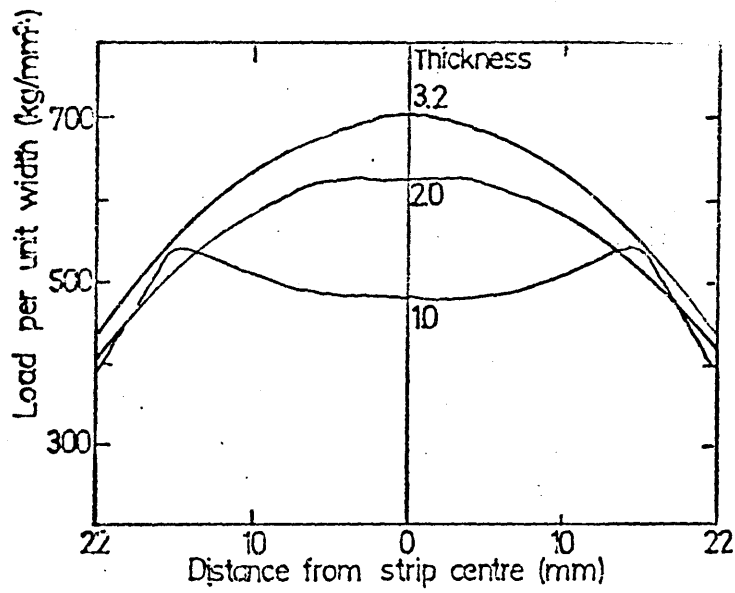


Fig.6.6.3

Table 2 Correcting factors to allow for transversal drop of roll pressure distribution.

<u>Experimental results</u>	<u>W_1/h_1</u>	<u>F_m/P_c</u>
Siebel (7) *	10	0.78
Matsuura (51)	13.75	0.81
Polukhine (65) **	-	0.82
Mean value used in the present work	6 - 8	0.8

* At high coefficients of friction

** For a constant thickness across the width of the plate.

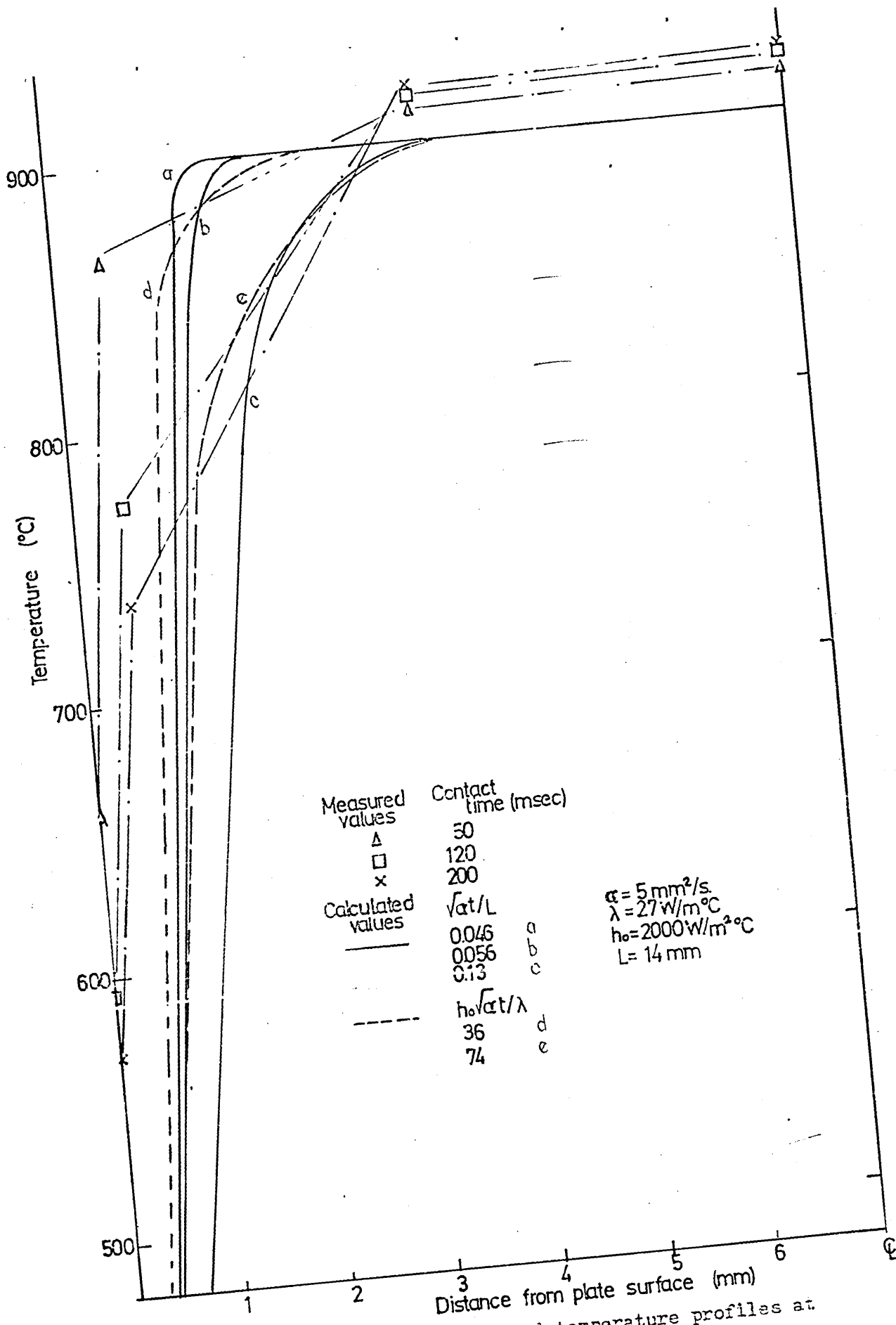
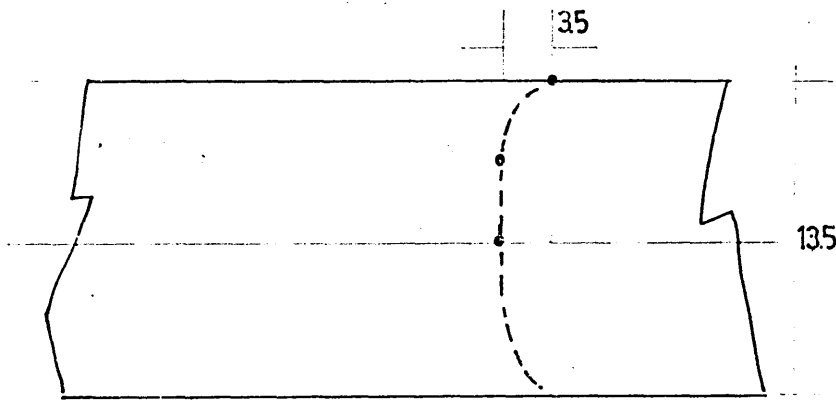


Fig.7.1 Measured and calculated temperature profiles at several instants during the time of contact.

Table 3 Values of the coefficient of friction determined from several empirical relationships.

Temperature(°C)	Present work r=30 - 40%	Ekelund (6)	Siebel (49)	Roberts (50) r=30-50%	Male et al. (45) r=50%
900	0.18 - 0.26	0.48	0.33	0.4	0.4 - 0.5
1000	0.45	0.44	0.3	0.475	-
1100	0.35	0.4	0.28	0.56	-
1200	0.32	0.36	0.25	0.6	-



• Thermocouple hot junction
 Dimensions in mm.

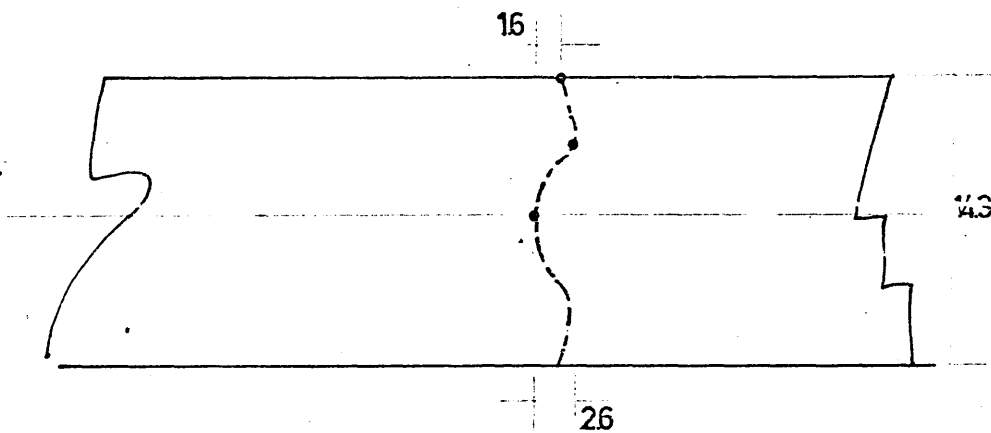


Fig.7.4.1 Reconstructed disposition of the hot junction of thermocouples in rolled plates.

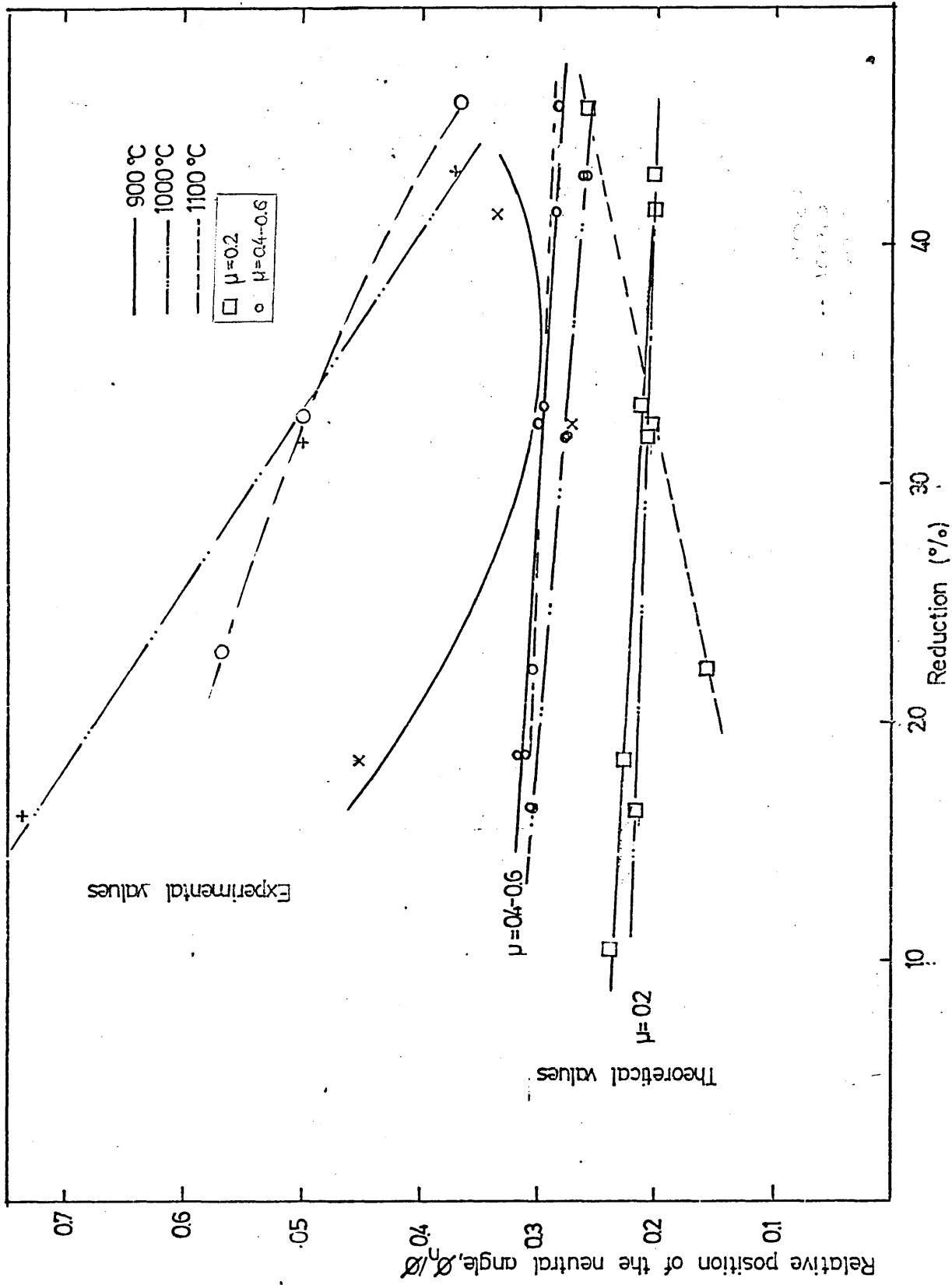


Fig.7.4.2 Relation between theoretical and experimental values of the neutral angle and percentage reduction (Series A).

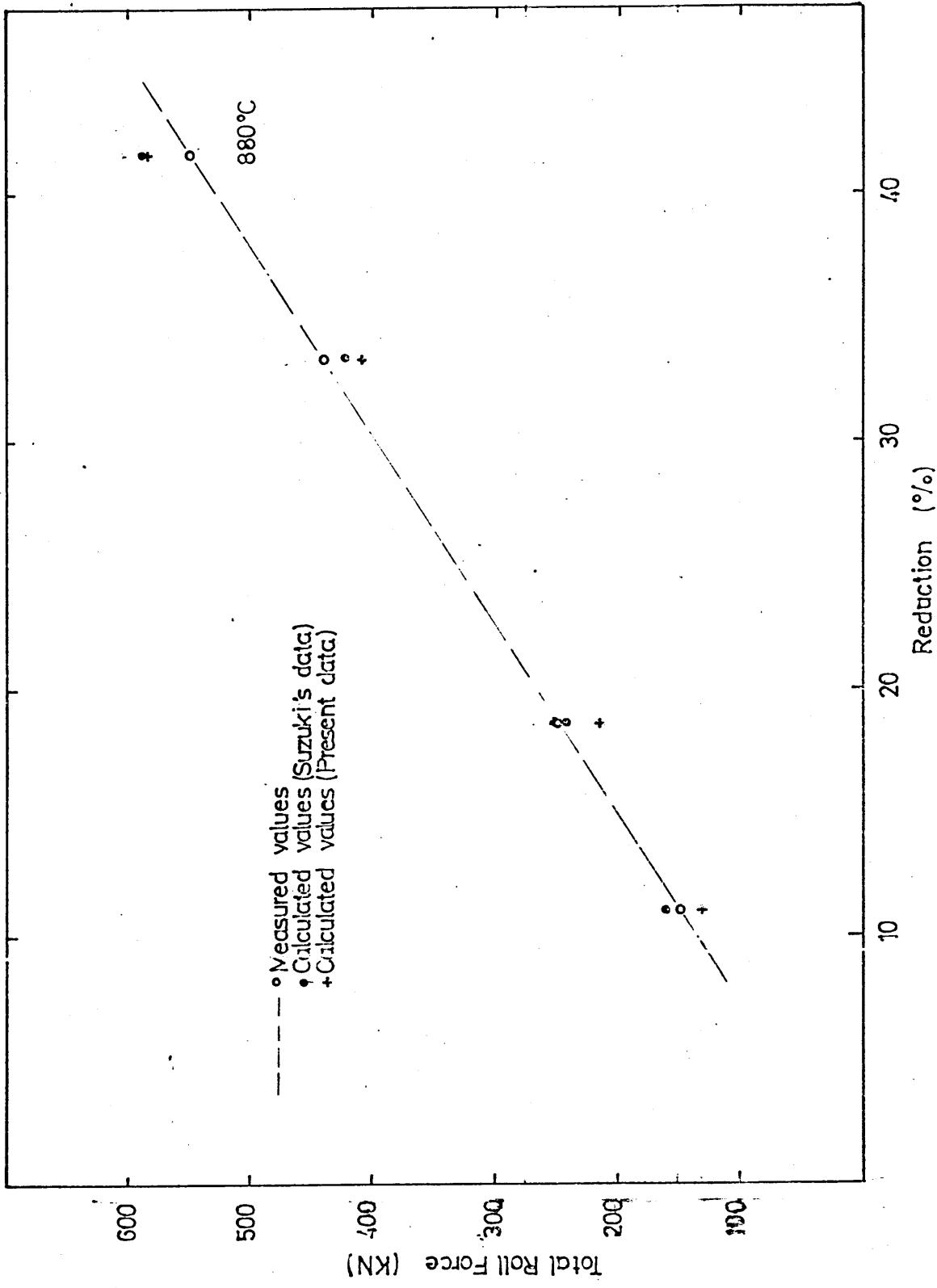


Fig.7.5.1 Comparison between calculated and measured values of roll force for the rolling conditions in Series A at 880 - 940°C

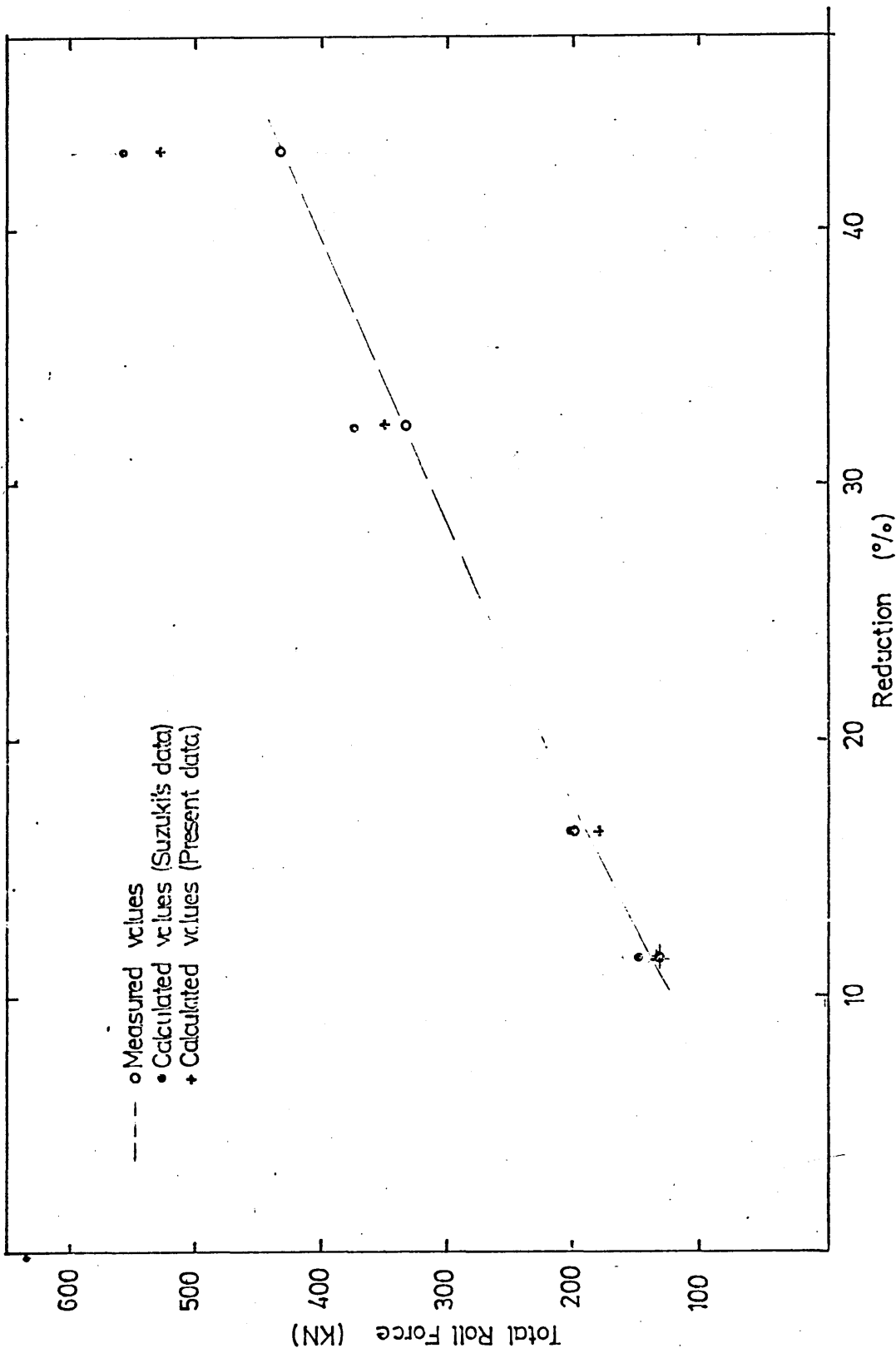


Fig.7.5.2 Comparison between calculated and measured values of roll force for the rolling conditions in Series A at 950 °C.

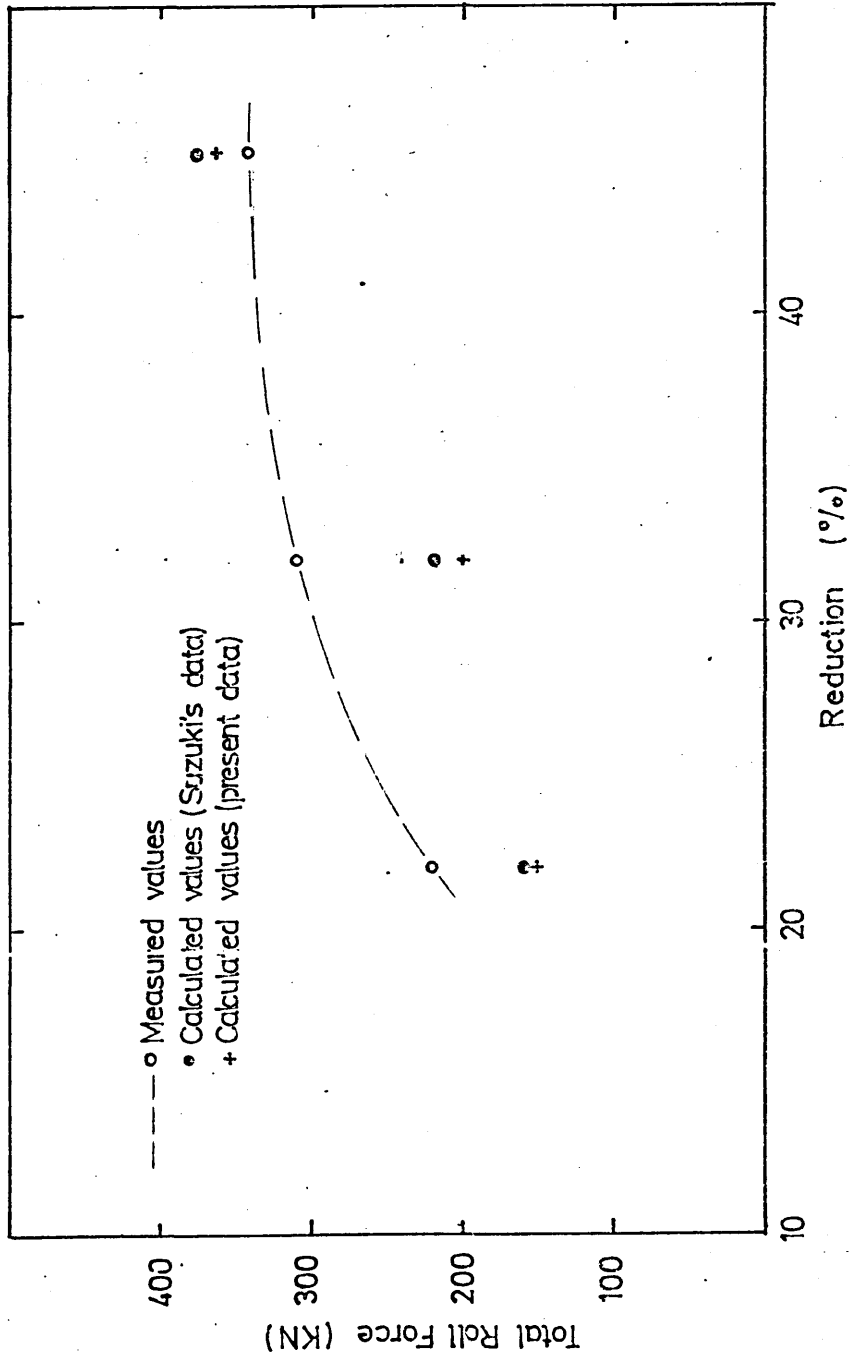


Fig.7.5.3 Comparison between calculated and measured values of roll force for the rolling conditions in Series A at 1080°C.

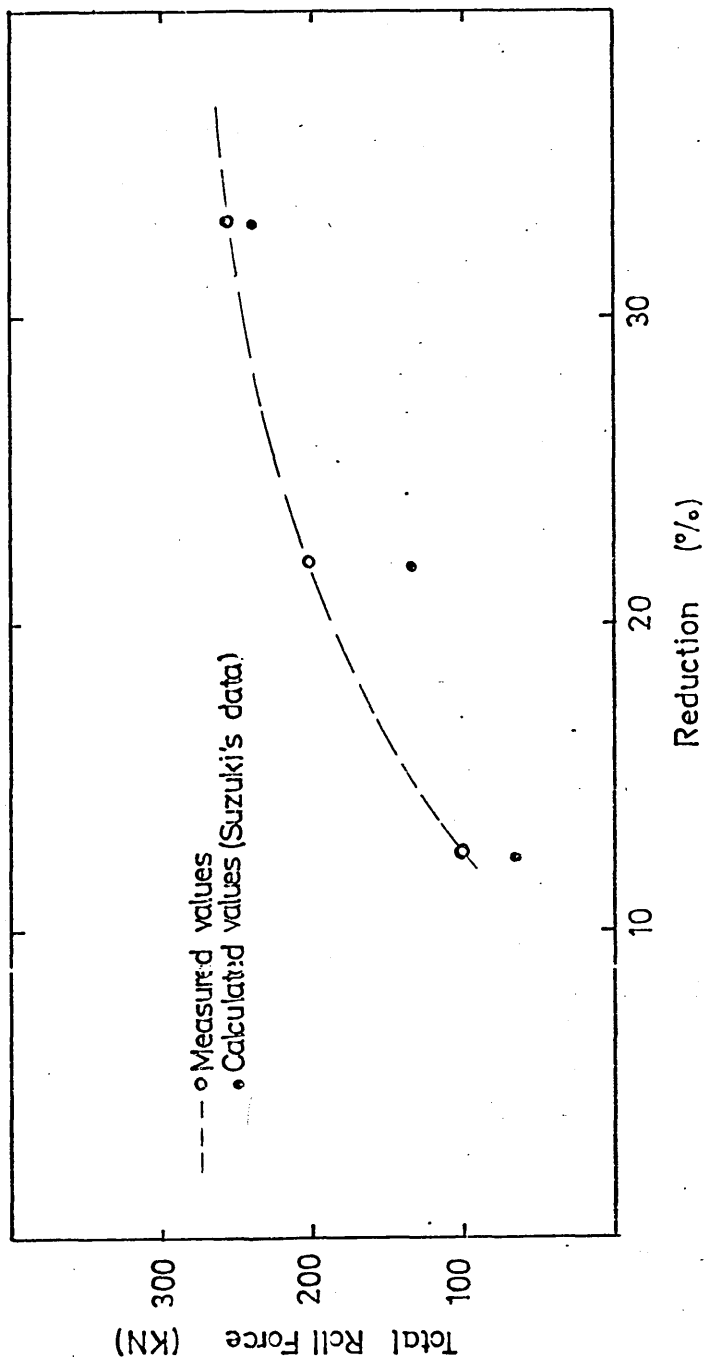


Fig.7.5.4 Comparison between calculated and measured values of roll force for the rolling conditions in Series A at 1150°C.

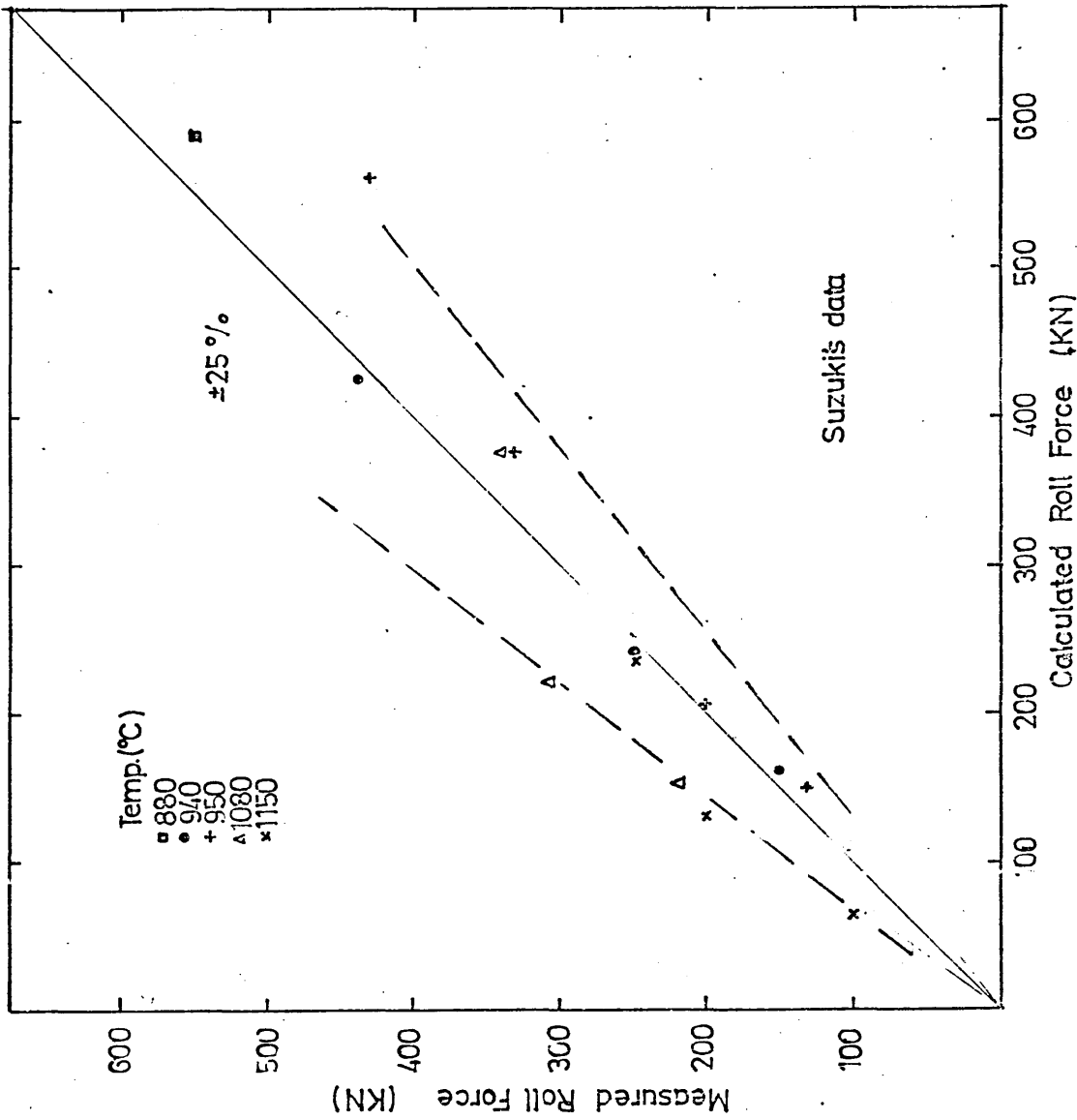


Fig. 7.5.5 Comparison between measured and calculated roll forces in Series A using published flow stress data.

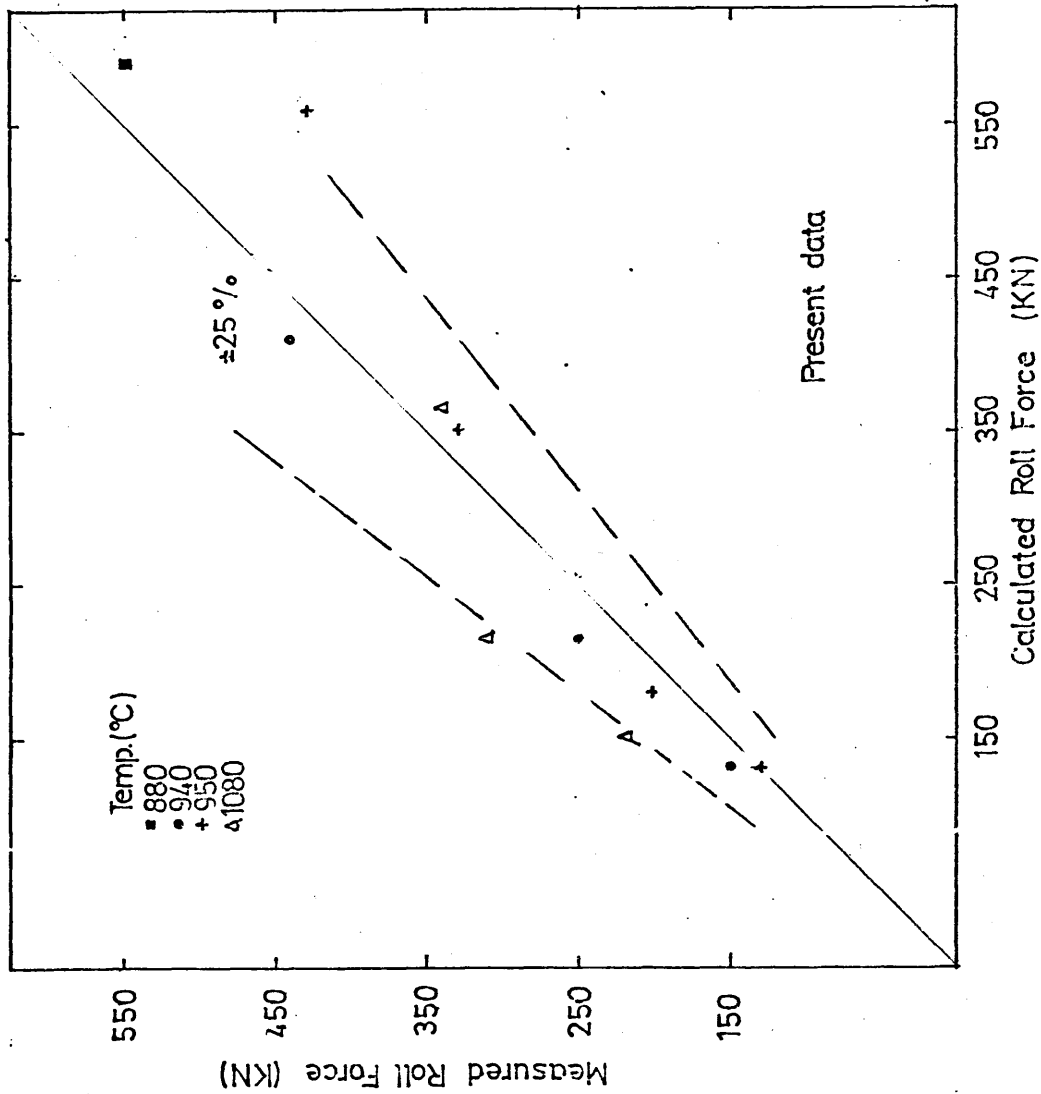


Fig.7.5.6 Comparison between measured and calculated roll forces in Series A using flow stress data determined in the present work.

Fig.7.6.1 Comparison between calculated and measured values of
roll torque for the rolling conditions in Series A at
880 - 940°C.

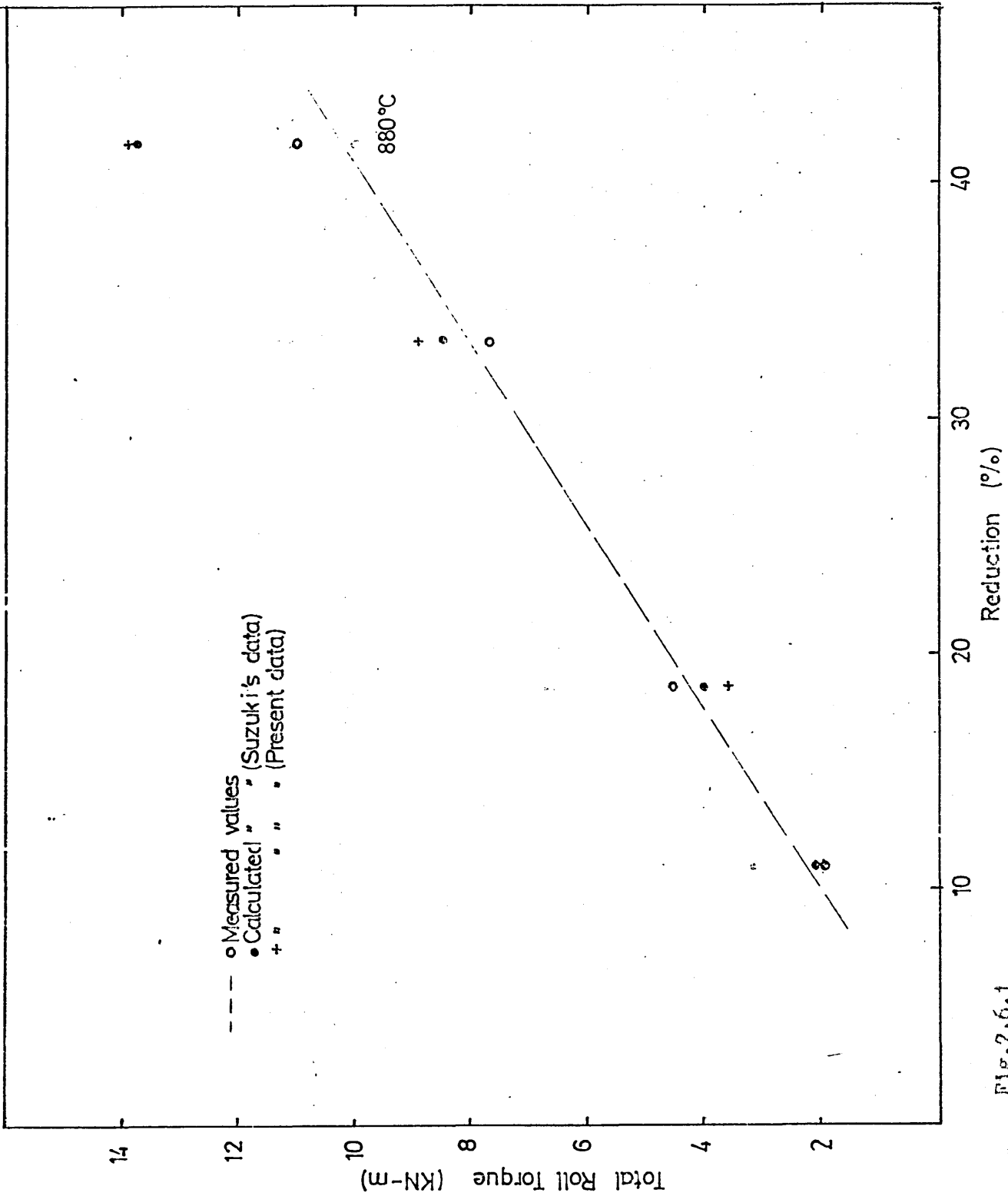


Fig.7.6.1

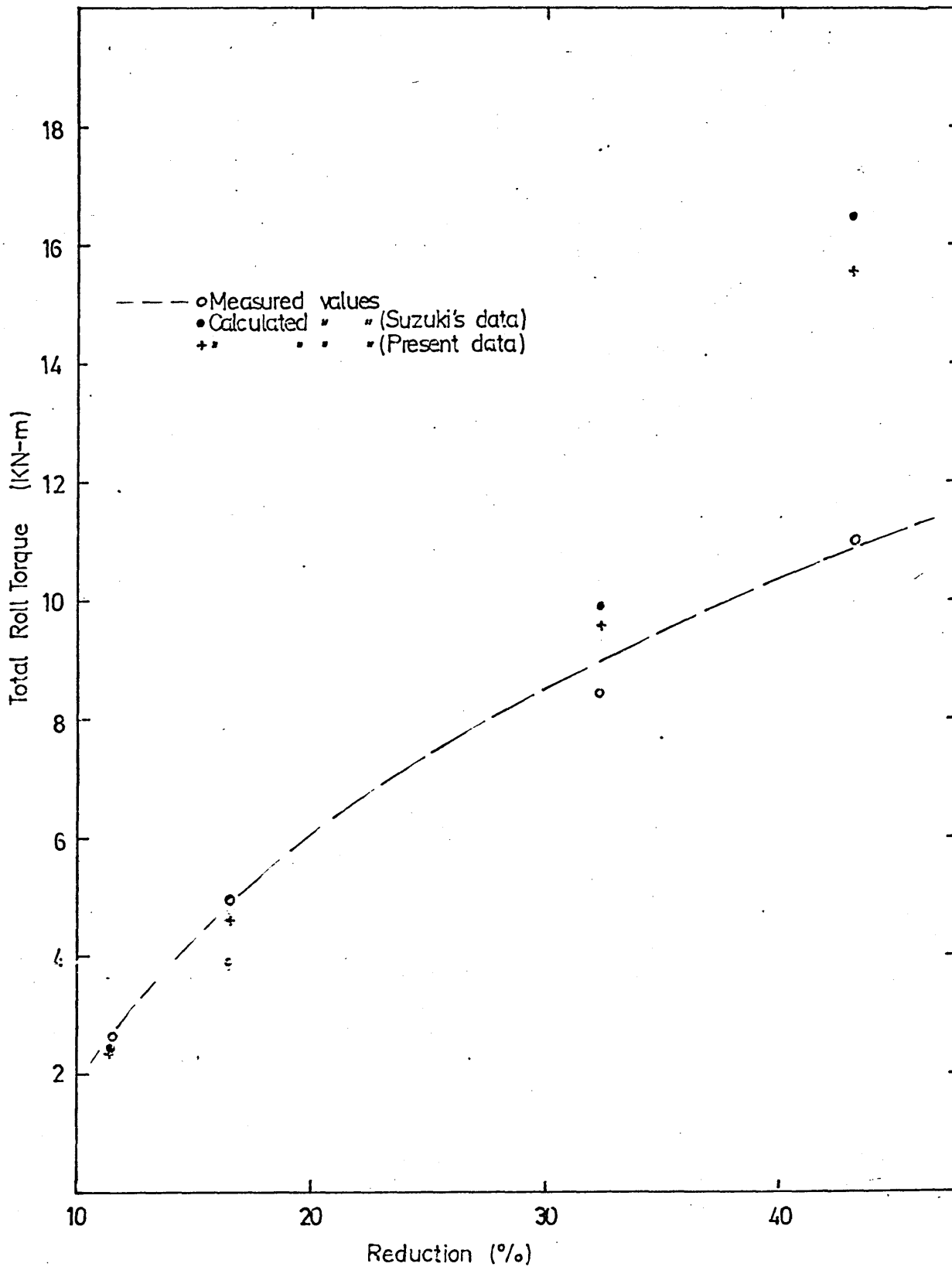


Fig.7.6.2 Comparison between calculated and measured values of roll torque for the rolling conditions in Series A at 950°C.

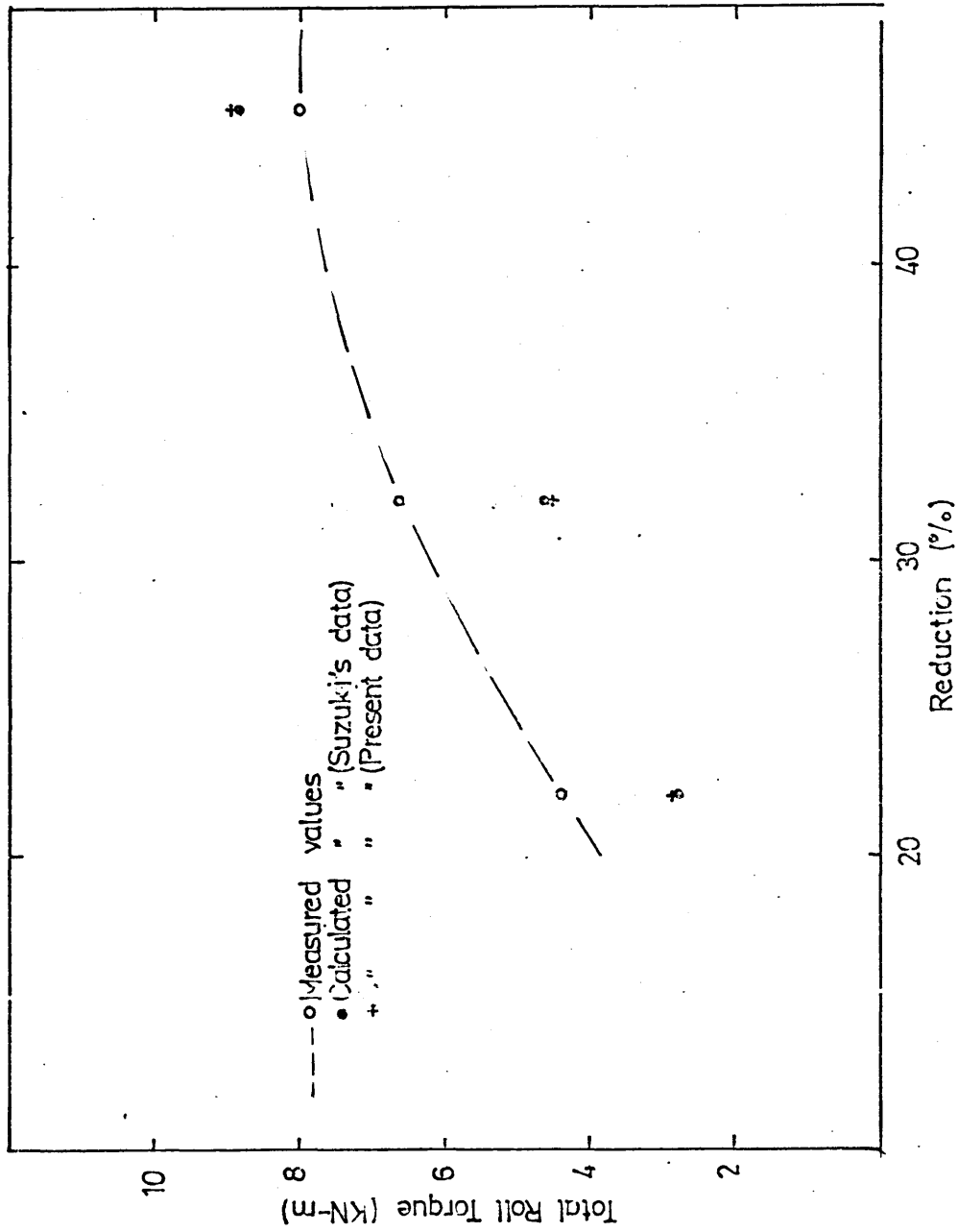


Fig.7.6.3 Comparison between calculated and measured values of roll torque for the rolling conditions in Series A at 1080°C.

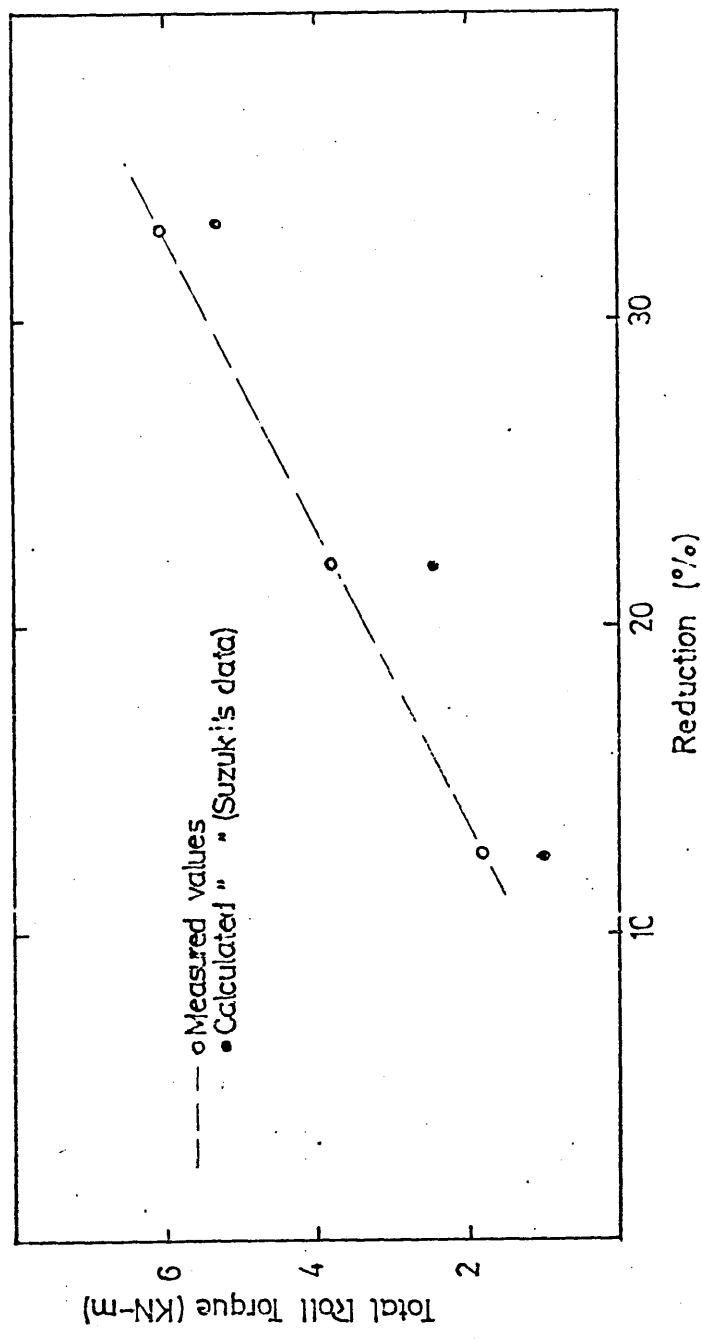


Fig.7.6.4 Comparison between calculated and measured values of roll torque for the rolling conditions in Series A at 1150°C.

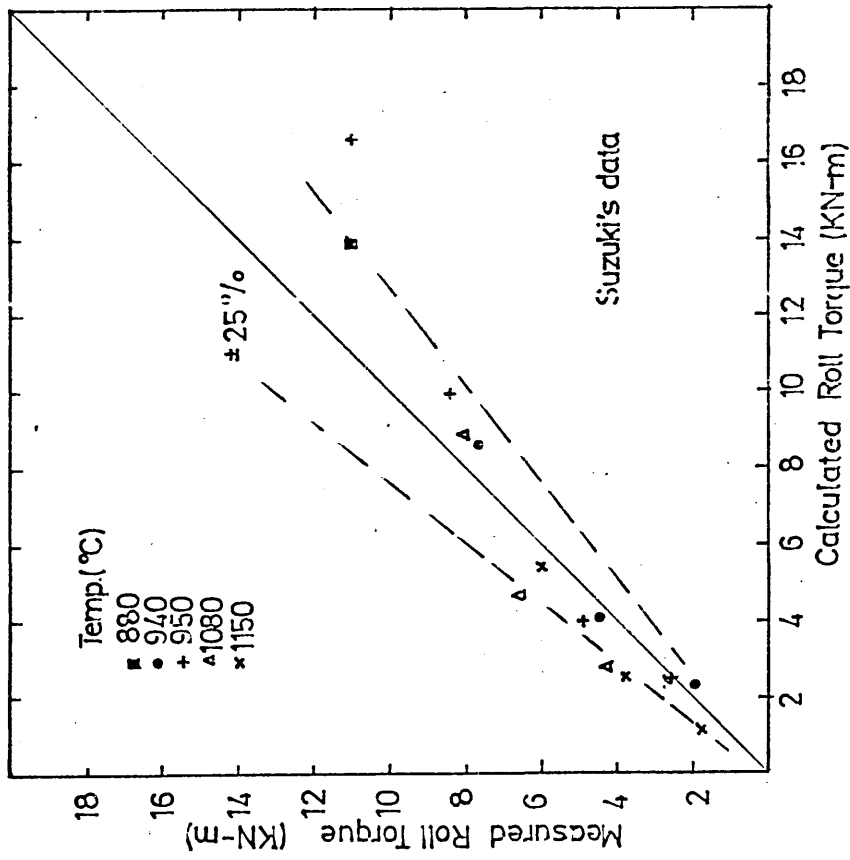


Fig.7.6.5 Comparison between measured and calculated roll torque in Series A using published flow stress data.

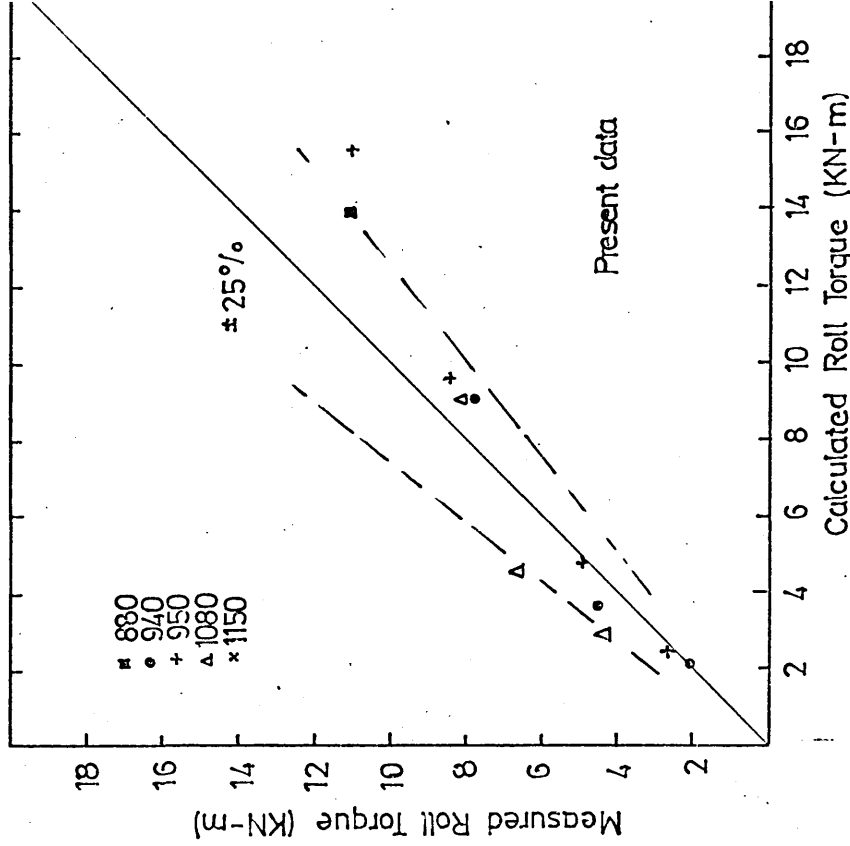


Fig.7.6.6 Comparison between measured and calculated roll torque in Series A using flow stress data determined in the present work.

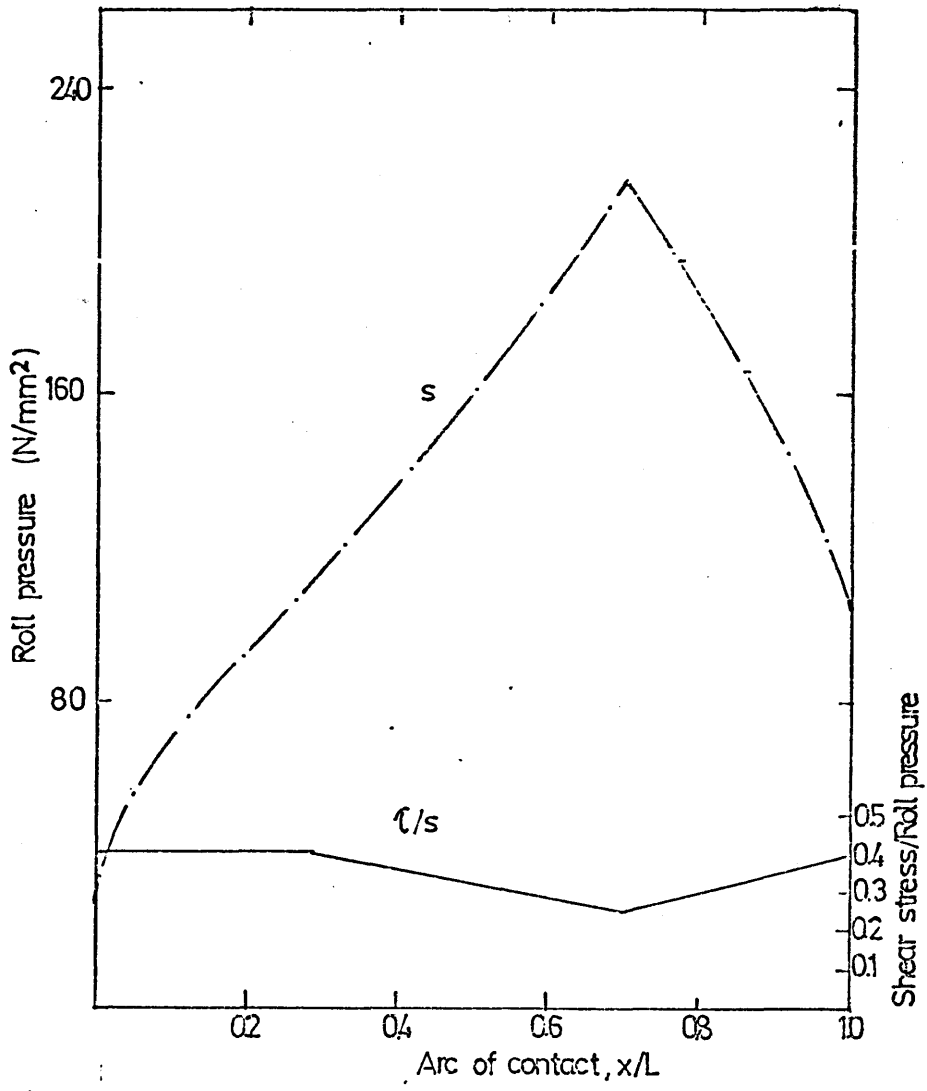


Fig.7.7 Distribution of roll pressure and shear stress/roll pressure ratio along the arc of contact (1100°C, $r=40\%$).